

Technische Universität München
Department Chemie
Lehrstuhl für Organische Chemie I

Photoredox Chemistry with Nickel-based Catalysts

Michael Grübel

Vollständiger Abdruck der von der Fakultät für Chemie der Technischen Universität München zur Erlangung des akademischen Grades eines

Doktors der Naturwissenschaften

genehmigten Dissertation.

Vorsitzender:	Prof. Dr. Klaus Köhler
Prüfer der Dissertation	1. Prof. Dr. Thorsten Bach 2. Prof. Dr. Corinna R. Hess

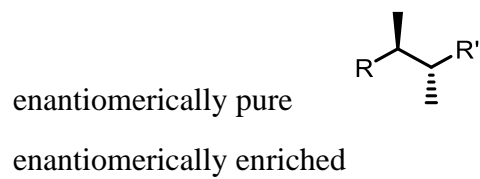
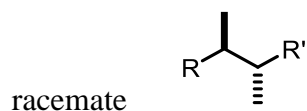
Die Dissertation wurde am 06.08.2019 bei der Technischen Universität München eingereicht und durch die Fakultät für Chemie am 02.09.2019 angenommen.

„Part of the journey is the end“

Tony Stark

This dissertation describes the work carried out at the Lehrstuhl für Organische Chemie I at the Technische Universität München between Juli 2016 and June 2019. The project described in this thesis was supervised by Prof. Dr. Thorsten Bach.

In this thesis, the relative configuration of racemates is represented by straight lines (bold or hashed). The absolute configuration of enantiomerically pure or enriched compounds is represented by wedge-shaped lines (bold or hashed)



Acknowledgements

Mein Dank gilt meinem Doktorvater Prof. Dr. Thorsten Bach für die freundliche Aufnahme in seinen Arbeitskreis und die Möglichkeit bei ihm promovieren zu können. Ich möchte mich für das entgegengebrachte Vertrauen bedanken, die hervorragenden Arbeitsbedingungen, die aufschlussreichen Diskussionen sowie die fachlichen Weiterbildungen durch Seminare und Übungen.

Ein weiterer Dank gilt meiner Doktormutter Prof. Dr. Corinna R. Hess für das Bereitstellen des interessanten Forschungsthemas, welches ich die letzten vier Jahre mit ihr zusammen bearbeiten durfte. Bei fachlichen und persönlichen Problemen hatte Sie immer ein offenes Ohr und Ich konnte immer auf Ihre Unterstützung bauen.

Des Weiteren bedanke ich mich bei Dr. Andreas Bauer und Dr. Stefan Breitenlechner, die mir im Labor durch ihre Kreativität und großes Engagement immer weiterhelfen konnten. Bei Problemen mit meiner Photochemie war Andreas sofort zur Stelle um mir zu Helfen. Gleichzeitig habe ich die Zeit mit Stefan am Säulenautomat oder bei den Autoklaven sehr genossen.

Frau Kerstin Voigt ist die gute Seele des Lehrstuhls und ich möchte einen großen Dank für die große Unterstützung abseits der Chemie aussprechen. Die zahlreichen bürokratischen Hürden, die Sie für mich bewältigte und die netten Gespräche zwischendurch haben den Arbeitsalltag vereinfacht. Für die Versorgung innerhalb des Labors möchte ich mich bei Herrn Olaf Ackermann bedanken, der zu jeder Zeit Laborutensilien und Chemikalien bereitstellte.

Für die Hilfe im Bereich der Analytik möchte ich mich bei Jürgen Kudermann bedanken der mir beim Aufsetzen meiner GC Proben oder beim IR Messen immer hilfreiche Tipps geben konnte. Weiter bedanke ich mich bei Christine Schwarz und Maria Matthews für die Unterstützung bei meinen NMR Messungen. Ein großer Dank geht an die Jungs aus dem SC XRD Labor (Alex, Philipp und Christian) die immer bereitwillig meine vielen Proben gemessen und mit denen ich viele nette Gespräche gehabt habe.

Für die tolle Zeit im Labor möchte ich zunächst der BOX1 danken, mit all den Ehemaligen und jetzigen Bewohnern. Die Anfangszeit mit Maïke und Zeyneb hat mich sehr geprägt aber mich nicht dazu gebracht sauberer zu arbeiten. Irene, meine Wegbegleiterin auf meinem Thema, Ich bedanke mich für die großartige Zeit und die vielen, vielen Stunden die wir zusammen im Labor waren und versucht haben Spanisch bzw. Deutsch zu lernen. Aber auch bei den jetzigen Bewohnern des AK Storch (Golo, Alex, Andi) und Lilla bedanke ich mich für die schöne Zeit.

Ein spezieller Dank gilt Lukas, mit dem ich meine Ideen für meinen neuen Photoreaktor realisieren konnte.

Weiter bedanke ich mich bei allen anderen Bewohnern der anderen BOXEN für das herausragende Arbeitsklima und die vielen unterhaltsamen und kurzweiligen Stunden im Labor. Mein großer Dank gilt: Allen die im Labor waren und sind!

Meinen Forschungspraktikanten Julia, Alexandra, Philipp, Micha, Manu, Vivien, Julian danke ich vielmals für die Hilfe im Labor und das Voranbringen meiner Projekte.

Für das akribische Korrekturlesen und die hilfreichen Anmerkungen bedanke ich mich herzlich bei Saner, Malte, Simon, Christian, Johannes, Noah, Fabi, Finn, Hanusch Golo und Lima.

Der größte Dank gilt meiner Familie, die mich zu jeder Zeit unterstützt hat und immer ein offenes Ohr hatte. Ich bedanke mich bei meinen Eltern und meinem Bruder die während meines Studiums und meiner Promotion immer moralisch für mich da waren. Als letztes möchte mich bei meiner Liebe Lima bedanken für die zahllosen Stunden die ich mit dir in guten und auch schlechten Tagen verbringen durfte. Für die rollenden Augen und die richtigen Worte, für dein Verständnis, deine Begeisterungsfähigkeit und deine viele Geduld. Danke, dass du immer für mich da warst und mir den Rücken freigehalten hast.

List of Abbreviations

Å	Ångström
ATRA	atom transfer radical addition
ATP/ADP	adenosine triphosphate/adenosine diphosphate
Bu/iBu	butyl/ <i>iso</i> -butyl
Bpy	2,2'-bipyridine
Cy	cyclohexyl
DMF	dimethylformamide
DFT	density functional theory
Dehal	dehalogenated
e.g.	latin for: <i>exempli gratia</i>
EPR	electron paramagnetic resonance
ee	enantiomeric excess
equiv	equivalents
Et ₂ O	diethylether
fs	femtoseconds
HAT	hydrogen atom transfer
HOMO	highest occupied molecular orbital
<i>hν</i>	denotes irradiation with photons of a specific wavelength
IC	internal conversion
ISC	intersystem crossing
IR	infrared
LC	ligand-centered
LED	light emitting diode
LUMO	lowest unoccupied molecular orbital
MLCT	metal-to-ligand charge transfer
MC	metal-centered
MeCN	acetonitrile
Me	methyl
NMR	nuclear magnetic resonance
NEt ₃	triethylamine

ns	nanoseconds
NADP	nicotinamide adenine dinucleotide phosphate
OLED	organic light emitting diode
Ox	oxidant
Ph	phenyl
PC	photocatalyst
PCET	proton-coupled electron transfer
rISC	reverse intersystem crossing
r.t.	room temperature
SET	single electron transfer
SCE	saturated calomel electrode
S ₀	singlet ground state
S ₁	singlet excited state
SC XRD	single crystal X-Ray diffraction analysis
SQUID	superconducting quantum interference device
THIQ	tetrahydroisoquinoline
TMS	trimethylsilyl
TADF	thermally activated delayed fluorescence
THF	tetrahydrofuran
UV/Vis	ultraviolet/visible region
μs	microseconds
τ	corresponds to lifetime
λ	wavelength

Publication List

- Grübel, M.; Bosque, I.; Altmann, P. J.; Bach, T.; Hess, C. R. *Chem. Sci.* **2018**, *9*, 3313-3317. “Redox and photocatalytic properties of a Ni(II) complex with a macrocyclicbiquinazoline (Mabiq) ligand.”
- Grübel, M.; Jandl, C.; Bach, T. *Synlett*, **2019**, *30*, 1825-1829. “Synthesis of Tetrahydroisoquinolines by Visible Light-mediated 6-exo-trig Cyclization of α -Aminoalkyl Radicals.”

Conferences Contributions

- Grübel, M.; Bach, T.; Hess, C. R. 26th Lecture Conference on Photochemistry **2018**, München Germany. “*New Nickel-Mabiq Compounds: Synthesis, Characterisation and Photochemical Properties*”; Poster
- Grübel, M.; Bosque, I.; Bach, T.; Hess, C. R. 256th ACS National Meeting and Exposition **2018**, Boston, Massachusetts, USA. “*New Nickel-Mabiq Compounds: Synthesis, Characterisation and Photochemical Properties*”; Poster
- Grübel, M.; Bach, T.; Hess, C. R. 13th National Coordination Chemistry Conference **2017**, Potsdam, Germany. “*New Nickel-Mabiq Compounds: Synthesis, Characterisation and Photochemical Properties*”; Poster
- Grübel, M.; Bach, T.; Hess, C. R. 12th National Coordination Chemistry Conference **2016**, Kiel, Germany. “*New Nickel-Mabiq Compounds: Synthesis, Characterisation and Photochemical Properties*”; Poster

Table of contents

Introduction	1
Concept behind photoredox chemistry	4
Photoredox catalysis with ruthenium or iridium based polypyridyl complexes.....	8
Net reductive reactions	8
Net oxidative reactions	10
Redox neutral reactions	12
Dual catalysis.....	15
Organocatalysis.....	15
Transition metal catalysis	17
Earth abundant photocatalysts	19
Mechanistic fundamentals	19
d ¹⁰ transition metal compounds	20
Chromium in visible light catalysis	24
Nickel complexes in photoredox catalysis	25
Scope of this work.....	27
Redox and photocatalytic properties of a Ni(II) complex with a macrocyclic biquinazoline (Mabiq) ligand.	29
Synthesis of Tetrahydroisoquinolines by Visible Light-mediated 6-exo-trig Cyclization of α-Aminoalkyl Radicals.	35
Unpublished results.....	47
Ligand modification	47
Photocatalytic studies with different metal Mabiq complexes	48
Bimetallic complexes	49

Summary and Outlook.....	50
Zusammenfassung und Ausblick.....	53
Appendix	57
Supporting Information Redox and photocatalytic properties of a Ni(II) complex with a macrocyclic biquinazoline (Mabiq) ligand.....	57
Supporting Information Synthesis of Tetrahydroisoquinolines by Visible Light-mediated 6-exo-trig Cyclization of α -Aminoalkyl Radicals	142
Bimetallic Nickel Mabiq complex.....	276
Synthesis of [NiNi(Mabiq)(Xanthphos)]OTf.....	276
Reprint permissions	279
Redox and photocatalytic properties of a Ni(II) complex with a macrocyclic biquinazoline (Mabiq) ligand.....	279
Synthesis of Tetrahydroisoquinolines by Visible Light-mediated 6-exo-trig Cyclization of α -Aminoalkyl Radicals.	280
References	285

Introduction

Light is the origin of all life on earth. Without light, there would be no photosynthesis, no conversion of solar energy to chemical energy performed in green plants. This seemingly simple process affects our daily life by maintaining the oxygen level in earth's atmosphere and is necessary for our food production. From a molecular perspective, the process of photosynthesis always begins when energy in the form of light is absorbed by enzymes that contain chlorophyll. These natural occurring pigments enjoyed keen interest from scientists in the early decades of the 20th century and peaked in 1915, when *Richard Willstätter* was awarded the *Nobel* prize for his studies on the structure of plant pigments including chlorophyll.^[1,2] Investigations, among others, *Hans Fischer* and later *Ian Fleming*, revealed the structural composition of chlorophyll and reported a metal complex bearing a magnesium central atom and a highly functionalized porphyrinogen ligand structure.^[3,4] The unique structure of the chlorophyll molecules provides the ability to absorb photons of light. Within the pigment molecules, the absorbed light energy excites electrons to higher states which will then trigger a variety of chemical processes such as the reduction of NADP to NADPH, the synthesis of carbohydrate molecules as chemical energy storage, and the splitting of water to produce oxygen.^[5] Chlorophyll can be described as a photosensitizer responsible for light harvesting and energy conversion in the plant cells.

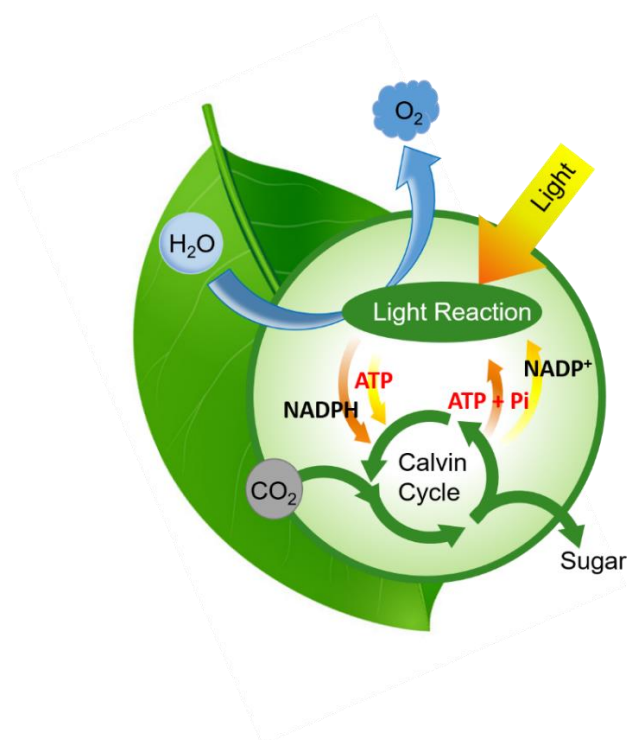


Figure 1: Processes inside a plant cell triggered by sunlight excitation involving water splitting, CO₂ conversion to carbohydrates, and electron transfer processes based on textbook depictions.

As there is a rapidly growing demand for more 'green' energy resources in today's society, one promising approach now is to use the principle of artificial photosynthesis in modern chemical industry and to thereby overcome the need for fossil fuels. The aim would be to generate solar fuels via artificial photosynthesis similar to natural photosynthesis. This would simultaneously solve the problem of CO₂ pollution and establish the idea to use the power of sunlight for chemical transformations. Nature provides examples for light-harvesting, electron transfer reactions or the machinery for solar energy conversion, which are optimized during millions of years.^[6] Light can be considered as an ideal reagent for environmentally friendly, 'green' chemical synthesis; unlike many conventional reagents, light is non-toxic, generates no waste, and can be obtained from renewable sources.

Gicomo Ciamician, an Italian chemist from Bologna already anticipated a major revolution in the chemical industry in 1912. He envisioned future chemical plants without fossil fuels such as coal or oil, but with implementation of nature's inventions to harvest the energy provided by the sun by technical photochemistry devices.^[7] He was the pioneer of artificial photosynthesis and the father of modern photochemistry. The increasing number of publications concerning photochemistry underlines that *Ciamician* had a crucial impact on today's chemical society and the realization of this concept.

A fundamental obstacle which limits the application of artificial photochemical reactions is the inability of most organic molecules to absorb light in the visible wavelength region.^[8] Photochemical activation often utilizes artificial UV light of higher energy, which is not abundant in the visible light solar spectrum. Nature has developed highly complex light harvesting systems to utilize the distinct wavelength regions. In order to overcome this impediment of most organic molecules and to perform photochemical reactions under visible light conditions, the use of strongly absorbing transition metal complexes as light harvesting compounds was investigated.^[9-11] Ru(bpy)₃²⁺, the best-known and most extensively studied representative of this kind of transition metal complexes is capable of transferring energy to an appropriate organic molecule or serving as a reductant after excitation with visible light.^[10,12-16] Generally, ruthenium or iridium polypyridyl complexes were extensively applied in artificial photosynthesis reactions, converting solar energy either directly into electricity or using the electrochemical potential of the excited states in water splitting or CO₂ reduction, organic light-emitting diodes or dye-sensitized solar cells.^[15,17-19] In the early 2000s, only a few examples were known for applications of transition metal complexes used as photosensitizers in synthetic organic chemistry.^[20,21] The utilization of photosensitizers such as the already mentioned transition metal polypyridyl complexes or fully organic dyes, together with visible

light radiation, marked the breakthrough for photoredox chemistry in synthetic organic chemistry. Starting around 2008, the number of publications on photoredox chemistry increased drastically as depicted in Figure 2.

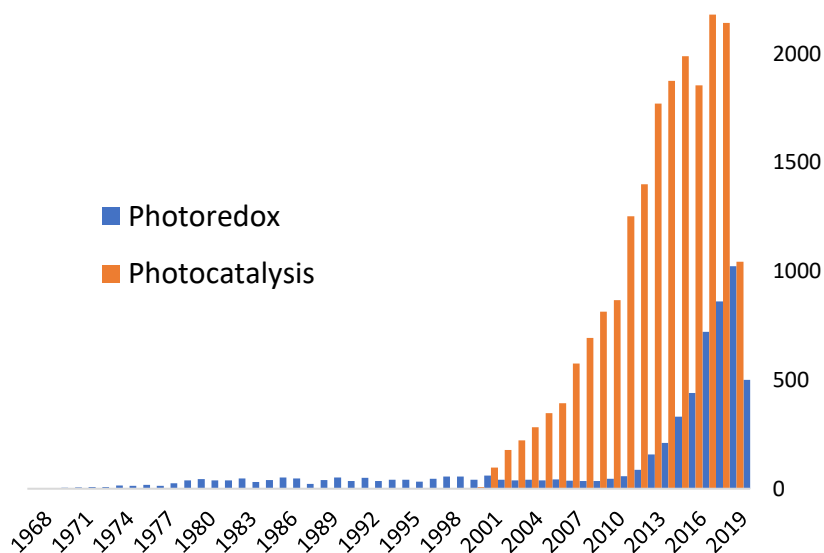


Figure 2: Number of publications per year. Orange: using the keyword “photocatalysis”, Blue: using the keyword “photoredox”. Scifinder search conducted 22.05.2019.

Outstanding solutions for different synthetic problems using visible light photoredox catalysis, were independently reported by *MacMillan*, *Yoon* and *Stephenson*. They are regarded as the main initiators who started the avalanche of the, nowadays integral, chemical research field of photoredox catalysis.^[22–24]

Concept behind photoredox chemistry

In general, the concept of photoredox chemistry is based on the ability of a metal complex or an organic dye to participate in a single-electron transfer (SET) reaction with an appropriate organic molecule upon excitation with visible light.^[25–30] Prior to 2008, the term to describe this process was photoinduced electron transfer. Especially in terms of ‘green’ chemistry, the use of photoredox catalysts under mild reaction conditions (use of visible light and at ambient temperature) offers an attractive alternative to more traditional systems, e.g. samarium diiodide in organic reduction reactions.^[31]

In contrast to the variety of literature-known examples using $\text{Ru}(\text{bpy})_3^{2+}$ as photocatalyst in organic transformations there is no “all-time-use” photocatalyst. The ideal photocatalyst for a specific reaction is determined by the kinetics and thermodynamics of the desired organic reaction system.^[27,32] In the following chapter $\text{Ru}(\text{bpy})_3^{2+}$ is employed as a model system to explain the photophysical properties required as well as the mechanistical fundamentals of transition metal photoredox chemistry. It has to be noted that the following description could be applied to most transition metal polypyridyl complexes.^[32]

The mechanism of photoinduced electron transfer in iridium or ruthenium based transition metal polypyridyl complexes, as well as in earth-abundant photocatalysts (based on e.g. copper), is discussed in further in-depth analysis. Complexes of second and third row d^6 transition metal ions such as Ru(II), Re(I) or Ir(III), have low spin ground states ($S = 0$) when coordinated to ligands with a strong ligand field (e.g. 2,2'-bipyridine, carbon monoxide).^[33] Polypyridyl scaffolds and their derivatives are established ligands in these complexes, and they are characterized by their σ donor orbitals at the nitrogen atoms as well as π donor and π^* acceptor orbitals, which are delocalized in the aromatic ring system.^[29,33,34] The photocatalytic process can be divided into three key steps: light absorption, MLCT (metal-to-ligand charge transfer) and the quenching process (electron transfer) (all processes are depicted in a *Jablonski* diagram^[35] in Figure 4). In the first step, upon irradiation and light absorption, three different electronic transitions are possible. The excitation of an electron is assigned to a ligand-centered transition ($\pi_L \rightarrow \pi_L^*$; LC).^[36] The second are transitions, most likely due to ligand-field transitions within the d-orbital manifold of the metal (d-d transition; MC = metal centered) (Figure 4 left).^[32] The contribution of those transitions to the excited state population are still under debate, since no distinct assignment is possible due to the overlap with ligand-centered and MLCT (metal to ligand charge transfer) transitions in the electronic spectra. On the other hand metal-to-ligand charge transfer events are known to be involved in the formation of the

excited state and describe the excitation of an electron from a d-orbital (t_{2g} -orbital) of the metal to the low lying π^* orbitals of the polypyridyl ligand framework ($PC^* {}^1MLCT_n$).^[25,27,32,33,37] This electronic transition is responsible for the enhanced redox activity of the excited state. After relaxation to the lowest spin-allowed singlet state ($PC^* {}^1MLCT_1$), intersystem crossing (ISC) occurs, which seems to be accelerated in the presence of a heavy metal atom in the complex (spin-orbit coupling).^[14]

Internal conversion (IC) leads to the formation of a long-lived triplet excited state ($PC^* {}^3MLCT$) (Figure 4 right).^[38] As a result, fluorescence or non-radiative relaxation from the singlet state ($PC^* {}^1MLCT_1$) are minor deactivation modes. Since the excited state properties depend on the energy level of the π^* orbital, it is possible to fine-tune the photophysical properties of the catalyst by modifications of the ligands.^[10,18,27,32,33,37]

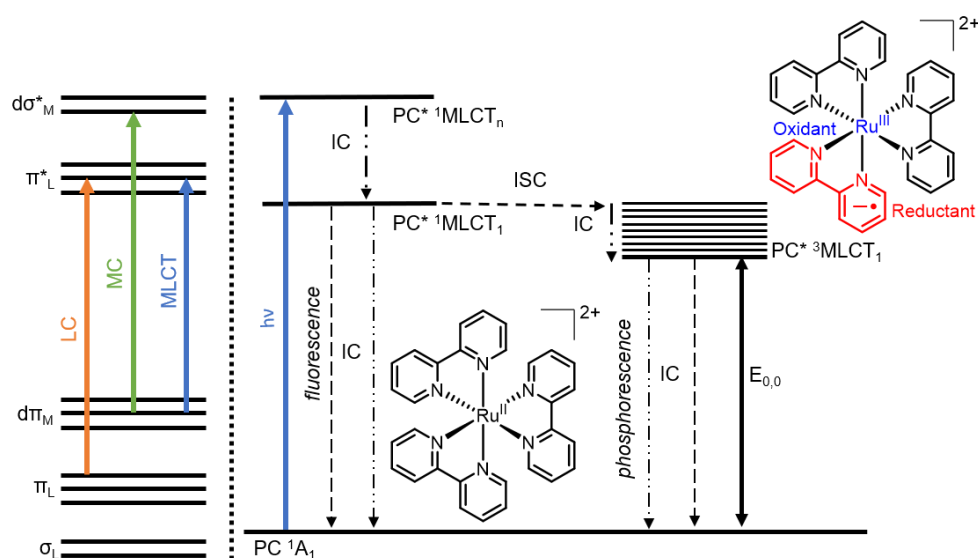


Figure 3: Left: simplified molecular orbital diagram for an octahedral complex with π -acceptor ligands; LC: ligand-centered transition, MC: metal-centered ligand-field transition, MLCT: metal-centered ligand charge transfer. Right: simplified Jablonski diagram; PC: photocatalyst, IC: internal conversion, ISC: intersystem crossing.

The energetically lowest lying triplet state ($PC^* {}^3MLCT_1$) can subsequently interact with other molecules that themselves are not able to absorb visible light, if the half-life of the photoexcited state is long enough to undergo bimolecular chemical reactions.^[32,37] Consequently, a quenching process of the excited state *via* electron transfer in an oxidative or reductive manner takes place.

A general mechanistic picture that describes the reductive and oxidative quenching cycle is depicted in Figure 5. In the term of ‘reductive quenching’, the photocatalyst reacts as an oxidant [$E_{1/2} (Ru^{II^*}/Ru^I) = + 0.77$ vs. SCE] from the triplet hypersurface by transferring an electron from the respective substrate or donor molecule into the t_{2g} -orbital of the metal complex.

Energetically the redox potential of donor molecules must be lower than the excited state redox potential of the photocatalyst to enable a SET. The resulting reduced Ru(I) complex, which is a strong reductant in the ground state [$E_{1/2}(\text{Ru}^{\text{II}}/\text{Ru}^{\text{I}}) = -1.33$ vs. SCE], transfers this electron to an appropriate substrate or acceptor molecule; the ground state of the photocatalyst is thereby restored.

The ‘oxidative quenching’ pathway includes the donation of an electron from the excited photocatalyst to a substrate (oxidative quencher). Hence, the excited photocatalyst acts as a strong reductant [$E_{1/2}(\text{Ru}^{\text{III}}/\text{Ru}^{\text{II}*}) = -0.81$ vs. SCE]. In this case, the redox potential of a suitable electron acceptors must be more positive than the excited state potential of the photocatalyst. The resulting Ru(III) complex, which is a strong oxidant [$E_{1/2}(\text{Ru}^{\text{III}}/\text{Ru}^{\text{II}}) = +1.29$ vs. SCE] in the ground state reacts with a sacrificial donor such as triethylamine to furnish the photocatalyst back in the ground state.^[25,27,32,37]

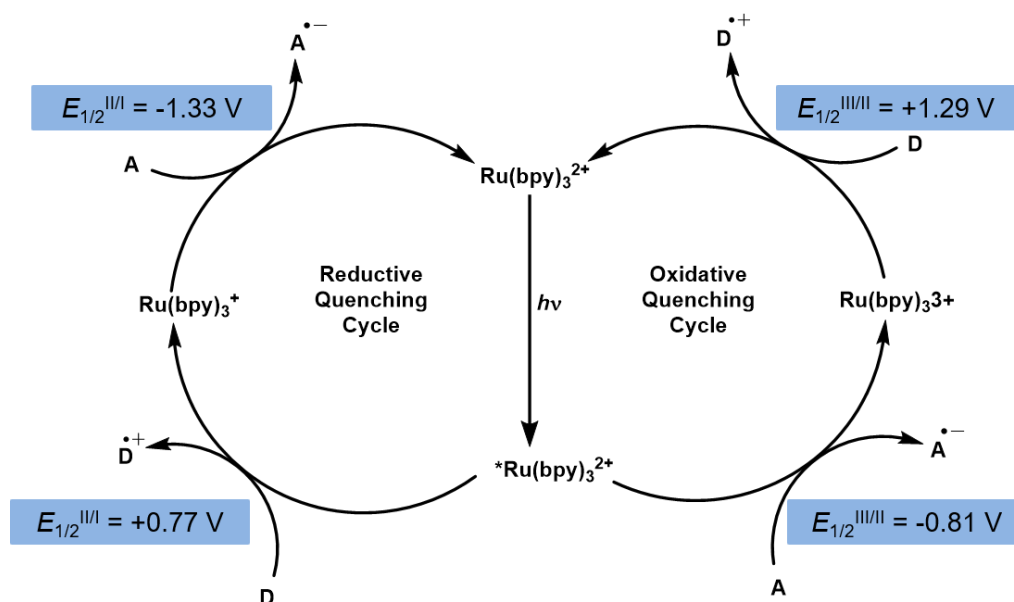


Figure 4: Photoredox catalysis with visible light: oxidative and reductive quenching cycles, A = electron acceptor, D = electron donor.

The excited state of the photocatalyst has a vacancy in a predominantly metal-centred orbital and a high-energy electron in a ligand-centred orbital, which implies that the photocatalyst simultaneously has oxidizing and reducing properties. Accordingly, an energetically higher excited state will therefore increase the redox strength of the photocatalyst, regardless of whether it acts as an oxidizing or reducing agent. Redox strength can be explained with how easily an electron can be transferred to the respective acceptors or donors. Increasing electron density at the metal centre through ligand design in general, therefore increases the reductive power of the complex and on the other hand reduces the oxidative power of the photocatalyst.

Also, the modulation of the ligand design or the change of symmetry at the ligand and the complex structure have a great impact on the photophysical and redox properties of the photocatalyst.^[10,18,37]

Some relevant representatives of iridium or ruthenium polypyridyl photoredox catalysts with different ligand structures and photophysical and redox properties are depicted in Figure 6. Further photophysical and redox properties of the depicted catalysts are noted in the literature.^[37,39–41]

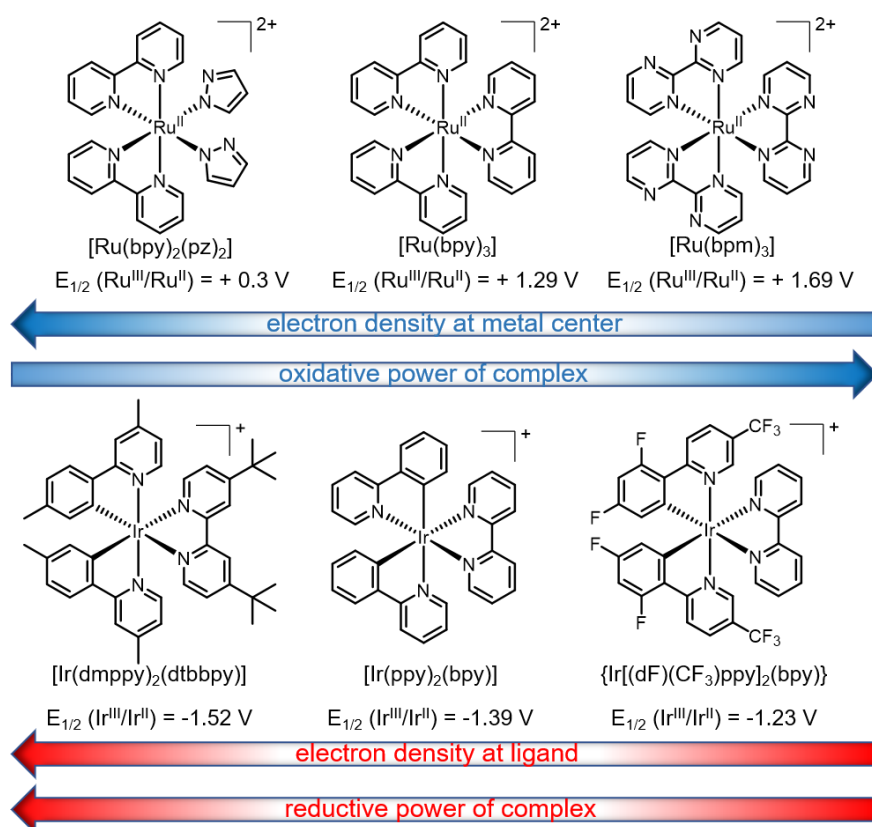


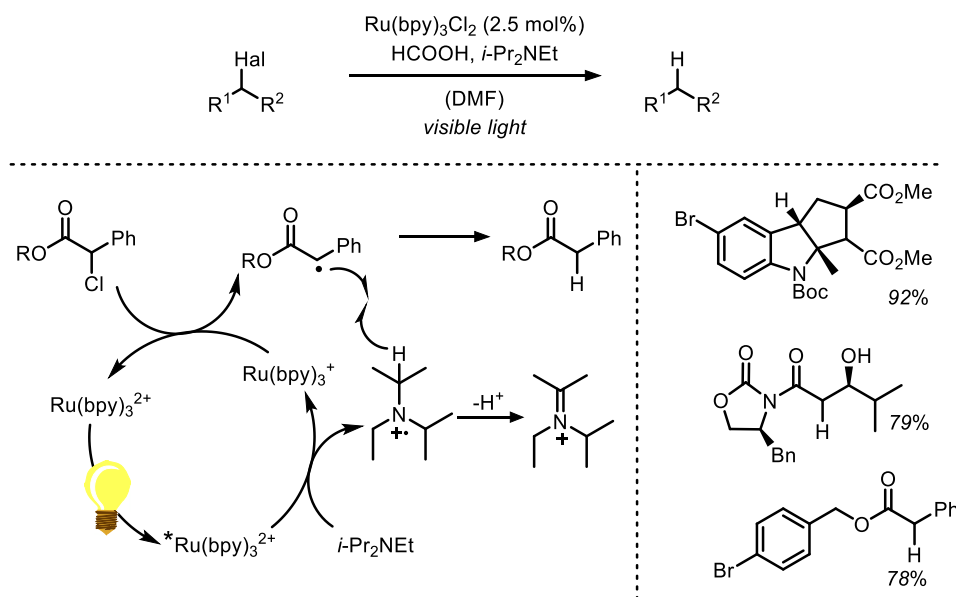
Figure 5: Common ruthenium or iridium based polypyridyl photocatalysts and effect of ligand on their ground state redox potential. All depicted potentials vs saturated calomel electrode (SCE). bpy: 2,2'-bipyridine, pz: pyrazole, bpm: 2,2'-bipyrimidine, dmppy: 4-methyl-2-(4-methylphenyl)pyridine, dtbbpy: 4,4'-di-tert-butyl-2,2'-dipyridine, ppy: 2-phenylpyridine, (dF)(CF₃)ppy: 2-(2',4'-difluorophenyl)-5-(trifluoromethyl)pyridine. Based on Tucker et al..^[37]

Photoredox catalysis with ruthenium or iridium based polypyridyl complexes

The reactive intermediates primarily formed in photoredox reactions, obtained by either oxidative or reductive quenching, are radical ions. Their further transformations are very valuable due to their *Umpolung* character. However, radical ions mostly undergo a subsequent chemical transformation to either radicals (loss of e.g. proton) or ions (ensuing electron transfer) quite fast. These secondarily formed radicals or ions are often key intermediates in subsequent chemical reactions. Photoredox reactions can be distinguished concerning different reaction pathways e.g. oxidative and reductive quenching. In the following section the pathways are displayed by one of each major breakthrough example reported in literature. Additionally, the topics of redoxneutral and dual photoredox (organophotoredox and metallaphotoredox) catalysis are elaborated due to the high importance and perspective in organic synthesis.

Net reductive reactions

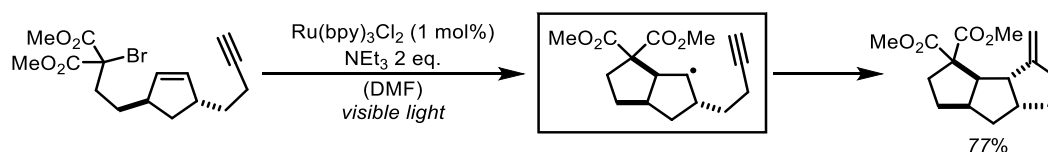
A sacrificial electron donor is necessary to serve as the stoichiometric reductant, if the reaction follows the reductive quenching pathway. In 1981, the group of *Pac* published an example utilizing 1-benzyl-1,4-dihydronicotinamide (BNAH) as stoichiometric reductant mimicking the biological reductant 1,4-dihydronicotinamide adenine dinucleotide (NADH). It was applied in a $\text{Ru}(\text{bpy})_3^{2+}$ catalyzed reduction of electron poor alkenes mediated by visible light irradiation.^[42] Besides previous reports on photoredox catalysis, the selective dehalogenation reaction published by the *Stephenson* group in 2009 is considered to be one of the major breakthrough reactions for photoredox chemistry.^[24] Scheme 1 depicts *Stephenson's* photoredox reductive dehalogenation as an explanatory example for all reactions that follow the reductive quenching cycle.



Scheme 1: Reductive dehalogenation using visible light photoredox chemistry, $\text{Ru}(\text{bpy})_3^{2+}$ as photocatalyst and an amine as the hydrogen atom source. Top: general reaction equation. Bottom left: mechanistic background; bottom right: selected products.^[24]

The reaction follows the reductive quenching pathway. The excited $\text{Ru}(\text{bpy})_3^{2+}$ [$E_{1/2}(\text{Ru}^{\text{II}*}/\text{Ru}^{\text{I}}) = +0.77 \text{ V vs. SCE}$] is quenched by SET from the stoichiometrically employed tertiary amine *Hünig's* base (*i*- Pr_2NEt) [$E_{\text{ox}}(\text{i-Pr}_2\text{NEt}^+/\text{i-Pr}_2\text{NEt}) = +0.60 \text{ V vs. SCE}$].^[43] The aminium radical cation and the Ru(I) species $\text{Ru}(\text{bpy})_3^+$ are generated, the latter species may reduce the α -chloroester to the corresponding α -carbonyl radical. After the single-electron oxidation of the amine, the bond strength of the α -C-H bond is significantly weakened, and the hydrogen atom can be transferred to the α -carbonyl radical, furnishing the dehalogenated product and an iminium ion. The addition of formic acid or a *Hantzsch* ester supports the hydrogen abstraction by a preformed ammonium formate complex. Deuterium labelling experiments proved, that the amine is most likely the cofactor which is delivering the hydrogen atom to the α -carbonyl radical. A huge advantage of this methodology is the superior chemoselectivity and the non-toxicity compared to traditional radical chemistry. The limitation of this dehalogenation protocol, namely the necessity of activated halides as substrates, was overcome by the utilization of photocatalysts with excited state oxidation potentials such as *fac*- $\text{Ir}(\text{ppy})_3$ [$E_{1/2}(\text{Ir}^{\text{IV}}/\text{Ir}^{\text{III}*}) = -1.73 \text{ V vs. SCE}$].^[44] Besides this major breakthrough, different functional group manipulations are possible, e.g. dehalogenation of *vic*-dibromides using NADPH or viologen in combination with photoredox catalysis.^[45,46] Another early example for an application of net reductive photoredox catalysis is the reductive cleavage of sulfonium and sulfonyl groups by 1,4-dihydropyridines as sacrificial electron donors.^[20,47] The reduction of nitrogen containing functional groups was accomplished by the groups of *Hirao* and *Liu*. They were able to reduce nitrobenzenes to aniline derivatives utilizing $\text{Ru}(\text{bpy})_3^{2+}$ as photocatalyst

and hydrazine as stoichiometric reductant and succeeded in the reduction of azides to amines using a catalytic system comprising $\text{Ru}(\text{bpy})_3^{2+}$, *Hünig's* base and *Hantzsch* ester.^[48,49]

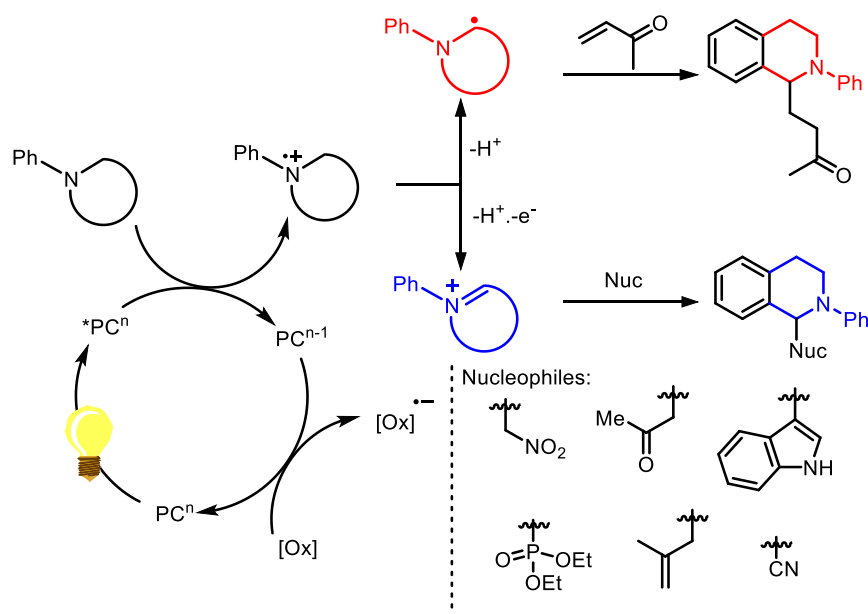


Scheme 2: Cascade photoredox cyclization reaction using NEt_3 as stoichiometric reductant.^[50]

All reaction types mentioned above enable only a single functional group modification. Furthermore, the utilization of radicals generated via photoredox catalysis in chemical reactions exhibits a great potential for building up molecular complexity. *Stephenson* successfully exploited the reactivity of the intermediary generated radical in a cascade cyclization reaction (Scheme 2).^[51] Analogous to the reductive dehalogenation, the ruthenium complex undergoes the reductive quenching cycle to generate the $\text{Ru}(\text{I})$ complex, which then reduces the alkyl halide to the reactive alkyl radicals. In a cyclization reaction, this radical adds to a tethered alkene or alkyne linker. Lastly, the hydrogen is abstracted, most likely from the amine, and furnishes the product. This protocol can also be applied in the cyclization of indoles or pyrroles^[52] or in a cascade reaction resulting in a tricyclic product as shown in Scheme 2.^[51]

Net oxidative reactions

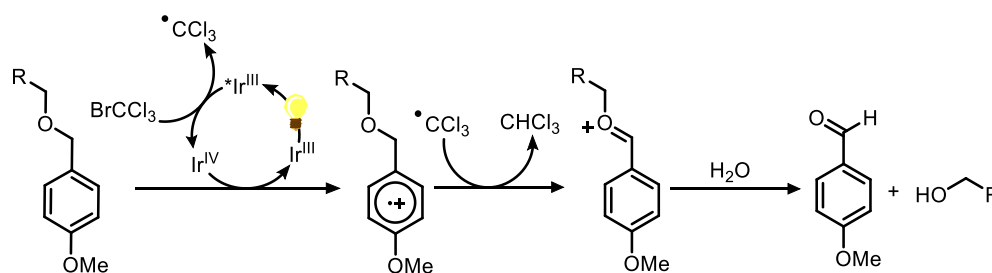
In a net oxidative photoredox reaction, stoichiometric amounts of an electron acceptor as the oxidant are necessary to close the catalytic cycle. Most of the previously described photoredox catalyzed reactions utilized a tertiary amine such as *Hünig's* base or triethylamine (NEt_3) as a reductive quencher. After oxidation, the corresponding trialkylammonium radical proved to be easily oxidizable to the iminium (scheme 3, blue) ion, which can further be attacked by nucleophiles.^[24] Another possible pathway originates from the loss of a proton and consecutive generation of the reactive α -aminoalkyl radical (scheme 3, red). This radical can add to different electron deficient alkenes (*Michael* acceptors).^[53–55] An explanatory catalytic cycle and the two generated key intermediates [α -aminoalkyl radical (red) and iminium ion (blue)] are depicted in scheme 3.



Scheme 3: Example for an oxidative photoredox catalytic cycle; Generation of a dialkylarylammonium radical and subsequent formation of either the α -aminoalkyl radical and addition to *Michael* acceptors (top) or the generation of iminium ions and the addition of various nucleophiles such as nitromethane, indoles, phosphates, enols (bottom right). PC: ruthenium or iridium based photocatalyst; [Ox]: O_2 , $BrCCl_3$, $(NH_4)_2S_2O_8$.

Early work on the single-electron oxidation pathway was performed by *Cano-Yelo* and *Deronzier* who examined the photoredox catalysed oxidation of benzylic alcohols to the corresponding aldehydes starting from aryldiazonium salts.^[56] Based on the evidence for the two key intermediates, after amine oxidation, several research groups focused on the modulation of the tertiary amine scaffolds. The *Stephenson* group reported a first example, employing photoredox conditions with the $Ir(ppy)_2(dtbbpy)PF_6$ catalyst in 2010. They investigated an oxidative *aza-Henry* reaction between nitroalkenes and tetrahydroisoquinolines (THIQ).^[57] In this reaction, the iminium ion is generated by a two electron oxidation and loss of the hydrogen atom of the tertiary amine substrate, which then reacts e.g. with nitromethane as a nucleophile. After the SET, the Ir(II) species is reoxidized by an electron transfer from ambient oxygen or other external oxidants such as bromotrichloromethane ($BrCCl_3$)^[50] or ammoniumpersulfate $[(NH_4)_2S_2O_8]$ ^[58] and the photoredox cycle is closed. Shortly after the work of *Stephenson*, the modification of the THIQ scaffold with different other nucleophiles was tested by other groups. Some examples are depicted in scheme 3.^[59–65]

As previously mentioned, the generation of the α -aminoalkyl radical from the respective tertiary amine is also possible by the abstraction of a proton from the trialkylammonium radical. The access to α -aminoalkyl radicals by photoinduced single-electron oxidation of amines was already established in previous reports.^[66–68] One of the first examples for a transition metal photoredox catalyzed reaction to α -aminoalkyl radicals and the subsequent addition to *Michael* acceptors such as methyl vinyl ketones was reported by the group of *Reiser*.^[53] Here, both $\text{Ru}(\text{bpy})_2\text{Cl}_2$ and $[\text{Ir}(\text{ppy})_2(\text{dtbbpy})]\text{PF}_6$ proved to be suitable for the reaction. However, it was demonstrated that the addition of Brønsted acids accelerates the carbon-carbon bond formation step, increasing the yield from 60% to 90%.^[55]



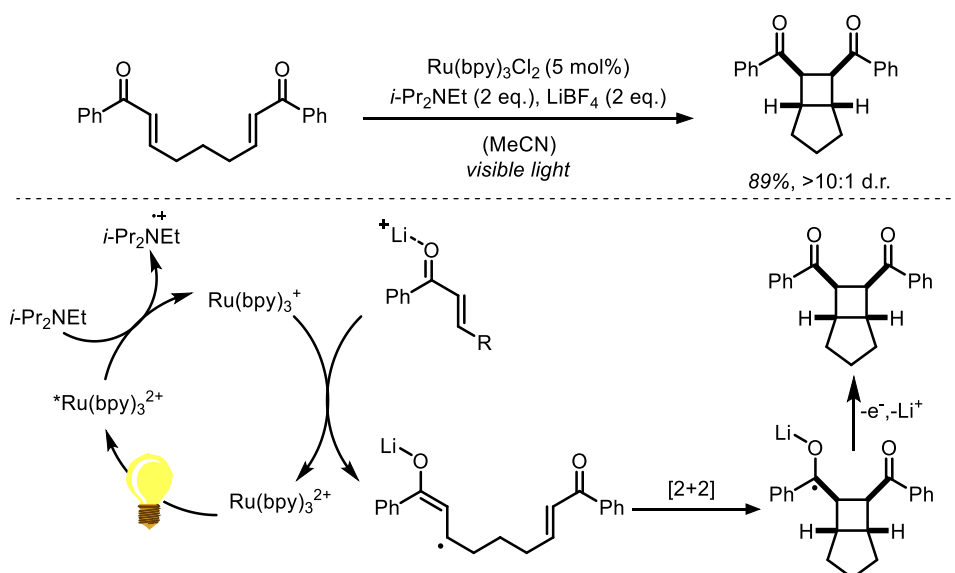
Scheme 4: Mechanistic proposal of the oxidative photoredox catalyzed cleavage of PMB ethers.

The iridium catalyzed oxidative photoredox deprotection of *para*-methoxybenzylethers (PMB) is another achievement of the *Stephenson* group.^[50] After photoexcitation, the iridium photocatalyst $[\text{Ir}(\text{df}(\text{CF}_3)\text{ppy})_2(\text{dtbbpy})]\text{PF}_6$ [$\text{df}(\text{CF}_3)\text{ppy}$ = 2-(2,4-difluorophenyl)-5-trifluoromethylpyridine], with a redox potential in the excited state of $[E_{1/2}(\text{Ir}^{\text{IV}}/\text{Ir}^{\text{III}*}) = -0.89$ V vs. SCE] is able to transfer an electron to BrCCl_3 . In addition, the resulting Ir(IV) species, as a strong oxidant [$E_{1/2}(\text{Ir}^{\text{IV}}/\text{Ir}^{\text{III}}) = +1.68$ V vs. SCE] performs the single-electron oxidation of electron-rich arenes. After hydrogen abstraction from the radical cation an oxocarbenium ion is generated and the final deprotected adduct is produced by subsequent hydrolysis. The full mechanistic proposal is depicted in scheme 4.

Redox neutral reactions

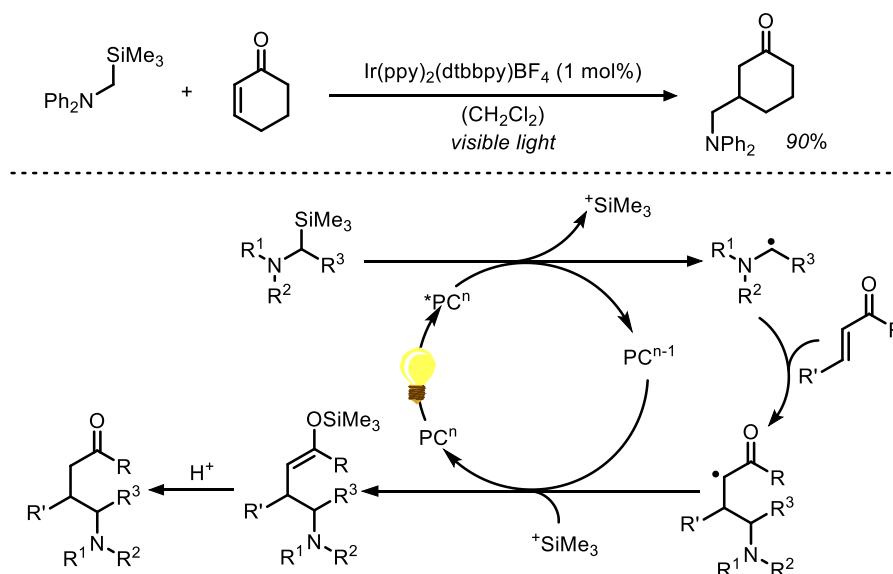
In contrast to the previously described reactions following the oxidative or reductive pathways, where a stoichiometric amount of an electron donor or acceptor is necessary to close the catalytic cycle, in a redox neutral photoredox reaction, the substrate itself undergoes both a single-electron oxidation and a single-electron reduction. The earliest example for a redox neutral reaction is the *Pschorr* reaction, investigated by *Cano-Yelo* and *Deronzier*. They established an intramolecular coupling of aryldiazonium salts with unsubstituted arenes.^[21,69] One of the first examples for modern visible light catalysed photoredox chemistry was reported by the group of *Yoon* in 2008,^[22] with the first example for a [2+2] photocycloaddition under

visible light photoredox conditions. Herein, $\text{Ru}(\text{bpy})_3^{2+}$ as the photocatalyst initiates the photocyclization of bis(enones) to cyclobutene adducts. For the first reduction step of the excited photocatalyst, *Hünig's* base needs to be present to undergo reductive quenching. The addition of a *Lewis* acid is essential for the activation of the enone towards the electron reduction by $\text{Ru}(\text{bpy})_3^+$. The [2+2] photocycloaddition of the lithium-bound radical anion results a ketyl radical which is further oxidized to the cyclobutene photoproduct. This oxidation may conceivably be performed by either the excited state of the photocatalyst [$^*\text{Ru}(\text{bpy})_3^{2+}$], the amine or a second *Lewis* acid-activated substrate molecule. To recapture the individual steps of a redox neutral reaction: the substrate itself does not change its oxidation state. On the one hand it accepts an electron, undergoes bond rearrangement and then donates an electron to an electron acceptor to turn over the catalytic cycle (scheme 5).



Scheme 5: Redox neutral photoredox enone [2+2] photocycloaddition established by *Yoon*. Bottom: Explanatory mechanistical proposal for this type of photocycloaddition reactions.

Besides his first encounter with this kind of photoredox catalysed photocycloadditions, *Yoon* also established [2+2] photocycloadditions of electron-rich bis(styrenes),^[70] an intermolecular [2+2] photocycloaddition reaction,^[71] and Diels-Alder reactions^[72,73] following the same mechanistical pathways.



Scheme 6: Reaction of α -silylamines with α,β -unsaturated compounds. Bottom: mechanistic proposal for generation of β -aminoalkyl radical and subsequent reaction with electron poor alkenes. PC: photocatalyst.

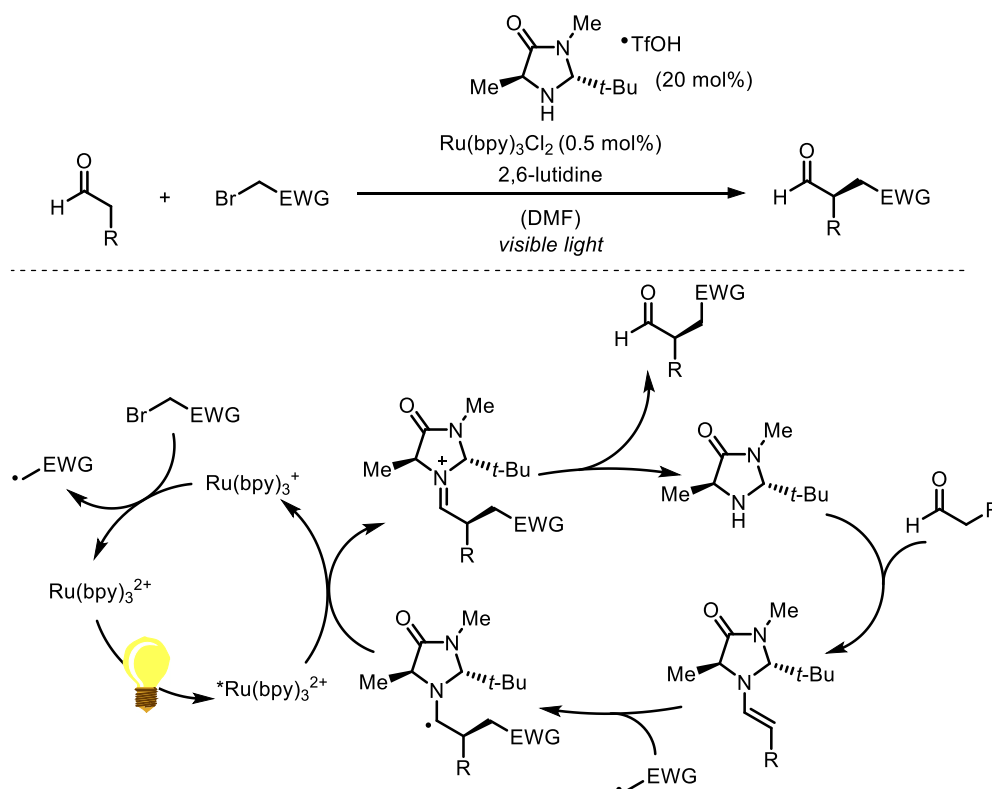
The group of *Nishibayashi* succeeded in the synthetic application of α -aminoalkyl radicals generated from tertiary α -silylamines and their subsequent addition to α,β -unsaturated carbonyl compounds.^[74] The α -aminoalkyl radicals are generated under photoredox conditions by dissociation of the C-Si bond. The SET from the excited state of the photocatalyst to the α -silylamine initiates this process. After the addition of the α -aminoalkyl radical to the *Michael* system, a SET from the photocatalyst reduces the ketyl radical, thereby closing the catalytic cycle. The trimethylsilyl (TMS) cation captures the enol and the silyl enol ether is hydrolyzed to the respective photoproduct. The strategy, to exploit the properties of the TMS cation as a ‘super proton’ and simultaneously good leaving group, consequentially giving easy access to carbon centered nucleophilic radicals, was applied by several other research groups.^[67,75–78] Photoredox catalysis offers a mild alternative for the generation of radical intermediates from carboxylic acids. This method can be employed for the radically initiated decarboxylation of α -amino acids and α -oxo acids.^[79,80] The generated radical intermediates generated can undergo coupling reactions to cyano-substituted aromatic compounds as shown by *MacMillan*.^[81] Further functional groups which readily leave the substrate molecule upon SET and generating carbon centered radicals are discussed later.

Dual catalysis

The term 'dual catalysis' describes a catalytic system with two intertwining catalytic cycles. With regard to photoredox catalysis, one catalytic cycle is visible light mediated. The second cycle can include organocatalysis or transition metal catalysis. In dual catalytic systems, the characteristic of photoredox catalysis, having both an oxidant and a reductant present significantly enhances the turnover of the interdependent catalytic cycles. The modulation of the oxidation states of transiently generated intermediates is highly dependent on this ability. First, the field of photoredox catalysis combined with organocatalysis is described.

Organocatalysis

So far only a few examples of photoredox catalysis induced enantioselective bond formation reactions are reported. One of the first reports on enantioselective photoredox reactions is dated back to the *MacMillan* group in 2008. They accomplished the merger between photoredox catalysis with enamine organocatalysis to perform enantioselective α -alkylation of aldehydes.^[23] In enamine catalysis, the α -position of a carbonyl compound is activated for further electrophilic functionalisation by the formation of an enamine with a secondary amine. The secondary amine such as an imidazolidinone serves as chiral catalyst to induce enantioselectivity.^[82,83] In the reaction of *MacMillan*, $\text{Ru}(\text{bpy})_3^{2+}$ was employed as photocatalyst, a chiral imidazolidinone is used as chiral secondary amine in catalytic amounts and electron deficient alkyl bromides and alkyl aldehydes were used as substrates (scheme 7).



Scheme 7: Dual catalysis approach of *Nicewicz* and *MacMillan* using a chiral imidazolidinone organocatalyst in an asymmetric α -alkylation of aldehydes under photoredox condition.

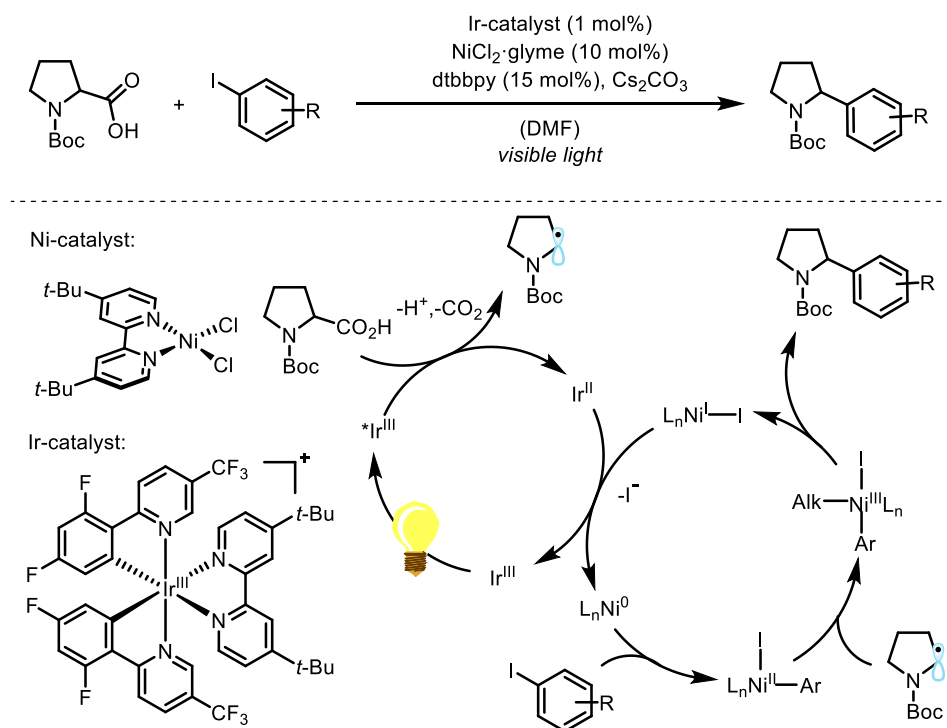
The reaction is initiated by a reductive quench of the excited $*\text{Ru}(\text{bpy})_3^{2+}$ by a sacrificial enamine molecule, providing the strong reductant $\text{Ru}(\text{bpy})_3^+$. Single-electron transfer to the alkyl bromide induces fragmentation to a bromide and an electron deficient radical. The chiral enamine is generated by the condensation of the aldehyde with the chiral imidazolidinone. The following addition of the photogenerated electrophilic radical to the enamine occurs in a stereocontrolled fashion and proceeds exclusively from the *Si* face. SET between the α -amino radical and the excited $*\text{Ru}(\text{bpy})_3^{2+}$ furnishes the iminium ion and the strongly reducing $\text{Ru}(\text{bpy})_3^+$. Hydrolysis of the iminium ion releases the product and regenerates the organocatalyst. The mechanistic proposal was supported with *Stern-Volmer* studies.^[23] After these initial results several other asymmetric α -functionalizations were investigated e.g. trifluoromethylation, benzylation, cyanoalkylation and amination.^[84-87]

Besides this example of photoredox dual catalysis using a covalent organocatalytic activation mode, there are several other reports for non-covalent interactions between transiently formed intermediates and an organocatalyst. *Ooi* reported an enantioselective *Brønsted* acid mediated photoredox catalyzed reaction,^[88] the group of *Knowles* established the proton-coupled electron transfer (PCET) mediated radical generation under visible light irradiation utilizing a dual photoredox hydrogen bonding catalyst system,^[89] and *Nicewicz* showed the broad applicability

of hydrogen atom transfer (HAT) catalysts in synthetically valuable photoredox-catalyzed organic transformations.^[90–94] For *Lewis* acid catalyzed photoredox reactions *vide supra*.

Transition metal catalysis

Transition metal catalysis has become a prominent synthetically useful tool, whose absence in organic transformations can no longer be imagined. The achievements in this field are acknowledged by the *Nobel* award for *Heck*, *Suzuki* and *Negishi*.^[95] The development of novel organometallic transformations necessitates the transition metal centre to change its oxidation state to the one required in the organic transformation. The merger of transition metal catalysis with visible light photoredox catalysis creates opportunities for the innovative design of new synthetic transformations. In recent years, this particular field of transition metal photoredox dual catalysis received outstanding attention from synthetic chemists. First reports concerning C-H arylations with aryldiazonium salts employing a photoredox palladium catalyst system demonstrated the great potential of this synergistic catalysis.^[96–98] *Molander*, *MacMillan* and *Doyle* independently provided easy solutions for synthetic problems either inaccessible or significantly challenging using traditional transition metal catalysis.^[99,100] They accomplished the merger of nickel and photoredox catalysis in a photoactivated cross-coupling reaction. While using different radical precursors, both examples share the same mechanistical background depicted in scheme 8.



Scheme 8: Dual photoredox C(sp³)-C(sp³) cross-coupling employing nickel as transition metal and a carboxylic acid as radical precursor.

In the depicted reaction the first steps include the oxidation of the carboxylic acid, employed here as a radical precursor. As described by *Molander*, *Fensterbank* or *Nishibayashi* it is also possible to use either organoborates,^[100] organosilicates,^[101,102] or 1,4-dihydropyridines^[103] as radical precursors.^[104] *Doyle* even employed unprotected amines or furanes as radical precursors in a photoredox cross-coupling reaction.^[105–107] The excited state of the Ir(III) catalyst oxidizes the radical precursor, generating a nucleophilic radical coupling partner by releasing CO₂. After oxidative addition of the Ni(0) catalyst into an aryl halide bond a Ni(II)-aryl species is formed. Subsequent addition of the carbon centred radical to the Ni(II)-aryl species results in a Ni(III) complex. Reductive elimination delivers the product. Last, the two intercepting cycles are closed by a SET from the Ir(II) species to the Ni(I) complex. After the first success Ni/Ir dual photoredox catalysis knew no boundaries in substrates and facilitated synthetical organic chemistry. Nearly every thinkable cross-coupling is currently accessible through this synergistic approach.^[108–113]

Besides nickel in photoredox dual catalysis, the use of other transition metals such as copper, gold or cobalt was also established.^[114] One of the first examples for copper in metallaphotoredox catalysis provided a mild and efficient catalyst system for cross-coupling between boronic acids and perfluoroalkyl iodides.^[115] The introduction of trifluoromethyl groups into complex molecule scaffolds such as biologically active compounds is highly desirable because of the enhanced metabolic stability of fluorinated molecules. The *MacMillan* group focused on Cu/Ir photoredox dual catalysis in C-N cross-coupling reaction of carboxylic acids with nitrogen nucleophiles.^[116] Gold photoredox dual catalysis is best represented by the groups of *Toste* and *Glorius*. Both reported synthetical protocols for arylative functionalization which typically require harsh oxidants. The broad range of gold-mediated functionalization of π -unsaturated substrates includes alkyne arylation,^[117] phosphonate arylation,^[118] ring expansion arylation^[119] or a new approach for a *Meyer-Schuster* rearrangement^[120]. Cobalt catalysts, which are commonly used in water splitting reaction or hydrogen evolution reaction were successfully applied in mild cross-coupling hydrogen evolution reactions catalyzed by a cobalt photoredox catalyst system. The cobaloxime catalyst was employed in a dual catalysis producing benzothiazoles and hydrogen gas as the only byproduct,^[121] or in a dehydrogenative decarboxyolefination of carboxylic acids^[122].

Earth abundant photocatalysts

As previously stated, the transition metal complexes most commonly used in photocatalysis are prominently based on precious and rare earth metals such as iridium or ruthenium. These metals are often rather expensive or impose significant environmental footprints due to their scarce occurrence in the earth's crust (see Figure 7).^[123] In recent years the interest in photoactive complexes utilizing less traditional but more earth abundant and cheaper first-row transition metals has grown rapidly.

Cr 1×10^{-2}	Mn 9×10^{-2}	Fe 4.7	Co 2×10^{-3}	Ni 7×10^{-3}	Cu 5×10^{-3}	Zn 0.007
Mo 1×10^{-4}	Re 1×10^{-7}	Ru 1×10^{-6}	Rh 5×10^{-7}	Pd 1×10^{-6}	Ag 7×10^{-6}	
W 6×10^{-4}		Os 5×10^{-7}	Ir 1×10^{-7}	Pt 1×10^{-6}	Au 4×10^{-7}	

Figure 6: Abundance in earth's crust of relevant chemical elements used in photoactive transition complexes. Values are given in mass percent.^[123]

Mechanistic fundamentals

As mentioned in previous sections, the photophysical properties determine the photochemistry of six-coordinated metal complexes with low-spin $4d^6$ and $5d^6$ electron configuration such as ruthenium or iridium. These metal complexes exhibit lifetimes in a microsecond time range, which favors the application in photoreactions. The sufficiently large energy gap between the electronic ground state and, the lowest lying excited state, as well as the association of molecular distortions with electronic excitation, plays a key role for photoactive compounds with long-lived excited states. Precious metal complexes display more favorable photophysics with regard to chemical applications due to their strong ligand field splitting energy and consequently long triplet $^3\text{MLCT}$ lifetimes.^[124,125] In contrast, first row transition metal complexes show exceptionally short charge-transfer lifetimes, which can be attributed to nonradiative deactivation modes through the low-lying ligand-field excited states.^[126] For $\text{Fe}(\text{bpy})_3^{2+}$, a d^6 homologue of $\text{Ru}(\text{bpy})_3^{2+}$ ($\tau = 0.63 \mu\text{s}$), a short $^3\text{MLCT}$ lifetime of $\tau = 100 \text{ fs}$ has been observed.^[127]

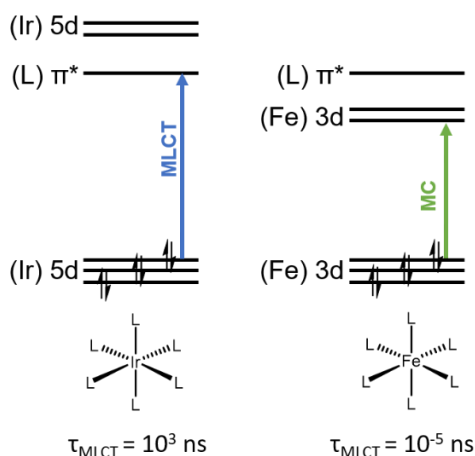


Figure 7: Schematic representation of the electronic structure in d^6 transition metal complexes e.g. Ir(III) or Fe(II) with corresponding lifetimes of excited MLCT states. Based on a report of Doyle.^[107]

For first row transition metal complexes, the non-emissive triplet metal-centered state (^3MC) and the emissive state ($^3\text{MLCT}$) are closer in energy relative to each other and less energetic compared to those of third row metal complexes (see Figure 8). As soon as a metal complex exhibits a ^3MC state which lies lower in energy than the $^3\text{MLCT}$ states, no luminescence is observed due to rapid non-emissive deactivation and poor photostability of the complexes.^[34] For heavy atoms such as 4d or 5d transition metals, an efficient intersystem crossing enhances the population of the emissive $^3\text{MLCT}$ and the subsequent slow radiative and nonradiative relaxation.^[128] Nevertheless, earth-abundant metal complexes have gained attention in the field of photochemistry. Cu(I), Cr(III) or Fe(II) complexes are well-known examples of the field.^[34,128] In the following sections, groundbreaking examples of photoactive first row transition metal complexes are discussed. The complexes displayed, exhibit unique photophysical and ground state properties e.g. excited state lifetimes, reactivity in photoredox transformations or exceptional redox properties.

d^{10} transition metal compounds

An attractive alternative to d^6 second and third row transition metals [Ru(II), Ir(III)] in photoactive complexes is represented by first row metal complexes incorporating a d^{10} electron configuration. The main advantage of these complexes is the lack of low-lying metal centered d-d transition states which could easily tend to non-emissive relaxation via thermal equilibration or energy transfer.^[129] One of the most extensively studied complexes are compounds coordinated to Cu(I), Ni(0) or Zn(II).^[34,128,130] However, due to the limited number of emissive and photo and benchstable Ni(0) compounds,^[126] and the fact, that metal-centered redox processes at Zn(II) central atoms are quite uncommon,^[34] Cu(I) complexes with redox-active ligands remain one of the largest subsets of earth-abundant photocatalysts and are therefore

discussed in detail. Luminescent zink complexes are mentioned in reviews.^[34,128] The most common oxidation states for copper in solution are +1 and +2. However, Cu(II) complexes exhibit a d^9 electron configuration and therefore have a relatively distinct metal-centered absorption which will deactivate in an ultrafast non-radiative fashion. Already in the 1970, McMillin investigated homoleptic Cu(I)-bisphenanthrolines as promising candidates for applications in photochemistry e.g. light emitting devices.^[131–134] Heteroleptic tri- or tetracoordinated complexes bearing a diimine and an additional mono or bisphosphine ligand showed promising photophysical properties as well.^[135] Besides those examples several other approaches towards photoactive Cu(I) complexes are reported.^[34,128] Here, only Cu(I) compounds coordinated by phenanthroline or phosphine ligands, as depicted in Figure 9, will be discussed.

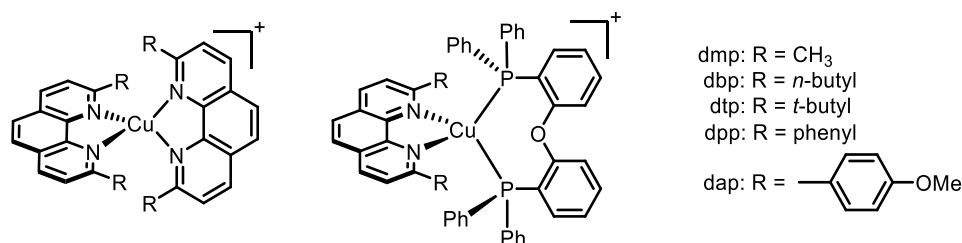
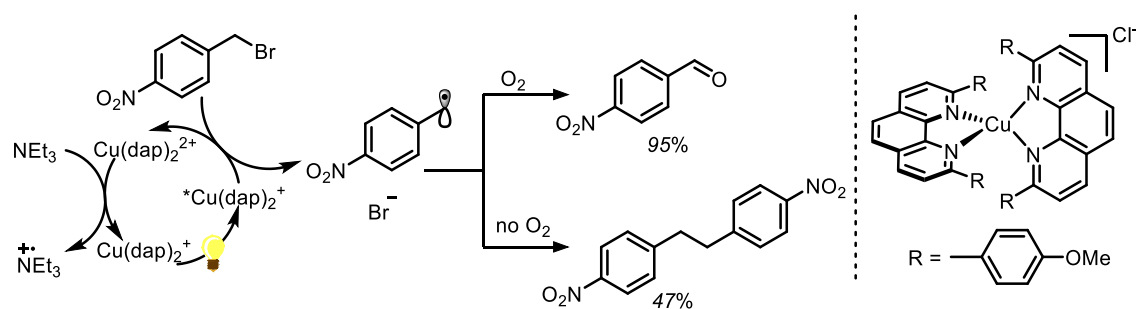


Figure 8: Main representatives for Cu(I) photocatalysts bearing ligand scaffolds with different substituents. Left: homoleptic bisphenanthroline based; right: heteroleptic Cu(I) diamine bisphosphine complexes.

Cu(I) complexes coordinated by diimine ligands are in fact the only examples for first row transition metal compounds with photophysical properties comparable to those of $\text{Ru}(\text{bpy})_3^{2+}$. The UV/Vis absorption is usually observed between $\lambda = 350\text{-}650$ nm with relatively high extinction coefficients ($\epsilon = 10^3\text{-}10^4 \text{ M}^{-1} \text{ cm}^{-1}$). In a homoleptic Cu(I) complex, substitution at the 2- and 9- position of the phenanthroline ligand increases the lifetime of the MLCT excited state to $\tau = 1 \text{ ns} - 10 \text{ }\mu\text{s}$. Heteroleptic Cu(I) complexes bearing a substituted phenanthroline and an additional POP ligand [(POP) = bis[2-(diphenylphosphino)phenyl]ether] exhibit increased lifetimes in the range $\tau = 1 \text{ }\mu\text{s}$.^[136] The advantages of the mixed-ligand POP complexes are the donor phosphine ligands and the angle of coordination of these to the metal center. Thereby, the charge-transfer excited state is elevated to higher energies which, increases the excited state lifetime.^[136]

The emission of copper(I) complexes originates from a complex synergy of phosphorescence and thermally activated delayed fluorescence (TADF).^[135,137] The main cause is the smaller spin-orbit coupling compared to 2nd and 3rd row transition metals. TADF is enhanced by the insignificantly small singlet-triplet energy gap and therefore a facile thermally activated reverse

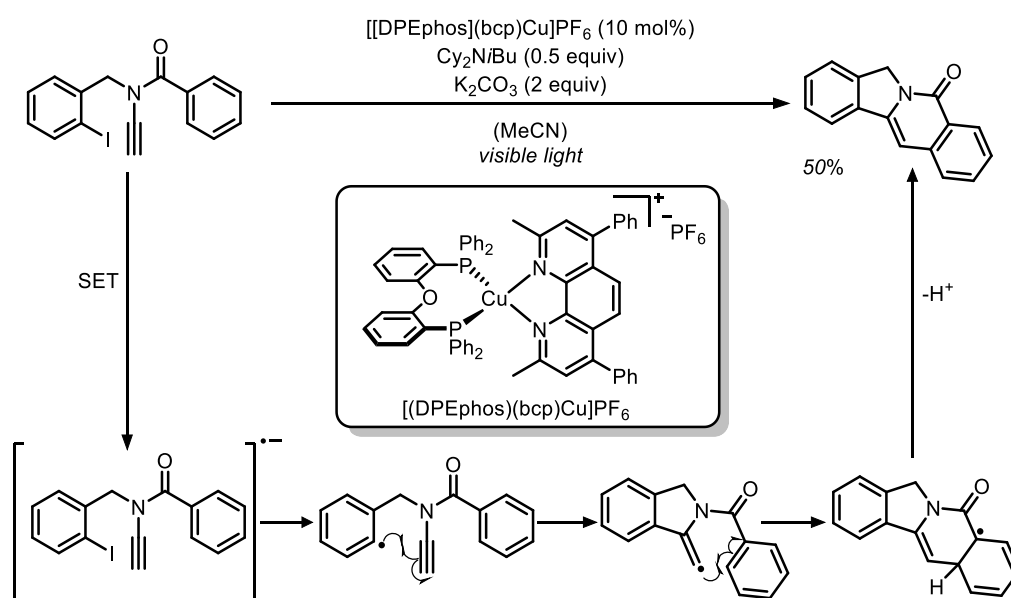
intersystem crossing (rISC). As a consequence, less energy is lost through intersystem crossing.^[34] Copper(I) exhibits a d^{10} electron configuration and therefore generally prefers a tetrahedron-like (D_{2d}) coordination sphere in the ground state (S_0). In bisdiimine coordinated complexes, both ligands are attached perpendicular to each other. In contrast to that, Cu(II) features a d^9 configuration and is situated generally in a *Jahn-Teller* distorted geometry with five or six coordination sites.^[130] As soon as the Cu(I) complex is excited, the lowest 3MLCT state is populated and consequently, the oxidation state of the central metal changes from +1 to +2. As previously mentioned, Cu(II) generally adopts a more ‘flattened’ coordination geometry leading to a ligand distortion. This flattening in the excited MLCT state results in a new open, fifth coordination site which can be attacked by nucleophiles e.g. solvent molecules. As a consequence, the lifetime of the excited state is shortened. The modulation of the ligand structure and the installation of bulky substituents such as phenyl or alkyl groups prevents this ligand distortion upon light excitation.^[129,130,137–140] Besides the application of photoactive copper complexes in organic light-emitting devices (OLED)^[135] or in the solar energy conversion of water splitting generating hydrogen,^[141] those complexes are nowadays extensively utilized in synthetic organic photoredox catalysis. *Sauvage et al.* reported in 1987 one of the first example employing the $Cu(dap)_2Cl$ [dap = 2,9-bis(*para*-anisyl)-1,10-phenanthroline] complex in a visible light driven transformation of nitrobenzyl bromides to either photodimerization products or the oxidized nitrobenzaldehydes (Scheme 9).^[142]



Scheme 9: Pioneering report of *Sauvage et al.* employing $Cu(dap)_2Cl$ visible light driven dimerization or oxidation of nitrobenzyl bromides.

After excitation, the copper catalyst is a strong reductant [$E_{1/2}(Cu^{II}/Cu^{*I}) = -1.43$ V vs. SCE]. Only *fac*- $Ir(ppy)_3$ exhibits a stronger reducing power [$E_{1/2}(Ir^{IV}/Ir^{*III}) = -1.73$ V vs. SCE]. The copper complex in its excited state transfers one electron to the benzyl bromide, leading to the formation of a benzylic radical. Depending on the reaction conditions and whether oxygen is present, a formal dimerization without oxygen or an oxidation to the corresponding benzaldehyde compounds proceeds. To close the catalytic cycle, stoichiometric reductant (triethylamine) is added and the $Cu(dap)_2^+$ ground state is regenerated. After nearly 25 years

the utilization of this complex was further elaborated by the group of *Reiser* in a visible light mediated atom transfer radical addition (ATRA) as well as allylation reactions.^[143] Other examples for $\text{Cu}(\text{dap})_2^+$ catalysed ATRA reactions include reactions between electron-deficient benzyl halides and electron rich styrenes or silyl enol ethers,^[144] trifluoromethylchlorosulfonylation of alkenes^[145] or azidation of styrenes-type double bonds^[146]. Photoredox reactions with copper photosensitizers following the reductive quenching pathway are relatively scarce due to the low redox potential of the excited state, e.g. for $\text{Cu}(\text{dap})_2^+$ [$E_{1/2}(\text{Cu}^{*\text{II}}/\text{Cu}^{\text{I}}) = +0.62 \text{ V vs. SCE}$]. Nevertheless, the group of *Evano* reported a copper-catalyzed visible light induced radical domino cyclization of ynamides and cyanamides in several natural products syntheses.^[147] The radical cascade reaction is depicted in Scheme 10.



Scheme 10: Copper catalyzed visible light induced radical cascade reaction.

Here, the catalysis follows, the reductive quenching cycle. The first step is the reduction of the photoexcited copper complex with a tertiary amine which generates a $\text{Cu}(0)$ species. In a SET from the $\text{Cu}(0)$ species to the substrate, the domino reaction is initiated by the cleaving of the halide ion, which regenerates the photocatalyst to the $\text{Cu}(\text{I})$ complex. Radical addition to the ynamide forms the first five-membered ring. Subsequent radical addition from the iminyl radical to the arene through a 6-endo-trig process results in the desired tetracyclic core structure. Finally, the product is generated by rearomatization.^[147] For other examples of copper complexes in photoredox chemistry see reports and reviews on earth-abundant photoactive metal complexes.^[32,34,128,140,148–151]

Chromium in visible light catalysis

Octahedral chromium(III) complexes with a $3d^3$ electron configuration exhibit low-lying d-d transition states with a spin-flip character. For d^3 metal complexes a spin flip occurs in the excited state from a quartet $[(t_{2g})^2(e_g)^1 \ ^4T_2]$ to a duplet $[(t_{2g})^3 \ ^2E]$ state during the intersystem crossing process. The large energy gap between quartet and duplet prevents reverse ISC resulting in exclusive population of the low energetic duplet state.^[152] This is favorable for a small molecular distortion and consequently leads to interesting photophysical properties. Two representatives for Cr(III) photoredox active complexes are the polypyridine complex $[\text{Cr}(\text{ddpd})_3]^{3+}$ (ddpd = N,N'-dimethyl-N,N'-dipyridine-2-ylpyridine-2,6-diamine) and the phenanthroline based $[\text{Cr}(\text{Ph}_2\text{phen})_3]^{3+}$ (Ph_2phen = 4,7-diphenyl-1,10-phenanthroline) which are depicted in Figure 10.

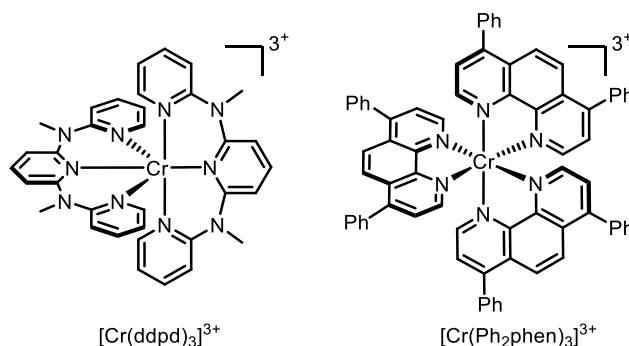
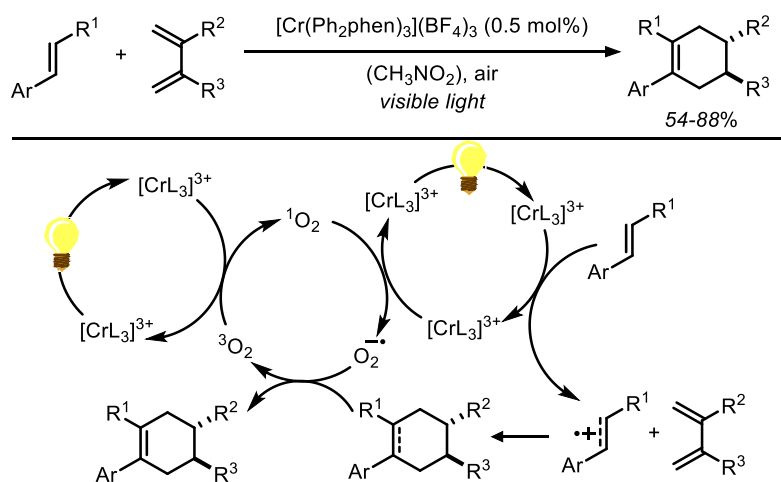


Figure 9: Photoredox active Cr(III) complexes. Left $[\text{Cr}(\text{ddpd})_3]^{3+}$ developed by *Heinze*.^[152,153] Right: $[\text{Cr}(\text{Ph}_2\text{phen})_3]^{3+}$ established by *Shores* and *Ferreira*.^[154]

The group of *Heinze* developed a molecular version of ruby by synthesizing a homoleptic Cr(III) complex with tridentate chelate ligands. Due to the nearly ideal bite angle of the ligand and its strong σ -donating properties, a very strong ligand-field splitting is observed in this Cr(III) complex. $[\text{Cr}(\text{ddpd})_3]^{3+}$ has a nearly perfect octahedral symmetry, which suppresses nonradiative relaxation. This results in a spectacular lifetime of the ${}^2E_g \rightarrow {}^4A_{2g}$ (spin-flip) luminescence of $\tau = 898 \mu\text{s}$ and a quantum yield of $\Phi = 11 \%$ in deaerated water at room temperature.^[152] *Heinze* et al. also reported the application of this complex in an oxidative C-H bond functionalization of amines by singlet oxygen.^[153] Surprisingly, only few literature reports for the application of chromium based photocatalyst in photoredox reactions are known. A report for the utilization of Cr(III) complexes in photoredox chemistry was published by *Shores* and *Ferreira*. Here the chromium catalyst $[\text{Cr}(\text{Ph}_2\text{phen})_3](\text{BF}_4)_3$, with a excited state redox potential of $[E_{1/2}(\text{Cr}^{*\text{III}}/\text{Cr}^{\text{II}}) = + 1.40 \text{ V vs. SCE}]$ was employed in a [4+2] cycloaddition reaction between electron rich styrenes and isoprenes (Scheme 11).^[154]



Scheme 11: Mechanistic proposal for the visible light chromium catalyzed photoredox *Diels-Alder* reaction.

After excitation, the excited Cr(III) complex transfers an electron to the electron-rich styrene resulting in a radical cation. Subsequent cycloaddition to isoprene yields a six-membered ring radical cation. Follow-up reduction with superoxide furnishes the desired *Diels-Alder* product. The Cr(II) species is oxidized by singlet oxygen, generated by another chromium catalyst molecule, and the photocatalyst is regenerated.^[154]

Nickel complexes in photoredox catalysis

As previously mentioned, nickel can be utilized in photoredox as a co-catalyst for visible light induced cross-coupling reactions. The use as stand-alone metal chromophore is however scarcely reported. Figure 11 presents examples for nickel based photoactive complexes which were applied in photoredox catalysis or show interesting photophysical properties.

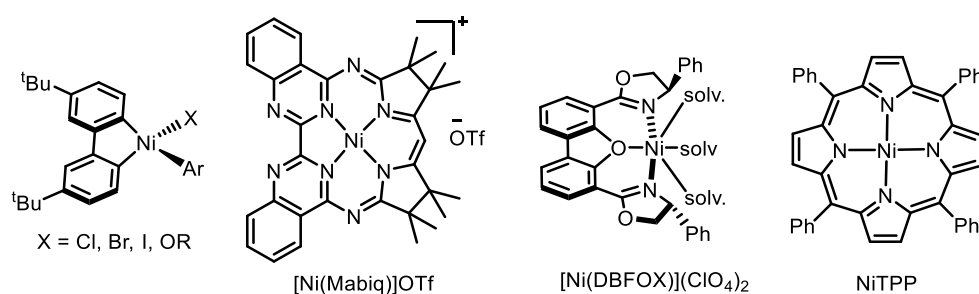


Figure 10: Ni-based photoredox catalyst. Left: Nickel catalyst reported by *Doyle*. Middleleft: Ni(Mabiq)OTf (Mabiq = [2-4:6-8-bis(3,3,4,4-tetramethyldihydropyrrolo)-10-15-(2,2'-biquinazolino)-[15]-1,3,5,8,10,14-hexaene-1,3,7,9,11,14-N₆] system developed by *Hess*). Middleright: Example for nickel photoredox catalyst employed by *Gong*. Right: NiTPP (TPP = tetraphenylporphyrin) complex developed by *Sakar*.

Nickel(II) aryl halide complexes, as reported by *Doyle*, show ³MLCT excited state lifetimes in the range of $\tau = 10$ ns. These excited states consist of both ligand centered UV and MLCT visible transitions.^[107] Additionally, it was demonstrated that the metal complex is active as photoredox catalyst in a reaction between aryl bromides and aliphatic alcohols resulting in

cross-coupled aryl species.^[107] A remarkable example for asymmetric photoredox catalysis employing nickel based complexes was reported by Gong.^[155] [Ni(DBFOX)](ClO₄)₂ (DBFOX = 4,6-bis((R)-4-phenyl-4,5-dihydrooxazol-2-yl)dibenzo[b,d]furan) was used as photoredox catalyst and the three open coordination sites were exploited for substrate-catalyst interaction to induce enantioselectivity. α,β -unsaturated carbonyl compounds were reacted with α -silylamines to yield γ -amino carboxylic acid derivatives and γ -lactam products. The photocatalyst is not only responsible for the visible light induced single electron transfer but also activates the α,β -unsaturated carbonyl substrates as *Lewis* acid and defines the radical transformation in an enantioselective fashion.^[155] Our group established a macrocyclic nickel based complex as photoredox catalyst in a cyclization reaction. We reported an estimated redox potential of the excited state of $[E_{1/2}(\text{Ni}^{*\text{II}}/\text{Ni}^{\text{I}}) = + 1.25 \text{ V vs. Fe}^{0/+}]$ and a lifetime of $\tau = 10 \text{ ns}$.^[156] Another macrocyclic nickel based photoredox catalyst was reported by Sarkar. The group investigated a Ni(II) tetraphenylporphyrin (NiTPP) complex which was applied in several different photoredox catalysed transformations. The photocatalysts exhibits a redox potential of the excited state of $[E_{1/2}(\text{Ni}^{*\text{II}}/\text{Ni}^{\text{I}}) = + 1.17 \text{ V vs. SCE}]$ and $[E_{1/2}(\text{Ni}^{\text{II}}/\text{Ni}^{*\text{II}}) = - 1.57 \text{ V vs. SCE}]$.^[157]

Scope of this work

In the last 15 years, photoredox chemistry evolved to one of the most popular research topics in the field of photocatalysis. The utilization of transition metal complexes in diverse visible light mediated organic reactions emphasises this trend towards the broad applicability of photoredox chemistry in catalysis. The main focus in photoredox catalysis lies on the investigation of new synthetically useful methods, employing iridium or ruthenium based photocatalysts. This includes also high costs for catalyst due to the low abundance of the mentioned metals in Earth's crust. To date, only a few examples of earth-abundant transition metal complexes are known to compete with the established $\text{Ru}(\text{bpy})_3^{2+}$ in photochemical transformations. The aim of this work was to establish a novel nickel based photocatalyst, to modulate the ligand design and to investigate the applicability of the photocatalyst in new organic photoredox transformations as well as in small molecule activation e.g. hydrogen evolution or CO_2 reduction. The macrocyclic ligand scaffold, introduced by the group of *Hess*, should serve as non-innocent platform. Ligand non-innocence plays a crucial role in small activation, as the ligand itself takes part in the catalytic process or supports the catalytic properties of the active metal centres. The employed ligand consists of two main fragments; the biquinazoline part and a diketiminate part as depicted in Figure 12.

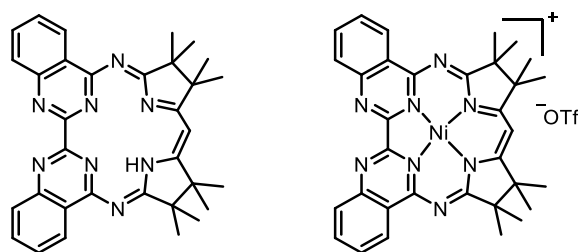


Figure 11: Macrocyclic ligand (left) and the corresponding nickel complex (right).

The aim was to first optimize the ligand synthesis due to low yields in several of the synthesis steps. Second, the goal was to insert nickel in the central coordination site and characterize the resulting metal complex with respect to redox and photophysical properties. The nickel complexes adds to the series of first-row transition metal Mabiq and helps to compare the studies on the different metal Mabiq complexes.^[158–161] Initial studies towards suitable applications should focus on the investigation of photochemical, organic transformations with the monometallic nickel complex. Therefore, all the photochemical and redox properties of the catalyst needed to be evaluated. This included cyclic voltammetry measurements, necessary for redox potentials but also the determination of excited state lifetime or evaluation of luminescence properties of the complex. With all data in hand, already literature-known

photoredox reactions were investigated to compare the novel nickel complex with commonly used photocatalysts. Besides literature-known photoreaction a novel substrate class needed to be tested with the nickel photocatalyst.

With a established photocatalytic system the second idea arose to apply the nickel complex in small molecule activation such as hydrogen evolution or CO₂ reduction in a photocatalytic fashion. Nickel incorporated in non-innocent macrocyclic ligand frameworks is a prominent representative for efficient small molecule activation.^[162,163] To date, no photocatalytic system for small molecule activation is known, which uses earth abundant metal complexes as photosensitizer and catalyst at the same time.

A third task was the modification of the ligand structure by designing a ligand with different steric and electronic properties. (Figure 13). Possible modifications can be introduced either at the biquinazoline fragment (blue, Figure 13) or at the diketiminate unit (red, Figure 13). Without the outer phenyl groups at the biquinazoline unit or with a change in sterics by replacing the phenyl groups with a thiophen or pyridine moiety the left ligand fragment could be modified. That would tune the photophysical and the ground state properties and enable new routes towards possible applications in photoredox catalysis. Another benefit is the larger access to the second binding site for transition metals e.g. ruthenium, palladium. Additionally, the diketiminate unit on the right molecule site could be customized by e.g. a full aromatic, porphyrinogen, dipyrrolo backbone. By substitution of the methyl groups with electron donating or withdrawing groups it would also be possible to tune the electron density at the metal enter. Comparable to literature reports, a template attached to the methylene carbon atom, would be possible to induce stereoselectivity by introduction of a facial shield.^[164,165]

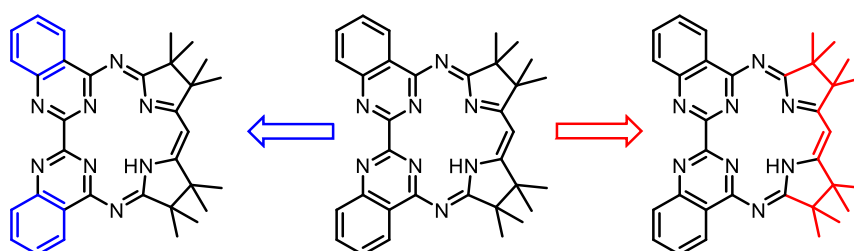


Figure 12: Possible changes in the structural motif of the Mabiq ligand.

As already mentioned, a third strategy was the introduction of a metal atom at the second binding site. Some biologically active enzymes exhibit enhanced catalytic properties through the introduction of a second active metal center. Bimetallic complexes e.g. Ni-Fe complexes are commonly found among enzymes in biochemical systems such as hydrogenases.

Redox and photocatalytic properties of a Ni(II) complex with a macrocyclic biquinazoline (Mabiq) ligand.

Title: “Redox and photocatalytic properties of a Ni(II) complex with a macrocyclic biquinazoline (Mabiq) ligand.”

Status: Edge Article, published online 23. February 2018

Journal: *Chemical Science*, **2018**, 9, 3313-3317

Publisher: Royal Chemical Society

DOI: 10.1039/C7SC05320G

Authors: Michael Grübel, Irene Bosque, Philipp J. Altmann, Thorsten Bach, Corinna, R. Hess

Content: This work was the entry for our group to the field of photoredox active earth-abundant metal complexes. The synthesis and characterization of a novel nickel(II) complex comprising a macrocyclic ligand framework was investigated. The nickel complex contributes to the series of first row transition metal Mabiq complexes. Starting from the Ni(II) compound it was also possible to synthesize its one-electron reduced form Ni(I)Mabiq which was further characterized by spectroscopic and DFT calculation methods. Irradiation of the Ni(II) compound, in the presence of triethylamine as sacrificial electron donor with an LED ($\lambda = 457$ nm) it was possible to obtain the reduced Ni(I) complex. This reaction could be followed by UV-Vis. The [Ni(II)Mabiq]OTf was applied in a visible light mediated photoredox cyclization of a bromoalkyl-substituted indole and exhibits a comparable if not superior activity in terms of turnover number and chemoselectivity to Ru(bpy)₃²⁺. The excited state redox potential was evaluated using a series of sacrificial donor amines in the aforementioned photoredox transformation indicating an excited state redox potential of $[E_{1/2}(\text{Ni}^{*\text{II}}/\text{Ni}^{\text{I}}) = + 1.25$ V vs. SCE]. Furthermore, a quantum yield for the photoconversion was determined, which provided an estimate for the excited state lifetime of $\tau = 1 - 10$ ns.

M. Grübel planned and executed all experiments and wrote the manuscript. I. Bosque helped with the quantum yield determination and proof reading. P. J. Altmann conducted all SC XRD-measurements and managed the processing of the respective data. All work was performed under the supervision of T. Bach and C. R. Hess.

Cite this: *Chem. Sci.*, 2018, 9, 3313

Redox and photocatalytic properties of a Ni^{II} complex with a macrocyclic biquinazoline (Mabiq) ligand†‡

Michael Grübel, Irene Bosque, Philipp J. Altmann, Thorsten Bach^{†*} and Corinna R. Hess^{‡*}

We present a late, first row transition metal photosensitizer that promotes photocatalytic C–C bond formation. The title compound, [Ni(Mabiq)]OTf, as well as its one-electron reduced form, Ni(Mabiq), were synthesized and molecular structures of both were obtained. The electronic structure of the reduced complex additionally was characterized by spectroscopic and DFT computational methods. Notably, [Ni^I(Mabiq)]OTf is photoactive: reduction of the compound was achieved photochemically upon irradiation at $\lambda = 457$ nm and reductive quenching by NEt₃. The performance of [Ni(Mabiq)]OTf as a photoredox catalyst was examined in the cyclization of a bromoalkyl-substituted indole. In this reaction, the first-row transition metal compound is comparable if not superior to [Ru(bpy)₃]²⁺ in terms of efficiency (turnover number) and chemoselectivity. Studies using a series of sacrificial donor amines indicate that the excited state redox potential of [Ni(Mabiq)]^{•+} is ≥ 1.25 V vs. SCE. This value is similar to the excited state potential of commonly employed noble metal based photocatalysts. The Ni-Mabiq compound thus provides a rare example of an earth-abundant photoredox catalyst.

Received 15th December 2017
Accepted 20th February 2018

DOI: 10.1039/c7sc05320g

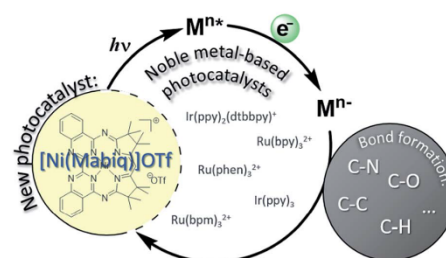
rsc.li/chemical-science

Introduction

Photoredox catalysis offers nascent opportunities to shift conventional chemical production methods to light-driven processes.¹ The design of new photoactive metal compounds is key to the development of new catalytic transformations. Chromophores can effect a wide array of functional group transformations and C–C bond formation reactions *via* the generation of active radical species, originating from excited state electron transfer processes (Scheme 1).² With very few exceptions, photoredox catalysis relies on the use of noble metal containing photosensitizers, mainly Ru- or Ir-polypyridyl complexes;³ other heavy metal complexes (*e.g.* Os^{II}, Re^I, Mo⁰, W⁰) also have occasionally been employed.^{4,5} [Ru(bpy)₃]²⁺ – with its long lived, charge separated excited state ([Ru^{III}(bpy^{•-})(bpy)₂]^{2+*}) – is the classic and universal photocatalyst for a plethora of applications.²

The use of less expensive, more abundant, late first row transition metal alternatives is generally precluded by their

inherently short excited-state lifetimes. In the first row, nickel complexes have been used in photocatalytic cross coupling reactions,⁶ though the use of an added photosensitizer (commonly Ir) still is required in all of these tandem systems. A class of Ni^{II} ligand-to-ligand charge transfer complexes recently were shown to possess advantageous properties as photosensitizers, but applications have not yet been demonstrated.⁷ In fact, reports describing catalytic applications or reactivity of systems using only non-noble metal photosensitizers are exceedingly scarce.^{8–10}



Scheme 1 Photoredox catalysis commonly relies on noble metal complexes for organic transformations, initiated by single electron transfer upon excitation of Ru or Ir compounds. The [Ni(Mabiq)]OTf catalyst offers an earth-abundant photosensitizer.

Department of Chemistry, Catalysis Research Center (CRC), Technische Universität München, 85747 Garching, Germany. E-mail: thorsten.bach@ch.tum.de; corinna.hess@ch.tum.de

† Dedicated to the memory of Inge Grübel.

‡ Electronic supplementary information (ESI) available: CIF files, synthetic procedures, spectroscopic, electrochemical and DFT computational data. CCDC 1538675, 1538676 and 1586948. For ESI and crystallographic data in CIF or other electronic format see DOI: 10.1039/c7sc05320g

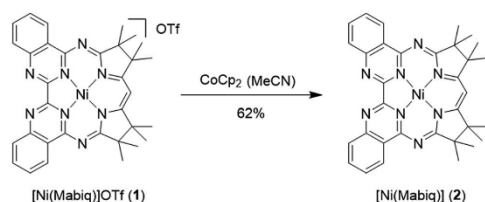


We now report a Ni^{II} complex with a macrocyclic biquinazoline (Mabiq) ligand,^{11,12} [Ni(Mabiq)]OTf (**1**), providing a rare example of a non-noble metal based photosensitizer. The divalent complex **1** can be photochemically reduced and the electronic structure of the product, [Ni(Mabiq)] (**2**), is described herein. Using a series of synthesized sacrificial donor molecules, the photo-excited state redox potential of **1** was assessed and compared to common noble-metal photocatalysts. We demonstrate the photoredox catalytic ability of **1** in a radical-based cyclization of a bromoalkyl-substituted indole. The reaction relies solely on the Ni-Mabiq photocatalyst, without the need for an additional noble metal photosensitizer.

Results and discussion

The yellow diamagnetic **1** (Scheme 2) was readily prepared by complexation of the ligand with Ni(OTf)₂ in ethanol solution (see ESI† for further details). The Ni ion adopts the expected square planar geometry in the solid state (Fig. S1†). The electronic spectrum of **1** in DCM exhibits intense absorption bands ($\epsilon \approx 10^4 \text{ M}^{-1} \text{ cm}^{-1}$) in the visible light region ($\lambda_{\text{max}} = 414, 435,$ and 457 nm ; $\epsilon = 13.6, 16.4, 22.3 \times 10^3 \text{ M}^{-1} \text{ cm}^{-1}$; Fig. 2 inset). Similar features were observed in the spectra of other M-Mabiq complexes, notably in the spectrum of Zn(Mabiq)Cl.^{12a} The Zn^{II}-complex displayed two strong absorption bands at 471 and 502 nm that were assigned as Mabiq $\pi \rightarrow \pi^*$ transitions. However, d-d or metal-to-ligand charge transfer (MLCT) processes may additionally contribute to the corresponding absorptions of **1**. The cyclic voltammogram of **1** in MeCN (Fig. S9†) exhibits a reversible, formally Ni^{II/I} redox couple at $-1.05 \text{ V vs. Fc}^{+/0}$ (Fc = ferrocene; $\text{Fc}^{+/0} = 0.4 \text{ V vs. SCE}$). Additional, seemingly reversible, reductive processes appear at potentials $< -1.5 \text{ V}$.

The one-electron reduced Ni(Mabiq) (**2**) was subsequently generated from **1** using CoCp₂ as the reductant (Scheme 2). The molecular structure of **2** (Fig. 1) reveals shorter Ni–N bond distances (Ni–N_{avg} = 1.874 Å vs. Ni–N_{avg} = 1.882 Å in **1**), as well as the hallmark changes in the diketiminate C–N bonds that signify reduction of the Mabiq ligand (Table S8†). The $S = 1/2$ ground state of the complex was verified by EPR spectroscopy. The spectrum is consistent with a ligand-centered radical, with $g_{\text{iso}} = 1.995$ (Fig. S4†). Low energy features at $\lambda_{\text{max}} = 641, 711$ and 801 nm ($1.4, 3.5, 5.4 \times 10^3 \text{ M}^{-1} \text{ cm}^{-1}$) are apparent in the electronic spectrum of **2** in THF (Fig. 2 inset), accounting for the}}



Scheme 2 Reaction of **1** with CoCp₂ (Cp = cyclopentadienyl) yields the one-electron reduced **2**.

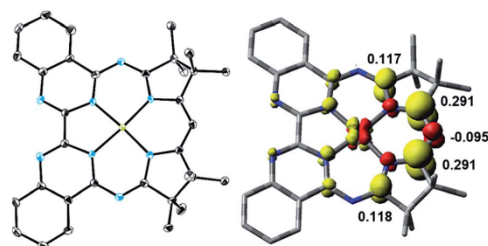


Fig. 1 Left: Molecular structure of **2** (50% probability ellipsoids; hydrogen atoms omitted for clarity). Right: DFT-derived (B3LYP) spin density plot for **2** based on Löwdin population analysis (isosurface value = ± 0.005).

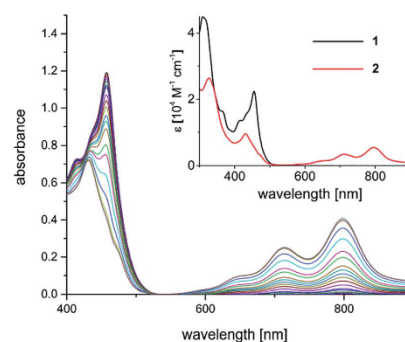


Fig. 2 Spectral evolution during photoconversion of **1** to **2** [**1**] = 0.05 mM; $c(\text{NET}_3) = 1.4 \text{ M}$; $\lambda = 457 \text{ nm}$, DMF. Inset: electronic spectra of **1** (black trace; CH₂Cl₂) and **2** (red trace; THF).

vibrant green color of the complex in solution. The spectrum again closely resembles that of the one-electron reduced Zn complex, Zn^{II}(Mabiq^{•−}).^{12a} The spectroscopic data thus point to ligand-centered reduction of **1**, such that the electronic structure of **2** corresponds to Ni^{II}(Mabiq^{•−}). Indeed, DFT calculations (B3LYP) on **2** further support this conclusion.

The DFT-derived (B3LYP) spin density plot (Fig. 1) describes a diamagnetic d⁸ Ni^{II} center with an unpaired electron localized primarily on the diketiminate unit of the Mabiq ligand. Four doubly occupied d-orbitals can be identified, while the SOMO possesses only ca. 4% d-orbital character and otherwise depicts a ligand π^* orbital (Fig. S5†). The latter molecular orbital is antibonding with respect to the diketiminate C–N p-orbital interactions, which explains the lengthening of these bonds in the structure of **2**. It is noteworthy that ligand-centered reduction appears to prevail across the series of metal-Mabiq compounds we have examined thus far.¹²

The well-behaved redox chemistry of [Ni(Mabiq)]OTf (**1**), its high absorbance in the visible region and its relatively high reduction potential warranted a study of its photoredox properties. As mentioned above, the compound exhibits a strong



multi-structured absorption band with a maximum at $\lambda = 457$ nm ($\epsilon = 22\,300$ M⁻¹ cm⁻¹), which invites excitation with a visible light source and quenching studies with a suitable reductant. Gratifyingly, it was indeed found that irradiation of a DMF solution of **1** at $\lambda = 457$ nm, in the presence of NEt₃ (7.5 mM to 1.4 M), leads to a color change from yellow to green and to the formation of complex **2**.

The formation of the reduced compound was complete after 15 minutes (using 1.4 M NEt₃; c (**1**) = 0.05 mM), as verified spectroscopically (Fig. 2). The photoconversion of **1** to **2** occurs on a much faster timescale in MeCN/THF or DMF/THF mixtures (the solvent combination solubilizes both forms), under identical conditions. The quantum yield for the photoconversion is $\approx 10^{-4}$ (THF : DMF 4 : 1), and correlates with the Et₃N concentration (14–56 mM; Table S3 and Fig. S29†). From the data, the lifetime of the excited state form that reacts with the Et₃N can be estimated as $\approx 1 \times 10^{-8}$ s (see ESI† for details). Steady-state emission spectra recorded at ambient temperature and at 77 K did not reveal any luminescence. Thus, we currently cannot comment in detail on the nature of the excited state processes involved in the photo-reduction of **1**. If one takes the longest wavelength absorption [$\lambda \cong 510$ nm, $E_0 \leq 235$ kJ mol⁻¹ (2.4 V)] of compound **1** to estimate the redox potential of photoexcited complex **1**^{*}, a value of $\leq +1.35$ V (vs. Fc^{+/0}) is obtained.¹³

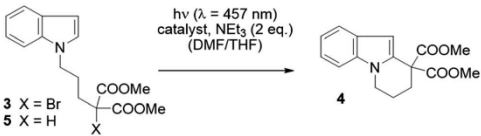
TDDFT (B3LYP) computational studies provide some insight into the nature of the absorptions in the visible region. The calculated transitions correlate well with the experimentally obtained absorbance spectrum of **1** (Fig. S6†). The absorptions at 400–500 nm include a prominent LL/CT transition that corresponds to the HOMO to LUMO transition. The HOMO is localized on the bipyrimidine moiety of the Mabiq ligand, while the LUMO is a diketiminate based π^* orbital (Fig. S7†). Other, less intense, transitions in the vicinity possess d–d (Ni d_{z²} → Ni

d_{x²-y²}) and MLCT (Ni d_{z²} → L π^*) character. These states may contribute to the unique photochemical properties of **1**. However, a detailed investigation regarding the photochemistry and excited state kinetics of this compound is warranted, and will be the subject of future investigations.

We examined whether the photochemical properties of **1** might render it a suitable photoredox catalyst for C–C bond formation reactions. The radical cyclization of the *N*-(ω -bromoalkyl)-substituted indole **3** was chosen as a test reaction.¹⁴ The reaction had been previously studied by the Stephenson group and was found to produce mainly product **4** by C–C bond formation under optimized conditions.¹⁵ Under non-optimized conditions, hydro-de-bromination was a competing side reaction and varying product ratios of **4** and **5** were observed. Optimal conditions were reported to include the use of [Ru(bpy)₃]Cl₂ as the catalyst (1 mol%) and NEt₃ (2 equiv.) in DMF solution and gave product **4** in 60% yield.¹⁵

Given the limited solubility of **2** in DMF, the reaction was initially attempted in a DMF/THF mixture ($v/v = 1/2$) with 2 mol% of catalyst **1** and 2 equiv. NEt₃ as the quencher (Table 1, entry 1).¹⁶ We were pleased to find that the desired cyclization proceeded smoothly and delivered with high chemoselectivity the desired product **4**. The inseparable hydro-de-brominated by-product **5** was detectable in minor quantities but the ratio of products was 95/5 in favor of cyclization product **4**. When increasing the relative volume of THF in the solvent mixture both conversion and yield improved slightly (entry 2). The selectivity towards the desired reaction was high with a yield of 86% at 94% conversion, *i.e.* 91% yield based on conversion. For comparison, the Ru^{II} complex [Ru(bpy)₃](PF₆)₂ was employed under identical conditions (entry 3). Although the ratio 4/5 was identical with this catalyst, the reaction suffered from a lower conversion and a lower chemoselectivity (63% yield based on conversion). Similar observations were made when the catalyst

Table 1 Photoredox-catalyzed cyclization of bromide **3** to tricyclic product **4** and reduction to hydro-de-brominated product **5**; influence of the catalyst and the reaction parameters on the yield and chemoselectivity



Entry ^a	Catalyst ^d	mol%	DMF/THF [v/v]	Conv. ^b [%]	Yield ^c [%]	4/5 ^d
1	1	2	1/2	93	84	95/5
2	1	2	1/4	94	86	95/5
3	[Ru(bpy) ₃](PF ₆) ₂	2	1/4	73	46	95/5
4	1	1	1/4	95	84	95/5
5	[Ru(bpy) ₃](PF ₆) ₂	1	1/4	59	23	95/5
6	1 ^e	2	1/4	n.d.	—	—
7	— ^f	—	1/4	12	12	55/45
8	1 ^g	2	1/4	<5	<5	—

^a All reactions were performed on a scale of 0.08 mmol ($c = 25$ mM) with a LED lamp (3 W power output) as light source. Irradiation time: 13 h. ^b The conversion was calculated from recovered starting material. ^c Total yield of isolated products **4** and **5**. ^d Ratio of cyclized to hydro-de-brominated product as determined by ¹H-NMR. ^e Attempted reaction without irradiation. ^f No catalyst was added. ^g No NEt₃ was added. n.d. = not detected.



loading was further decreased to 1 mol%: while the performance of Ni^{II} catalyst **1** remained unchanged (entry 4) the reaction with the Ru^{II} catalyst was sluggish and a decrease in yield was observed (entry 5).

The above reaction is induced by visible light as no conversion occurs without irradiation (entry 6). In the absence of the Ni^{II} catalyst,¹⁷ only 12% of a product mixture was obtained, which was composed of the cyclized product **4** and the reduced product **5** in a 55/45 ratio (entry 7). In the absence of the reductant, no reaction was observed (entry 8). The free HMabiq ligand is not photocatalytically active. The quantum yield for the [Ni(Mabiq)]OTf catalysed cyclization reaction was determined to be $\phi = 0.006$.

Mechanistically, it is suggested that the photoreduction of complex **1** by NEt₃ (reductive quenching cycle)¹ generates complex **2**, which may engage in SET to the bromide **3** (Scheme 3). Complex **2** was shown to be competent to reduce **3**. We note that modification of the Ni-Mabiq complex during the cyclization reaction was not observed, as verified by ESI-MS and ¹H-NMR (Fig. S8 and S41†).

To experimentally verify the estimated photoexcited state redox potential of **1**^{*}, we synthesized a series of amines with oxidation potentials in the range of 0.78–1.59 V (vs. SCE; Tables 2 and S1†), as determined by CV. The amines were employed as sacrificial donors in the cyclization reaction. Excellent yields of **4** were obtained using the donor molecules with oxidation potentials up to 1.25 V (Table 2, amines **6a–6c**), whereas a drastic decrease in yield was observed using those with higher redox potentials. Only 40% and 20% product yields were obtained with **6d** ($E_{\text{ox}} = 1.41$ V vs. SCE) and **6e** ($E_{\text{ox}} = 1.59$ V vs. SCE), respectively. The product yield in the control reaction using **6e** in the absence of photocatalyst **1** was 7%, a result that is comparable to that obtained using NEt₃ (Table 1, entry 7). The results confirm that the excited state redox potential of **1**^{*} is at least 1.25 V (vs. SCE). Thus, our new Ni-Mabiq complex is a more powerful oxidant than [Ru(bpy)₃]²⁺ ($E_{1/2}[\text{Ru}^{2+}/\text{Ru}^{\cdot+}]$ 0.78 V vs. SCE),¹⁸ and comparable to [Ir(dF(CF₃)ppy)₂(dtbbpy)]⁺ ($E_{1/2}[\text{Ir}^{3+}/\text{Ir}^{2+}]$ 1.21 V vs. SCE).¹⁹

We additionally generated a sterically hindered amine, N(CH₂Me)₂Cy₂ (**6f**), to assess whether coordination of the sacrificial donor molecules influences the reactivity of **1**. In contrast to the bpy- and phen-based photosensitizers, the Ni-Mabiq complexes are coordinatively unsaturated and intramolecular electron transfer from a coordinated amine to the

Table 2 Comparison of the oxidation potentials for different sacrificial donors **6** with the yields obtained for the catalytic reaction of **3** to **4** and **5**

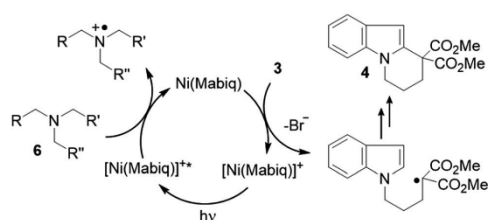
Amine ^a	E_{ox} (vs. SCE)	Yield ^b [%]
Et ₃ N (6a)	0.83	84
6b	1.05	97
6c	1.25	95
6d	1.41	40
6e	1.59	20 ^c
6f	0.78	84

^a All reactions were performed on a scale of 0.08 mmol ($c = 2.5$ mM) with a 457 nm LED lamp (3 W power output) as the light source. Irradiation time: 13 h. ^b Total yield of isolated products **4** and **5**, with a 95 : 5 ratio of cyclized to hydro-de-brominated product as determined by ¹H-NMR. ^c Average of two runs. $\text{Fe}^{10} = 0.4$ V vs. SCE. Cy = cyclohexyl.

divalent metal center could potentially occur. The molecular structure of **6f** (Fig. S3†) suggests that coordination of this amine group to the Ni center is unlikely; the cyclohexyl and mesityl groups encapsulate the nitrogen atom rendering the lone pair inaccessible. Whereas noticeable changes in the absorption spectrum of **1** were observed upon addition of Et₃N (400 equiv.) to a solution of the complex in THF/DMF, the addition of **6f** has no effect (Fig. S30 and S31†). However, the yield of the catalytic reaction using **6f** as sacrificial donor was found to be 84%, a value that is comparable to the one obtained using Et₃N (**6a**) and **6b–6e** as sacrificial donors.

Conclusions

In summary, we have discovered a new photoredox catalyst, [Ni(Mabiq)]OTf (**1**) that is based on the earth-abundant metal nickel. The diamagnetic, bench-stable compound was readily prepared, its redox properties were studied and the one-electron reduced form Ni(Mabiq) (**2**) likewise was isolated. Further studies to elucidate the detailed photophysical properties of **1**^{*} are warranted. However, we have already demonstrated that the photoexcited complex is a strong oxidant, with the capacity to induce C–C bond formation in an initial test reaction. The Ni-Mabiq compound may offer an alternative to noble metal photosensitizers for other synthetic transformations in organic photoredox chemistry, as well as for energy conversion processes. The Mabiq ligand also features a second metal binding site that could be exploited for tandem catalysis. Thus, the macrocycle represents a new type of platform for the development of photoactive systems. With evidence of the ability of **1** to act as a photosensitizer and photoredox catalyst, the broader photocatalytic applications of our system subsequently will be investigated.



Scheme 3 Proposed catalytic cycle for the cyclization of **3** to give **4**.



Conflicts of interest

There are no conflicts to declare.

Acknowledgements

We thank Dr Alex Pöthig for contributions to the crystallography, and Dr Andreas Bauer for assistance with fluorescence and quantum yield measurements. We are grateful to Prof. Klaus Köhler for the use of his EPR instrument, and to Dr Carmen Haefßner and Manuel Kaspar for technical assistance. I. B. acknowledges the Ramón Areces Foundation (Becas para Estudios Postdoctorales) and the Alexander von Humboldt Foundation for a postdoctoral fellowship. M. G acknowledges the TUM Graduate School for financial support.

Notes and references

- For seminal studies, see: (a) M. A. Ischay, M. E. Anzovino, J. Du and T. P. Yoon, *J. Am. Chem. Soc.*, 2008, **130**, 12886–12887; (b) D. A. Nicewicz and D. W. C. MacMillan, *Science*, 2008, **322**, 77–80; (c) J. M. R. Narayanan, J. W. Tucker and C. R. J. Stephenson, *J. Am. Chem. Soc.*, 2009, **131**, 8756–8757.
- Reviews: (a) D. M. Schultz and T. P. Yoon, *Science*, 2014, **343**, 985; (b) Y. Xi, H. Yi and A. Lei, *Org. Biomol. Chem.*, 2013, **11**, 2387–2403; (c) M. Reckenthäler and A. G. Griesbeck, *Adv. Synth. Catal.*, 2013, **355**, 2727–2744; (d) C. K. Prier, D. A. Rankic and D. W. C. MacMillan, *Chem. Rev.*, 2013, **113**, 5322–5363; (e) J. M. R. Narayanan and C. R. J. Stephenson, *Chem. Soc. Rev.*, 2011, **40**, 102–113; (f) K. Zeitler, *Angew. Chem., Int. Ed.*, 2009, **48**, 9785–9789.
- D. M. Arias-Rotondo and J. K. McCusker, *Chem. Soc. Rev.*, 2016, **45**, 5803–5820.
- (a) L. A. Büldt and O. S. Wenger, *Angew. Chem., Int. Ed.*, 2017, **56**, 5676–5682; (b) L. A. Büldt, X. Guo, A. Prescimone and O. S. Wenger, *Angew. Chem., Int. Ed.*, 2016, **55**, 11247–11250; (c) J.-P. Sauvage, J.-P. Collin, J.-C. Chambron, S. Guillerez and C. Coudret, *Chem. Rev.*, 1994, **94**, 993–1019; (d) D. J. Stufkens and A. Vlcek Jr, *Coord. Chem. Rev.*, 1998, **177**, 127–179; (e) K. S. Schanze, D. B. MacQueen, T. A. Perkins and L. A. Cabana, *Coord. Chem. Rev.*, 1993, **122**, 63–89; (f) S. Meister, R. O. Reithmeier, M. Tschurl, U. Heiz and B. Rieger, *ChemCatChem*, 2015, **7**, 690–697.
- For the use of organic compounds as photoredox catalysts, see: N. A. Romero and D. A. Nicewicz, *Chem. Rev.*, 2016, **116**, 10075–11166.
- (a) Z. Zuo, D. T. Ahneman, L. Chu, J. A. Terrett, A. G. Doyle and D. W. C. MacMillan, *Science*, 2014, **345**, 437–440; (b) D. T. Ahneman and A. G. Doyle, *Chem. Sci.*, 2016, **7**, 7002–7006; (c) M. Jouffroy, D. N. Primer and G. A. Molander, *J. Am. Chem. Soc.*, 2016, **138**, 475–478; (d) B. P. Woods, M. Orlandi, C.-Y. Huang, M. S. Sigman and A. G. Doyle, *J. Am. Chem. Soc.*, 2017, **139**, 5688–5691; (e) M. K. Nielsen, B. J. Shields, J. Liu, M. J. Williams, M. J. Zacuto and A. G. Doyle, *Angew. Chem., Int. Ed.*, 2017, **56**, 7191–7194; (f) J. Twilton, C. Le, P. Zhang, M. H. Shaw, R. W. Evans and D. W. C. MacMillan, *Nat. Rev. Chem.*, 2017, **1**, 1–18; (g) E. R. Welin, C. Le, D. M. Arias-Rotondo, J. K. McCusker and D. W. C. MacMillan, *Science*, 2017, **355**, 380–385.
- L. A. Cameron, J. W. Ziller and A. F. Heyduk, *Chem. Sci.*, 2016, **7**, 1807–1814.
- For a recent review of earth-abundant photosensitizers see: C. B. Larsen and O. S. Wenger, *Chem.–Eur. J.*, 2018, **24**, 2039–2058.
- (a) F. J. Sarabia and E. M. Ferreira, *Org. Lett.*, 2017, **19**, 2865–2868; (b) S. M. Stevenson, M. P. Shores and E. M. Ferreira, *Angew. Chem., Int. Ed.*, 2015, **54**, 6506–6510; (c) A. Gualandi, M. Marchini, L. Mengozzi, M. Natali, M. Lucarini, P. Ceroni and P. G. Cozzi, *ACS Catal.*, 2015, **5**, 5927–5931; (d) P. Zimmer, P. Müller, L. Burkhardt, R. Schepper, A. Neuba, J. Steube, F. Dietrich, U. Flörke, S. Mangold, M. Gerhards and M. Bauer, *Eur. J. Inorg. Chem.*, 2017, 1504–1509; (e) S. Otto, A. M. Nauth, E. Ermilov, N. Scholz, A. Friedrich, U. Resch-Genger, S. Lochbrunner, T. Opatz and K. Heinze, *ChemPhotoChem*, 2017, **1**, 344–349.
- S. J. Hwang, D. C. Powers, A. G. Maher, B. L. Anderson, R. G. Hadt, S.-L. Zheng, Y.-S. Chen and D. G. Nocera, *J. Am. Chem. Soc.*, 2015, **137**, 6472–6475.
- E. Müller, G. Bernardinelli and A. von Zelewsky, *Inorg. Chem.*, 1988, **27**, 4645–4651.
- (a) P. Banerjee, A. Company, T. Weyermüller, E. Bill and C. R. Hess, *Inorg. Chem.*, 2009, **48**, 2944–2955; (b) E. V. Puttock, P. Banerjee, M. Kaspar, L. Drennan, D. S. Yufit, E. Bill, S. Sproules and C. R. Hess, *Inorg. Chem.*, 2015, **54**, 5864–5873; (c) M. Kaspar, P. J. Altmann, A. Pöthig, S. Sproules and C. R. Hess, *Chem. Commun.*, 2017, **53**, 7282–7285.
- The redox potential of $\mathbf{1}^{*/2}$ was calculated from the redox potential of $\mathbf{1}/2$ (–1.05 V vs. $\text{Fc}^{+/0}$) by adding the energy of the excited state E_0 (see ref. 3).
- For recent work on photoredox-induced alkylation reactions at the indole core, see: D. Alpers, M. Gallhof, J. Witt, F. Hoffmann and M. Brasholz, *Angew. Chem., Int. Ed.*, 2017, **56**, 1402–1406 and refs cited therein.
- J. W. Tucker, J. M. R. Narayanan, S. W. Krabbe and C. R. J. Stephenson, *Org. Lett.*, 2010, **12**, 368–371.
- For the reaction set-up, see: (a) D. Rackl, V. Kais, P. Kreitmeier and O. Reiser, *Beilstein J. Org. Chem.*, 2014, **10**, 2157–2165; (b) D. Lenhart, A. Pöthig and T. Bach, *Chem.–Eur. J.*, 2016, **22**, 6519–6523.
- Radical reactions of amines can be initiated in the absence of a photoredox catalyst if an alkyl halide is present: (a) J. F. Franz, W. B. Kraus and K. Zeitler, *Chem. Commun.*, 2015, **51**, 8280–8283; (b) A. Böhm and T. Bach, *Chem.–Eur. J.*, 2016, **22**, 15821–15928; (c) A. M. Nauth, J. C. O. Pacheco, S. Pusch and T. Opatz, *Eur. J. Org. Chem.*, 2017, 6966–6974.
- A. Juris, V. Balzani, P. Belser and A. von Zelewsky, *Helv. Chim. Acta*, 1981, **64**, 2175–2182.
- M. S. Lowry, J. I. Goldsmith, J. D. Slinker, R. Rohl, R. A. Pascal Jr, G. G. Mailliaras and S. Bernhard, *Chem. Mater.*, 2005, **17**, 5712–5719.



Synthesis of Tetrahydroisoquinolines by Visible Light-mediated 6-exo-trig Cyclization of α -Aminoalkyl Radicals.

Title: "Synthesis of Tetrahydroisoquinolines by Visible Light-mediated 6-exo-trig Cyclization of α -Aminoalkyl Radicals."
Status: Letter, published online 17.07.2019
Journal: *Synlett*
Publisher: Thieme Verlag
DOI: 10.1055/s-0039-1690006
Authors: Michael Grübel, Christian Jandl, Thorsten Bach

Content: In this report our group investigated a novel synthetic method towards tetrahydroisoquinoline (THIQ) compounds utilizing visible light and a photoredox active iridium polypyridyl catalyst. It is well established that α -silylalkyl amines can be utilized as α -aminalkyl radical precursors as previously reported by *Mariano*, *Nishibayashi* and *Yoon*. Our group established a visible light mediated intramolecular cyclization, resulting in substituted THIQ compounds. The reported substrates incorporate both, the α -silylalkyl amine and the Michael acceptor functionality. The substrate scope comprises 13 substrates which could be synthesized from *ortho*-alkylbenzaldehydes in a three-step procedure. The conditions for the photoreactions include the use of 5 mol% of the respective iridium catalyst, equimolar amounts of water and cesium carbonate and dimethylformamide as solvent. After optimization, the photoreaction delivered the THIQ products in moderate to good yields (41-83%). In three cases a diastereoselectivity of d.r. = 80/20 was observed and SC XRD data provided evidence for the respective relative configuration of the major diastereoisomer.

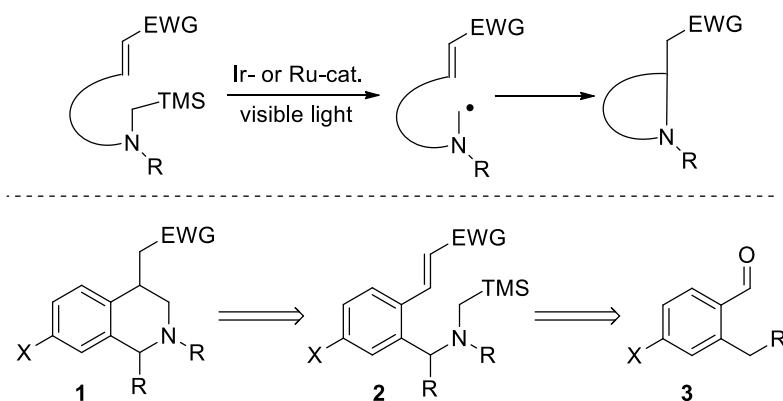
M. Grübel planned and executed all experiments and wrote the manuscript. C. Jandl conducted all SC XRD-measurements and managed the processing of the respective data. All work was performed under the supervision of T. Bach.

Abstract Starting from the respective tertiary α -silylmethyl amines, the intramolecular cyclization of α -aminoalkyl radicals to Michael acceptors was found to produce tetrahydroisoquinolines. The reaction conditions included the use of 5 mol% of an iridium photoredox catalyst, dimethylformamide as solvent and equimolar amounts of water and cesium carbonate as additives. 13 substrates were synthesized from *ortho*-alkylbenzaldehydes in a three-step procedure involving a carbonyl condensation, a radical bromination, and a substitution by a secondary α -silylmethyl amine. After optimization of the photocyclization, the reaction delivered tetrahydroisoquinolines in moderate to high yields (41-83%). A facial diastereoselectivity (d.r. \cong 80/20) was observed with chiral substrates and a crystal structure provided evidence for the relative configuration of the major diastereoisomer. A catalytic cycle with direct electron transfer to the photo-excited metal catalyst is proposed.

Photoinduced single electron oxidation of amines provides access to nucleophilic α -aminoalkyl radicals which can act as reactive intermediates.¹ Besides the generation of α -aminoalkyl radicals by single electron transfer (SET) and subsequent deprotonation,² the radicals can be produced by oxidative decarboxylation of α -amino acid derivatives,³ by hydrogen atom transfer,⁴ or by oxidative desilylation of α -silylalkyl amines.⁵ The silyl group renders the formation of α -aminoalkyl radicals regioselective⁶ and avoids overoxidation of the α -aminoalkyl radicals to the corresponding iminium ions.⁷

Several research groups reported the utilization of the trimethylsilyl (TMS) group as a suitable electrophilic leaving group in photosensitized electron transfer reactions. Frequently, a consecutive reaction is the addition of the photochemically generated α -aminoalkyl radical to electron deficient alkenes (Michael acceptors) in an inter- or intramolecular fashion.⁵ Typically, the α -aminoalkyl radical is generated from α -silylmethyl amines employing ultraviolet irradiation or visible light with different sensitizers, such as anthraquinone,⁸ benzophenones,⁹ 1,4-dicyanonaphthalenes,^{5d,f} or 9,10-dicyanoanthracene^{5c,e} to induce the SET.

In recent years, several protocols have been reported for the generation of α -aminoalkyl radicals by photoredox active iridium- or ruthenium-polypyridyl complexes. Visible light irradiation induces an electron transfer from the amine to the photoexcited transition metal complex. Subsequent formation of an α -aminoalkyl radical allows for a conjugate addition to a double bond which results – if performed intramolecularly – in a cyclization (Scheme 1).^{10,11,12}



Scheme 1: Generation of α -aminoalkyl radicals via a SET and consecutive addition to a Michael system in an intramolecular fashion (top) and its application to the synthesis of tetrahydroisoquinolines **1** (bottom).

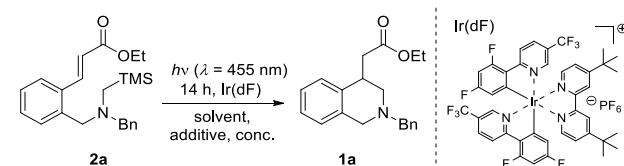
Herein, we present a visible light-mediated cyclization reaction to tetrahydroisoquinolines **1** (THIQs) that relies on a conjugate addition of SET-generated α -aminoalkyl radicals to Michael acceptors and that is catalyzed by an iridium-polypyridyl complex. THIQs are usually synthesized from a β -arylethylamine and an aldehyde or ketone following the Pictet-Spengler protocol.¹³ Although photoredox-based methods have been established in recent years to further modify the THIQ core structure^{10b,14-17} there is not yet a method to access this skeleton by photoredox catalysis.

The synthesis of the respective starting materials **2** for the photoreactions required in all cases the corresponding *ortho*-alkyl substituted benzaldehydes **3**. Aldehyde substrates with substituents at the phenyl skeleton ($X = \text{OMe}, \text{Cl}$) and $R^1 = \text{CH}_3$ were prepared by a halogen-metal exchange and subsequent formylation with *N,N*-dimethylformamide (DMF).¹⁸ In the next synthetic step, the electron-withdrawing groups (EWG) were introduced by either an aldol condensation (nitriles, ketones) or a *Wittig* reaction (methyl and ethyl ester). For compounds **2a** and **2b** it was also possible to commence the synthesis with the respective cinnamates **4** (EWG = $\text{CO}_2\text{Me}, \text{CO}_2\text{Et}$). A literature procedure was adapted to introduce the sulfone by addition of thiophenol to 1-ethynyltoluene and subsequent oxidation.¹⁹ The radical bromination at the benzylic position of substrates **4** was performed using *N*-bromosuccinimide (NBS) in chloroform and dibenzoylperoxide (DBP) as radical initiator. A nucleophilic substitution of bromides **5** by secondary α -silylmethyl amines in acetone with K_2CO_3 concluded the synthesis (Table 1).

Table 1: Synthesis of amine substrates **2** starting from *ortho*-alkyl substituted styrenes **4** by bromination (4→5) and nucleophilic substitution (5→2).

substrate	X	R ¹	R ²	EWG	Yield [%] 4→5	Yield [%] 5→2
2a	H	H	Ph	CO ₂ Et	70	81
2b	H	H	Ph	CO ₂ Me	80	75
2c	H	H	Ph	COCH ₃	57	76
2d	H	H	Ph	CN	69	80
2e	Cl	H	Ph	CO ₂ Me	36	72
2f	OMe	H	Ph	CO ₂ Me	34	90
2g	H	H	<i>iso</i> -butyl	CO ₂ Me	80	56
2h	H	Me	Ph	COCH ₃	72	58
2i	H	Me	Ph	CO ₂ Me	85	72
2j	H	Me	Ph	CN	quant.	71
2k	H	H	Ph	COPh	29	90
2l	H	H	Ph	SO ₂ Ph	54	95
2m	H	H	Ph-CF ₃	CO ₂ Me	80	33

The corresponding amines for substrate **2g**, **2m** were synthesized as previously reported.²⁰ All substrates exhibit oxidation potentials between $E_{\text{ox}}(2^{+\bullet}/2) = +0.75$ V and $+0.95$ V vs. SCE (for further details, see the Supporting Information). Our investigation of the intramolecular cyclization commenced with model substrate **2a** which was irradiated in the presence of 5 mol% $[\text{Ir}\{\text{dF}(\text{CF}_3)\text{ppy}\}_2(\text{tbbpy})]\text{PF}_6$ $[\text{Ir}(\text{dF})]$ $[E_{1/2}(\text{Ir}^{\text{III}*}/\text{Ir}^{\text{II}}) = +1.21$ V vs. SCE]²¹ as photocatalyst. After irradiation for 14 hours in DMF at 25 °C with a blue LED (30 W, $\lambda = 455$ nm), 29% of the desired product was obtained (Table 2, entry 1).



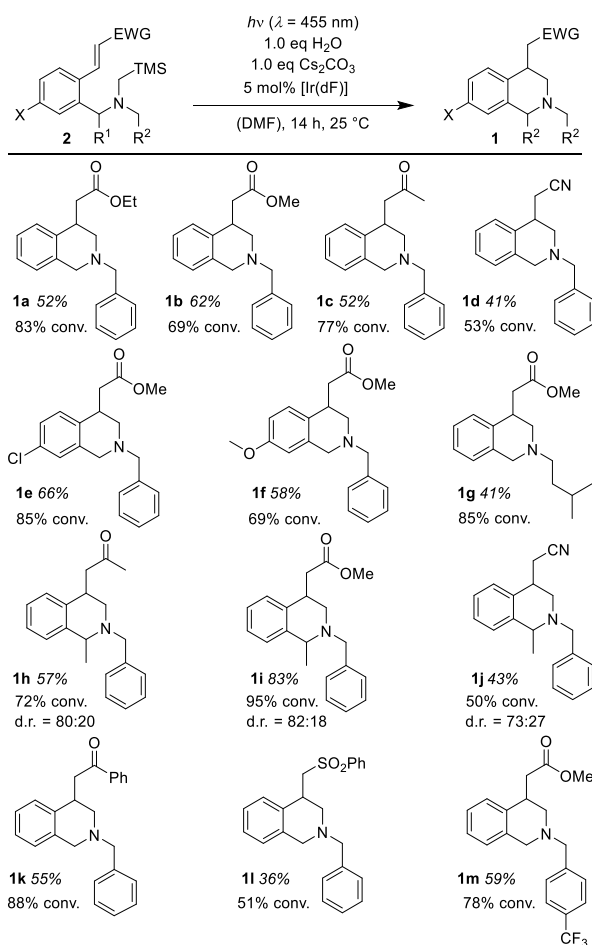
entry	Ir cat. [mol%]	solvent	conc. [mM]	additive ^a	Yield [%] ^b
1	5	DMF	50	—	29
2	5	MeCN	50	—	7
3	5	CH ₂ Cl ₂	50	—	12
4	5	DMF	25	—	17
5	5	DMF	100	—	22
6	5	DMF	50	AcOH	28
7	5	DMF	50	H ₂ O	40
8	5	DMF	50	H ₂ O/LiBF ₄	32
9	5	DMF	50	H ₂ O/Cs ₂ CO ₃	52
10	2	DMF	50	H ₂ O/Cs ₂ CO ₃	23
11 ^c	5	DMF	50	H ₂ O/Cs ₂ CO ₃	0
12 ^d	—	DMF	50	H ₂ O/Cs ₂ CO ₃	0
13 ^e	5	DMF	50	H ₂ O/Cs ₂ CO ₃	0
14 ^f	5	DMF	50	H ₂ O/Cs ₂ CO ₃	28
15 ^g	5	DMF	50	H ₂ O/Cs ₂ CO ₃	55

^aAddition of additive in stoichiometric amounts. ^bYield of isolated product after chromatographic purification. ^cNo light. ^dNo photocatalyst (71% recovered starting material.). ^eRu(bpy)₃(PF₆)₂ as photocatalyst. ^f[Ir(dF-CF₃-ppy)₂(bpy)]PF₆ as photocatalyst. ^gIrradiation of photoproduct **1a** under optimized conditions.

Variation of the solvent led to decomposition of the starting material and a low product yield (entries 2-3). Entries 4 and 5 show that a change in the substrate concentration did not improve the yield. The addition of Brønsted acid has been reported to accelerate the rate-determining carbon-carbon bond formation step^{10b} but using acetic acid as proton source did not alter the reaction outcome (entry 6). However, the addition of water in stoichiometric amounts had a positive effect, improving the yield to 40% (entry 7). From a screening of several Lewis acids and inorganic bases (for further additive screening, see the SI), cesium carbonate evolved as the most beneficial additive increasing the yield up to 52% at a conversion of 83% (entry 9). Lowering the catalyst loading only decreased the yield (entry 10). Control experiments (entry 11 and 12) validated the necessity of light and catalyst in the reaction. Only 71% of starting material and no product could be re-isolated after irradiation of a sample without a catalyst demonstrating the limited stability of the starting material. Neither Ru(bpy)₂(PF₆)₂ nor a different iridium catalyst [Ir{dF(CF₃)ppy}₂(bpy)]PF₆ proved to be a suitable catalyst in the cyclization reaction (entry 13 and 14). The excited state potential of Ru(bpy)₂(PF₆)₂ [E_{1/2}(Ru^{II*}/Ru^I) = +0.80 V vs. SCE]²² might be too low to oxidize the tertiary amine. Eventually, we checked the stability of the photoproduct under the optimized condition and observed decomposition during irradiation (entry 15). With an oxidation potential of E_{ox}(**1a**⁺/**1a**) = +1.15 vs. SCE, the photoproduct could potentially still be oxidized by the excited state of the

iridium catalyst, resulting in decomposition as previously described.²³ No reaction was observed with an amine substrate without a trimethylsilyl group in the α -position (see the SI).

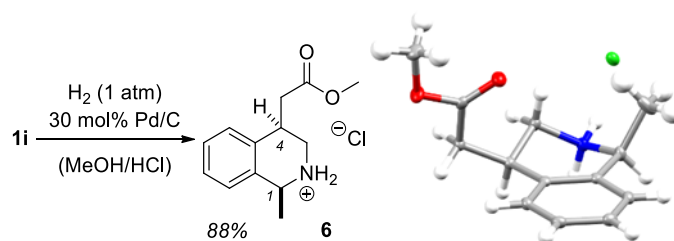
In the next set of experiments, we examined the substrate scope of this transformation under optimized reaction conditions (entry 9, Table 1).²⁴ As shown in scheme 2 the reaction seems to be fairly general and applicable to a range of substrates with moderate to high yields (41-83%). By changing the EWG from the model substrate **2a** to a methoxycarbonyl substitution (**2b**) the yield increased to 62% but the conversion dropped to 69%. With a stronger EWG such as cyano or sulfonyl the yields decreased to 41% (**1d**) and 36% (**1l**) and in both cases the conversion was only around 50% (53% for **1d**, 51% for **1l**). With acetyl or benzoyl as EWG, products **1c** and **1k** were isolated in 52% and 55% yield, respectively, at a conversion of 77% for **1c** and 88% for **1k**. Variation of the substituents at the aryl core resulted in a yield of 66% for **1e** with a weakly deactivating chloro substituent and 58% for **1f** with a strongly activating methoxy group attached to the phenyl ring. In both reactions, the starting material was not fully converted to the products (85% and 69% conversion). Different substituents at the amine moiety such as a 4-trifluoromethylbenzyl group **1m** (59%) or an aliphatic *iso*-butyl group **1g** (41% yield) were also tolerated with conversions of 78% and 85%, respectively. Acetyl- (**2h**), methoxycarbonyl- (**2i**), and cyano-substituted (**2j**, *E/Z* = 73/27) substrates with a methyl group at the 1-position of the THIQ core successfully afforded the desired products **1h-1j** in 57%, 83%, and 43% yield. The conversion in the three reactions was 72%, 95%, and 50%.



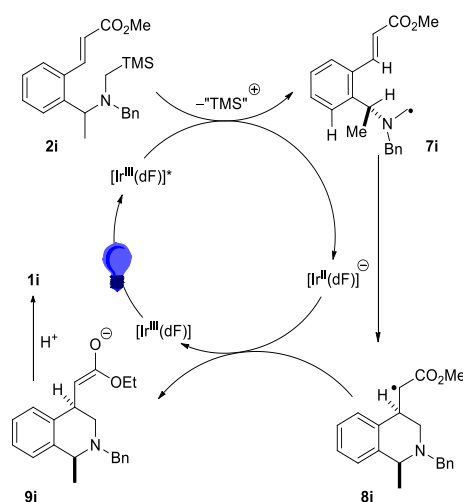
Scheme 2: Intramolecular photocatalytic cyclization of α -silylated amines **2** to products **1** under optimized reaction conditions. Yields are given for isolated products and are not based on conversion.

THIQs **1h–1j** were isolated as a mixture of diastereomeric products, which could be separated by column chromatography. In all three cases, the formation of a major diastereoisomer was observed (d.r. \cong 80/20). The assignment of the relative configuration of product **1i** was accomplished after a palladium-catalyzed debenzoylation of the tertiary amine (scheme 3). The crystal structure of the corresponding ammonium salt **6** revealed for the major diastereoisomer a *cis*-configuration of the substituents in positions C1 and C4. Comparing the $^1\text{H-NMR}$ spectra for products **1i**, the shift of the signal for the proton in position C1 is distinctly different for the major (3.75 ppm) and minor (4.10 ppm) diastereoisomer. The same chemical shift difference was also observed for products **1h** and **1j** suggesting that in all diastereomeric mixtures the major product displays a *cis*-configuration of the substituents in positions C1 and C4. The diastereoselectivity can be rationalized by assuming that the conformation of the cyclization precursor is governed by 1,3-allylic strain.²⁵ Accordingly, the hydrogen atom at the stereogenic center is located in the plane of the aryl group, minimizes the steric strain between the Michael system and substituents in *ortho*-position. The conjugate addition of the α -aminoalkyl radical **7i** presumably proceeds from the bottom face generating the major product with a *cis*-

configuration (scheme 4). Scheme 4 describes a reasonable mechanistic scenario for the photocatalytic cyclization of 2i to THIQ 1i as representative substrate. The first step involves a reductive quench of the photoexcited iridium complex by the amine producing a radical cation, which loses the TMS group generating the α -aminoalkyl radical.



Scheme 3: Palladium-catalyzed deprotection of the *N*-benzyl group and conformation of the relative configuration of the major diastereoisomer by X-Ray analysis.



Scheme 4: Mechanistic scenario for the catalytic cycle in the photochemical transformation of 2j to the THIQ 1i and model for an 1,3-allylic strain stereocontrol.

Intramolecular addition of the radical to the double bond closes the ring in a 6-*exo*-trig fashion. The catalytic cycle is completed by oxidation of the photocatalyst and the formation of enolate 9i, which gets trapped by a TMS source or is directly hydrolyzed. Intermediate 9i can also be formed from 8i by simultaneous oxidation of amine 2i (chain process).

In summary, we have described a new intramolecular 6-*exo*-trig photocyclization to tetrahydroisoquinolines induced by visible light-mediated photoredox catalysis with an iridium complex. A three-step synthesis route has been developed to access a variety of substrates incorporating the α -silylmethyl amine. The latter entity proved to be essential for the generation of the nucleophilic α -aminoalkyl radical. All substrates show relatively high redox potentials compared to other α -silylmethyl anilines.²⁶ The photocyclization has been found to occur in moderate to high yields and offers a yet unexplored entry to biologically relevant tetrahydroisoquinolines.

Acknowledgment This project was supported by the Deutsche Forschungsgemeinschaft (DFG). M.G. acknowledges the TUM graduate school for financial support and Prof. Corinna Hess for valuable discussions.

Supporting Information Supporting information for this article is available online at <https://doi.org/10.1055/s-0039-1690006>

References and Notes

- (1) Reviews: (a) Nakajima, K.; Miyake, Y.; Nishibayashi, Y. *Acc. Chem. Res.*, 2016, 49, 1946-1956. (b) Renaud, P.; Giroud L. *Synthesis* 1996, 913-926. (c) Pandey, G. *Synlett* 1992, 546-552. (d) Yoon, U. C.; Mariano, P. S. *Acc. Chem. Res.*, 1992, 25, 233-240.
- (2) (a) Pienta, N. J.; McKimney, J. E. *J. Am. Chem. Soc.* 1982, 104, 5501-5502. (b) Dunn, D. A.; Schuster, D. I. *J. Am. Chem. Soc.*, 1985, 107, 2802-2804 (c) Dinnocenzo, J.P.; Banach, T.E. *J. Am. Chem. Soc.*, 1989, 111, 8646-8653. (d) Miyake, Y.; Nakajima, K.; Nishibayashi, Y. *J. Am. Chem. Soc.* 2012, 134, 3338-3341.
- (3) (a) Chu, L.; Ohta, C.; Zuo, Z.; MacMillan, D. W. C. *J. Am. Chem. Soc.* 2014, 136, 10886-10889. (b) Fan, L.; Jia, J.; Lefebvre, H. Q.; Rueping, M. *Chem. Eur. J.*, 2016, 22, 16437-16440. (c) Zuo, Z.; Cong, H.; Li, W.; Choi, J.; Fu, G. C.; MacMillan, D. W. C. *J. Am. Chem. Soc.*, 2016, 138, 1832-1835.
- (4) Ashley, M. A.; Yamauchi, C.; Chu, J. C. K.; Otsuka, S.; Yorimitsu, H.; Rovis, T. *Angew. Chem. Int. Ed.* 2019, 58, 4002-4006.
- (5) (a) Yoon, U. C.; Kim, J. U.; Hasegawa, E.; Mariano, P. S. *J. Am. Chem. Soc.* 1987, 109, 4421-4423. (b) Hasegawa, E.; Xu, W.; Mariano, P. S.; Yoon, U. C.; Kim, J. U. *J. Am. Chem. Soc.* 1988, 110, 8099-8111. (c) Xu, W.; Yoon, T. J.; Hasegawa, E.; Yoon, U. C.; Mariano, P. S. *J. Am. Chem. Soc.* 1989, 111, 406-408. (d) Pandey, G. Kumaraswamy, G. Bhalerao, U. T. *Tetrahedron Lett.* 1989, 30, 6059-6062. (e) Jung, Y. S.; Swartz, W. H.; Xu, W.; Mariano, P. S.; Green, N. J.; Schultz, A. G. *J. Org. Chem.* 1992, 57, 6037-6047. (f) Pandey, G.; Reddy, G. D.; Kumaraswamy, G. *Tetrahedron*, 1994, 50, 8185-8194. (g) Jonas, M.; Blechert, S.; Steckhan, E. *J. Org. Chem.* 2001, 66, 6896-6904. (h) Cho, D. W.; Yoon, U. C.; Mariano, P. S. *Acc. Chem. Res.* 2011, 44, 204-215.
- (6) Nakajima, K.; Kitagawa, M.; Ahida, Y.; Miyake, Y.; Nishibayashi, Y. *Chem. Commun.* 2014, 50, 8900-8903

- (7) Wayner, D. D. M.; Dannenberg, J. J.; Griller, D. *Chem. Phys. Lett.* 1986, 131, 189-191.
- (8) (a) Das, J.; Kumar, J. S. D.; Thomas, K. G.; Shivaramayya, K.; George, M. V. *J. Org. Chem.* 1994, 59, 628-634. (b) Das, J.; Kumar, J. S. D.; Thomas, K. G.; Shivaramayya, K.; George, M. V. *Tetrahedron* 1996, 52, 3425-3434.
- (9) (a) de Alvarenga, E. S.; Mann, J. *Chem. Soc. Perkin Trans. 1*, 1993, 2141-2142. (b) de Alvarenga, E. S.; Cardin, C. J.; Mann, J. *Tetrahedron* 1997, 40, 3169-3172. (c) Bertrand, S.; Glapski, C.; Hoffmann, N.; Pete, J.-P. *Tetrahedron Lett.* 1999, 40, 3169-3172. (d) Bertrand, S.; Hoffmann, N.; Pete, J.-P. *Eur. J. Org. Chem.* 2000, 2227-2238; (e) Bauer, A.; Westkämper, F.; Grimme, S.; Bach, T. *Nature* 2005, 436, 1139-1140.
- (10) For non-functionalized amines, see: (a) McNally, A.; Prier, C. K.; MacMillan, D. W. C. *Science* 2011, 334, 1114-1117. (b) Ruiz Espelt, L.; Wiensch, E. M.; Yoon, T. P. *J. Org. Chem.* 2013, 78, 4107-4114. (c) Zhu, S.; Das, A.; Bui, L.; Zhou, H.; Curran, D. P.; Rueping, M. *J. Am. Chem. Soc.* 2013, 135, 1823-1829. (d) Dai, X.; Cheng, D.; Guan, B.; Mao, W.; Xu, W.; Li, X. *J. Org. Chem.* 2014, 79, 7212-7219. (e) Dai, X.; Mao, R.; Guan, B.; Xu, X.; Li, X. *RSC Adv.* 2015, 5, 55290-55294. (f) Murphy, J. J.; Bastida, D.; Paria, S.; Fagnoni, M.; Melchiorre, P. *Nature*, 2016, 532, 218-222
- (11) For silylated amines, see: (a) Miyake, Y.; Ashida, Y.; Nakajima, K.; Nishibayashi, Y. *Chem. Commun.* 2012, 48, 6966-6968. (b) Lenhart, D.; Bach, T. *Beilstein J. Org. Chem.*, 2014, 10, 890-896. (c) Ruiz Espelt, L.; McPherson, I. S.; Wiensch, E. M.; Yoon, T. P. *J. Am. Chem. Soc.*, 2015, 137, 2452-2455. (d) Lenhart, D.; Bauer, A.; Pöthig, A.; Bach, T. *Chem. Eur. J.* 2016, 22, 6519-6523.
- (12) Recent reviews: (a) Schultz, D. M.; Yoon, T. P. *Science* 2014, 343, 1239176/1-8. (b) Reckenthäler, M.; Griesbeck, A. G.; *Adv. Synth. Catal.* 2013, 355, 2727-2744. (c) Xi, Y.; Yi, H.; Lei, A. *Org. Biomol. Chem.* 2013, 11, 2387-2403. (d) Prier, C. K.; Rankic, D. A.; MacMillan, D. W. C. *Chem. Rev.* 2013, 113, 5322-5363. (e) Tucker, J. W.; Stephenson, C. R. *J. J. Org. Chem.* 2012, 77, 1617-1622. (f) Zeitler, K. *Angew. Chem. Int. Ed.* 2009, 48, 9785-9789.
- (13) (a) Pictet, A.; Spengler, T. *Ber. Dtsch. Chem. Ges.* 1911, 44, 2030. (b) Cox, E. D.; Cook, J. M. *Chem. Rev.* 1995, 95, 1797-1842.
- (14) Key publications: (a) Rueping, M.; Zhu, S.; Koenigs, R. M. *Chem. Commun.* 2011, 47, 12709-12711. (b) Rueping, M.; Vila, C.; Koenigs, R. M.; Poschorny, K.; Fabry, D. C. *Chem.*

Commun. 2011, 47, 2360-2362. (c) Rueping, M.; Zhu, S.; Koenigs, R. M. Chem. Commun. 2011, 47, 8679-8681. (d) Pan, Y.; Wang, S.; Kee, C. W.; Dubuisson, E.; Yang, Y.; Loh, K. P.; Tan, C.-H. Green Chem. 2011, 13, 3341-3344. (e) Zhao, G.; Yang, C.; Guo, L.; Sun, H.; Chen, C.; Xia, W. Chem. Commun. 2012, 48, 2337-2339. (f) Freeman, D. B.; Furst, L.; Condie, A. G.; Stephenson, C. R. J. Org. Lett. 2012, 14, 94-97.

(15) Condie, A. G.; González-Gómez, J. C.; Stephenson, C. R. J. J. Am. Chem. Soc. 2010, 132, 1464-1465.

(16) Kohl, P.; Jadhav, D.; Pandey, G.; Reiser, O. Org. Lett. 2012, 14, 672-675.

(17) Liu, X.; Bureš, F.; Liu, H.; Jiang, Z. Angew. Chem. Int. Ed. 2015, 54, 11443-11447.

(18) Nakamura, Y.; O-kawa, K.; Minami, S.; Ogawa, T.; Tobita, S., Nishimura, J. J. Org. Chem. 2002, 67, 1247-1252.

(19) Xue, Q.; Mao, Z.; Shi, Y.; Mao, H.; Cheng, Y.; Zhu, C. Tetrahedron Lett. 2012, 53, 1851-1854.

(20) Jeong, H. C.; Lim, S. H.; Cho, D. W.; Kim, S. H.; Mariano, P. S. Org. Biomol. Chem. 2016, 14, 10502-10510.

(21) Juris, A.; Balzani, V.; Barigelletti, F.; Campagna, S.; Belser, P.; von Zelewsky, A. Coord. Chem. Rev. 1988, 84, 85-277.

(22) Lowry, M. S.; Goldsmith, J. I.; Slinker, J. D.; Rohl, R.; Pascal, R. A.; Maillaras, G. G.; Bernhard, S. Chem. Mater. 2005, 17, 5712-5719.

(23) Böhm, A.; Bach, T. Chem. Eur. J. 2016, 22, 15921-15928.

(24) General procedure for the cyclization: 1.00 eq. substrate, 1.00 eq. Cs₂CO₃, 1.00 eq. of H₂O and 0.05 eq. photoredox catalyst [Ir{dF(CF₃)ppy} (dtbpy)]PF₆ [Ir(dF)] were dissolved in dry DMF (ca. 2 mL per 0.1 mmol substrate). The yellow mixture was degassed by repeating three times a freeze-pump-thaw cycle and was irradiated for 14 hours with 30 W blue LED lamps ($\lambda = 455$ nm) at room temperature while continuously stirring under an argon atmosphere. After 14 hours, water (ca. 5 mL/0.1 mmol) was added. The layers were separated and the aqueous layer was extracted with diethyl ether (3 \times ca. 6 mL/0.1 mmol). The combined organic layers were washed with brine and dried over Na₂SO₄. After filtration, residual solvent was removed under reduced pressure. The crude product was purified by column chromatography to obtain the photoproduct. Representative NMR data: (1a): ¹H NMR (500 MHz, CDCl₃): δ

(ppm) = 7.40–7.34 (m, 2H, 2 × meta-CPh-H), 7.34–7.28 (m, 2H, 2 × ortho-CPh-H), 7.27–7.21 (m, 1H, para-CPh-H), 7.17–7.07 (m, 3H, H-6, H-7, H-8), 7.00–6.94 (m, 1H, H-5), 4.13–3.99 (m, 2H, CH₂CH₃), 3.80 (d, 2J = 14.9 Hz, 1H, CHH-1), 3.71 (d, 2J = 13.1 Hz, 1H, Ph-CHH), 3.58 (d, 2J = 13.1 Hz, 1H, Ph-CHH), 3.42 (d, 2J = 14.9 Hz, 1H, CHH-1), 3.38–3.31 (m, 1H, H-4), 2.88 (dd, 2J = 16.0 Hz, 3J = 9.7 Hz, 1H, CHHCO₂Et), 2.80 (ddd, 3J = 11.7 Hz, 4J = 3.2 Hz, 4J = 1.3 Hz, 1H, CHH-3), 2.61–2.58 (m, 2H, CHH-3, CHHCO₂Et), 1.20 (t, 3J = 7.1 Hz, 3H, CH₂CH₃). ¹³C-NMR (101 MHz, CDCl₃): δ (ppm) = 172.9 (s, CO₂Et), 138.7 (s, CH₂-CPh), 137.6 (s, C-4a), 135.3 (s, C-8a), 129.1 (d, meta-CHPh), 128.4 (d, C-8), 128.4 (d, ortho-CHPh), 127.2 (d, para-CHPh), 126.7 (d, C-6*), 126.5 (d, C-7*), 126.2 (d, C-5), 62.8 (t, CH₂-CPh), 60.4 (t, CH₂CH₃), 56.5 (t, C-1), 54.7 (t, C-3), 41.2 (t, CH₂CO₂Et), 35.8 (d, C-4), 14.3 (q, CH₂CH₃). *Assignment is interconvertible. (1i): Major diastereoisomer ¹H NMR (400 MHz, CDCl₃): δ (ppm) = 7.39–7.36 (m, 2H, 2 × meta-CPh-H), 7.33–7.29 (m, 2H, 2 × ortho-CPh-H), 7.27–7.22 (m, 1H, para-CPh-H), 7.22–7.13 (m, 4H, H-5, H-6, H-7, H-8), 4.10 (d, 2J = 13.6 Hz, 1H, Ph-CHH), 3.75 (q, 3J = 6.3 Hz, 1H, H-1), 3.55 (s, 3H, CO₂CH₃), 3.40 (d, 2J = 13.6 Hz, 1H, Ph-CHH), 3.26 (dq, 3J = 9.0 Hz, 3J = 5.0 Hz, 1H, H-4), 2.90–2.80 (m, 2H, CHH-3, CHHCO₂CH₃), 2.66 (dd, 2J = 16.0 Hz, 3J = 5.0 Hz, 1H, CHHCO₂CH₃), 2.62–2.56 (m, 1H, CHH-3), 1.53 (d, 3J = 6.3 Hz, 3H, CH₃). ¹³C NMR (101 MHz, CDCl₃): δ (ppm) = 173.2 (s, CO), 140.4 (s, C-8a), 139.6 (s, CH₂-CPh), 137.7 (s, C-4a), 128.9 (d, meta-CHPh), 128.3 (d, ortho-CHPh), 128.1 (d, C-8*), 127.3 (d, C-5*), 127.0 (d, para-CHPh), 126.4 (d, C-6**), 126.1 (d, C-7**), 58.9 (t, CH₂-CPh), 57.8 (d, C-1), 51.5 (q, CO₂CH₃), 50.9 (t, C-3), 39.9 (t, CH₂CO₂H₃), 35.1 (d, C-4), 21.9 (q, CH₃). */**Assignments are interconvertible. Minor diastereoisomer ¹H NMR (400 MHz, CDCl₃): δ (ppm) = 7.39–7.35 (m, 2H, 2 × meta-CPh-H), 7.33–7.28 (m, 2H, 2 × ortho-CPh-H), 7.27–7.22 (m, 1H, para-CPh-H), 7.17–7.09 (m, 3H, H-6, H-7, H-8), 7.06–7.00 (m, 1H, H-5), 4.10 (q, 3J = 6.6 Hz, 1H, H-1), 3.83 (d, 2J = 13.1 Hz, 1H, Ph-CHH), 3.63 (d, 2J = 13.1 Hz, 1H, Ph-CHH), 3.52 (s, 3H, CO₂CH₃), 3.23–3.17 (m, 1H, H-4), 3.00 (d, 2J = 10.6 Hz, 1H, CHH-3), 2.88 (dd, 2J = 16.2 Hz, 3J = 10.1 Hz, 1H, CHHCO₂CH₃), 2.55–2.45 (m, 2H, CHH-3, CHHCO₂CH₃), 1.28 (d, 3J = 6.6 Hz, 3H, CH₃). ¹³C NMR (101 MHz, CDCl₃): δ (ppm) = 173.5 (s, CO), 141.4 (s, C-8a), 139.4 (s, CH₂-CPh), 137.5 (s, C-4a), 129.2 (d, meta-CHPh), 128.8 (d, C-8), 128.3 (d, ortho-CHPh), 127.4 (d, para-CHPh), 127.0 (d, C-5), 126.4 (d, C-6*), 126.2 (d, C-7*), 58.4 (t, CH₂-CPh), 56.0 (d, C-1), 51.5 (q, CO₂CH₃), 45.8 (t, C-3), 41.1 (t, CH₂CO₂CH₃), 35.9 (d, C-4), 14.8 (q, CH₃). *Assignment is interconvertible.

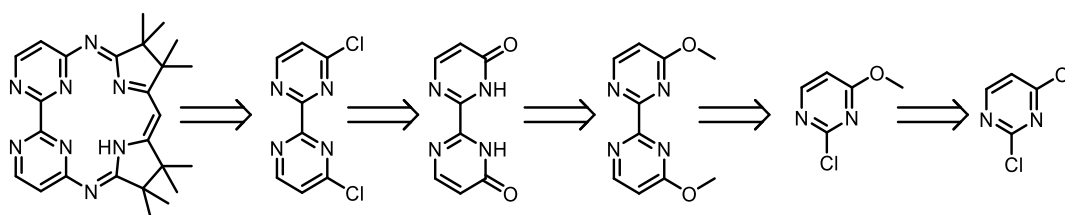
(25) Hoffmann, R. W. Chem. Rev. 1989, 89, 1841-1860.

(26) Cooper, B. E.; Owen, W. J. J. Organomet. Chem. 1971, 29, 33-40.

Unpublished results

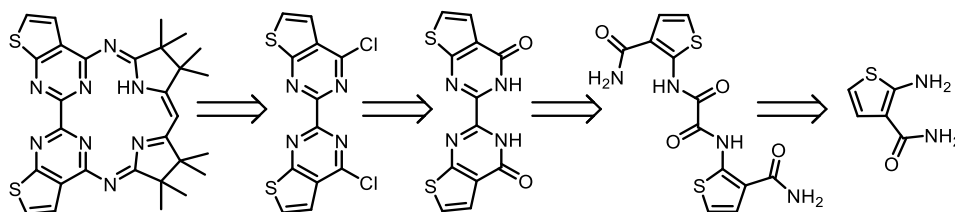
Ligand modification

As previously mentioned, the aim was to modify the ligand scaffold. The following depictions describe four approaches to modify the ligand macrocycle at different fragments of the molecule. The first approach towards new ligand motifs or modifications at the macrocyclic ligand scaffold focused on the removal of the external aromatic ring (scheme 12). The synthesis route started with a nucleophilic aromatic substitution^[166] followed by a homo coupling of the bipyrimidine.^[167] Methoxy deprotection resulted in the bipyrimidone product^[166] which can be converted into the dichloropyrimidine compound. All literature-known transformations could be performed in good yield. Unfortunately, the chlorination of the bipyrimidone was unsuccessful and further, extensive screening for reaction conditions did not result in conversion to the desired dichlorobipyrimidin.



Scheme 12: Synthesis route towards a ligand without external phenyl groups at the biquinazoline fragment.

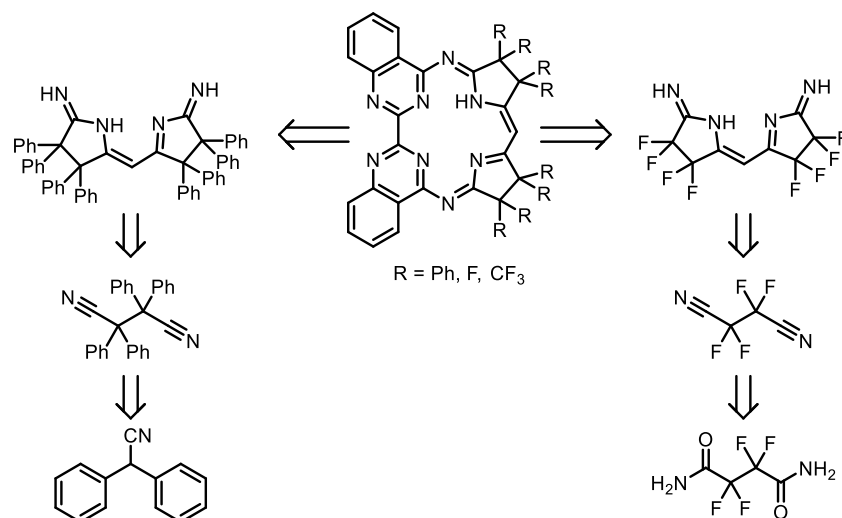
Another possible approach is the substitution of the external aromatic ring of the biquinazoline fragment with thiophene (scheme 13). The synthesis route towards a thiophene substituted biquinazoline ligand includes similar transformations compared to the reported synthesis of the Mabiq ligand. Unfortunately, the intramolecular condensation to the bipyrimidone derivative did not work and even after optimization no reaction product was obtained.



Scheme 13: Synthesis route towards a thiophene modified biquinazoline backbone.

The modification of the diketiminate unit included the variation of the precursors for the *Grignard* cyclization. Two different synthetic routes were investigated, introducing phenyl groups or fluorine atoms (scheme 14). The *Grignard* precursor was obtained by an electrolysis of the diphenylnitrile in quantitative yield. Unfortunately, the *Grignard* reactions to the desired

modified diketiminate unit could not be achieved and no product was isolated. The introduction of the fluorine atoms failed during the reaction towards the dinitrile compound.

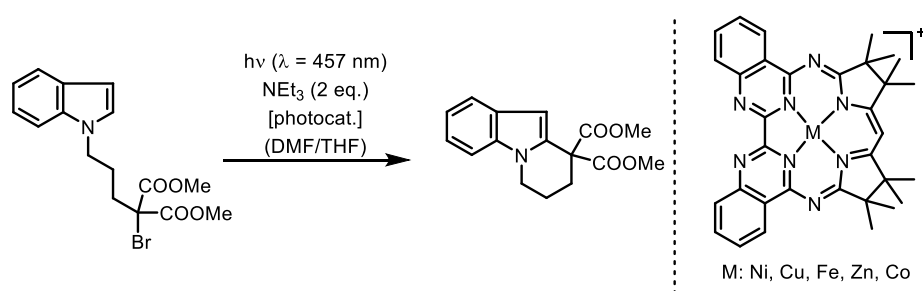


Scheme 14: Different modifications introduced at the diketiminate unit. Left: introduction of phenyl groups instead of CH_3 groups. Right: Attachment of fluorine atoms substituting methyl groups.

For further ligand modification approaches, see the Masters thesis of Michael Grübel.

Photocatalytic studies with different metal Mabiq complexes

Further photocatalytic studies were performed with different metal Mabiq complexes to compare their photocatalytic behavior. To evaluate the activity, the already known cyclization of the alkyl substituted indole derivative was chosen and photoreactions were performed under the optimized conditions reported by our group (scheme 15).^[156] The obtained yields and the different ratios between cyclization and dehalogenation product are given in table 1.



Scheme 15: Photocatalytic cyclization of an alkyl substituted indole derivative catalyzed by different metal Mabiq complexes.

Table 1: Reaction yields and ratio of cyclized and dehalogenated product for the different employed metal Mabiq complexes. Reactions were performed under reported, optimized reaction conditions.^[156]

	Yield [%]	Selectivity Cy/Dehal
(NiMabiq)OTf	84	95/5
(CuMabiq)OTf	31	72/28
[FeMabiq(MeCN) ₂]PF ₆	19	95/5
(ZnMabiq)OTf	35	15/85
[CoMabiq(MeCN) ₂]PF ₆	10	55/45

The nickel complex was the superior catalyst for this specific organic transformation with a reaction yield of 84% and a ratio of 95/5 for the cyclized product. A comparable ratio was only obtained with the iron complex. In the cases of the zinc and cobalt Mabiq complexes, a nearly one to one mixture or a reverse relation between cyclized and dehalogenated product was observed. Except for the nickel complex, all reaction yields were low. For the (ZnMabiq)OTf, this can be rationalized by decomposition of the metal complex.

Bimetallic complexes

It was possible to generate a bimetallic Mabiq complex with two nickel atoms as metal centers. For synthesis details see appendix. The second nickel atom at the outer binding site needs further stabilization through supporting due to its instability. Phosphine based ligands such as xanthphos or triphenylphosphine seemed to be suitable ligands as strong donating ligands. For the bimetallic nickel complex with xanthphos the molecular structure was solved by X-Ray analysis (see appendix). Preliminary DFT calculations revealed an electron distribution similar to the monometallic Ni(I)Mabiq complex.

Summary and Outlook

Driven by the need for novel earth-abundant metal complexes, active in photocatalysis this work focused on the synthesis, characterization and modification of a nickel complex comprising a macrocyclic ligand. The investigation of photoredox reactions with the nickel complexes was another target which was tackled. Initially the synthesis, characterization and modification of the ligand and the complex was examined. The ligand synthesis could be optimized from literature-known procedures and the nickel complex was obtained in a good yield by adjusting the reaction conditions. Furthermore, it was possible to synthesize the one-electron reduced Ni(I)Mabiq complex. The nickel complexes were characterized using different spectroscopic methods and electronic measurements e.g. NMR, IR, UV-Vis, SC XRD and cyclic voltammetry giving information about the photophysical and electronic properties of the respective complexes. DFT calculations and EPR measurements of the Ni(I) compound revealed a ligand centered radical and Ni(II) central atom. It was not possible to synthesize the formally two-electron reduced complex due to its instability already in the glove-box.

The photoconversion from the Ni(II) to the Ni(I) compound was accomplished by irradiation at $\lambda = 457$ nm of a solution of the complex in dimethylformamide and triethylamine as sacrificial electron donor. The reaction was monitored by UV-Vis. This experiment gave rise to the application in photoredox catalysis. First experiments with literature-known photoredox reactions were unsuccessful. After several attempts, an intramolecular cyclization reaction starting from a bromo-alkyl substituted indole exhibited the first positive results. After optimization of the reaction conditions, the product was isolated in high yield. This catalytic activity led the way to the investigation of the photophysical properties of the nickel complex. Without luminescence the excited state lifetime as well as the excited state redox potential and the quantum yield for the photoconversion needed to be evaluated on a different experimental way. The excited state redox potential was estimated by performing the cyclization reaction using different sacrificial amines with increasing redox potential. The yields dropped significantly with amines with a redox potential higher than ($E_{ox} = + 1.25$ V vs. SCE), resulting in an estimated excited state potential of $[E_{1/2}(\text{Ni}^{*\text{II}}/\text{Ni}^{\text{I}}) = + 1.25$ V vs. SCE]. The excited state lifetime was determined by monitoring the photoconversion by UV-Vis and calculation the quantum yield for that reaction. A literature-known direct correlation between the quantum yield and the lifetime gave rise to the excited state lifetime, depending on the solvent of $\tau = 1\text{-}10$ ns. The photophysical properties might be further evaluated using e.g. transient absorption measurements. Besides the quantum yield for the photoconversion, the quantum

yield for the catalysis was determined using the same experimental set-up and the nickel catalyst as well as the $\text{Ru}(\text{bpy})_3^{2+}$.

After its first success the $[\text{Ni}(\text{Mabiq})]\text{OTf}$ required further utilization in the field of photoredox catalysis. Here, catalytic reactions underlying different mechanistic pathways e.g. oxidative or redox neutral would prove the broad applicability. A new substrate class, incorporating an α -silylalkylamine and a *Michael* acceptor, was investigated. The novel substrate was synthesized in a three-step procedure involving a carbonyl condensation, a radical bromination and a substitution by a secondary α -silylamine. However, after extensive screening of reaction conditions with the nickel photocatalyst no conversion to the product was observed. Contrary, a common iridium photocatalyst proved to be active in the photoredox cyclisation reaction towards tetrahydroisoquinoline compounds. After optimisation, 13 substrates could be converted to the corresponding THIQ product in moderate to good yields. In three cases the formation of diastereoisomers was observed and by the aid of X-Ray analysis the relative configuration of the major diastereoisomer could be solved. To give evidence for the mechanistic pathway, quantum yield experiments were performed and the determined yields hinted towards a closed catalytic cycle with a direct electron transfer to the metal catalyst. Unfortunately, to this date, no further catalytic reaction was found in which the nickel catalyst could be utilized.

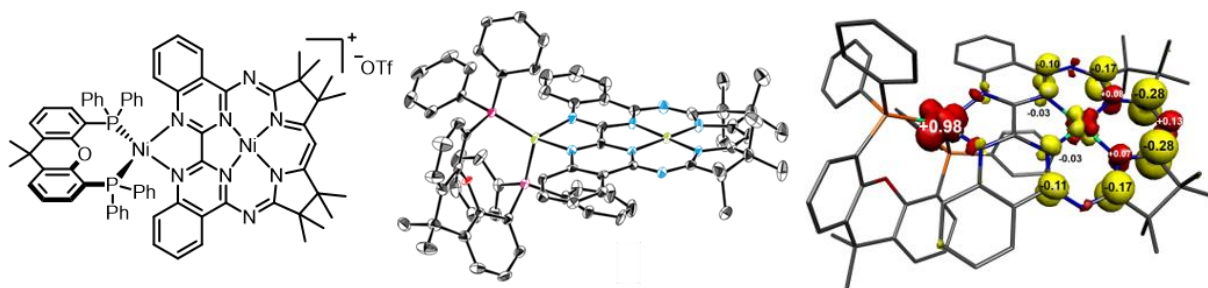


Figure 13: Bimetallic NiNiMabiqXanthphos complex; Middle crystal structure, Right: DFT calculation for electron density distribution.

Furthermore, the goal was to attach a second metal at the outer binding site of the ligand scaffold. It was possible to obtain a complex with two nickel centers at the Mabiq ligand by reaction of $\text{Ni}(\text{II})\text{MabiqOTf}$, additional $\text{Ni}(\text{0})(\text{COD})_2$ salt and a stabilizing xanthphos ligand. The isolated complex was paramagnetic, which suggests a comproportionation of the two nickel atoms resulting in a $\text{Ni}(\text{I})\text{Ni}(\text{I})$ electron distribution. DFT calculations pointed towards an electron density distribution over the ligand and an outer $\text{Ni}(\text{I})$ metal centre, comparable to the monometallic $\text{Ni}(\text{I})$ complex. Further studies including SQUID measurements might contribute to solve the electron distribution throughout the ligand and on the metal centres. Cyclic

voltammetry experiments of the bimetallic complex gave initial information about the redox potentials, though the experiments need to be repeated due to impurities and instability of the samples. Besides characterization, first reactivity studies concerning photoactivity were performed with a sacrificial super donor.

Given the fact, that the [Ni(Mabiq)]OTf complex is active in photoredox transformation further screening for novel reactions is necessary. Possible applications can not only be found in organic transformations but also in light-driven small molecule activation e.g. CO₂ reduction. The utilization of the nickel complex in organic transformations needs further elaboration of mechanistical aspects such as aggregation of substrate and catalyst or kinetic studies. These investigations might also solve the problem of so far only limited applicability of the photoactive catalyst. The photocatalytic activity of the other metal Mabiq complexes (Fe, Co, Cu, Zn) needs to be evaluated and applications need to be found.

Besides all the unsuccessful trails towards ligand modification there are still some starting points for a novel ligand, active in either photoredox catalysis or small molecule activation. The attachment of carboxylic or sulfuric groups would give rise to a water-soluble catalyst. A phenanthroline or bipyridine based catalyst would on the one-hand-side erase the possibility for a bimetallic complex but would also alter the electronic and photophysical properties. Phenanthroline or bipyridine based complexes are also easier to modify due to commercially available precursors or easily synthetically accessible starting materials.

The potential of the bimetallic complexes is still unknown but with further investigation these highly interesting complexes might have properties suitable for catalysis. With the preliminary data in hand, a first glance on highly active bimetallic complexes was given, but further studies with different supporting ligands or different second site metals atoms need to be performed.

In conclusion, the Mabiq ligand in combination with various metal atoms, but especially with a nickel central atom exhibits unique properties concerning light-driven catalysis and further investigation on this metal complex is of high interest.

Zusammenfassung und Ausblick

Basierend auf der starken Nachfrage nach neuartigen, kostengünstigen Metallkomplexen zur Anwendung in der Photokatalyse, fokussiert diese Arbeit auf die Synthese, Charakterisierung und die Modifikation eines Nickel Komplexes mit einem makrocyclischen Liganden. Weiterhin beschäftigte sich diese Arbeit mit der Evaluation von Photoredox-Reaktionen, welche durch den Nickel Komplex katalysiert werden können. Zuerst wurden die Synthese, Charakterisierung und die Modifikation des Liganden und des Komplexes untersucht. Die literatur-bekanntesten Bedingungen für die Ligandensynthese konnten optimiert und der Nickel Komplex konnte nach Reaktionsoptimierung in guten Ausbeuten erhalten werden. Des Weiteren war es möglich, den ein-Elektron reduzierten Ni(I)-Mabiq Komplex zu synthetisieren. Die photophysikalischen und elektronischen Eigenschaften der Nickel Komplexe konnten durch verschiedenste spektroskopische Analysemethoden wie z.B. NMR, IR, UV-Vis, SC XRD und Cyclische Voltammetrie evaluiert werden. Im Falle des Ni(I)Mabiq offenbarten DFT Berechnungen und EPR Experimente die Existenz eines Ligand zentriertes Radikals und eines Ni(II) Metallzentrums. Es war nicht möglich, den formal zweifach reduzierten Metallkomplex herzustellen.

Die photoinduzierte Reduktion des Ni(II) zu dem entsprechenden Ni(I) Komplex konnte durch Bestrahlung einer Lösung des Komplexes in Dimethylformamid in Gegenwart von Triethylamin als Elektrondonor bei einer Wellenlänge von $\lambda = 457 \text{ nm}$ erreicht werden. Die Reaktion konnte mittels UV/Vis Spektroskopie verfolgt werden. Dieses Experiment deutete auf eine mögliche Anwendung in der Photoredox Katalyse hin. Erste Experimente zur Katalyse literatur-bekannteste photoredox Reaktionen schlugen fehl. Schließlich zeigte sich, dass die intramolekulare Cyclisierung eines brom-alkyl substituierten Indolderivats durch den [Ni(Mabiq)]OTf Komplex katalysiert durchgeführt werden kann. Nach Optimierung der Reaktionsbedingungen konnte das Produkt in hoher Ausbeute erhalten werden. Die photophysikalischen Eigenschaften des Nickel Komplexes konnten auf Basis dieser katalytischen Aktivität untersucht werden. Ohne vorhandene Lumineszenz mussten das Redoxpotential im angeregten Zustand, die Lebenszeit des angeregten Zustandes und die Quantenausbeute des photochemischen Umsatzes auf eine alternative Art und Weise Fluoreszenz Lösung bestimmt werden. Um das Redoxpotential im angeregten Zustand zu bestimmen, wurde die Cyclisierungsreaktion mit Elektronendonoren durchgeführt, welche Redoxpotentiale mit einem zunehmendem Wert aufweisen. Ab einem Redoxpotential größer als ($E_{\text{ox}} = + 1.25 \text{ V vs. SCE}$) nahm die Ausbeute des Cyclisierungsprodukts ab. Daraus konnte

ein Redoxpotential für den angeregten Zustand von mindestens $[E_{1/2}(\text{Ni}^{*\text{II}}/\text{Ni}^{\text{I}}) = + 1.25 \text{ V vs. SCE}]$ abgeschätzt werden. Durch eine literatur bekannte Korrelation zwischen der Lebenszeit des angeregten Zustandes und der Quantenausbeute für die licht-induzierte Reduktion des Metallkomplexes konnte eine Lösungsmittel abhängige Lebenszeit des angeregten Zustandes von $\tau = 1 - 10 \text{ ns}$ bestimmt werden. Die Quantenausbeute wurde mit Hilfe von UV-Vis Experimenten bestimmt. Des Weiteren wurde die Quantenausbeute für die Cyclisierungsreaktion unter Verwendung des Nickel Katalysators sowie $\text{Ru}(\text{bpy})_3^{2+}$ bestimmt.

Nach ersten erfolgreichen Photoredox-Experimenten wurde die Suche nach weiteren Anwendungen intensiviert. Die Verwendung des $[\text{Ni}(\text{Mabiq})]\text{OTf}$ Komplexes in Reaktionen mit unterschiedlichem mechanistischem Hintergrund sollte die Anwendbarkeit in der Photoredoxkatalyse untermauern. Eine neue Substratklasse, welche gleichzeitig α -Silylalkylamine und ein *Michael* Akzeptor als strukturelle Einheit enthalten, wurde untersucht. Die neuartigen Substrate konnten in einer drei-stufigen Synthese erhalten werden. Die Sequenz beinhaltete eine Carbonyl Kondensation, eine benzyliche, radikalische Bromierung sowie eine nukleophile Substitution durch eine sekundäres α -Silylalkylamin. Jedoch konnte auch nach intensiver Reaktionsoptimierung mit dem Nickel Katalysator kein Umsatz zum gewünschten Produkt erzielt werden. Ein gängiger Iridium-basierter Photokatalysator erwies sich in der Photocyclisierung zu Tetrahydroisoquinolinprodukten als aktiv. Unter optimierten Bedingungen konnten 13 Substrate zu den entsprechenden THIQ Produkten in mäßigen bis guten Ausbeuten umgesetzt werden. In drei Fällen wurde die Bildung von Diastereomeren beobachtet. Die Relativkonformation im bevorzugten Diastereoisomer konnte durch Röntgenbeugungsexperimente evaluiert werden. Um Hinweise bezüglich des Mechanismus zu erhalten, wurde die Quantenausbeute bestimmt. Diese gab erste Hinweise auf einen geschlossenen Katalysezyklus mit einem direkten Elektronentransfer vom Substrat zum Metallkatalysator.

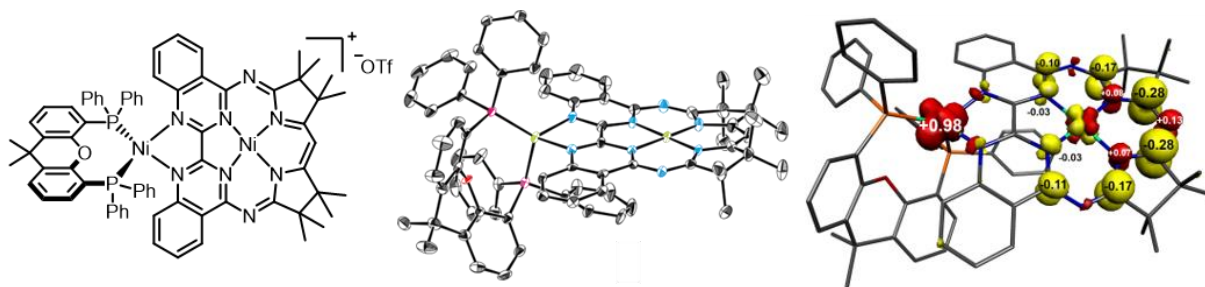


Figure 1314: Bimetallische NiNiMabiqXanthphos Komplexe; Mitte: Kristallstruktur, rechts: DFT Berechnungen der Elektronenverteilung über den Metallkomplex.

Ein weiteres Ziel war es, ein zusätzliches Metall in die zweite Bindungstasche zu koordinieren. Der bimetallischen NiNi Komplex konnte durch Reaktion des Ni(II)MabiqOTf mit Ni(0)(COD)₂ und Xanthphos als stabilisierendem Liganden synthetisiert werden. Der isolierte Komplex weist paramagnetische Eigenschaften auf, was auf eine Komproportionierung der Oxidationzustände der Metallzentren und eine Elektronenverteilung zu einem entsprechenden Ni(I)Ni(I) Komplex hindeutet. DFT Berechnungen untermauerten die Annahme einer Elektronenverteilung über den Liganden welche vergleichbar mit der des monometallischen Ni(I)Mabiq Komplexes und einem äußeren Ni(I) Metallzentrum ist. Weitere Experimente wie z.B. SQUID könnten weitere Informationen bezüglich der Elektronendistribution beisteuern. CV Experimente lieferten erste Informationen bezüglich der Redoxeigenschaften des bimetallischen Komplexes. Jedoch sollten diese Experimente mit hochreinem Metallkomplex erneut durchgeführt werden. Neben der Charakterisierung wurde erste photochemische Experimente mit Superelektronen Donoren durchgeführt.

Weitere Anwendungen für den photoaktiven [Ni(Mabiq)]OTf Komplex in der Photoredoxkatalyse wurden getestet. Nicht nur organische Transformationen, auch die Licht induzierte Aktivierung kleiner Moleküle wie CO₂ stellen dabei eine Option dar. Um weitere Anwendungen in der organischen Photoredoxkatalyse zu finden, sollten zusätzliche mechanistische Studien durchgeführt werden. Kinetische Studien oder Experimente, welche Hinweise auf eine Aggregation zwischen Substrat und Katalysator liefern, könnten auch Probleme bezüglich der bis dato limitierten Anwendbarkeit des Nickel Katalysators lösen. Außerdem sollte die photokatalytische Aktivität der anderen Metall Mabiq Komplexen (Fe, Co, Cu, Zn) untersucht werden.

Neben den nicht erfolgreichen Ligand Modifikationen gab es weitere, noch nicht verfolgte Ansätze, um neuartige Liganden zu designen und zu synthetisieren. Die Installation von Carbon- oder Sulfon-Säuregruppen könnte die Löslichkeit des Liganden stark verbessern. Ein Phenanthrolin- oder Bipyridin-basierter Ligand würde zwar die zweite Bindungsstelle einbüßen, gleichzeitig jedoch die elektronischen und photophysikalischen Eigenschaften des Liganden stark beeinflussen. Diese Art von Liganden wären auch später einfacher zu modifizieren, da alle Edukte käuflich erwerblich oder in wenigen Schritten zu synthetisieren sind.

Das Potential der bimetallischen Komplexe ist immer noch nicht vollständig evaluiert und weitere Untersuchungen bezüglich der Eigenschaften müssen durchgeführt werden. Jedoch deuten die erhaltenen, vorläufigen Daten auf hohe katalytische Aktivität hin. Durch Austausch

des unterstützenden Liganden oder den Einsatz anderer Metalle als sekundäres Zentrum könnten die Eigenschaften des Komplexes weiter angepasst werden.

Zusammenfassend ist zu sagen, dass der Mabiq Ligand in Kombination mit verschiedenen Metallen, im Speziellen mit Nickel, einzigartige Eigenschaften in Licht induzierten Photoreaktionen aufweist und die weitere Untersuchung dieser Komplexe von großem Interesse ist.

Appendix

Supporting Information Redox and photocatalytic properties of a Ni(II) complex with a macrocyclic biquinazoline (Mabiq) ligand.

Electronic Supplementary Information for:

Redox and Photocatalytic Properties of a Ni^{II} Complex with a Macrocyclic Biquinazoline (Mabiq) Ligand

Michael Grübel, Irene Bosque, Philipp J. Altmann, Thorsten Bach, and Corinna R. Hess**

Department of Chemistry and Catalysis Research Center (CRC)
Technische Universität München, 85747 Garching, Germany

Table of Contents

Experimental	2
Materials	2
Physical Measurements	2
Crystallographic Data	3
Density Functional Theory Calculations	4
Photochemical experiments	5
General method for the photocatalytic cyclization	6
Performance of the photocatalytic cyclization using different amines	7
Stoichiometric reaction of 2 with 3	8
Syntheses	9
Molecular Structures	24
Molecular Structure of Ni(Mabiq)OTf (1)	24
Molecular structure of Ni(Mabiq) (2)	27
Molecular structure of Cy ₂ NCH ₂ Mes (6f)	30
EPR Data for Ni(Mabiq) (2)	34
DFT Computational Data	35
ESI-MS of Ni(Mabiq)OTf (1) after the photocatalytic reaction	43
Cyclic Voltammetry (CV) experiments	44
Cyclic Voltammogram of Ni(Mabiq)OTf (1)	44
Cyclic Voltammograms for Amines 6a to 6n	45
Chemical actinometry: Determination of the photon-flux	53
Emission spectra of the LED (455 nm)	57
Determination of the quantum yield for the photoconversion of 1 to 2	58
Determination of the quantum yield for the photocatalytic conversion of 3 to 4	63
Absorption spectra of Ni(Mabiq)OTf (1) in the presence of Et ₃ N (6a) or Cy ₂ NCH ₂ Mes (6f)	65
NMR Spectra	66
References	100

Experimental

Materials

Chemicals were purchased from *Sigma Aldrich* and used without further purification, unless otherwise mentioned. Nickel containing compounds were synthesized and handled under Argon atmosphere, using Schlenk techniques or in a glovebox, using anhydrous solvents. Tetrahydrofuran (THF), diethyl ether (Et₂O), pentane (P) and dichloromethane (DCM) were purified using a MBSPS 800 *MBraun* solvent purification system. All solvents were deoxygenized via freeze-pump-thaw procedure prior to use. Dimethylformamide (DMF; 99.8% stored over molecular sieves) and Triethylamine (TEA; >99.5% BioUltra) (**6a**) were purchased as anhydrous grade from *Sigma Aldrich*. *N,N*-dimethylbenzylamine (**6h**) was purchased from *Sigma Aldrich*. Tetrabutylammonium hexafluorophosphate was recrystallized four times from EtOH before use. Ferrocene was sublimed before use.

Physical Measurements

Solution state NMR spectra were recorded at room temperature on a *Bruker* AVA 400. ¹H-NMR spectra were calibrated to the residual solvent signal of chloroform-d₁ (CHCl₃ δ = 7.26 ppm). ¹³C-NMR spectra were calibrated to the ¹³C-D triplet of CDCl₃ (δ = 77.16 ppm). The following abbreviations for single multiplicities were used: s-singlet, d-doublet, t-triplet, q-quartet, quin.-quintet. X-band EPR spectra were recorded on a JEOL JES-FA 200 spectrometer. Electronic spectra were measured on a Shimadzu UV-3600 Plus UV-vis-NIR spectrophotometer or an Agilent Cary 60 UV-vis spectrophotometer.

ESI mass spectra were measured on a Thermo Scientific™ UltiMate™ 3000 HPLC System using loop mode. Microanalyses were carried out at the Technische Universität München. Electrochemical measurements were carried out with an EmStat³⁺ potentiostat using a three-electrode cell equipped with glassy carbon working and counter electrode and a Ag/AgNO₃ or a Pt wire as reference electrode. Potentials are reported with reference to an internal standard of ferrocenium/ferrocene (Fc⁺⁰). Infrared spectra were recorded on a PerkinElmer IR 4100 spectrometer directly measuring in substance via a total reflexion method (ATR). Intensities are assigned as: w = weak, m = medium, s = strong. GC analysis was performed on an Agilent 7890B instrument (FID) with a HP 5 column (30 mm × 320 μm, 0.25 μm).

Crystallographic Data

Data were collected on an X-ray single crystal diffractometer equipped with a CMOS detector (Bruker Photon-100), a IMS microsource with MoK α radiation ($\lambda = 0.71073 \text{ \AA}$) and a Helios mirror optic by using the APEX III software package.^[1] The measurements were performed on a single crystal coated with perfluorinated ether. The crystal was fixed on top of a microsampler, transferred to the diffractometer and frozen under a stream of cold nitrogen. A matrix scan was used to determine the initial lattice parameters. Reflections were merged and corrected for Lorentz and polarization effects, scan speed, and background using SAINT.^[2] Absorption corrections, including odd and even ordered spherical harmonics, were performed using SADABS.^[2] Space group assignments were based upon systematic absences, E statistics, and successful refinement of the structures. Structures were solved by direct methods with the aid of successive difference Fourier maps, and were refined against all data using SHELXLE^[3] in conjunction with SHELXL-2014^[4]. Hydrogen atoms were assigned to ideal positions and refined using a riding model with an isotropic thermal parameter 1.2 times that of the attached carbon atom (1.5 times for methyl hydrogen atoms). If not mentioned otherwise, non-hydrogen atoms were refined with anisotropic displacement parameters. Full-matrix least-squares refinements were carried out by minimizing $\sum w(F_o^2 - F_c^2)^2$ with SHELXL-97^[5] weighting scheme. Neutral atom scattering factors for all atoms and anomalous dispersion corrections for the non-hydrogen atoms were taken from International Tables for Crystallography.^[6] Images of the crystal structures were generated by PLATON.^{[7]-[8]}

Density Functional Theory Calculations

Density Functional Theory (DFT) calculations were performed with the ORCA program package.^[9] Geometry optimizations of the complexes were performed at either the BP86^{[10]-[11]} (1) or the B3LYP^{[12]-[14]} (2) level of DFT. The all-electron Gaussian basis sets were those developed by the Ahlrich's group.^{[15]-[16]} Triple- ζ quality basis sets (TZV(P)) with one set of polarization functions on the metals and on the atoms directly coordinated to the metal center were used.^[16] For the carbon and hydrogen atoms, slightly smaller polarized split-valence SV(P) basis sets were used that were of double- ζ quality in the valence region and contained a polarizing set of d functions on the non-hydrogen atoms. Auxiliary basis sets used to expand the electron density in the resolution-of-the-identity (RI) approach were chosen,^{[17]-[18]} where applicable, to match the orbital basis. SCF calculations were tightly converged (1×10^{-8} Eh in energy, 1×10^{-7} Eh in the density change, and 1×10^{-7} Eh in maximum element of the DIIS error vector). Geometry optimizations were carried out in redundant internal coordinates without imposing symmetry constraints. In all cases the geometries were considered converged after the energy change was less than 5×10^{-6} Eh, the gradient norm and maximum gradient element were smaller than 1×10^{-4} and 3×10^{-4} Eh Bohr⁻¹, respectively, and the root-mean square and maximum displacements of all atoms were smaller than 2×10^{-3} and 4×10^{-3} Bohr, respectively. Orbital/spin density plots were created using GaussView.^[19]

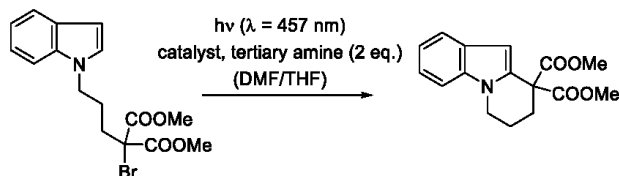
TD-DFT calculations were performed on the optimized using the B3LYP functional (Triple- ζ quality basis sets (def2-TZVP) were used for all atoms), with dichloromethane as the solvent. The conductor like screening model (COSMO) was used for all calculations and RIJCOSX approximation^[20] combined with appropriate Ahlrichs auxiliary basis sets were routinely employed to speed up the calculations.^{[17],[21]} Relativistic effects were accounted for using the zero order regular approximation (ZORA).^[22] The first 40 states were calculated, whereas the maximum dimension of the expansion space in the Davidson procedure (MAXDIM) was set to 400. The full width at half maximum (FWHM) was set to 3000 cm⁻¹.

Photochemical experiments

All photochemical experiments were carried out using the set-up previously described.^[23]

Photoconversion experiments using a LED were carried out in a preheated Schlenk tube (diameter 1 cm) with a polished quartz rod as an optical fiber, which was roughened by sandblasting at one end. 20.0 mg (267 μ mol) of [Ni(Mabiq)]OTf were dissolved in 5.0 ml of a solvent mixture (TEA/MeCN/THF: 2/2/1 or TEA/DMF: 1/4). The reaction mixture was deoxygenated once via a *freeze-pump-thaw* cycle and the glass rod was placed inside the solution under an Ar atmosphere. The solution was protected from light and the LED was switched on.

General method for the photocatalytic cyclization



A flame dried Schlenk-tube was charged with 90.7 μmol (1.00 eq.) of dimethyl 2-(3-(1H-indol-1-yl)propyl)-2-bromomalonate, 1.81 μmol (0.02 eq.) or 0.91 μmol (0.01 eq.) of catalyst and 0.18 mmol, (2.00 eq.) of the corresponding tertiary amine in 3.0 ml of a solvent mixture of THF/DMF (4/1 or 2/1). The mixture was deoxygenated three times by the freeze-pump-thaw procedure. The Schlenk-tube was equipped with the LED and the reaction was irradiated for 13 h. The reaction was stopped by addition of 5.0 ml water and 10 ml Et₂O. The aqueous phase was extracted with Et₂O (3 x 15 ml). The combined organic layers were dried over Na₂SO₄ and the solvent removed under vacuum. The residue subsequently was purified by chromatography on SiO₂ (20:1, P/EtOAc).

TLC: R_f (EtOAc/Pentane 1:4) 0.38 [UV]

The NMR data for the product are in agreement with literature values.^[24]

¹H NMR (400 MHz, CDCl₃, 300K): δ (ppm) = 7.60 (dt, ³J = 8.0, 1.0 Hz, 1H), 7.29 (dq, ³J = 8.1, 0.9 Hz, 1H), 7.21 (ddd, ³J = 8.2, 7.0, 1.2 Hz, 1H), 7.12 (ddd, ³J = 8.0, 7.0, 1.1 Hz, 1H), 6.60 (d, ³J = 0.9 Hz, 1H), 4.08 (t, ³J = 6.2 Hz, 2H), 3.80 (s, 6H), 2.57 – 2.51 (m, 2H), 2.17 – 2.08 (m, 2H).

¹³C NMR (101 MHz, CDCl₃, 300K): δ (ppm) = 170.4, 136.4, 131.0, 127.6, 121.8, 120.8, 120.2, 109.2, 102.2, 56.2, 53.3, 42.0, 28.9, 19.9.

Performance of the photocatalytic cyclization using different amines

The oxidation potentials of the various amines were measured by cyclic voltammetry (see Figures S9-S22) and the photocatalytic cyclization was performed using the amines as sacrificial donors following the general method described above. The yields of **4** + **5** were obtained after column chromatography in a ratio of 95:5 cyclized to hydro-de-brominated product as determined by ¹H-NMR.

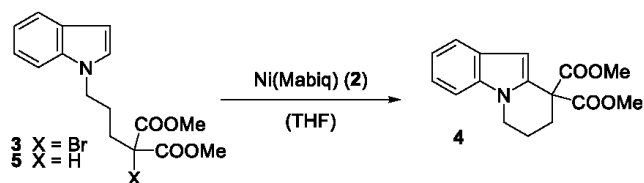
Table S1: Yields of the photocatalytic reaction using different amines with varied oxidation potentials.

$3 \text{ X} = \text{Br}$
 $5 \text{ X} = \text{H}$

$\text{hv } (\lambda = 457 \text{ nm})$
 $\text{Ni}(\text{Mebiq})\text{OTf } (2 \text{ mol}\%)$
 $\text{Amine } (2 \text{ eq.})$
 (DMF/THF)

4

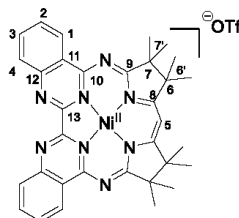
Amine	$E_{1/2}$ (V vs. SCE)	Yield 4+5 [%]	Amine	$E_{1/2}$ (V vs. SCE)	Yield 4+5 [%]
	6f 0.78 V	84%		6i 1.22 V	84%
	6a 0.83 V	84%		6c 1.25 V	95%
	6g 0.93 V	97%		6d 1.41 V	40%
	6h 0.99 V	89%		6m 1.43 V	65%
	6l 1.05 V	91%		6e 1.59 V	20%, 21% (2 runs)
	6b 1.05 V	97%		6n 1.61	32%
	6j 1.08 V	90%			
	6k 1.20 V	85%			

Stoichiometric reaction of 2 with 3

In a Schlenk tube, 13.7 mg (22.8 μmol , 1.00 eq.) of **2** and 8.40 mg (22.8 μmol , 1.00 eq.) of **3** were each dissolved in 5 ml anhydrous THF. The substrate was added to the catalyst and the mixture was stirred for three hours. The reaction was stopped by adding 5 ml water. The aqueous phase was extracted with Et₂O (3 x 10 ml), the organic phase dried over Na₂SO₄ and the solvents were removed under vacuum. 3.21 mg (11.2 μmol , 49 %) of the product mixture of **4** and **5** was obtained after chromatography on SiO₂ (20:1, P/EtOAc).

Syntheses

[Ni^{II}(Mabiq)]OTf (1)



C₃₄H₃₃F₃N₈NiO₃S
Mw: 749.44 g/mol

Ni(OTf)₂ (98.6 mg, 276 μmol, 1.00 eq.) was added in one portion to a solution containing 150 mg (276 μmol, 1.00 eq.) HMabiq in 10.0 ml EtOH and 40.2 μL (290 μmol, 1.10 eq.) NEt₃. The reaction mixture was stirred for 48 h at 60°C, during which time the product precipitated as a yellow powder. The suspension was cooled to ambient temperature, and the solution was filtered. Diffusion of hexane into a solution of the crude product in DCM, yielded 175 mg (84 %, 0.23 mmol) of **1** as yellow needles suitable for X-ray analysis.

¹H NMR (400 MHz, CDCl₃, 300K): δ (ppm) = 9.15 (ddd, ³J = 8.3, ⁴J = 1.5, ⁵J = 0.59 Hz, 2H, H1), 8.50 (ddd, ³J = 8.4, ⁴J = 1.1, ⁵J = 0.6 Hz, 2H, H4), 8.20 (ddd, ³J = 8.4, ³J = 7.0, ⁴J = 1.5 Hz, 2H, H3), 7.95 (ddd, ³J = 8.3, ³J = 7.04, ⁴J = 1.1 Hz, 2H, H2), 6.77 (s, 1H, H5), 1.46 (s, 24H, H6' & H7').

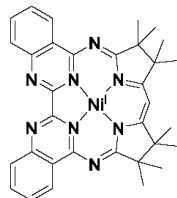
¹³C NMR (101 MHz, CDCl₃, 300K): δ (ppm) = 186.8 (C8), 179.2 (C9), 155.8 (C10), 153.3 (C13), 150.2 (C11), 136.7 (C3), 130.6 (C2), 129.3 (C4), 127.2 (C1), 123.1 (C12), 97.5 (C5), 52.1 (C6), 51.8 (C7), 24.6 (C7'), 23.8 (C6')

Anal. Calcd for C₃₄H₃₃F₃N₈NiO₃S (*M_r* = 749.44 g mol⁻¹): C, 54.49; H, 4.44; N, 14.95; S, 4.28 %. Found: C, 54.42; H, 4.31; N, 14.97; S, 4.21 %.

FTIR: ν cm⁻¹: 2978 (w, L), 2293 (w), 1603 (m), 1578 (m), 1562 (m), 1508 (m), 1467 (s), 1368 (m), 1262 (s, OTf), 1239 (m), 1220 (m), 1029 (s, OTf), 775 (s).

UV-Vis (in CH₂Cl₂): λ / nm 310 (ε = 44500 M⁻¹ cm⁻¹), 366 (ε = 16300 M⁻¹ cm⁻¹), 414 (ε = 13600 M⁻¹ cm⁻¹), 437 (ε = 16400 M⁻¹ cm⁻¹), 457 (ε = 22300 M⁻¹ cm⁻¹).

ESI-MS *m/z* (rel. Int. %): 599.63 (100) [⁵⁸M-OTf]⁺, 601.48 [⁶⁰M-OTf]⁺.

[Ni^I(Mabiq)] (2)

C₃₃H₃₃N₈Ni
Mw: 600.38 g/mol

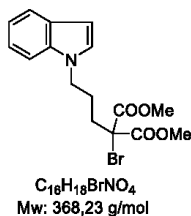
A mixture of 50.0 mg (66.7 μmol , 1.00 eq.) **1** and 12.6 mg (66.7 μmol , 1.0 eq.) CoCp₂ in 10 ml MeCN was stirred for 12 h at room temperature. A distinct colour change from yellow to green was observed directly after addition of the solvent. The mixture was filtered, the solid was washed three times with 2.0 ml MeCN, and the solvent removed under reduced pressure, affording 34 mg (85 %, 56.6 μmol) of crude **2** as a green powder. Single crystals suitable for X-ray diffraction were obtained via diffusion from THF/Hexane, yielding 24 mg (62 %, 41.6 μmol) of **2**.

Anal. Calcd for C₃₃H₃₃N₈Ni ($M_r = 744.17 \text{ g mol}^{-1}$): C, 66.02; H, 5.54; N, 18.66; %. Found: C, 65.48; H, 5.60; N, 18.39 %.

FTIR: $\nu \text{ cm}^{-1}$: 3066 (w), 2969 (s), 2905 (m), 2863 (m), 2549 (m), 1581 (m), 1561 (m), 1525 (s), 1483 (s), 1466 (s), 1439 (s), 1387 (m), 1360 (s), 1336 (m), 1326 (m), 1313 (m), 1273 (m), 1233 (s), 1183 (m), 1151 (m), 1132 (s), 1111 (m), 1084 (m), 1067 (m), 1031 (m), 1016 (m), 966 (m), 957 (m), 932 (m), 906 (m), 870 (m), 862 (m), 848 (m), 825 (m), 796 (w), 790 (w), 766 (s), 739 (m), 726 (s), 689 (m), 675 (s), 654 (m).

UV-Vis (in THF): λ / nm : 297 ($\epsilon = 23300 \text{ M}^{-1} \text{ cm}^{-1}$), 329 ($\epsilon = 26200 \text{ M}^{-1} \text{ cm}^{-1}$), 435 ($\epsilon = 9200 \text{ M}^{-1} \text{ cm}^{-1}$), 474 ($\epsilon = 2700 \text{ M}^{-1} \text{ cm}^{-1}$), 641 ($\epsilon = 1400 \text{ M}^{-1} \text{ cm}^{-1}$), 711 ($\epsilon = 3500 \text{ M}^{-1} \text{ cm}^{-1}$), 801 ($\epsilon = 5400 \text{ M}^{-1} \text{ cm}^{-1}$).

ESI-MS m/z (rel. Int. %): 599.59 (100) [⁵⁸M]⁺, 601.51 [⁶⁰M]⁺.

Dimethyl 2-(3-(1H-indol-1-yl)propyl)-2-bromomalonate (3)

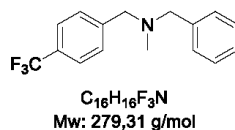
The compound was synthesized according to literature procedure, with the following modification.^[24] NaH was used, instead of NaHMDS, in the reaction procedure. A reaction mixture of 260 mg (0.89 mmol, 1.00 eq.) dimethyl 2-(3-(1H-indol-1-yl)propyl)-malonate, 41.3 mg (1.03 mmol, 1.15 eq.) NaH and 175 mg (0.98 mmol, 1.1 eq.) NBS in 50 ml dry THF afforded 300 mg (91 %, 0.82 mmol) **3** after purification by chromatography on SiO₂ (9:1, Pentane/EtOAc) (5 h reaction time)

TLC: R_f (EtOAc/Pentane 1:4) 0.41 [UV]

The NMR data matched reported literature values.^[24]

¹H NMR (400 MHz, CDCl₃, 300K): δ (ppm) = 7.63 (d, ³J = 7.7 Hz, 1H), 7.32 (d, ³J = 8.3 Hz, 1H), 7.21 (t, ³J = 7.7 Hz, 1H), 7.13 – 7.08 (m, 2H), 6.50 (d, ³J = 3.1 Hz, 1H), 4.18 (t, ³J = 6.9 Hz, 2H), 3.71 (s, 6H), 2.34 – 2.25 (m, 2H), 2.06 – 1.94 (m, 2H).

¹³C NMR (101 MHz, CDCl₃, 300K): δ (ppm) = 167.2, 135.9, 128.8, 127.7, 121.7, 121.2, 119.5, 109.3, 101.5, 62.0, 54.0, 45.7, 35.7, 26.3.

***N*-benzyl-*N*-methyl-(4-trifluoromethyl)benzylamine (6b)**

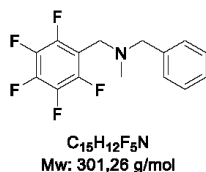
To a solution of 500 mg (2.09 mmol, 1.00 eq.) 4-(Trifluoromethyl)-benzylbromide in 4.00 ml anhydrous THF, 270 μ L (253 mg, 2.09 mmol, 1.00 eq) of *N*-benzylmethylamine was added dropwise. The reaction mixture was stirred for 16 h at room temperature. The suspension was diluted in 10 mL EtOAc and treated with saturated NaHCO₃ solution (10 ml). The aqueous phase was extracted with EtOAc (3 x 10 ml), the combined organic phases were dried over Na₂SO₄ and the solvent was removed under reduced pressure. Purification by column chromatography (P/EtOAc 10/1 – 4/1) afforded the product. 422 mg (72%, 1.51 mmol) of the product was obtained as a yellow oil.

TLC: R_f (EtOAc/Pentane 1:4) 0.62 [UV]

¹H NMR (400 MHz, CD₂Cl₂, 300K): δ (ppm) = 7.59 (d, ³J = 8.1 Hz, 1H), 7.52 (d, ³J = 8.1 Hz, 1H), 7.41 – 7.29 (m, 2H), 7.28 – 7.22 (m, 1H), 3.57 (s, 1H), 3.54 (s, 1H), 2.17 (s, 2H).

¹³C NMR (101 MHz, CD₂Cl₂, 300K): δ (ppm) = 144.8, 139.9, 129.6, 129.4, 128.8, 127.6, 125.6 (q, ¹J = 3.9 Hz), 62.5, 61.7, 42.6.

HRMS (ESI): [M+H]⁺ calculated for C₁₆H₁₆F₃N: 280.1308; found: 280.1308.

***N*-benzyl-*N*-methyl-2,3,4,5,6-pentafluorobenzylamine (6c)**

To a solution of 500 mg (1.92 mmol, 1.00 eq.) 2,3,4,5,6-pentafluorobenzylbromide in 4.00 ml anhydrous THF, 247 μ L (232 mg, 1.92 mmol, 1.00 eq) of *N*-benzylmethylamine was added dropwise. The reaction mixture was stirred for 16 h at room temperature. The suspension was diluted in 10 mL EtOAc and treated with saturated NaHCO₃ solution (10 ml). The aqueous phase was extracted with EtOAc (3 x 10 ml), the combined organic phases were dried over Na₂SO₄ and the solvent was removed under reduced pressure. Purification by column chromatography (P/EtOAc 10/1 – 4/1) afforded the product. 434 mg (75%, 1.44 mmol) of the product was obtained as a yellow oil.

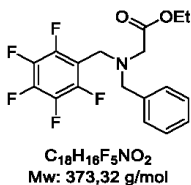
TLC: R_f (EtOAc/Pentane 1:4) 0.64 [UV]

¹H NMR (400 MHz, CD₂Cl₂, 300K): δ (ppm) = 7.35 – 7.22 (m, 5H), 3.71 (s, 2H), 3.56 (s, 2H), 2.17 (s, 3H).

¹³C NMR (101 MHz, CD₂Cl₂, 300K): δ (ppm) = 139.4, 129.4, 128.7, 127.7, 62.3, 48.6, 41.8.

HRMS (ESI): [M+H]⁺ calculated for C₁₅H₁₂F₅N: 302.0963; found: 302.0963.

Ethyl *N*-benzyl-*N*-(2,3,4,5,6-pentafluoro)benzylglycinate (6d)



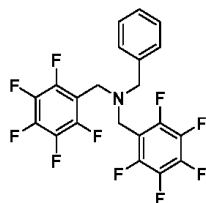
To a flame dried 25 mL round-bottom flask containing 242 mg (2.3 mmol, 1.10 equiv.) of Na_2CO_3 , were added 5 mL of THF followed by 300 mg (1.04 mmol, 1.00 equiv.) of *N*-benzyl-2,3,4,5,6-pentafluorobenzylamine. The mixture was stirred at room temperature for 10 min. Then, 128 μ L of ethyl bromoacetate (1.15 mmol, 1.10 equiv.) were added and the reaction mixture was stirred at room temperature for 12 h. The heterogeneous mixture was filtered and the filtrate was concentrated and the crude product was purified by column chromatography (95:5 to 9:1 hexane:EtOAc) to give 356 mg of product (91% yield) as a colorless oil.

TLC: R_f (EtOAc/Pentane 1:4) 0.51 [UV]

1H NMR (400 MHz, $CDCl_3$, 400K): δ (ppm) = 7.37 – 7.27 (m, 4H), 7.30 – 7.21 (m, 1H), 4.19 (q, $^3J = 7.1$ Hz, 2H), 4.08 (s, 2H), 3.92 (s, 2H), 3.33 (s, 2H), 1.30 (t, $^3J = 7.1$ Hz, 3H).

^{13}C NMR (101 MHz, $CDCl_3$, 300K): δ (ppm) = 170.9, 145.7 (d, $^1J = 247.1$ Hz), 140.6 (d, $^1J = 253.3$ Hz), 138.3, 137.2 (d, $^1J = 252.8$ Hz), 128.7, 128.3, 127.4, 111.9 (t, $^1J = 19.0$ Hz), 60.4, 57.9, 53.1, 44.9, 14.2.

HRMS (ESI): $[M+H]^+$ calculated for $C_{18}H_{16}F_5NO_2$: 374.1174; found: 374.1174.

***N,N*-bis-(2,3,4,5,6-pentafluorobenzyl)benzylamine (6e)**

$C_{21}H_{11}F_{10}N$
Mw: 467,31 g/mol

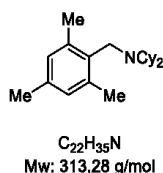
To a flame dried 25 mL round-bottom flask containing 439 mg (8.4 mmol, 2.10 equiv.) of Na_2CO_3 , were added 5 mL of THF followed by 1.25 mL (8.4 mmol, 2.10 equiv.) of 2,3,4,5,6-pentafluorobenzyl bromide. The mixture was stirred at room temperature for 10 min. 440 μ L (4.02 mmol) of benzylamine were added and the reaction mixture was stirred at room temperature for 12 h. The heterogeneous mixture was filtered and the filtrate was concentrated. The crude product was purified by column chromatography (95:5 to 9:1 hexane:EtOAc) to give 1.30 g of an inseparable 1:2 mixture of desired product and 2,3,4,5,6-pentafluorobenzyl bromide as a colorless oil, and 509 mg (44% yield) of *N*-benzyl-*N*-(2,3,4,5,6-pentafluorobenzyl)amine as a white solid. The desired product was separated from the excess 2,3,4,5,6-pentafluorobenzyl bromide by the addition of this mixture to a stirred mixture of 316 μ L (2.9 mmol, 1 equiv. with respect to the remaining 2,3,4,5,6-pentafluorobenzyl bromide) of benzylamine and 307 mg (2.9 mmol, 1 equiv. with respect to the remaining 2,3,4,5,6-pentafluorobenzyl bromide) of Na_2CO_3 in 5 mL of THF. The reaction mixture was stirred for 12 h and subsequently filtered. The filtrate was evaporated and the crude material was purified by column chromatography (95:5 to 9:1 hexane:EtOAc) to give 660 mg of **6e** (37% yield after the two steps) as a colorless oil, and 631 mg (76% yield) of *N*-benzyl-*N*-perfluorobenzylamine as a white solid.

TLC: R_f (EtOAc/Pentane 1:9) 0.62 [UV]

1H NMR (400 MHz, $CDCl_3$, 300K): δ (ppm) = 7.38 – 7.11 (m, 5H), 3.78 (s, 4H), 3.64 (s, 2H).

^{13}C NMR (101 MHz, $CDCl_3$, 300K): δ (ppm) 145.63 (d, $^1J = 240.1$ Hz), 140.7 (d, $^1J = 254.0$ Hz), 137.9, 137.3 (d, $^1J = 253.0$ Hz), 128.3, 128.1, 127.4, 111.7 (t, $^1J = 17.3$ Hz), 58.3, 45.7.

HRMS (ESI): $[M+H]^+$ calculated for $C_{21}H_{11}F_{10}N$: 468.0805; found: 468.0804.

***N*-(2,4,6-trimethylbenzyl)dicyclohexylamine (6f)**

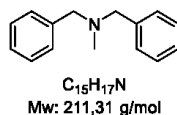
To a suspension of 400 mg (2.9 mmol, 2.90 eq.) in 2.00 ml anhydrous DMF in a pressure tube, 600 μ L (3.00 mmol, 3.00 eq) of dicyclohexylamine were added followed by 169 mg (1.00 mmol, 1.00 eq) of 2,4,6-trimethylbenzyl chloride. The tube was sealed and the reaction mixture was stirred for 72 h at 140 °C. The mixture was allowed to reach room temperature and the suspension was diluted in 10 mL EtOAc and filtered. The filtrate was concentrated under reduced pressure. Purification by column chromatography (pentane/EtOAc 40:1) afforded 131 mg of product (42%, 0.42 mmol) as a white solid. Further recrystallization from DMF afforded the product as colorless needles.

TLC: R_f (pentane/EtOAc 30:1) 0.48 [UV]

¹H NMR (400 MHz, CDCl₃, 300K): δ (ppm) = 6.78 (s, 2H), 3.72 (s, 2H), 2.44 – 2.37 (m, 2H), 2.36 (s, 6H), 2.25 (s, 3H), 1.78 – 1.64 (m, 8H), 1.60 – 1.52 (m, 2H), 1.49 – 1.29 (m, 4H), 1.25 – 0.96 (m, 6H).

¹³C NMR (101 MHz, CDCl₃, 300K): δ (ppm) = 138.3, 135.5, 133.8, 128.9, 56.5, 43.7, 32.1, 26.68, 26.3, 20.8, 20.3.

HRMS (ESI): [M+H]⁺ calculated for C₂₂H₃₆N: 314.2842; found: 314.2841.

***N*-benzyl-*N*-methylbenzylamine (6g)**

To a solution of 347 μ l (500 mg, 2.92 mmol, 1.00 eq.) benzylbromide in 4.00 ml anhydrous THF, 377 μ l (354 mg, 2.92 mmol, 1.00 eq) of *N*-benzylmethylamine was added dropwise. The reaction mixture was stirred for 16 h at room temperature. The suspension was diluted in 10 mL EtOAc and treated with saturated $NaHCO_3$ solution (10 ml). The aqueous phase was extracted with EtOAc (3 x 10 ml), the combined organic phases were dried over Na_2SO_4 and the solvent was removed under reduced pressure. Purification by column chromatography (P/EtOAc 10/1 – 4/1) afforded the product. 512 mg (83%, 2.42 mmol) of the product was obtained as a yellow oil.

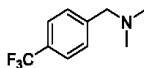
TLC: R_f (EtOAc/Pentane 1:4) 0.54 [UV]

1H NMR (400 MHz, $CDCl_3$, 300K): δ (ppm) = 7.44 – 7.18 (m, 10H), 3.53 (s, 4H), 2.19 (s, 3H).

^{13}C NMR (101 MHz, $CDCl_3$, 300K): δ (ppm) = 139.5, 129.1, 128.4, 127.1, 62.0, 42.4.

The NMR data matched reported literature values.^[25]

HRMS (ESI): $[M+H]^+$ calculated for $C_{15}H_{17}N$: 212.1434; found: 212.1434.

***N,N*-dimethyl-(4-trifluoromethyl)benzylamine (6i)**

$C_{10}H_{12}F_3N$
Mw: 203,21 g/mol

To a solution of 1.00 g (4.18 mmol, 1.00 eq.) of 4-(Trifluoromethyl)benzylbromide in 4.00 ml anhydrous Et₂O, 4.14 ml (3.14 g, 20.9 mmol, 5.00 eq.) of a 30 wt% Diethylamine solution was added in one portion. The reaction mixture was stirred for 12 h at room temperature. The suspension was diluted in 10 ml Et₂O and extracted with 1 M HCl solution. The combined aqueous phases were neutralized with 2 M NaOH solution until a precipitate formed. The aqueous phase was then extracted with 20 ml Et₂O. The combined organic phases were dried over Na₂SO₄ and the solvent was removed under reduced pressure. 838 mg (98%, 4.12 mmol) of the **6h** was obtained as a clear oil.

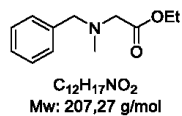
TLC: R_f (EtOAc/Pentane 1:4) 0.41 [UV]

¹H NMR (400 MHz, CDCl₃, 300K): δ (ppm) = 7.57 (d, ³J = 8.0 Hz, 2H), 7.43 (d, ³J = 8.0 Hz, 2H), 3.47 (s, 2H), 2.25 (s, 6H).

¹³C NMR (101 MHz, CDCl₃, 300K): δ (ppm) = 143.2, 129.14, 125.2 (q, ¹J = 3.8 Hz), 63.8, 45.4.

The NMR data matched reported literature values.^[26]

HRMS (ESI): [M+H]⁺ calculated for C₁₀H₁₂F₃N: 204.0995; found: 204.0995

Ethyl *N*-benzyl-*N*-methylglycinate (6j)

To a solution of 1.93 ml (1.81 g, 15.0 mmol, 1.25 eq.) *N*-benzylmethylamine in 20.0 ml anhydrous MeCN, 1.33 mL (2.00 g, 12.0 mmol, 1.00 eq) of ethylbromoacetate was added dropwise at 0°C. The reaction mixture was stirred for 16 h at room temperature. The suspension was diluted in 20 mL Et₂O and treated with NaHCO₃ solution (40 ml). The aqueous phase was extracted with Et₂O (3 x 30 ml), the combined organic phases were dried over Na₂SO₄ and the solvent was removed under reduced pressure. Purification by column chromatography (P/EtOAc 10/1 – 4/1) afforded the product. 1.26 g (51%, 6.08 mmol) of the product was obtained as a yellow oil.

TLC: R_f (EtOAc/Pentane 1:4) 0.58 [UV]

¹H NMR (400 MHz, CDCl₃, 300K): δ (ppm) = 7.38 – 7.21 (m, 5H), 4.18 (q, ³J = 7.1 Hz, 2H), 3.68 (s, 2H), 3.25 (s, 2H), 2.39 (s, 3H), 1.27 (t, ³J = 7.1 Hz, 3H).

¹³C NMR (101 MHz, CDCl₃, 300K): δ (ppm) = 171.1, 138.3, 129.3, 128.4, 127.3, 61.3, 60.5, 57.7, 42.4, 14.4.

The NMR data matched reported literature values.^[27]

HRMS (ESI): [M+H]⁺ calculated for C₁₂H₁₇NO₂: 208.1332; found: 208.1332.

***N,N*-dimethyl-2,3,4,5,6-pentafluorobenzylamine (6k)**

To a solution of 1.00 g (3.83 mmol, 1.00 eq.) of 2,3,4,5,6-Pentafluorobenzylbromide in 4.00 ml anhydrous Et₂O, 3.79 ml (2.88 g, 19.2 mmol, 5.00 eq.) of a 30 w% diethylamine solution was added in one portion. The reaction mixture was stirred for 12 h at room temperature. The suspension was diluted in 10 ml Et₂O and extracted with 1 M HCl solution. The combined water phases were neutralized with 2 M NaOH solution until a precipitate formed. The aqueous phase was extracted with 20 ml Et₂O. The combined organic phases were dried over Na₂SO₄ and solvent removed under reduced pressure. 830 mg (96%, 3,69 mmol) of the product was obtained as a clear oil.

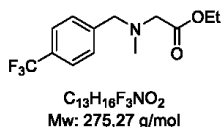
TLC: R_f (EtOAc/Pentane 1:4) 0.41 [UV]

¹H NMR (400 MHz, CDCl₃, 300K): δ (ppm) = 7.57 (d, ³J = 8.0 Hz, 1H), 7.43 (d, ³J = 8.0 Hz, 1H), 3.47 (s, 1H), 2.25 (s, 3H).

¹³C NMR (126 MHz, CDCl₃, 300K): δ (ppm) = 145.5 (dddd, ¹J = 247.4, ²J = 13.8, ²J = 8.6, ⁴J = 4.0 Hz), 140.5 (dddd, ¹J = 253.4, ²J = 18.9, ³J = 12.7, ⁴J = 5.4 Hz), 137.3 (dddd, ¹J = 251.1, ²J = 17.6, ³J = 12.5, ⁴J = 4.8 Hz), 110.8 (td, ²J = 18.7, ³J = 3.7 Hz), 49.4, 44.5.

The NMR data matched reported literature values.^[28]

HRMS (ESI): [M+H]⁺ calculated for C₁₀H₁₂F₅N: 204.0995; found: 204.0995.

Ethyl *N*-(4-trifluoromethyl)benzyl-*N*-methylglycinate (6l)

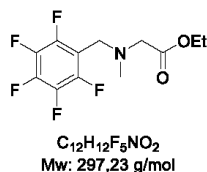
To a solution of 856 mg (3.58 mmol, 1.10 eq.) 4-(Trifluoromethyl)-benzylbromide and 288 μ l (282 mg, 3.58 mmol, 1.10 eq.) pyridin in 10 ml anhydrous CH₂Cl₂, 500 mg (3.26 mmol, 1.00 eq) of sarcosineethylester hydrochloride in 10 ml anhydrous CH₂Cl₂ was added dropwise at 0°C. The reaction mixture was stirred for 16 h at room temperature. The suspension was diluted in 25 mL CH₂Cl₂ and treated with saturated NaHCO₃ solution (25 ml). The aqueous phase was extracted with CH₂Cl₂ (3 x 20 ml), the combined organic phases were dried over Na₂SO₄ and the solvent was removed under reduced pressure. Purification by column chromatography (P/EtOAc 10/1 – 4/1) afforded the product. 312 mg (35%, 1.13 mmol) of the product could be obtained as a yellow oil.

TLC: R_f (EtOAc/Pentane 1:4) 0.58 [UV]

¹H NMR (400 MHz, CDCl₃, 300K): δ (ppm) = 7.57 (d, ³J = 8.0 Hz, 2H), 7.47 (d, ³J = 8.0 Hz, 2H), 4.18 (q, ³J = 7.1 Hz, 2H), 3.74 (s, 2H), 3.27 (s, 2H), 2.38 (s, 3H), 1.28 (t, ³J = 7.1 Hz, 3H).

¹³C NMR (101 MHz, CDCl₃, 300K): δ (ppm) = 171.0, 142.9, 129.3, 125.4 (q, ¹J = 3.8 Hz), 60.7, 60.6, 57.9, 42.4, 14.4.

HRMS (ESI): [M+H]⁺ calculated for C₁₃H₁₆F₃NO₂: 276.1206; found: 276.1206.

Ethyl *N*-methyl-*N*-(2,3,4,5,6-pentafluoro)benzylglycinate (6m)

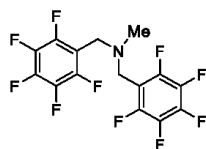
To a solution of 934 mg (3.58 mmol, 1.10 eq.) 2,3,4,5,6-pentafluorobenzoylbromide and 288 μ l (283 mg, 3.58 mmol, 1.10 eq.) pyridin in 10 ml anhydrous CH_2Cl_2 , 500 mg (3.26 mmol, 1.00 eq) of sarcosineethyl ester hydrochloride in 10 ml anhydrous CH_2Cl_2 was added dropwise at 0°C. The reaction mixture was stirred for 16 h at room temperature. The suspension was diluted in 25 mL CH_2Cl_2 and treated with saturated $NaHCO_3$ solution (25 ml). The aqueous phase was extracted with CH_2Cl_2 (3 x 20 ml), the combined organic phases were dried over Na_2SO_4 and the solvent was removed under reduced pressure. Purification by column chromatography (P/EtOAc 10/1 – 4/1) afforded the product. 161 mg (17%, 542 μ mol) of the product was obtained as a yellow oil.

TLC: R_f (EtOAc/Pentane 1:4) 0.54 [UV]

1H NMR (400 MHz, $CDCl_3$, 300K): δ (ppm) = 4.19 (q, $^3J = 7.1$ Hz, 2H), 3.93 (s, 2H), 3.30 (s, 2H), 2.40 (s, 3H), 1.28 (t, $^3J = 7.1$ Hz, 3H).

^{13}C NMR (101 MHz, $CDCl_3$, 300K): δ (ppm) = 170.6, 145.8 (dddd, $^1J = 247.5$, $^2J = 15.0$, $^3J = 8.5$, $^4J = 4.1$ Hz), 140.8 (ddd, $^1J = 253.5$, $^2J = 13.3$, $^3J = 2.5$ Hz), 137.5 (ddd, $^1J = 251.1$, $^2J = 17.6$, $^3J = 12.5$ Hz), 110.3 (td, $^2J = 18.7$, $^3J = 3.7$ Hz), 60.8, 57.5, 47.0, 41.7, 14.4.

HRMS (ESI): $[M+H]^+$ calculated for $C_{12}H_{12}F_5NO_2$: 298.0861; found: 298.0861.

***N,N*-bis-(2,3,4,5,6-pentafluorobenzyl)methylamine (6n)**

$C_{15}H_7F_{10}N$
Mw: 391,04 g/mol

To a flame dried 25 mL round-bottom flask containing 773 mg (5.6 mmol, 2.1 equiv.) of K_2CO_3 were added 5 mL of THF followed by 850 μ L (5.6 mmol, 2.1 equiv.) of 2,3,4,5,6-pentafluorobenzyl bromide. The mixture was stirred at room temperature for 10 min. 1.34 mL of a 2M solution of methylamine in THF (2.7 mmol, 1 equiv.) were added and the reaction mixture was stirred at room temperature for 72 h. The heterogeneous mixture was filtered and the filtrate was concentrated. The crude product was purified by column chromatography (98:2 to 95:5 hexane:EtOAc) to give 942 mg of product (89% yield) as a colorless oil.

TLC: R_f (EtOAc/Pentane 1:9) 0.62 [UV]

1H NMR (400 MHz, $CDCl_3$, 300K): δ (ppm) = 3.77 (s, 4H), 2.24 (s, 3H)

^{13}C NMR (101 MHz, $CDCl_3$, 300K): δ (ppm) = 145.8 (dddd, $^1J = 247.8$, $^2J = 14.9$, $^3J = 8.3$, $^4J = 4.0$ Hz), 141.0 (dddd, $^1J = 253.7$, $^2J = 18.7$, $^3J = 13.3$, $^4J = 5.3$ Hz), 138.6 (ddd, $^1J = 251.1$, $^2J = 17.6$, $^3J = 12.5$ Hz), 111.2 (t, $^2J = 17.9$ Hz), 48.0, 40.7.

HRMS (ESI): $[M+H]^+$ calculated for $C_{15}H_7F_5N$: 392.0492; found: 392.0492.

Molecular Structures

Molecular Structure of Ni(Mabiq)OTf (1)

A clear yellow fragment-like specimen of $C_{35}H_{35}Cl_2F_3N_8NiO_3S$, approximate dimensions 0.110 mm x 0.126 mm x 0.245 mm, was used for the X-ray crystallographic analysis. The X-ray intensity data were measured on a Bruker D8 Venture Duo IMS system equipped with a Helios optic monochromator and a Mo IMS microsource ($\lambda = 0.71073 \text{ \AA}$).

A total of 1843 frames were collected. The total exposure time was 15.36 hours. The frames were integrated with the Bruker SAINT software package using a narrow-frame algorithm. The integration of the data using a triclinic unit cell yielded a total of 39797 reflections to a maximum 2θ angle of 25.68° (0.82 Å resolution), of which 6667 were independent (average redundancy 5.969, completeness = 99.8%, $R_{int} = 3.99\%$, $R_{sig} = 2.51\%$) and 5772 (86.58%) were greater than $2\sigma(F_2)$. The final cell constants of $a = 10.0222(8) \text{ \AA}$, $b = 12.1506(11) \text{ \AA}$, $c = 16.0254(14) \text{ \AA}$, $\alpha = 69.063(4)^\circ$, $\beta = 75.075(4)^\circ$, $\gamma = 81.389(4)^\circ$, volume = $1757.6(3) \text{ \AA}^3$, are based upon the refinement of the XYZ-centroids of 125 reflections above $20 \sigma(I)$ with $4.544^\circ < 2\theta < 43.92^\circ$. Data were corrected for absorption effects using the Multi-Scan method (SADABS). The ratio of minimum to maximum apparent transmission was 0.933. The calculated minimum and maximum transmission coefficients (based on crystal size) are 0.8230 and 0.9140.

The structure was solved and refined using the Bruker SHELXTL Software Package in conjunction with SHELXL, using the space group $P -1$, with $Z = 2$ for the formula unit, $C_{35}H_{35}Cl_2F_3N_8NiO_3S$. The final anisotropic full-matrix least-squares refinement on F_2 with 725 variables converged at $R_1 = 2.88\%$, for the observed data and $wR_2 = 7.55\%$ for all data. The goodness-of-fit was 1.032. The largest peak in the final difference electron density synthesis was 0.451 e-/\AA^3 and the largest hole was -0.438 e-/\AA^3 with an RMS deviation of 0.053 e-/\AA^3 . On the basis of the final model, the calculated density was 1.577 g/cm^3 and $F(000)$, 860 e-.

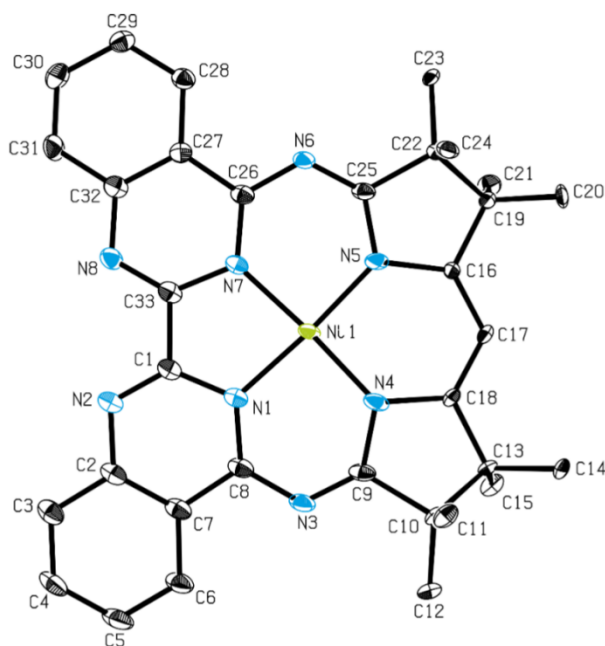


Figure S1: ORTEP style representation of **1**. Ellipsoids are shown at the 50% probability level. Hydrogen atoms, dichloromethane molecule and triflate counterion are omitted for clarity.

Table S2: Sample and crystal data for **1**.

Identification code	GruMi1 AP8017-100	
Chemical formula	$C_{35}H_{35}Cl_2F_3N_8NiO_3S$	
Formula weight	834.38	
Temperature	100 (2) K	
Wavelength	0.71073 Å	
Crystal size	0.110 x 0.126 x 0.245 mm	
Crystal habit	Clear yellow fragment	
Crystal system	Triclinic	
Space group	P -1	
Unit cell dimensions	a = 10.0222 (8) Å	$\alpha = 69.063 (4)$
	b = 12.1506 (11) Å	$\beta = 75.075 (4)$
	c = 16.0254 (14) Å	$\gamma = 81.389 (4)$
Volume	1757.6 (3) Å ³	
Z	2	
Density	1.577 g/cm ³	
Absorption	0.839 mm ⁻¹	
F (000)	860	

Table S3: Data collection and structure refinement of **1**.

Diffractometer	Bruker D8 Venturo Duo IMS		
Radiation source	IMS microsource, Mo		
Theta range for data collection	2.48 to 25.68°		
Index ranges	-12<=h<=12, -14<=k<=14, -19<=l<=19		
Reflections collected	39797		
Independent reflections	667 [R(int) = 0.0399]		
Coverage of independent reflections	99.8 %		
Absorption correction	Multi-Scan		
Max. and. Min. transmission	0.9149 and 0.8230		
Structure solution technique	Direct methods		
Structure solution program	XT, VERSION 2014/4		
Refinement method	Full-matrix least-squares on F ²		
Refinement program	SHELXL-2014/7 (Sheldrick, 2014)		
Function minimized	$\sum w (F_o^2 - F_c^2)^2$		
Data/ restraints / parameters	6667 / 381 / 725		
Goodness-of-fit on F²	1.032		
Δ / σ_{\max}	0.001		
Final R indices	5772 data; I>2 σ	R1 = 0.0288,	wR2 = 0.0711
	All data	R1 = 0.0375	wR2 = 0.0755
Weighting scheme	$w = 1/[\sigma^2/(F_o^2) + (0.0390P)^2 + 0.9346P]$		
	Where P = (F _o ² +2F _c ²)/3		
Largest diff. peak and hole	0.451 and -0.438 eÅ ⁻³		
R.M.S. deviation from mean	0.053 eÅ ⁻³		

Molecular structure of Ni(Mabiq) (2)

A green needle-like specimen of $C_{33}H_{33}N_8Ni$, approximate dimensions 0.040 mm x 0.055 mm x 0.417 mm, was used for the X-ray crystallographic analysis. The X-ray intensity data were measured on a Bruker D8 Venture Duo IMS system equipped with a Helios optic monochromator and a Mo IMS microsource ($\lambda = 0.71073 \text{ \AA}$).

A total of 2322 frames were collected. The total exposure time was 58.05 hours. The frames were integrated with the Bruker SAINT software package using a narrow-frame algorithm. The integration of the data using an orthorhombic unit cell yielded a total of 192057 reflections to a maximum θ angle of 25.03° (0.84 \AA resolution), of which 9767 were independent (average redundancy 19.664, completeness = 99.9%, $R_{int} = 8.57\%$, $R_{sig} = 3.29\%$) and 8669 (88.76%) were greater than $2\sigma(F_2)$. The final cell constants of $a = 10.1802(7) \text{ \AA}$, $b = 20.4136(17) \text{ \AA}$, $c = 26.689(2) \text{ \AA}$, volume = $5546.4(7) \text{ \AA}^3$, are based upon the refinement of the XYZ-centroids of 9623 reflections above $2\sigma(I)$ with $4.471^\circ < 2\theta < 50.39^\circ$. Data were corrected for absorption effects using the Multi-Scan method (SADABS). The ratio of minimum to maximum apparent transmission was 0.875. The calculated minimum and maximum transmission coefficients (based on crystal size) are 0.7480 and 0.9710.

The structure was solved and refined using the Bruker SHELXTL Software Package in conjunction with SHELXLE, using the space group P 21 21 21, with $Z = 8$ for the formula unit, $C_{33}H_{33}N_8Ni$. The final anisotropic full-matrix least-squares refinement on F_2 with 773 variables converged at $R_1 = 3.08\%$, for the observed data and $wR_2 = 6.73\%$ for all data. The goodness-of-fit was 0.946. The largest peak in the final difference electron density synthesis was 0.221 e-/\AA^3 and the largest hole was -0.312 e-/\AA^3 with an RMS deviation of 0.052 e-/\AA^3 . On the basis of the final model, the calculated density was 1.438 g/cm^3 and $F(000)$, 2520 e-.

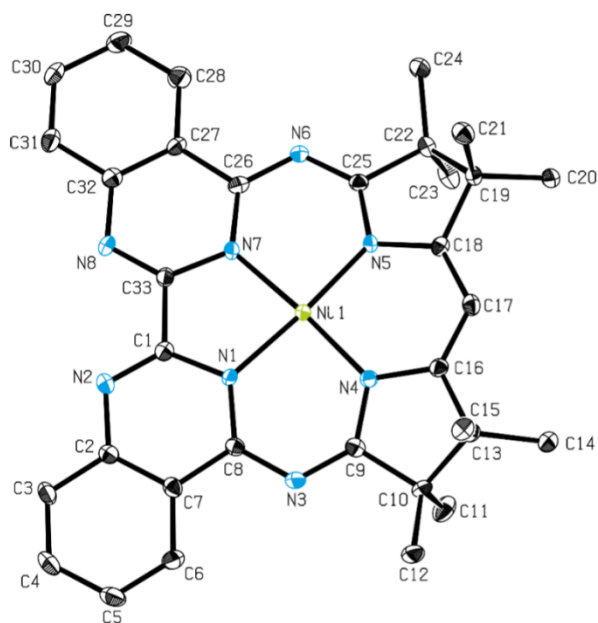


Figure S2: ORTEP style representation of **2**. Ellipsoids are shown at the 50% probability level. Hydrogen atoms are omitted for clarity.

Table S4: Sample and Crystal data for **2**.

Identification code	GruMi1 AP8030-100	
Chemical formula	$C_{33}H_{33}N_8Ni$	
Formula weight	600.38	
Temperature	100 (2) K	
Wavelength	0.71073 Å	
Crystal size	0.040 x 0.055 x 0.417 mm	
Crystal habit	Green needle	
Crystal system	Orthorhombic	
Space group	P 21 21 21	
Unit cell dimensions	a = 10.1802 (7) Å	$\alpha = 90^\circ$
	b = 20.4136 (17) Å	$\beta = 90^\circ$
	c = 26.689 (2) Å	$\gamma = 90^\circ$
Volume	5546.4 (7) Å ³	
Z	8	
Density	1.438 g/cm ³	
Absorption	0.740 mm ⁻¹	
F (000)	2520	

Table S5: Data collection and structure refinement for 2.

Diffractometer	Bruker D8 Venturo Duo IMS		
Radiation source	IMS microsource, Mo		
Theta range for data collection	2.24 to 25.03°		
Index ranges	-12<=h<=12, -24<=k<=24, -31<=l<=31		
Reflections collected	192057		
Independent reflections	9767 [R(int) = 0.0857]		
Coverage of independent reflections	99.9 %		
Absorption correction	Multi-Scan		
Max. and Min. transmission	0.9710 and 0.7480		
Structure solution technique	Direct methods		
Structure solution program	XT, VERSION 2014/4		
Refinement method	Full-matrix least-squares on F ²		
Refinement program	SHELXL-2014/7 (Sheldrick, 2014)		
Function minimized	$\sum w (F_o^2 - F_c^2)^2$		
Data/ restraints / parameters	9767 / 0 / 773		
Goodness-of-fit on F²	0.946		
Δ / σ_{\max}	0.001		
Final R indices	8669 data; I>2 σ	R1 = 0.0308,	wR2 = 0.0632
	All data	R1 = 0.0410	wR2 = 0.0673
Weighting scheme	$w = 1/[\sigma^2/(F_o^2) + (0.0248P)^2 + 6.2581P]$		
	Where $P = (F_o^2 + 2F_c^2)/3$		
Absolute structure parameter	0.5 (0)		
Largest diff. peak and hole	0.221 and -0.312 eÅ ⁻³		
R.M.S. deviation from mean	0.052 eÅ ⁻³		

Molecular structure of $\text{C}_{22}\text{H}_{35}\text{N}$ (6f)

A clear colourless fragment-like specimen of $\text{C}_{22}\text{H}_{35}\text{N}$, approximate dimensions 0.136 mm x 0.139 mm x 0.174 mm, was used for the X-ray crystallographic analysis. The X-ray intensity data were measured on a Bruker D8 Venture system equipped with a Helios optic monochromator and a Mo TXS rotating anode ($\lambda = 0.71073 \text{ \AA}$).

A total of 1272 frames were collected. The total exposure time was 1.57 hours. The frames were integrated with the Bruker SAINT software package using a narrow-frame algorithm. The integration of the data using a monoclinic unit cell yielded a total of 33127 reflections to a maximum θ angle of 25.03° (0.84 \AA resolution), of which 3359 were independent (average redundancy 9.862, completeness = 99.9%, $R_{\text{int}} = 3.67\%$, $R_{\text{sig}} = 1.81\%$) and 2978 (88.66%) were greater than $2\sigma(F_2)$. The final cell constants of $a = 17.6983(15) \text{ \AA}$, $b = 6.2954(6) \text{ \AA}$, $c = 17.4420(15) \text{ \AA}$, $\beta = 102.677(3)^\circ$, volume = $1896.0(3) \text{ \AA}^3$, are based upon the refinement of the XYZ-centroids of 117 reflections above $20 \sigma(I)$ with $7.564^\circ < 2\theta < 48.35^\circ$. Data were corrected for absorption effects using the Multi-Scan method (SADABS). The ratio of minimum to maximum apparent transmission was 0.905. The calculated minimum and maximum transmission coefficients (based on crystal size) are 0.9890 and 0.9920.

The final anisotropic full-matrix least-squares refinement on F^2 with 211 variables converged at $R_1 = 3.92\%$, for the observed data and $wR_2 = 10.02\%$ for all data. The goodness-of-fit was 1.061. The largest peak in the final difference electron density synthesis was 0.180 e-/\AA^3 and the largest hole was -0.202 e-/\AA^3 with an RMS deviation of 0.038 e-/\AA^3 . On the basis of the final model, the calculated density was 1.098 g/cm^3 and $F(000)$, 696 e-.

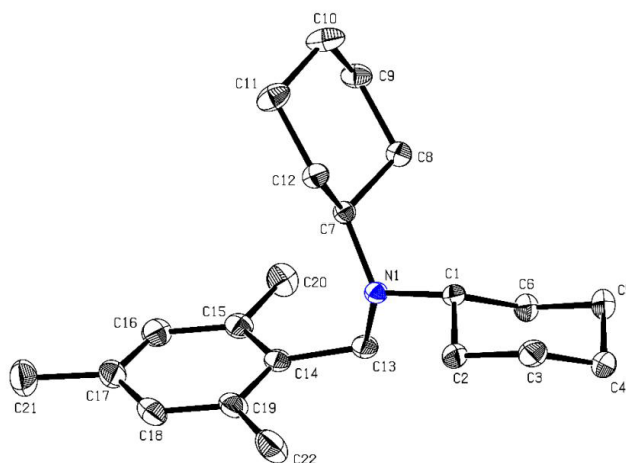


Figure S3: ORTEP style representation of **6f**. Ellipsoids are shown at the 50% probability level. Hydrogen atoms are omitted for clarity.

Table S6: Sample and Crystal data for **6f**.

Identification code	GruMi20 AP9266-135	
Chemical formula	$C_{22}H_{35}N$	
Formula weight	313.51	
Temperature	135 (2) K	
Wavelength	0.71073 Å	
Crystal size	0.136 x 0.139 x 0.174 mm	
Crystal habit	Clear colourless fragment	
Crystal system	monoclinic	
Space group	P 1 21/c1	
Unit cell dimensions	a = 17.6983 (15) Å	$\alpha = 90^\circ$
	b = 6.2954 (6) Å	$\beta = 102.677 (3)^\circ$
	c = 17.4420 (15) Å	$\gamma = 90^\circ$
Volume	1896.0 (7) Å ³	
Z	4	
Density	1.098 g/cm ³	
Absorption	0.062 mm ⁻¹	
F (000)	696	

Table S7: Data collection and structure refinement for **6f**.

Diffractometer	Bruker D8 Venture
Radiation source	TXS rotating anode, Mo
Theta range for data collection	2.36 to 25.03°
Index ranges	-21<=h<=21, -7<=k<=7, -20<=l<=20
Reflections collected	33127
Independent reflections	3359 [R(int) = 0.0367]
Coverage of independent reflections	99.9 %
Absorption correction	Multi-Scan
Max. and. Min. transmission	0.9920 and 0.9890

Structure solution technique	Direct method		
Structure solution program	XT, VERSION 2014/4		
Refinement method	Full-matrix least-squares on F^2		
Refinement program	SHELXL-2014/7 (Sheldrick, 2014)		
Function minimized	$\Sigma w (F_o^2 - F_c^2)^2$		
Data/ restraints / parameters	3359 / 0 / 221		
Goodness-of-fit on F^2	1.061		
Δ / σ_{\max}	0.001		
Final R indices	2978 data; $ >2\sigma$	R1 = 0.0391,	wR2 = 0.0964
	All data	R1 = 0.0445	wR2 = 0.1002
Weighting scheme	$w = 1/[\sigma^2/(F_o^2) + (0.0455P)^2 + 0.7786P]$		
	Where $P = (F_o^2 + 2F_c^2)/3$		
Absolute structure parameter	0.5 (0)		
Largest diff. peak and hole	0.180 and -0.202 $e\text{\AA}^{-3}$		
R.M.S. deviation from mean	0.038 $e\text{\AA}^{-3}$		

Table S8: Selected bond distances for **1** and **2**.

	1	2
Ni1-N5	1.8599(15)	1.871(3)
Ni1-N4	1.8599(16)	1.873(3)
Ni1-N7	1.8861(15)	1.891(3)
Ni1-N1	1.8885(14)	1.894(3)
N3-C9	1.288(2)	1.313(5)
N4-C9	1.372(2)	1.352(5)
N4-C18	1.481(4)(N4-C18a 1.302(4))	1.390(5)
N6-C25	1.285(2)	1.314(5)
N5-C25	1.363(2)	1.351(5)
N5-C16	1.482(4)(N5-C16a 1.297(4))	1.389(5)
C16-C17	1.381(4)(C16a-C17a 1.386(4))	1.374(5)
C17-C18	1.375(5)(C17a-C18a 1.383(5))	1.370(5)
C16-C19	1.516(4)	1.516(5)
C13-C18	1.519(4)	1.513(5)

EPR Data for Ni(Mabiq) (2)

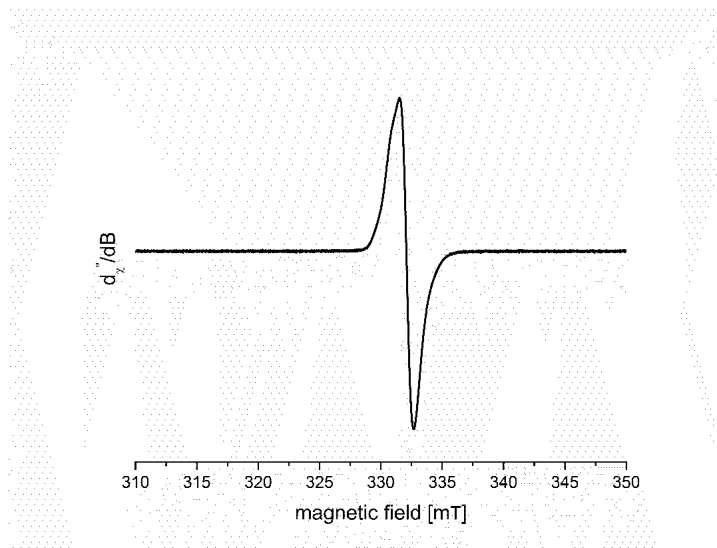


Figure S4: EPR data for **2** in THF at 140 K, frequency = 9.265 GHz, mod. Amp. = 100 G, power = 0.4 mW

DFT Computational Data

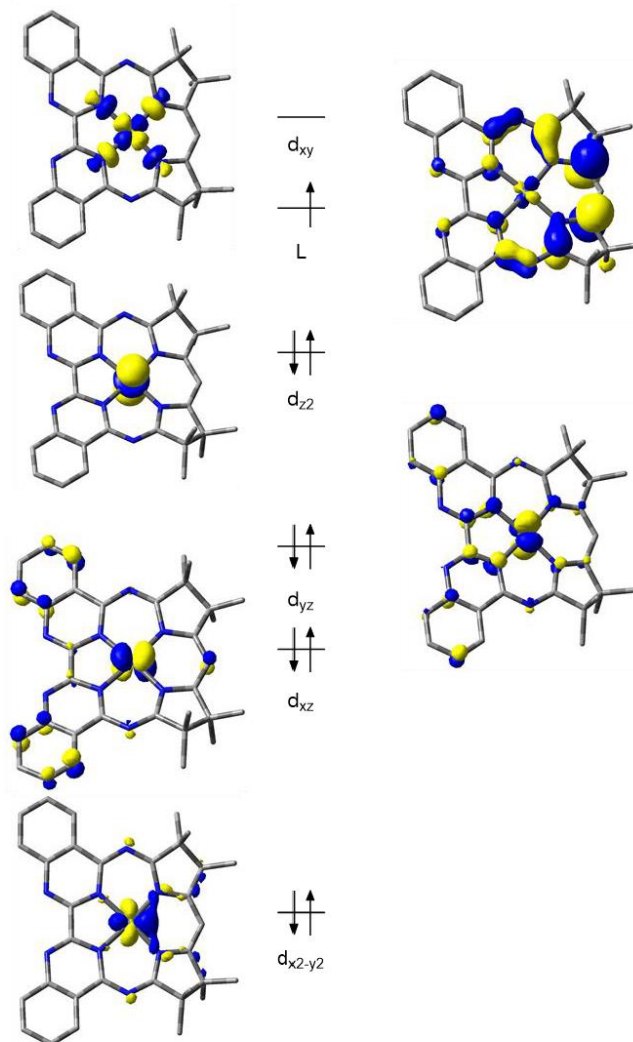


Figure S5: DFT-derived (B3LYP) qualitative MO diagram of **2**.

Table S9: DFT-derived (B3LYP, UKS) Löwdin atomic charges and spin population for **2**.-----
LOEWDIN ATOMIC CHARGES AND
SPIN POPULATIONS

0 Ni:	-0.062782	0.030413
1 N :	-0.005364	0.034975
2 N :	-0.058331	0.023622
3 N :	-0.135668	0.009777
4 N :	0.021644	-0.038146
5 N :	0.021302	-0.037944
6 N :	-0.135733	0.009957
7 N :	-0.005326	0.034850
8 N :	-0.058293	0.023558
9 C :	0.018471	-0.006404
10 C :	0.004359	0.007854
11 C :	-0.109773	0.000230
12 C :	-0.104640	0.010991
13 C :	-0.117509	-0.000522
14 C :	-0.092874	0.009824
15 C :	-0.052655	-0.002523
16 C :	0.055213	0.044715
17 C :	0.045312	0.117837
18 C :	-0.068280	0.001360
19 C :	-0.295378	0.000496
20 C :	-0.291145	0.007548
21 C :	-0.063440	-0.003515
22 C :	-0.291365	0.016174
23 C :	-0.297371	0.003549
24 C :	0.015015	0.291700
25 C :	-0.188980	-0.095639
26 C :	0.015161	0.291265
27 C :	-0.063407	-0.003503
28 C :	-0.291497	0.016152
29 C :	-0.297485	0.003494
30 C :	-0.068442	0.001399
31 C :	-0.295087	0.000468
32 C :	-0.291214	0.007519
33 C :	0.045397	0.117291
34 C :	0.055405	0.044444
35 C :	-0.052742	-0.002483
36 C :	-0.092709	0.009759
37 C :	-0.117636	-0.000497
38 C :	-0.104721	0.010912
39 C :	-0.109562	0.000256

40 C : 0.004352 0.007791
41 C : 0.018608 -0.006383
42 H : 0.131877 -0.000027
43 H : 0.123530 -0.000365
44 H : 0.122381 0.000011
45 H : 0.131615 -0.000327
46 H : 0.119976 0.000105
47 H : 0.109743 0.000078
48 H : 0.115182 -0.000096
49 H : 0.114554 -0.000215
50 H : 0.112701 0.000584
51 H : 0.119933 -0.000318
52 H : 0.116325 -0.000415
53 H : 0.112800 0.002639
54 H : 0.112918 -0.000088
55 H : 0.115315 0.000231
56 H : 0.112642 -0.000053
57 H : 0.115025 0.000433
58 H : 0.125896 0.003006
59 H : 0.116243 -0.000423
60 H : 0.112938 -0.000077
61 H : 0.113011 0.002625
62 H : 0.115358 0.000236
63 H : 0.115043 0.000434
64 H : 0.112683 -0.000047
65 H : 0.115095 -0.000092
66 H : 0.109637 0.000073
67 H : 0.120005 0.000112
68 H : 0.120002 -0.000315
69 H : 0.112715 0.000579
70 H : 0.114561 -0.000208
71 H : 0.131632 -0.000324
72 H : 0.122414 0.000011
73 H : 0.123566 -0.000362
74 H : 0.131855 -0.000028

Table S10: DFT-optimized (B3LYP, UKS) geometry (.XYZ format) for the monomeric unit of **2**.

```

-----
CARTESIAN COORDINATES (ANGSTROEM)
-----
Ni -0.014436  0.018188  0.106099
N  -1.447801 -1.266475  0.141766
N  -3.821927 -1.377673 -0.149570
N  -0.203437 -3.228146  0.661655
N   1.283214 -1.363237  0.330066
N   1.300647  1.400895  0.045893
N  -0.161928  3.312350 -0.014034
N  -1.430928  1.301267 -0.124729
N  -3.802968  1.380152 -0.443471
C  -2.696839 -0.731329 -0.090584
C  -3.784193 -2.730325  0.068556
C  -4.988805 -3.472077  0.006782
C  -4.973870 -4.836951  0.241535
C  -3.761365 -5.497417  0.545281
C  -2.571821 -4.787702  0.608384
C  -2.565719 -3.395433  0.367589
C  -1.350378 -2.598393  0.394406
C   0.976904 -2.644633  0.629048
C   2.233236 -3.434380  1.000757
C   2.157433 -4.914772  0.608234
C   2.377629 -3.332557  2.540385
C   3.329076 -2.592030  0.247611
C   3.486730 -3.053545 -1.224820
C   4.713335 -2.601925  0.913813
C   2.652656 -1.224171  0.235792
C   3.295060 -0.005429  0.072843
C   2.668448  1.228913 -0.014984
C   3.361263  2.563081 -0.277869
C   3.519648  2.717300 -1.813200
C   4.746931  2.688852  0.372734
C   2.276534  3.552233  0.291107
C   2.219466  4.927061 -0.385505
C   2.420268  3.756167  1.820688
C   1.010630  2.719962  0.079303
C  -1.316350  2.655176 -0.152789
C  -2.520482  3.444815 -0.351045
C  -2.507925  4.856681 -0.405029
C  -3.687637  5.553132 -0.619166
C  -4.908587  4.859758 -0.784111
C  -4.941741  3.476221 -0.730565
C  -3.747378  2.747980 -0.510904

```

C	-2.686910	0.745749	-0.246080
H	-5.911013	-2.933962	-0.225477
H	-5.905607	-5.409616	0.193992
H	-3.763138	-6.576027	0.730639
H	-1.627132	-5.282607	0.838853
H	1.399470	-5.429369	1.221038
H	3.130954	-5.410324	0.780457
H	1.875422	-5.057910	-0.446605
H	2.476993	-2.285364	2.875676
H	3.260299	-3.894138	2.893308
H	1.483781	-3.763219	3.023463
H	2.514998	-3.095575	-1.746596
H	3.952734	-4.052988	-1.282906
H	4.132266	-2.344901	-1.772253
H	4.708290	-2.127237	1.908184
H	5.452920	-2.067613	0.291304
H	5.078631	-3.638845	1.027539
H	4.383542	-0.021912	-0.007417
H	2.545447	2.672858	-2.330368
H	4.148106	1.900823	-2.209562
H	4.003744	3.675591	-2.071437
H	4.737620	2.423555	1.442013
H	5.126472	3.722376	0.276014
H	5.478044	2.030670	-0.129553
H	1.947500	4.862070	-1.450428
H	3.196480	5.438238	-0.302893
H	1.461247	5.558230	0.106057
H	1.531321	4.283130	2.207776
H	3.308192	4.369007	2.055243
H	2.510470	2.796684	2.359345
H	-1.556764	5.376143	-0.278812
H	-3.675069	6.646657	-0.661974
H	-5.832424	5.422205	-0.953012
H	-5.870756	2.913636	-0.850400

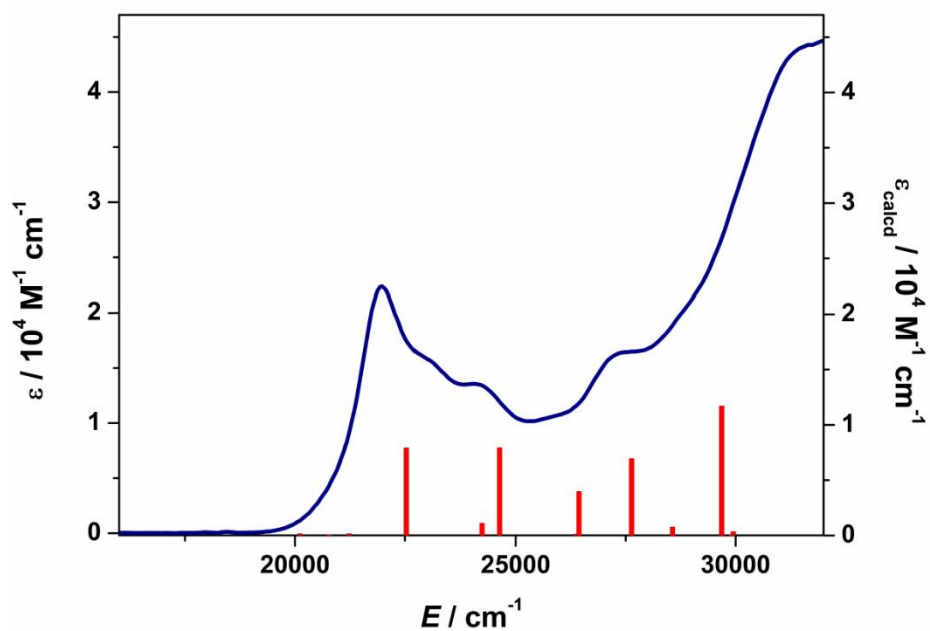


Figure S6: Calculated (B3LYP) electronic absorption spectrum for **1**.

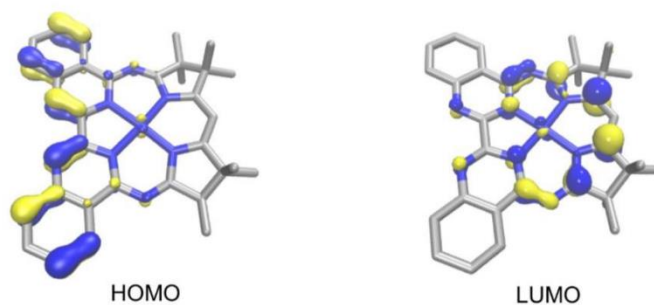


Figure S7: Orbitals involved in the electronic transition calculated at 22,532 cm^{-1} of **1**.

Table S11: DFT-optimized (BP86) coordinates for **1**.

Ni	0.05896768067087	0.01125961724558	0.07875142176482
N	-1.30389672401400	1.34211427903215	0.20670282654254
N	-3.64860743173783	1.54197828550295	0.71659820275700
N	0.00297864949814	3.29821002671260	-0.22445283849090
N	1.39803509496731	1.32966071862351	-0.06393807329299

N	1.30878107950911	-1.39633496309796	0.00515063342351
N	-0.21067012916504	-3.27550740113458	-0.09535505622629
N	-1.38953805317275	-1.22177025097025	0.24524864435922
N	-3.74759924319598	-1.24805181766321	0.73290787328206
C	-2.56812561033255	0.84183918037599	0.49386776530804
C	-3.55585188299511	2.90382561343707	0.65857200738819
C	-4.70964950973742	3.69505153716963	0.91346308822739
C	-4.61907416443092	5.08169178389264	0.84151337947031
C	-3.38729625550859	5.71189793622875	0.51125429392084
C	-2.24504404374482	4.95623741531668	0.25688826217288
C	-2.31201494046510	3.53997954424162	0.33197644664654
C	-1.16795509699796	2.68579624208167	0.10145350259182
C	1.13826317107800	2.67654064156293	-0.30261727896173
C	2.41431431358134	3.40268973827658	-0.71712401450544
C	2.48660268327061	3.31416154985387	-2.26875850249557
C	2.43492067479703	4.87843386435410	-0.29467310931339
C	3.49601975997316	2.48086817347099	-0.03112580211743
C	4.85399556029897	2.42969553412413	-0.75228556358605
C	3.72679347126024	2.88460598892188	1.45350093741749
C	2.66632740955362	-1.30200493420988	0.06534217864482
C	3.36334556763726	-0.09533449009169	0.08110192557043
C	2.74673953360994	1.15120199435507	-0.01494551748608
C	3.32308219851971	-2.67644451608637	0.15625352946870
C	4.70323915609521	-2.76637372516377	-0.51614638634592
C	3.47428274548920	-2.99602865416013	1.67172791724580
C	2.20058083246131	-3.56398841710626	-0.50839910903367
C	2.11369656063704	-5.01191834947483	-0.00652140955541
C	2.31795418145902	-3.56918358846114	-2.05942985361628
C	0.96545933378259	-2.73397816977749	-0.16965804996342
C	-1.34425600896421	-2.57410701970874	0.17877217273932
C	-2.54985165730238	-3.34145761660585	0.40268524226114
C	-2.58218913789837	-4.75999575223473	0.35171330342337
C	-3.77978921023864	-5.42857329562497	0.59524995503897
C	-4.96912444250755	-4.70755846287938	0.89371199993503
C	-4.96182329046575	-3.31702777873359	0.94411736929682
C	-3.75080984297161	-2.61379077435573	0.69703991229491
C	-2.61897343025502	-0.62949509688736	0.50801702963150
H	-5.65065744468287	3.18070106571700	1.16154960125318
H	-5.50950925863144	5.70108122652264	1.03827301379494
H	-3.33894400962932	6.81160695349657	0.45500126768881
H	-1.28842524447009	5.43356737281825	-0.00027759030390
H	2.51587674771707	2.26346413411684	-2.63222240680277
H	3.39093867511252	3.83889845519275	-2.64478624148801
H	1.59673925157257	3.80807238051132	-2.71491438467204
H	1.67189295108304	5.44893758848649	-0.86465939546418
H	3.42872771576815	5.32805795059953	-0.51386220153110
H	2.21511739956222	5.01811115837704	0.78354212640951
H	4.79166665702188	1.97062924899172	-1.76086366836135
H	5.60187053165034	1.85789866473239	-0.16039498694457
H	5.26023558950087	3.45865689064105	-0.86650128481355
H	4.26701455215161	3.85412386382915	1.50819824354855
H	4.34875298576362	2.12120075242665	1.96915378995574

H	2.77286845506659	2.98412967759782	2.01598590792728
H	4.45932264256710	-0.13091099135950	0.13516833928771
H	5.03732480267650	-3.82666201215492	-0.55384719503742
H	5.47106344471426	-2.21381572932219	0.06843865748924
H	4.70569317476917	-2.36726770717078	-1.55165236990510
H	2.49550101609677	-2.99175615047448	2.19916697796041
H	4.12943166488923	-2.24341159268438	2.16156410395831
H	3.94170993296146	-3.99451484801323	1.81046836560864
H	1.86235399435147	-5.07853223952969	1.07185864326761
H	3.07941531593206	-5.53797564070429	-0.17638515654436
H	1.32692531515803	-5.56213678756451	-0.56408596912348
H	1.41293054328283	-4.03741989821398	-2.50274402533799
H	3.19968130772788	-4.16478164630662	-2.37939748518194
H	2.41716445866612	-2.54514167292084	-2.48203194638303
H	-1.65763769448834	-5.30806077812238	0.11987087919857
H	-3.80877078566006	-6.52969055882942	0.55563195024876
H	-5.90456983514263	-5.25909226948151	1.08328927983791
H	-5.86776054410666	-2.73328279555698	1.16794395362672

ESI-MS of Ni(Mabiq)OTf (1) after the photocatalytic reaction

D:\0698107\Masse\mg49435

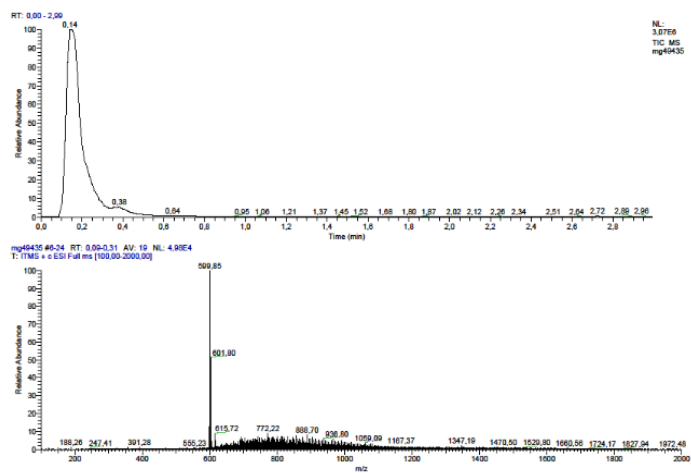


Figure S8: GC-MS of product mixture (after photoredox catalysis with 1 and 3).

Cyclic Voltammetry (CV) experiments

Cyclic Voltammogram of Ni(Mabiq)OTf (1)

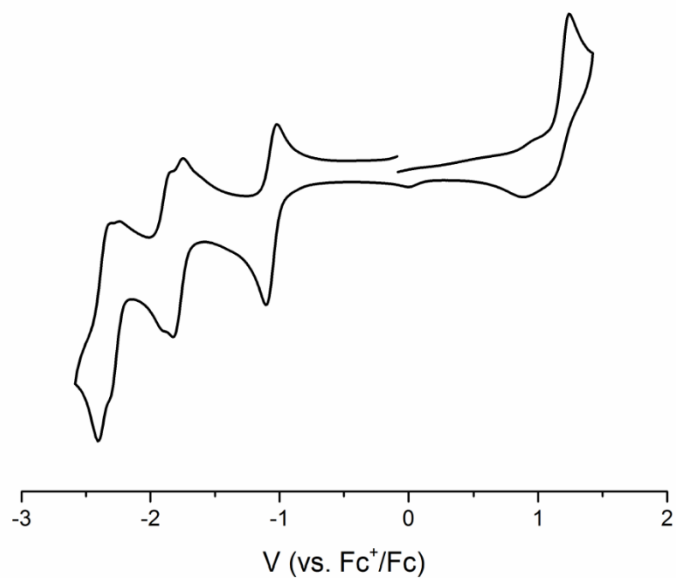


Figure S9: Cyclic voltammogram of **1** (1 mM) in MeCN; 0.1 M [N(*n*-Bu)₄]PF₆; scan rate: 0.1 V/s.

Cyclic Voltammograms for Amines 6a to 6n

The CV measurements were performed with the corresponding amine **6** (1 mM) in 0.1 M of $[N(n\text{-Bu})_4]PF_6$ in MeCN. Glassy carbon electrode was used as working electrode, a platinum wire as counter electrode, $Ag/AgNO_3$ (0.01 M in MeCN) as reference electrode, and a scan rate of 100 mV/s. The value of the potential at the inflexion point of each oxidation curve was selected as the oxidation potential of the given amine **6**. 300 mV were added to this value to give the corresponding oxidation potentials (E^{ox}) vs. the Saturated Calomel Electrode (SCE).

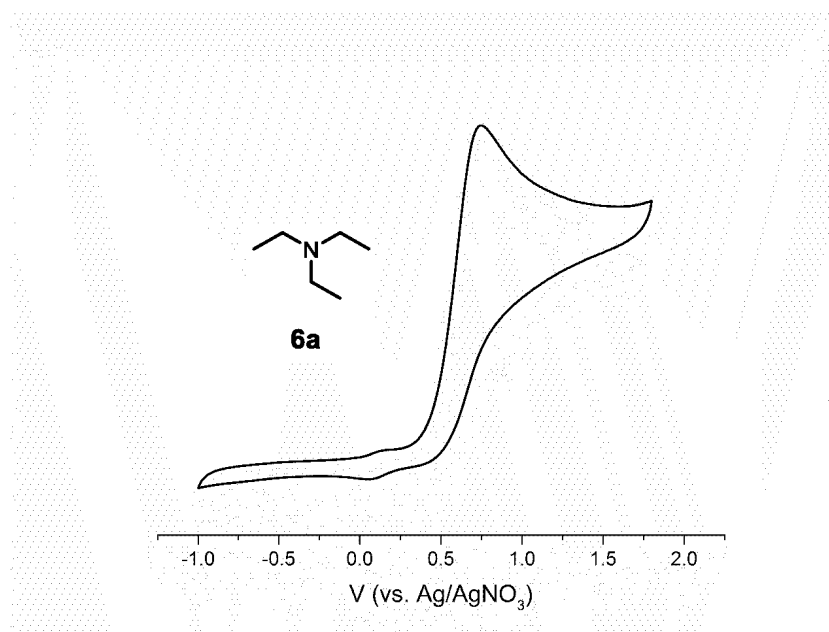


Figure S10: Cyclic voltammogram of **6a**.

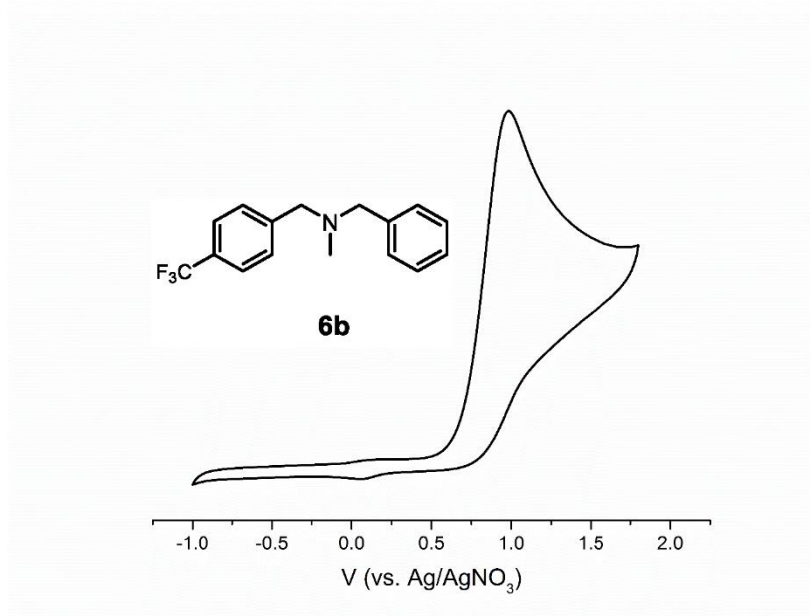


Figure S11: Cyclic voltammogram of **6b**.

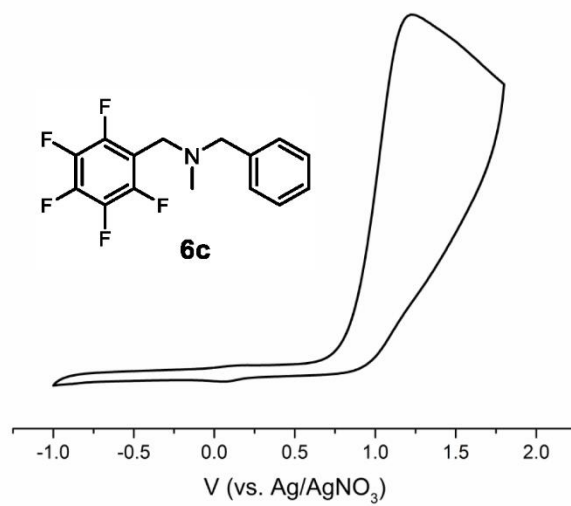


Figure S12: Cyclic voltammogram of **6c**.

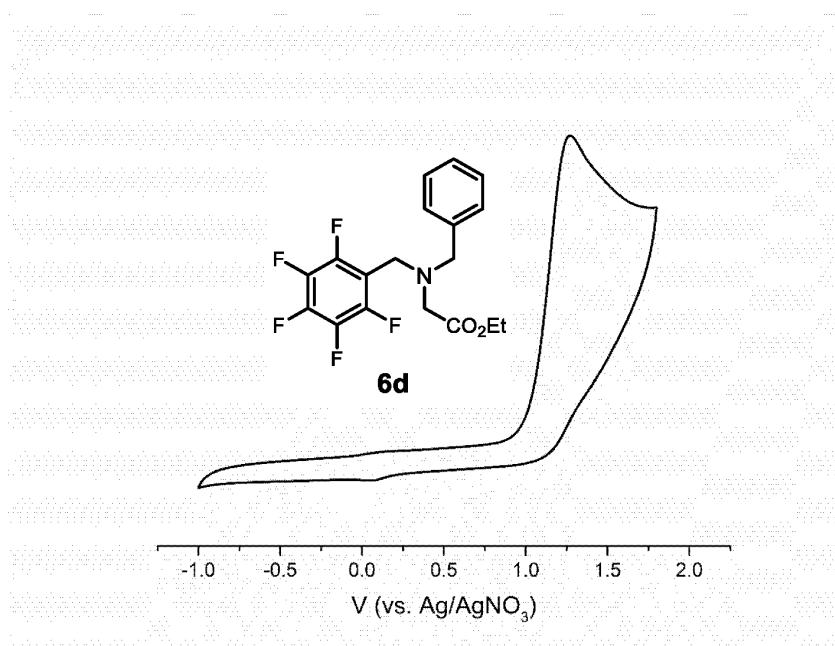


Figure S13: Cyclic voltammogram of **6d**.

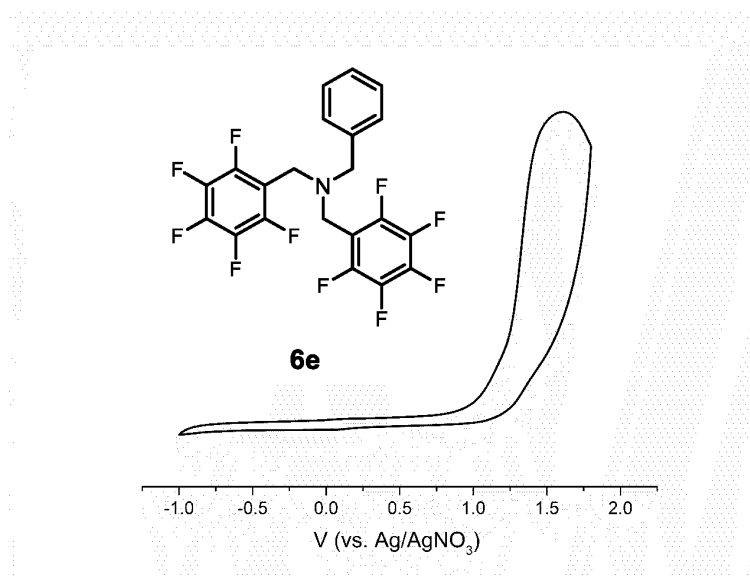


Figure S14: Cyclic voltammogram of **6e**.

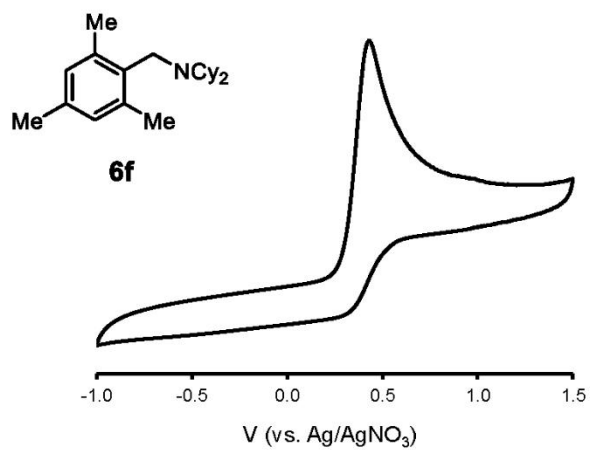


Figure S15: Cyclic voltammogram of **6f**.

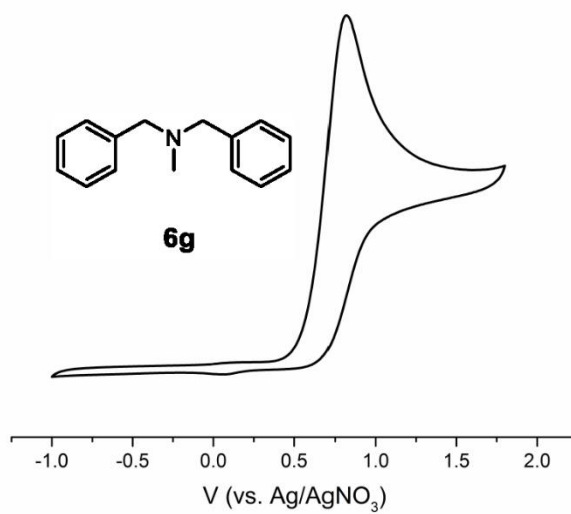


Figure S16: Cyclic voltammogram of **6g**.

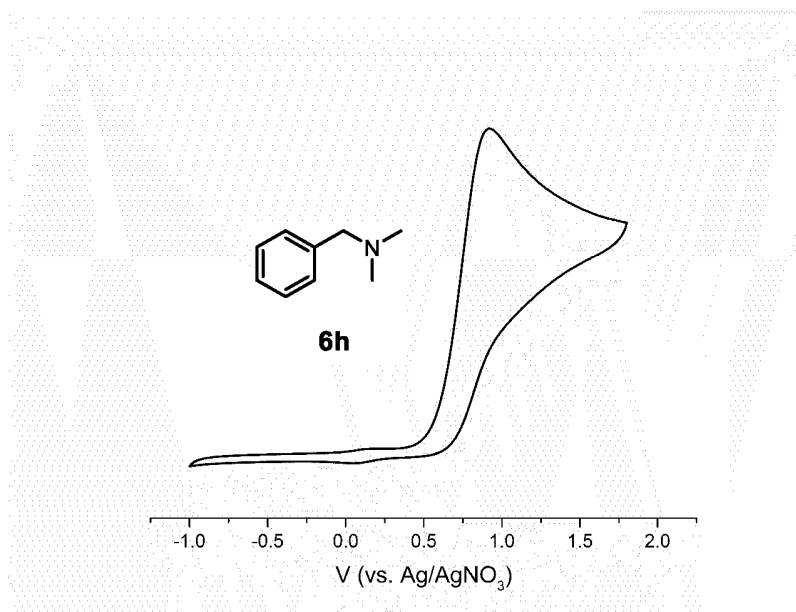


Figure S17: Cyclic voltammogram of **6h**.

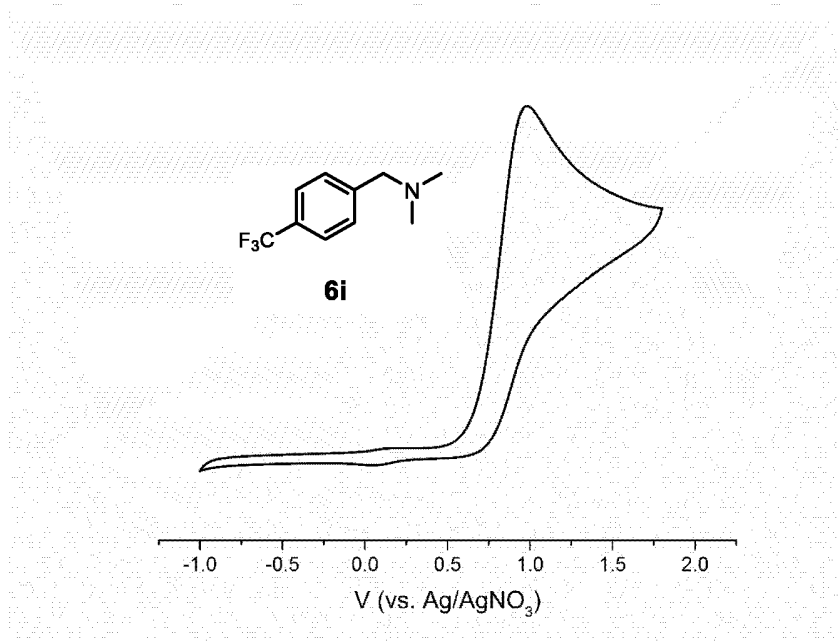


Figure S18: Cyclic voltammogram of **6i**.

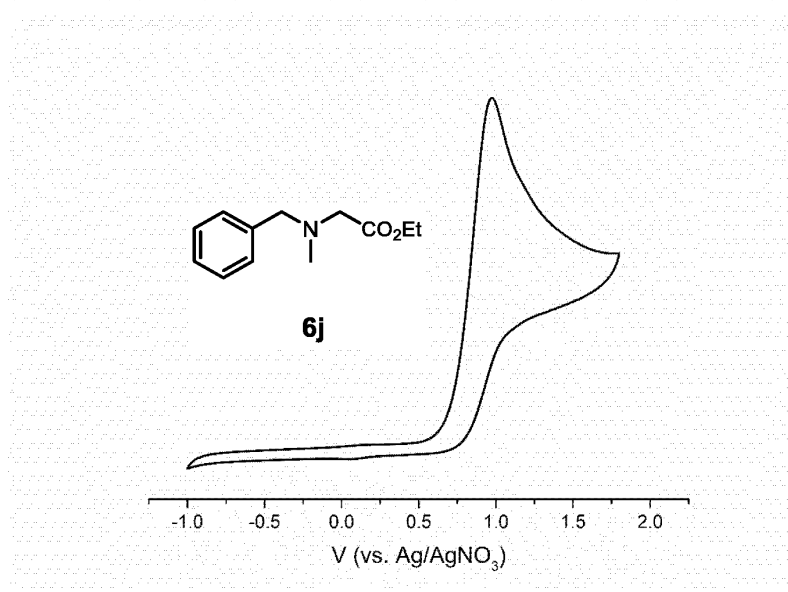


Figure S19: Cyclic voltammogram of **6j**.

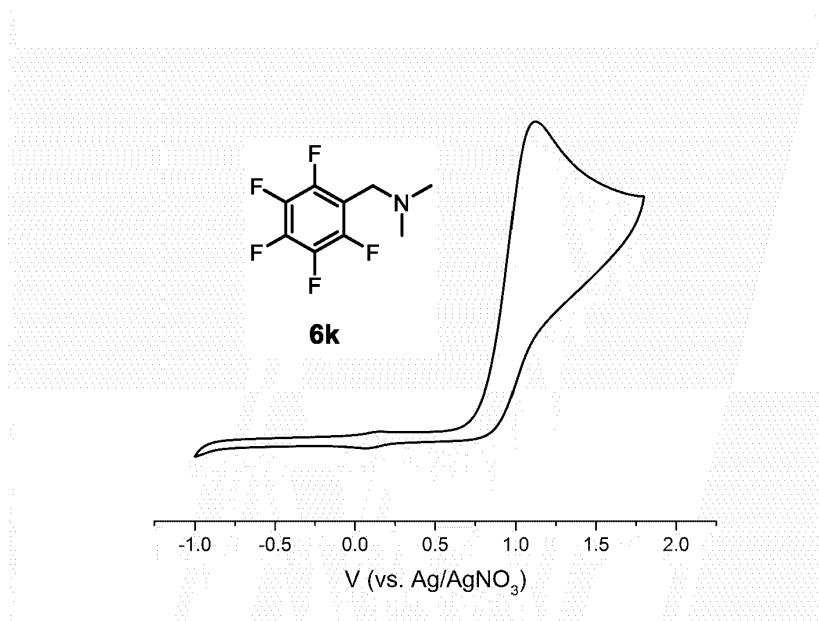


Figure 20 Cyclic voltammogram of **6k**.

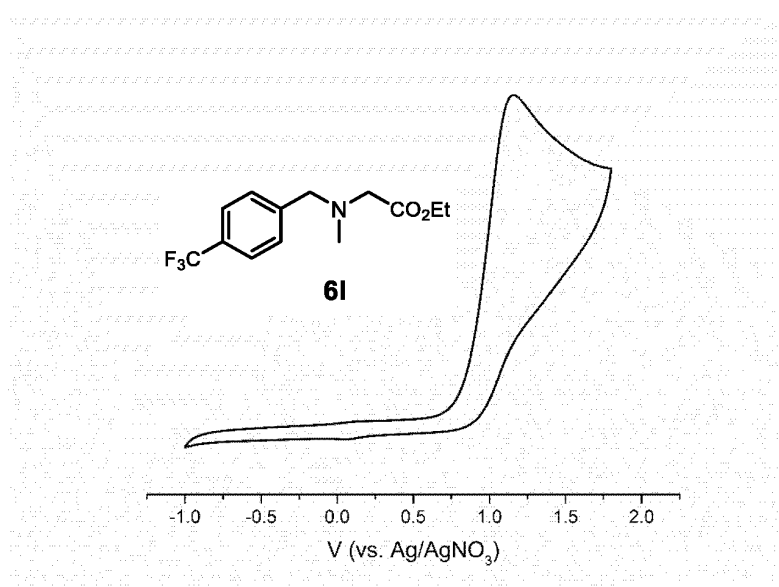


Figure S21: Cyclic voltammogram of **6l**.

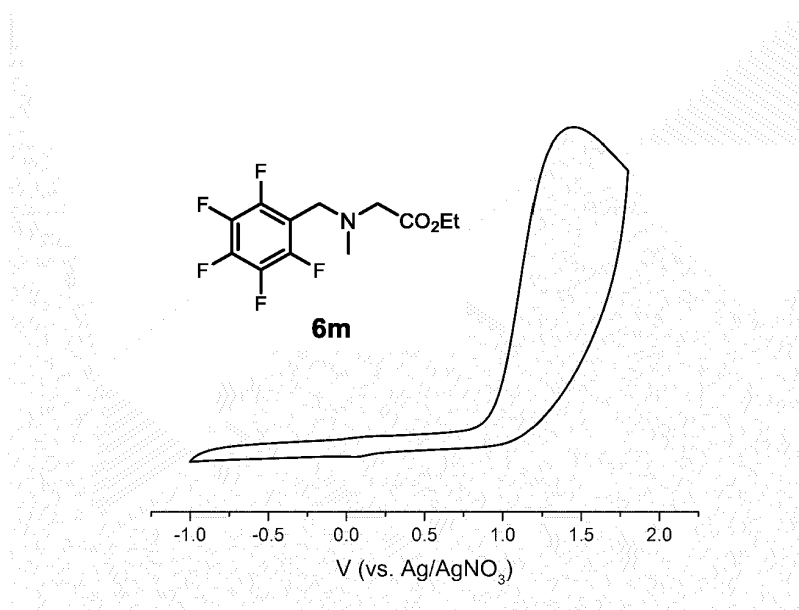


Figure S22: Cyclic voltammogram of **6m**.

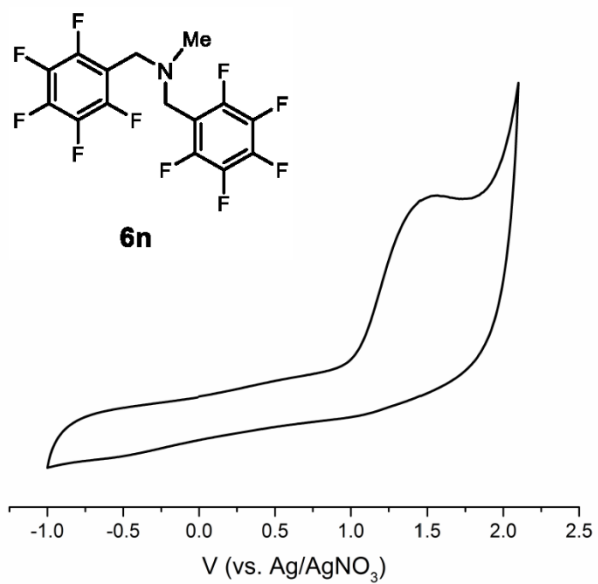


Figure S23: Cyclic voltammogram of **6n**.

Chemical actinometry: Determination of the photon-flux

The set up used for the chemical actinometry consisted of a LED (455 ± 10 nm) mounted on a heat sink and a set of focussing lenses ($f = 25$, $f = 150$) to direct the light into the cuvette, which was placed in a cuvette holder situated at 21 cm distance from the LED (Figure S24). A magnetic stirbar drive (2mag, cuvetteMixdrive1) was installed under the cuvette holder.

The photon flux in the cuvette after thermal equilibration of the LED (working at a constant current of 0.7 V) was measured using a radiometrically calibrated setup (USB-4000, Ocean Optics) connected by a fiber and a cosine corrector^[29] which gave 104 mW/cm^2 on an irradiated area of $9.5 \text{ mm} \times 9.5 \text{ mm}$. These values correspond to 94 mV or $3.56 \times 10^{-7} \text{ Einstein} \cdot \text{s}^{-1}$.

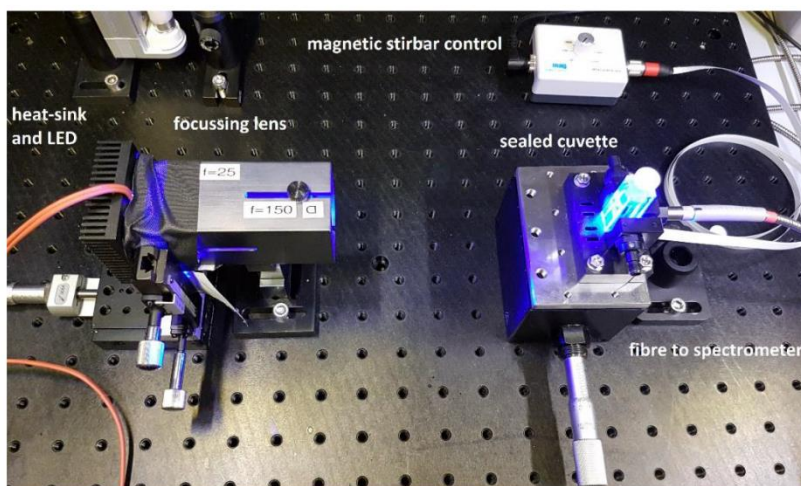


Figure S24: Set up used for the actinometry and quantum yield experiments.

Chemical actinometry was used to verify this value:^{[30]-[31]} A potassium ferrioxalate solution (150 mM) was prepared under strict exclusion of light (dark room under red light conditions) by dissolving 1.639 g of $\text{K}_3[\text{Fe}(\text{C}_2\text{O}_4)_3]$ in 2.5 mL of a 0.5 M H_2SO_4 aqueous solution, and water

was added to a final sample volume of 25 mL. The solution was stored in a dark 10 mL volumetric flask, and used on the same day as prepared.

The 1,10-phenanthroline solution (10 mM) was prepared by dissolving 45.1 mg of 1,10-phenanthroline and 2.05 g of NaOAc in 10 mL of water and 9.7 mL of 0.5 M H₂SO₄ aqueous solution, and water was added to a final volume of 25 mL. The solution was stored in a dark 10 mL volumetric flask, and used on the same day as prepared.

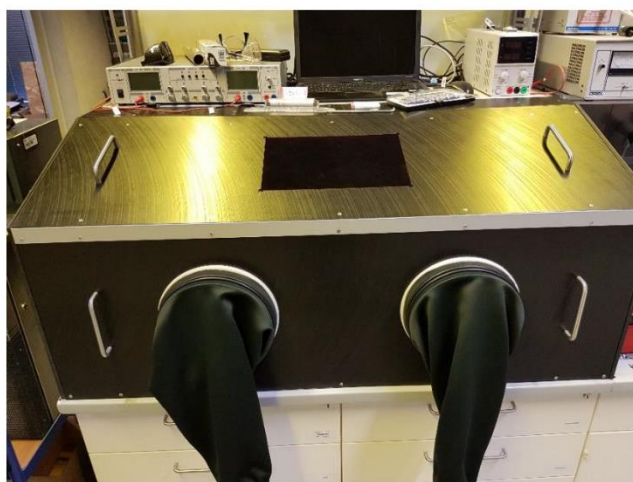


Figure S25: Black box with a red window used for the actinometry and quantum yield experiments.

In a black box under red-light conditions (Figure S25), 3 mL samples of the ferrioxalate solution were irradiated in a 10 x 10 mm cuvette for 5, 10, 20 and 30 seconds. After irradiation, 100 μ L aliquots of each sample and a non-irradiated blank were transferred into brown GC-vials. 900 μ L of the 1,10-phenanthroline solution were added to each GC-vial and the cuvettes were left for 60 min in the black box, after which time the UV-visible spectra were measured (Figure S26). The fit of the $\Delta A/t$ plot (Figure S26) yields a slope of = 0.0696 s⁻¹.

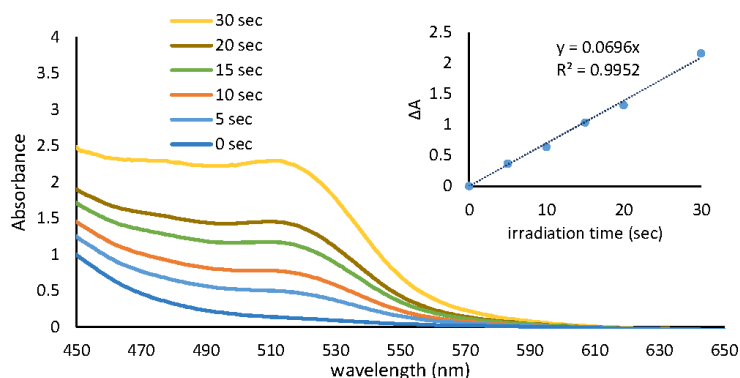


Figure S26: UV-visible spectra for the potassium ferrioxalate solutions after 0, 5, 10, 15, 20 and 30 s of irradiation at 455 nm. Inset: change in absorbance (510 nm) vs irradiation time plot.

The experimental photon flux was calculated according to the following equation:

$$\text{photon flux} = \frac{\text{mol Fe}^{2+}}{\Phi \times t \times f}$$

Where Φ is the reference quantum yield for the ferrioxalate actinometer (0.845 for a 0.15 M solution at $\lambda = 457 \text{ nm}$)^[32], t is the irradiation time (in s) and f is the fraction of light absorbed at $\lambda = 457 \text{ nm}$ ($f = 1$, as the optical density of the ferrioxalate solution at 457 nm is > 3).

Given the following equation for the calculation of the mols of Fe^{2+} generated:

$$\text{mol Fe}^{2+} = \frac{V \times d \times \Delta A}{l \times \epsilon}$$


where V is the total volume in the cuvette of the analysis (0.001 L), d is the dilution factor (30, as 0.1 mL out of 3 mL of initial solution were taken for the analysis), ΔA is the increment of absorbance after certain irradiation time, l is the path length of the cuvette (1 cm) and ϵ is the molar absorption coefficient at 510 nm ($11,100 \text{ M}^{-1} \text{ cm}^{-1}$)^[36], the photon flux can be determined by:

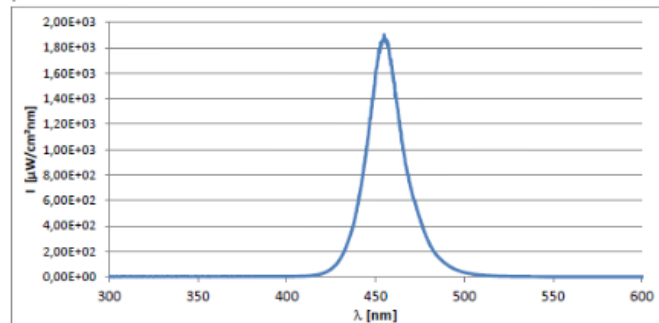
$$\text{photon flux} = \frac{V \times d}{\Phi \times f \times l \times \epsilon} \times \frac{\Delta A}{t}$$

where $\Delta A/t$ is the slope of the absorbance vs time (0.0696 s^{-1} , vide supra). The photon flux calculated accordingly was found to be:

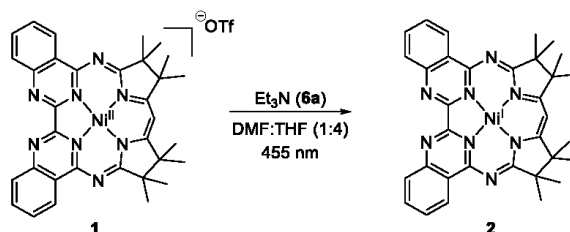
$$\text{photon flux} = \frac{0.001 \text{ L} \times 30 \times 0.0696 \text{ s}^{-1}}{0.845 \times 1 \times 1.00 \text{ cm} \times 11100 \text{ L} \cdot \text{mol}^{-1} \cdot \text{cm}^{-1}} = 2.226 \cdot 10^{-7} \text{ Einstein s}^{-1}$$

Emission spectra of the LED (455 nm)

Lehrstuhl OC 1 - TUM	
	
Datasheet LED028	Av-455-3W
Basic Information	
Type	High-Power-LED
Description	Avonec 455-460 nm / 3 W
Manufacturer / Supplier	n/a / Avonec
Order number / Date of purch.	n/a / 01/2016
Internal lot / serial number	2016-01 / LED028
Specification Manufacturer	
Type / size	single emitter / ca. 1 x 1 mm
Mechanical specification	
Electrical specification	700 mA, UF 3.7 V
Wavelength (range, typ.)	455-460 nm, typ. n/a
Spectral width (FWHM)	n/a
Datasheet	n/a
Characterization	
Description of measurement	Measured with Ocean-optics USB4000 spectrometer using a calibrated setup (cosine corrector/fibre). The distance between the emitting surface and the surface of the cosine corrector was 20 mm. The LED was operated at 700 mA on a passive heat-sink at approx. 20 °C
Measured wavelength	455 nm
Measured spectral width	22 nm
Integral Reference intensity	50200 $\mu\text{W}/\text{cm}^2$ (400-550 nm @ 20 mm distance, 4 mm cosine corr.)
Spectrum	



Determination of the quantum yield for the photoconversion of **1** to **2**



The reaction mixture was prepared in a glove box equipped with a red LED in a dark room, using a cuvette fitted with a J-Young tap and equipped with a stir bar inside.

Two stock solutions were prepared: A stock solution of **1** was prepared by dissolving 4 mg of **1** in 25 mL of THF:DMF (4:1) ($[1] = 2.13 \cdot 10^{-4}$ M). A stock solution of Et₃N (**6a**) was prepared by diluting 118.8 μ L of Et₃N (**6a**) in 10 mL of THF:DMF (4:1) ($[6a] = 8.50 \cdot 10^{-2}$ M).

For each measurement, 1 mL of the stock solution of **1** was added to a cuvette, followed by 0.5 mL of the stock solution of **6a** (200 equiv. of **6a**). 1.5 mL of a THF:DMF (4:1) solution was subsequently added to a total volume of 3 mL. Therefore, the final reaction solution contained $2.13 \cdot 10^{-4}$ mmol of **1** ($7.13 \cdot 10^{-5}$ M) and $4.27 \cdot 10^{-2}$ mmol of Et₃N (**6a**) ($1.43 \cdot 10^{-2}$ M).

The cuvette was sealed, covered with aluminum foil to avoid any light exposure, and transferred to a dark room equipped with a UV-visible spectrometer and a dark box. A UV-visible spectrum of the reaction mixture was recorded for $t = 0$ min. The reaction mixture was subsequently irradiated at 455 nm for three 10 min periods (10, 20 and 30 min total). After each of these periods, the absorption spectra were recorded.

The same procedure was followed using 300, 400, 600 or 800 equivalents of Et₃N.

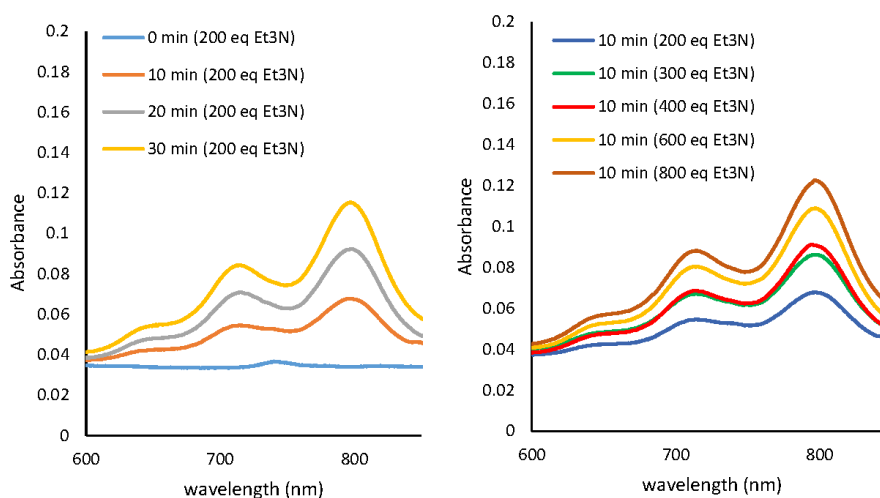


Figure S27: Left: UV-visible spectra for mixtures of **1** in the presence of 200 equiv. of Et₃N in THF:DMF (4:1) after 0, 10, 20 or 30 min irradiation at 455 nm; Right: UV-visible spectra for mixtures of **1** in the presence of different concentrations of Et₃N in THF:DMF (4:1) after 10 min irradiation at 455 nm.

We note that in the region from 600 – 850 nm the absorption observed in the UV-visible spectra is only due to Ni(Mabiq) (**2**), whereas in the region from 400 – 500 nm both Ni(Mabiq)OTf (**1**) and Ni(Mabiq) (**2**) absorb (see Figure 2 in the manuscript). The concentration of **1** was chosen to avoid saturation of the signal at 455 nm, allowing us to determine the photons absorbed exclusively by **1**.

The absorbance due to **1** was corrected using the molar absorption coefficient of **2** at 455 nm ($\epsilon_{455} = 5493 \text{ M}^{-1} \text{ cm}^{-1}$) and the known concentration of **2** as determined at 796 nm ($\epsilon_{796} = 5551 \text{ M}^{-1} \text{ cm}^{-1}$) at 10 min. Although this is a slight overcorrection, the data treatment revealed that (e.g. for the 200 equiv. Et₃N, 10 min data) a maximum of 5% of the light is absorbed by Ni(Mabiq) (**2**) while 95% is absorbed by Ni(Mabiq)OTf (**1**). The correction provides a value of $f = 0.95$ used in the quantum yield calculations.

From the absorbance at 796 nm (Figure S27, left), the concentration of Ni(Mabiq) (**2**) generated after irradiation was calculated. The slope of the plot of [**2**] vs the irradiation time (Figure S28), gives the observed rate of product formation ($k_p = [\mathbf{2}]/_t = 7.13 \cdot 10^{-9} M \cdot s^{-1}$), from which the quantum yield was determined according to the following equation:

$$\phi_{pc} = \frac{k_p \cdot V}{\text{photon flux} \cdot f} = \frac{7.13 \cdot 10^{-9} M \cdot s^{-1} \cdot 0.003 L}{2.226 \cdot 10^{-7} \text{Einstein} \cdot s^{-1} \cdot 0.95} = 1.011 \cdot 10^{-4}$$

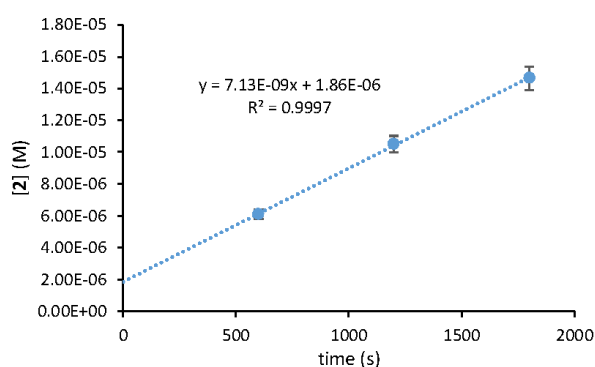


Figure S28: Concentration of Ni(Mabiq) (**2**) generated in solution vs irradiation time, in a reaction mixture with 200 equiv. Et₃N, measured at 796 nm.

In this manner, the quantum yield of the photoconversion at various concentrations of Et₃N was calculated (Table S3).

Table S3: Quantum yields calculated for the different concentrations of Et₃N.

[Et ₃ N] (M)	0.0142	0.0214	0.0285	0.0428	0.0570
k_p (M · s ⁻¹)	$7.13 \cdot 10^{-9}$	$1.07 \cdot 10^{-8}$	$1.24 \cdot 10^{-8}$	$1.72 \cdot 10^{-8}$	$2.30 \cdot 10^{-8}$
$\phi_{pc,[Et_3N]}$	$1.01 \cdot 10^{-4}$	$1.52 \cdot 10^{-4}$	$1.76 \cdot 10^{-4}$	$2.44 \cdot 10^{-4}$	$3.26 \cdot 10^{-4}$
1/[Et ₃ N] (M ⁻¹)	70.12	46.75	35.06	23.37	17.53
1/ $\phi_{pc,[Et_3N]}$	9886.4	6587.8	5684.7	4098.3	3064.8

As described by Kaneko *et al.*^[33] a relationship between the excited state lifetime and the reciprocal of the quantum yield can be described as:

$$\frac{1}{\phi_{pc}} = \frac{1}{f_{CS} \phi^*} \left(1 + \frac{1}{k_d \tau^* [Et_3N]} \right)$$

Where ϕ_{pc} is the quantum yield of the photoconversion, f_{CS} is a factor that takes into account the efficiency for charge separation and the rate for reverse electron transfer, ϕ^* is the quantum yield for the production of the reactive excited state specie, k_d is the diffusion rate constant and τ^* is the lifetime of the excited state of the photocatalyst.

Consequently, the life time of the excited state of Ni(Mabiq)OTf (**1***) can be estimated from the plot of the reciprocal of the calculated quantum yields vs the reciprocal of the various Et₃N concentrations (Figure S29). The reciprocal of the intercept affords $\phi^* f_{CS} = 9.72 \cdot 10^{-4}$ and division of the intercept by the slope gives $1/k_d \tau^* = 0.12 M$.

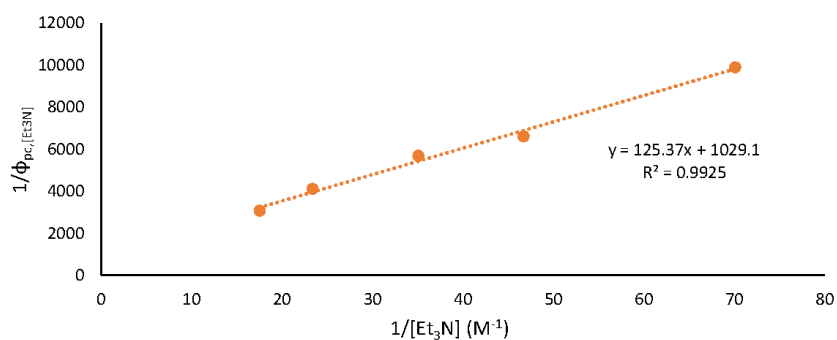


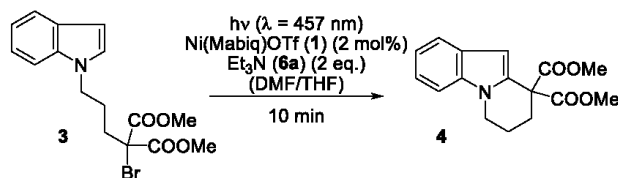
Figure S29: Representation of the reciprocal of the quantum yield of Ni(Mabiq) (**2**) generated after 10 min irradiation at 455 nm vs the reciprocal of the concentration of the Et₃N for individual samples.

The diffusion rate constant (k_d) can be calculated from the dynamic viscosity of the solvent according to the following equation:

$$k_d = \frac{8 \cdot N_A \cdot kT}{3 \cdot \eta}$$

Where N_A is the Avogadro number ($6.022 \cdot 10^{23} \text{ mol}^{-1}$), k is the Boltzman constant ($1.38 \cdot 10^{-23} \text{ m}^2 \text{ Kg s}^{-2} \text{ K}^{-1}$), T is the temperature (298 K) and η is the viscosity of the solvent. Since a 4:1 THF:DMF mixture was used for the experiments, the diffusion rate constant was calculated for both solvents from their corresponding viscosities ($\eta_{THF} = 0.0047 \text{ Pa s}$; ^[34] $\eta_{DMF} = 0.00724 \text{ Pa s}$ ^[35]), yielding $k_{d,THF} = 1.41 \cdot 10^9 \text{ s}^{-1} \text{ M}^{-1}$ and $k_{d,DMF} = 9.12 \cdot 10^8 \text{ s}^{-1} \text{ M}^{-1}$, which gives a lifetime range of $5.82 \cdot 10^{-9} \text{ s} - 9 \cdot 10^{-9} \text{ s}$.

Determination of the quantum yield for the photocatalytic conversion of **3** to **4**



The reaction mixture was prepared in a glove box equipped with a red LED in a dark room, using a cuvette (equipped with a stir bar) fitted with a J-Young tap.

For these experiments, three stock solutions were prepared: A stock solution of **3** was prepared by dissolving 216 mg of **3** in 14.4 mL of THF. A stock solution of NEt_3 (**6a**) was prepared by dissolving 164 μL of NEt_3 in 4.8 mL of THF. A stock solution of Ni(Mabiq)OTf (**1**) was prepared by dissolving 4.4 mg of Ni(Mabiq)OTf in 2.4 mL of DMF.

1.8 mL of the stock solution of **3** were added to a cuvette, after which 0.6 mL of the stock solution of NEt_3 (**6a**) were added, followed by 0.6 mL of the Ni(Mabiq)OTf (**1**) stock solution. The final reaction mixture contained $7.34 \cdot 10^{-2}$ mmol of **3**, 0.148 mmol of NEt_3 (**6a**) (2 equiv.) and $1.47 \cdot 10^{-3}$ mmol of Ni(Mabiq)OTf (**1**) (2 mol%) in 3 mL of a 4:1 THF:DMF mixture.

The cuvette was sealed, covered with aluminum foil, removed from the glove box and introduced into a black box equipped with a red LED and a red window. The reaction mixture was irradiated at 455 nm for 60 min (with stirring at 400 rpm).

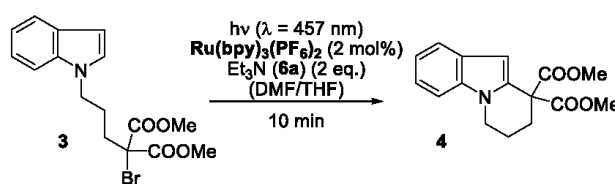
During the irradiation time a dibromomethane stock solution was prepared. 128 mg of dibromomethane were added to a 10 mL volumetric flask and diluted with CDCl_3 to a final volume of 10 mL. With 0.5 mL aliquots of this solution the NMR sample was prepared.

After the irradiation time the reaction was stopped by addition of 5 mL water. The mixture was poured into a separation funnel and extracted with ether (3 x 10 mL). The combined organic phases were washed with 20 mL brine solution, dried over 3.00 g of Na_2SO_4 and filtered. After removing the solvents under vacuum a NMR sample was prepared by adding 0.5 mL aliquots of the dibromomethane stock solution.

The product yield, based on the NMR analysis, was determined as 6%, which yields a quantum yield of 0.006:

$$\Phi (1, 1 \text{ h}) = \frac{\text{mol of } 4}{\text{photon flux} \times t \times f} = \frac{4.41 \cdot 10^{-6}}{2.226 \cdot 10^{-7} \times 3600 \times 1} = 0.006$$

An analogous reaction was carried out using $\text{Ru}(\text{bpy})_3(\text{PF}_6)_2$ as the catalyst.



Stock solutions of **3** and Et_3N (**6a**) were as previously described. A stock solution of $\text{Ru}(\text{bpy})_3(\text{PF}_6)_2$ was prepared by dissolving 5.0 mg of $\text{Ru}(\text{bpy})_3(\text{PF}_6)_2$ in 2.4 mL of DMF.

Samples were prepared as described above, such that the final reaction mixture contained $7.34 \cdot 10^{-2}$ mols of **3**, 0.148 mmol of NEt_3 (**6a**) (2 equiv.) and $1.47 \cdot 10^{-3}$ mmol of $\text{Ru}(\text{bpy})_3(\text{PF}_6)_2$ (2 mol%) in 3 mL of a 4:1 THF:DMF mixture.

The analogous procedure to the one described for **1** was followed to determine the quantum yield for the $\text{Ru}(\text{bpy})_3(\text{PF}_6)_2$ catalyzed reaction.

The product yield was determined to be 36%, from which the quantum yield was calculated to be 0.033.

$$\Phi ([\text{Ru cat}], 1 \text{ h}) = \frac{\text{mols of } 4}{\text{photon flux} \times t \times f} = \frac{2.65 \cdot 10^{-5}}{2.226 \cdot 10^{-7} \times 3600 \times 1} = 0.033$$

We note that we observe decomposition of the $[\text{Ru}(\text{bpy})_3]^{2+}$ catalyst during the 1 h reaction period (as analyzed by mass spectrometry, where peaks corresponding to brominated complex can be observed). Thus, the decomposition of the Ru catalysts presents a limitation to any direct comparison of quantum yields.

Absorption spectra of Ni(Mabiq)OTf (1) in the presence of Et₃N (6a) or Cy₂NCH₂Mes (6f)

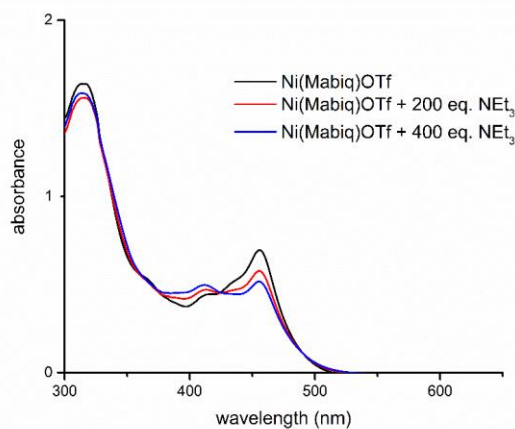


Figure S30: Absorption spectra of a 10⁻⁴ M solution of Ni(Mabiq)OTf in DMF:THF (1:4), and after addition of 200 or 400 equivalents of Et₃N (6a).

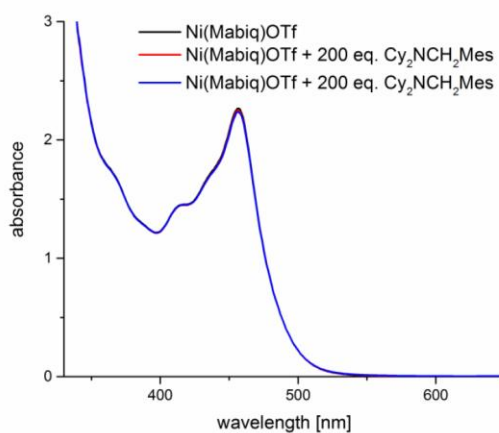


Figure S31: Absorption spectra of a 10⁻⁴ M solution of Ni(Mabiq)OTf in DMF:THF (1:4), and after addition of 200 or 400 equivalents of Cy₂NCH₂Mes (6f).

NMR Spectra

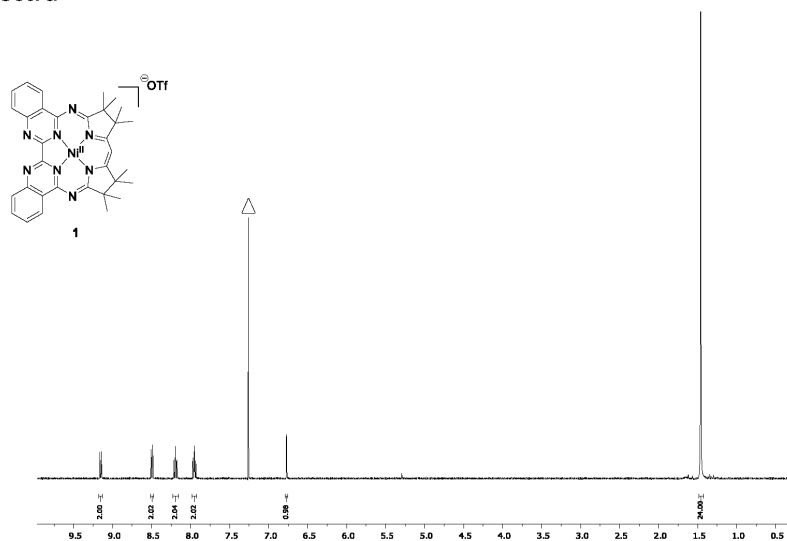


Figure S32: ¹H NMR (400 MHz, CDCl₃) of **1**; (Δ= CDCl₃ solvent residual signal in all NMR spectra throughout).

66

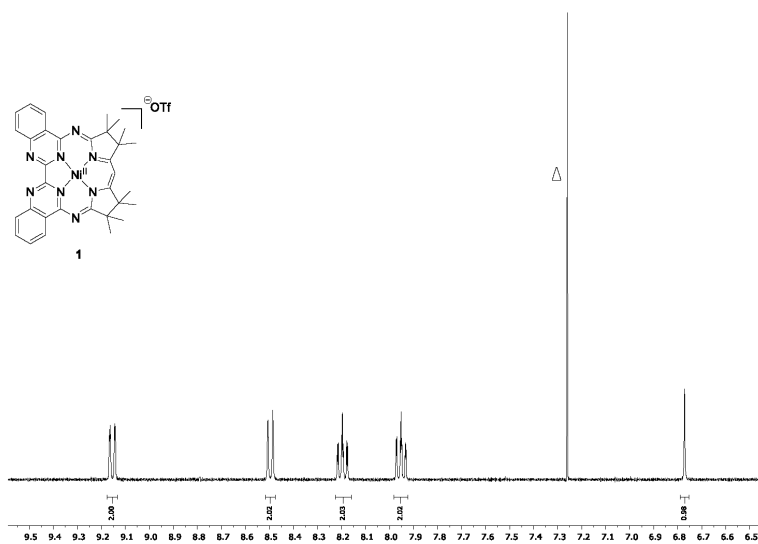


Figure S33: ¹H NMR (400 MHz, CDCl₃) of **1** in the range 6.5 ppm and 9.5 ppm.

67

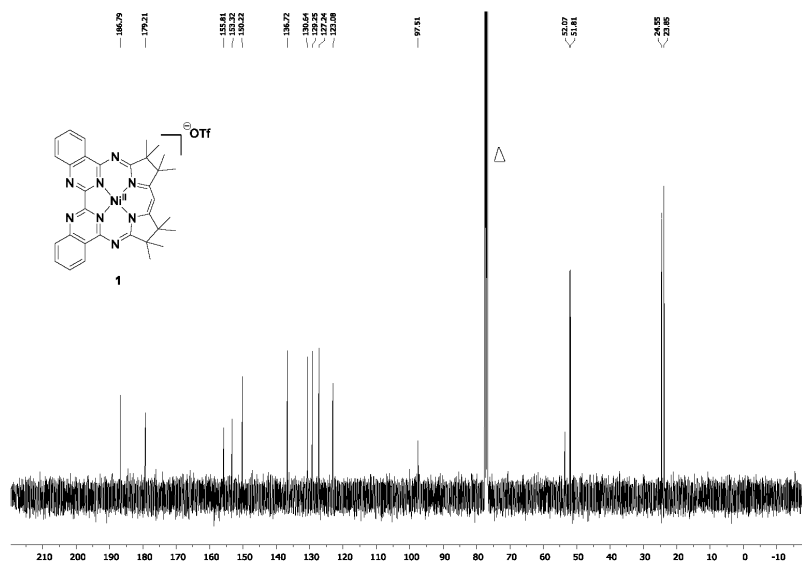


Figure S34: ^{13}C NMR (101 MHz, CDCl_3) of **1**.

68

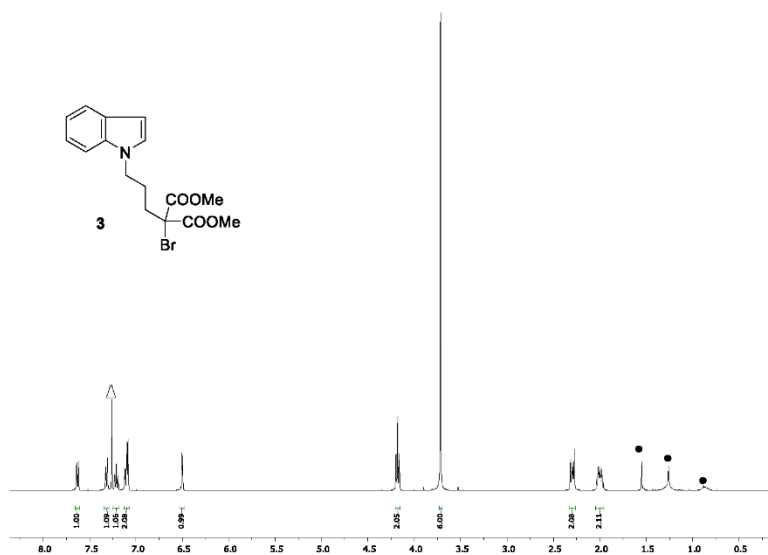


Figure S35: ^1H NMR (400 MHz, CDCl_3) of **3**; Δ= solvent peaks (CDCl_3 solvent residual signal); • = water, grease.

69

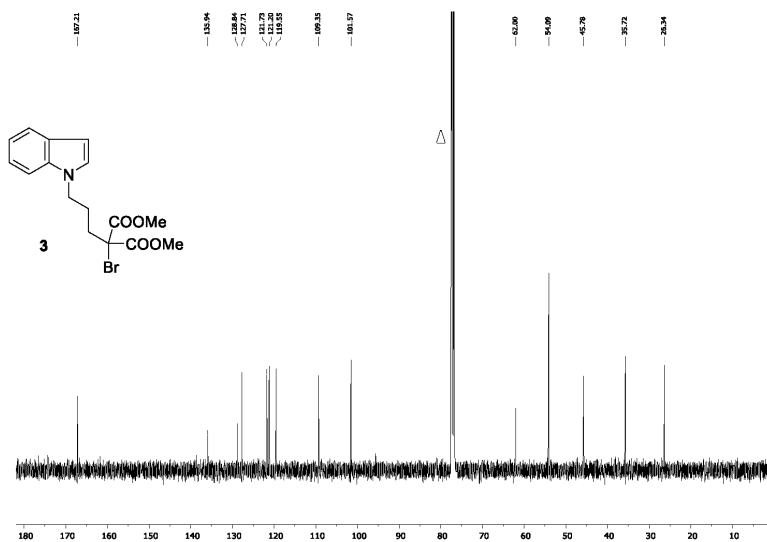


Figure S36: ¹³C NMR (101 MHz, CDCl₃) of **3**.

70

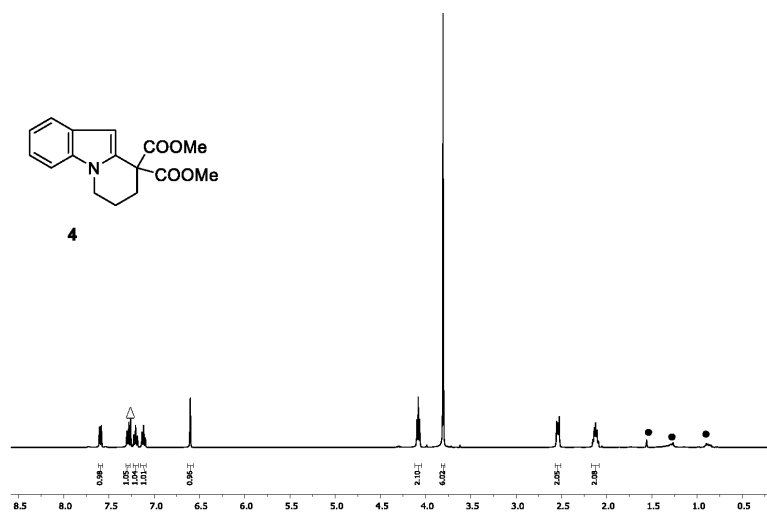


Figure S37: ¹H NMR (400 MHz, CDCl₃) of **4** Δ = solvent peaks (CDCl₃ solvent residual signal); • = water, grease.

71

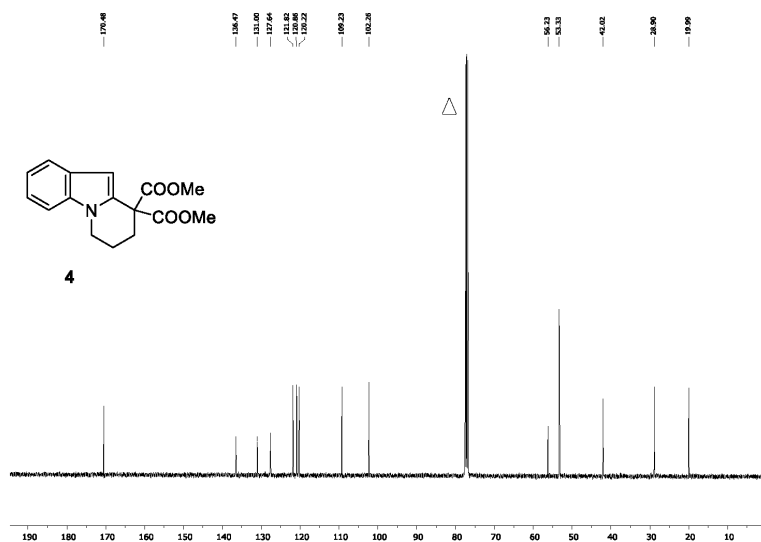


Figure S38: ¹³C NMR (101 MHz, CDCl₃) of **4**.

72

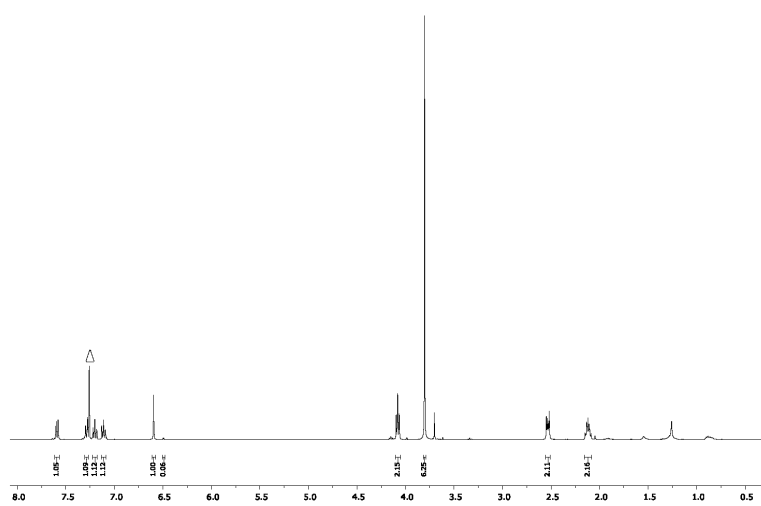


Figure S39: ¹H NMR (400 MHz, CDCl₃) of product mixture (photoredox catalysis with **1** and **3**).

73

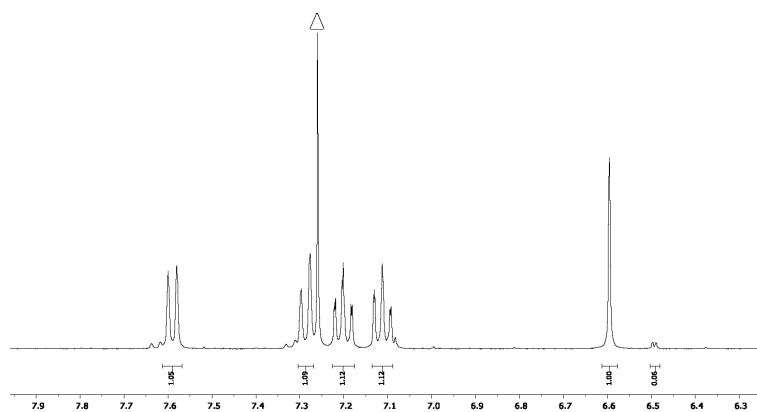


Figure S40: ¹H NMR (400 MHz, CDCl₃) of product mixture (photoredox catalysis with **1** and **3**) in the range between 6.3 ppm and 7.8 ppm.

74

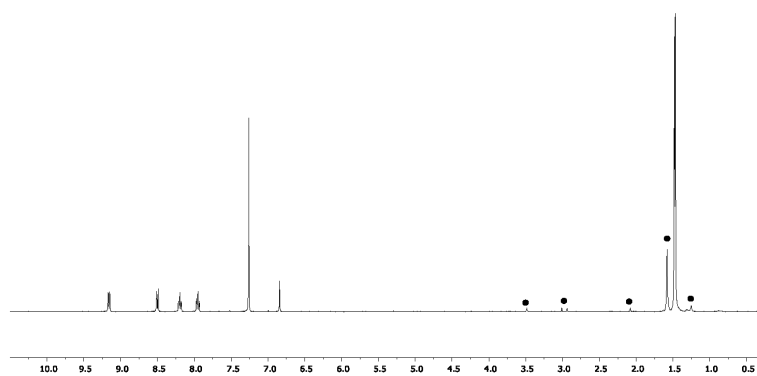


Figure S41: ¹H NMR (400 MHz, CDCl₃) of **1** after catalytic reaction; ● = water, grease, DMF, MeOH.

75

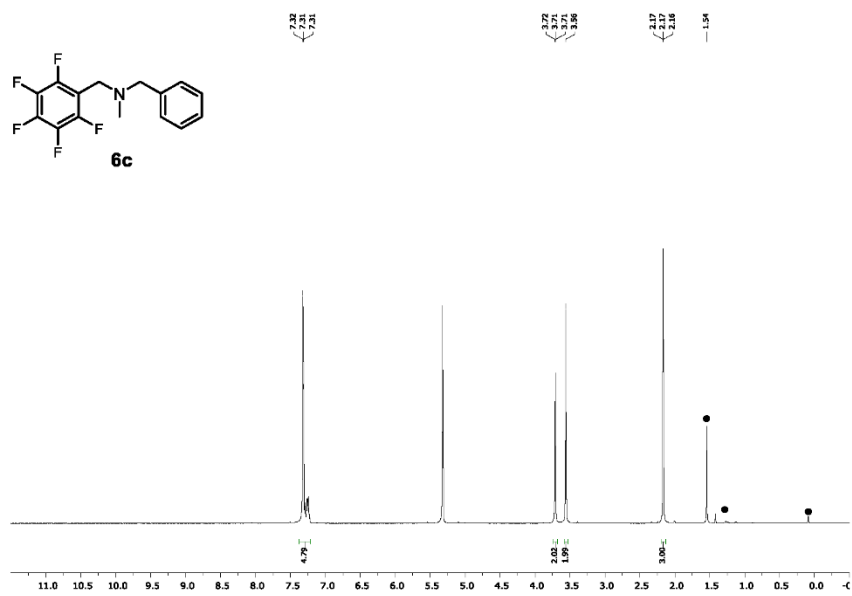


Figure S44: ¹H NMR (400 MHz, CD₂Cl₂) of **6c**, ● = water, grease.

78

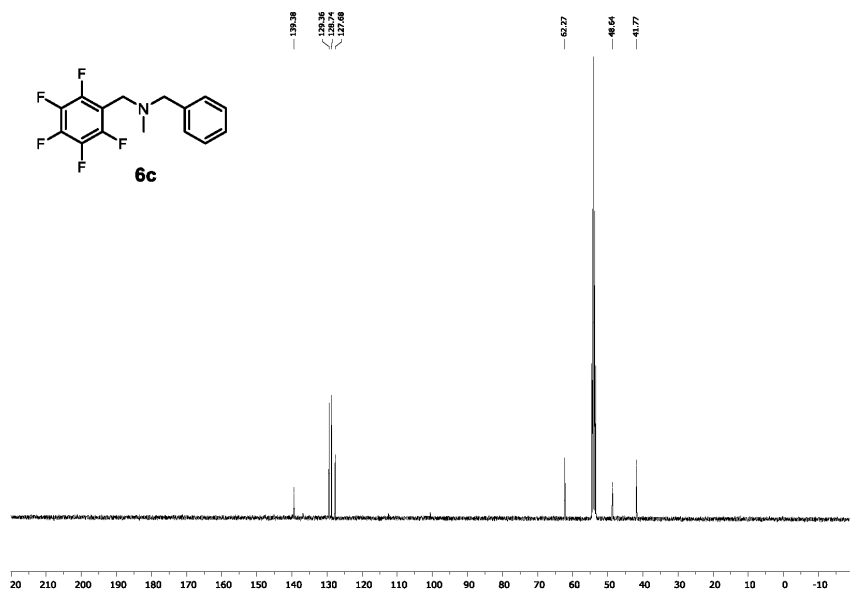
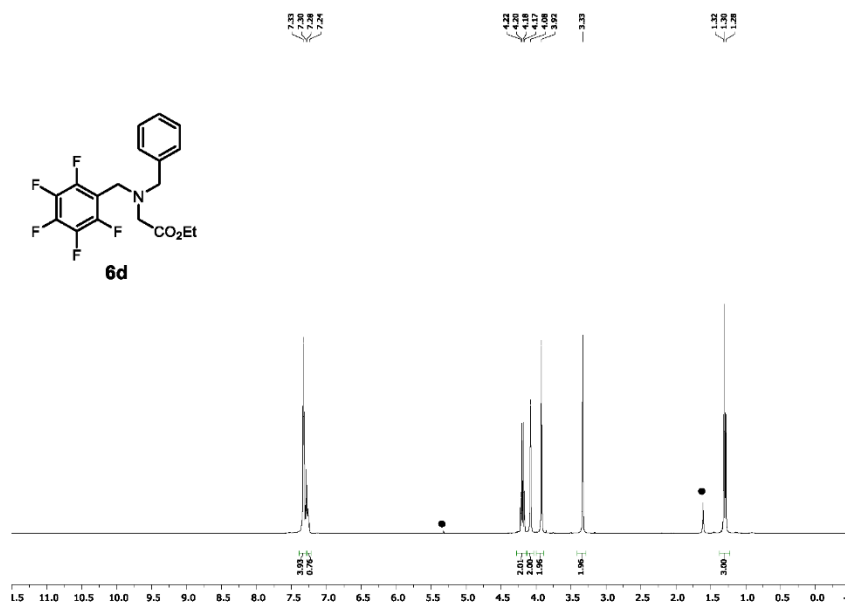
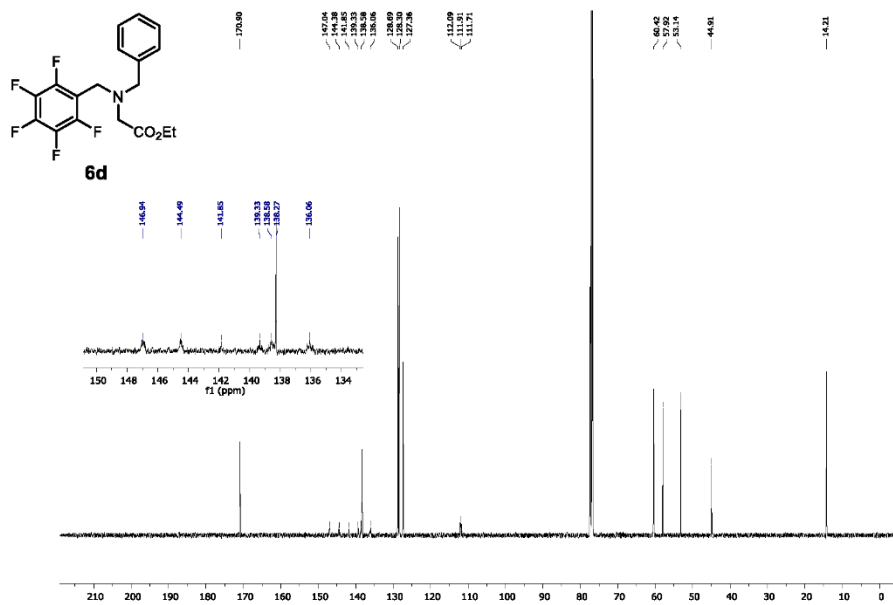


Figure S45: ¹³C NMR (101 MHz, CD₂Cl₂) of **6c**.

79

Figure S46: ¹H NMR (400 MHz, CDCl₃) of **6d**, • = water, CH₂Cl₂.

80

Figure S47: ¹³C NMR (101 MHz, CDCl₃) of **6d**.

81

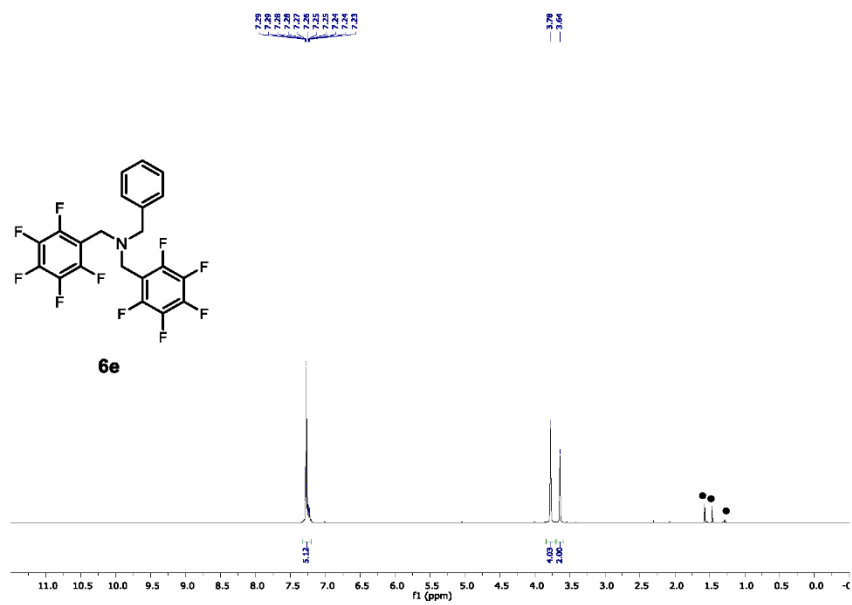


Figure S48: ^1H NMR (400 MHz, CDCl_3) of **6e**, ● = water, grease, cyclohexane.

82

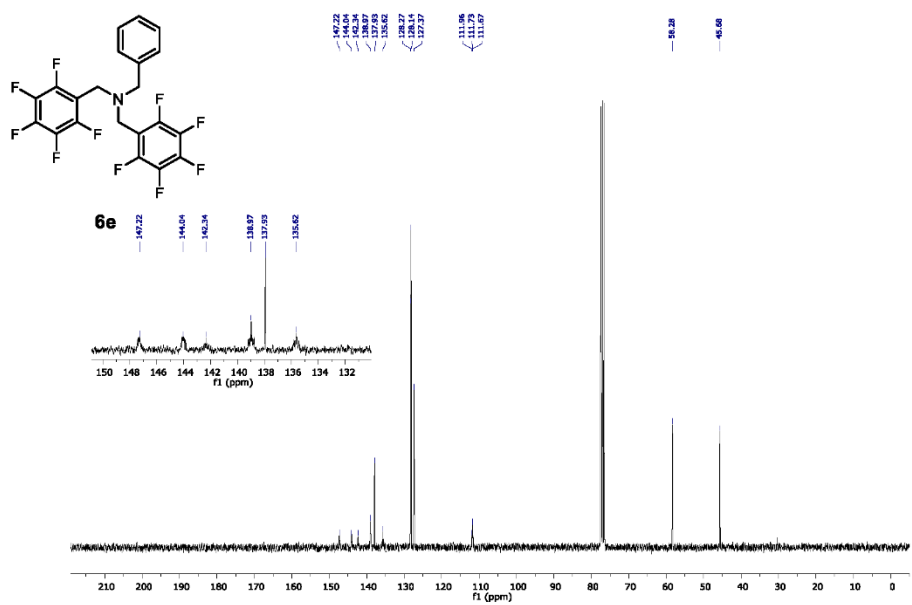
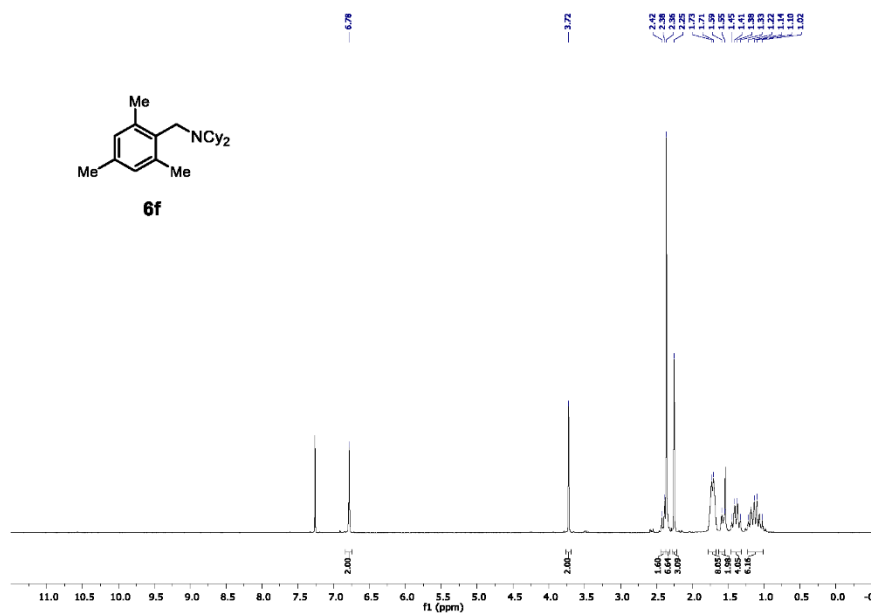
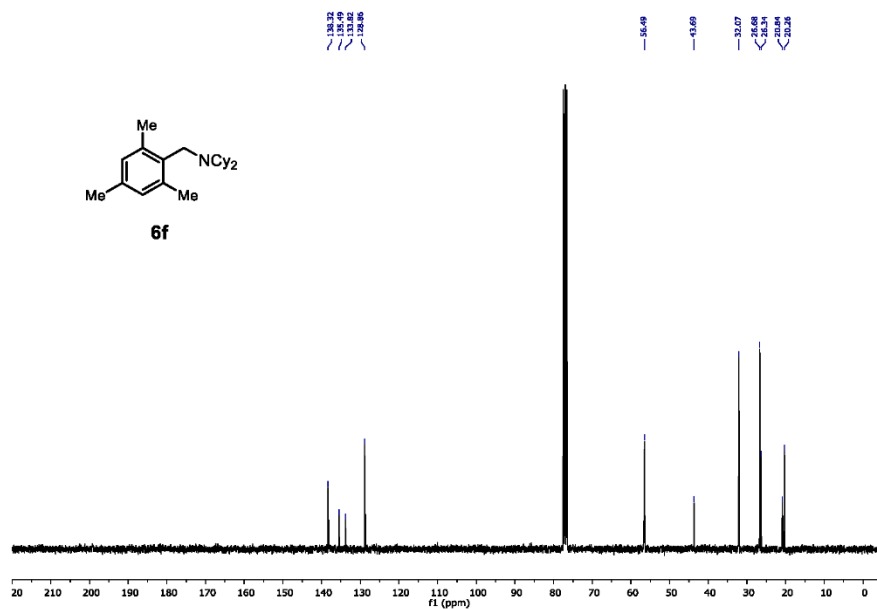


Figure S49: ^{13}C NMR (101 MHz, CDCl_3) of **6e**.

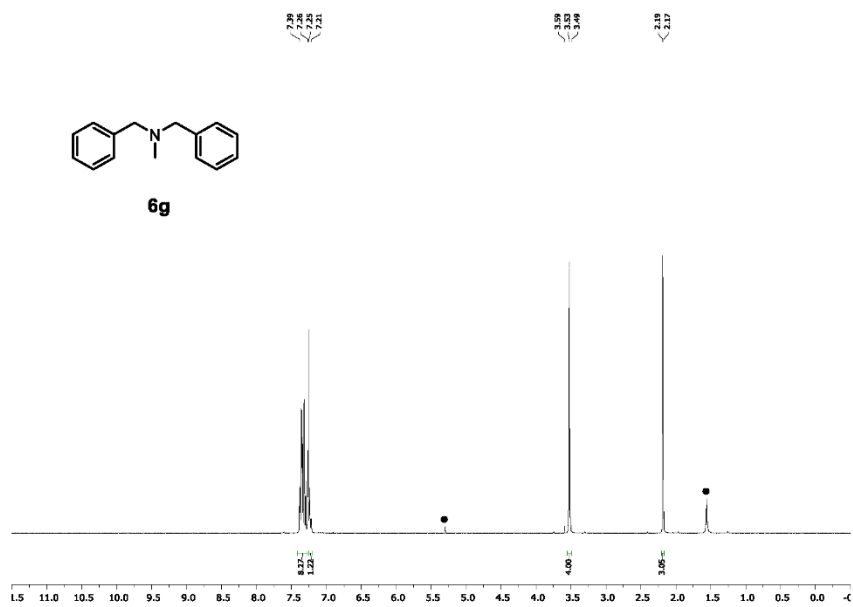
83

Figure S50: ¹H NMR (400 MHz, CDCl₃) of **6f**.

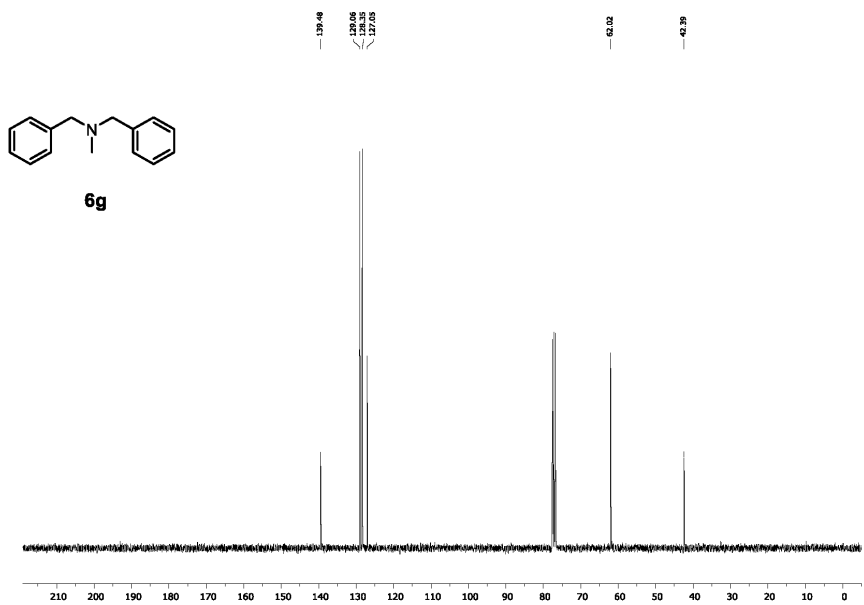
84

Figure S51: ¹³C NMR (101 MHz, CDCl₃) of **6f**.

85

Figure S52: ¹H NMR (400 MHz, CDCl₃) of **6g**, ● = water, CH₂Cl₂.

86

Figure S53: ¹³C NMR (101 MHz, CDCl₃) of **6g**.

87

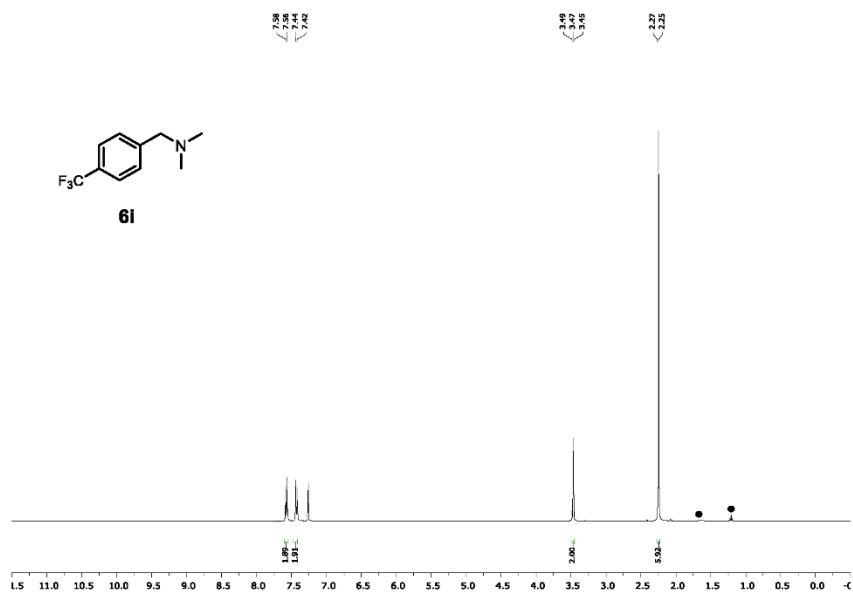


Figure S54: ¹H NMR (400 MHz, CDCl₃) of **6i**, ● = water, grease.

88

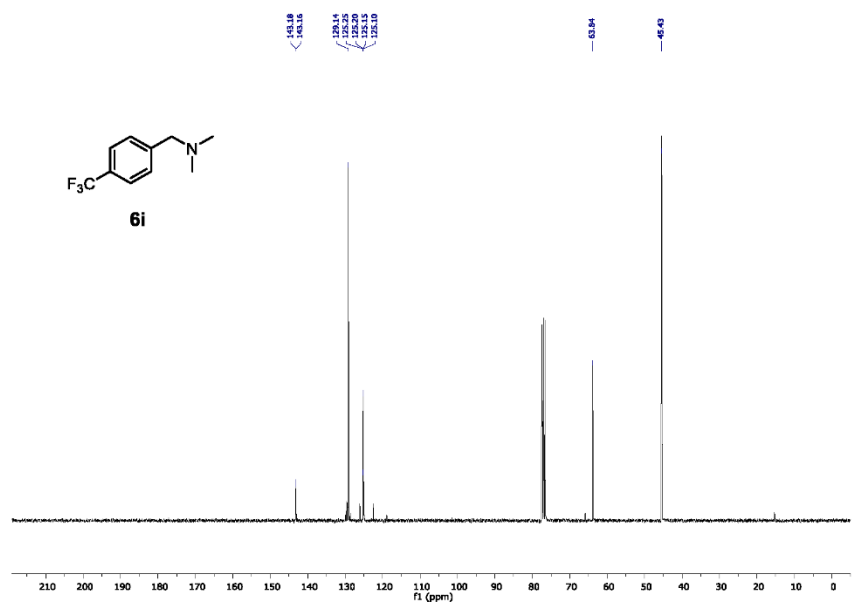


Figure S55: ¹³C NMR (101 MHz, CDCl₃) of **6i**.

89

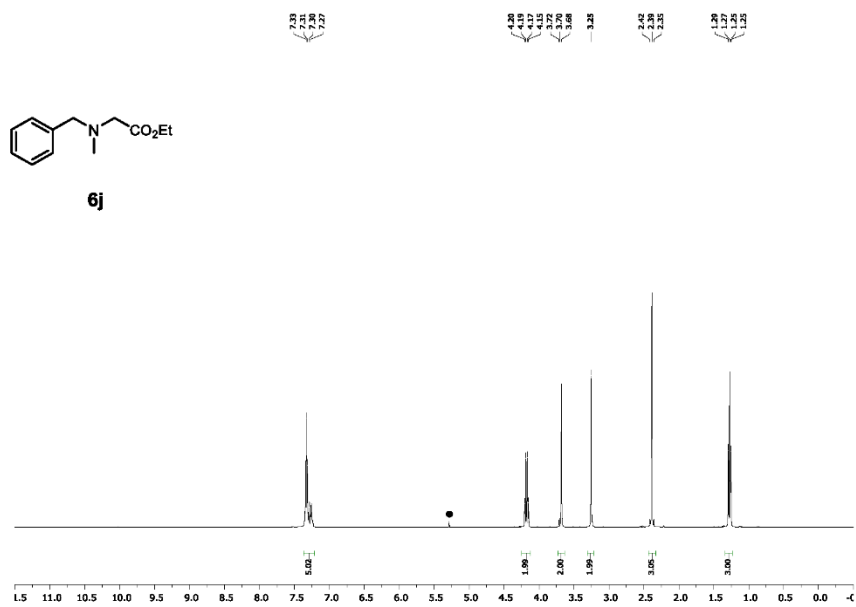


Figure S56: ¹H NMR (400 MHz, CDCl₃) of **6j**, • = CH₂Cl₂.

90

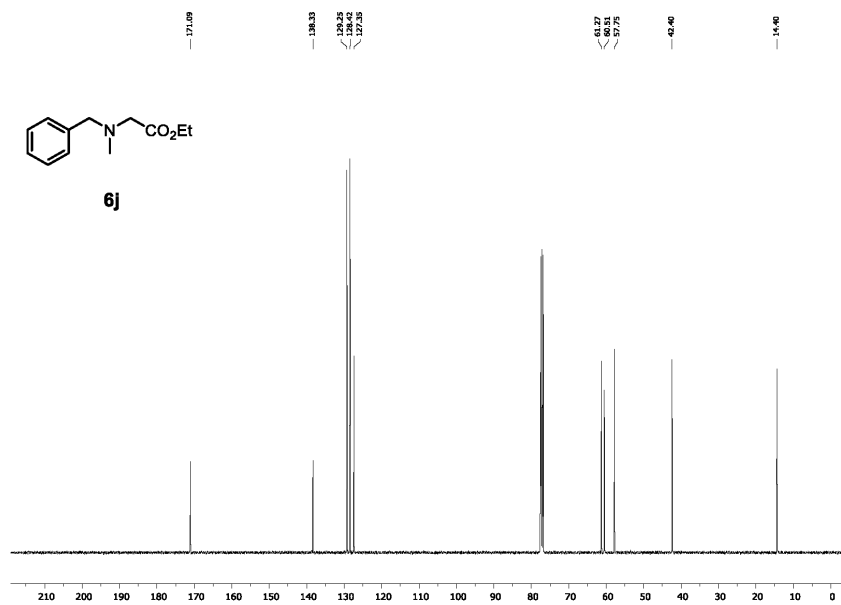
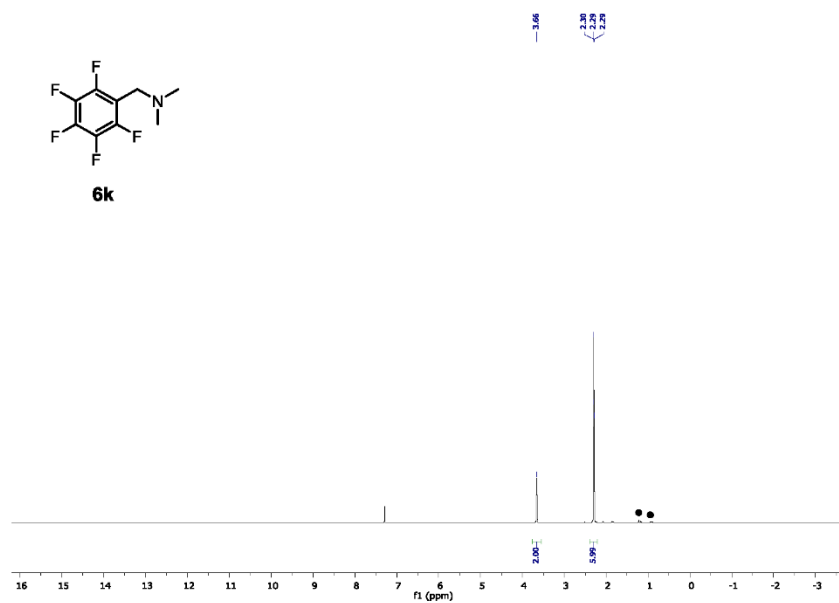
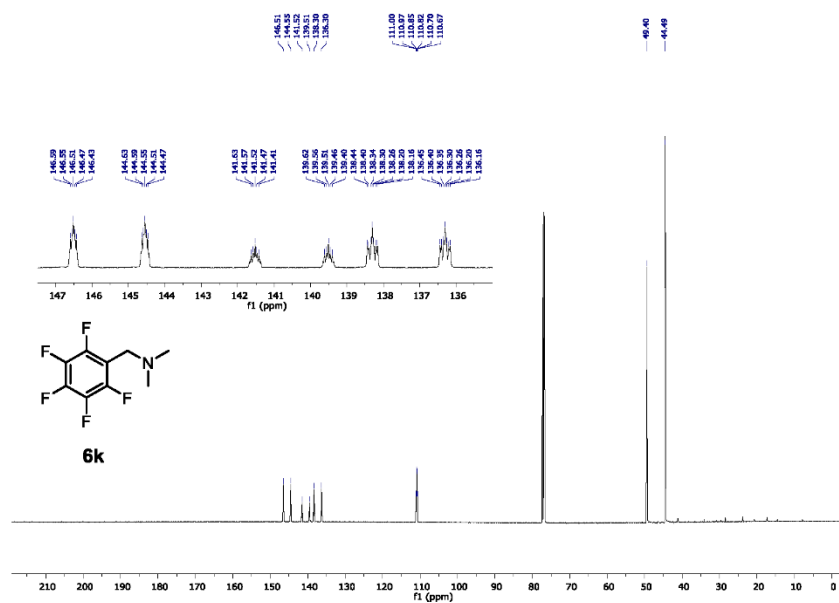


Figure S57: ¹³C NMR (101 MHz, CDCl₃) of **6j**.

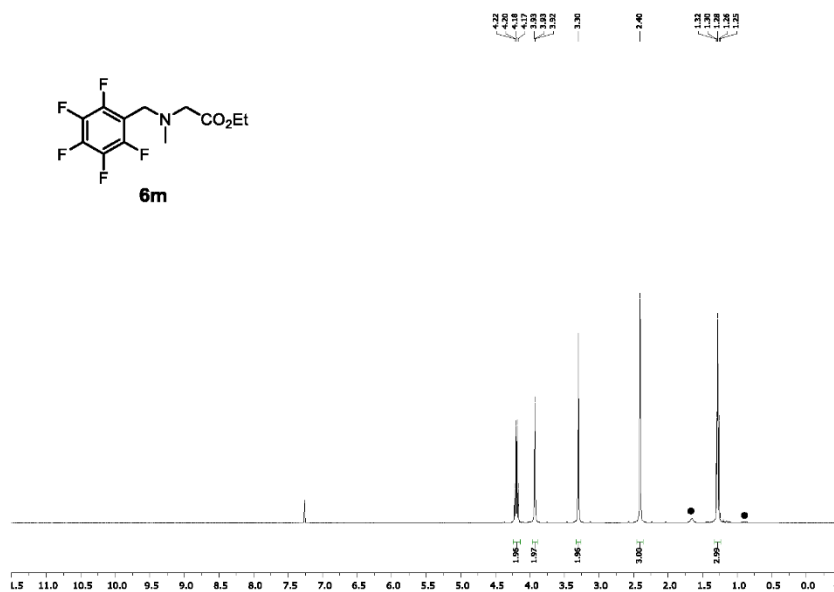
91

Figure S58: ¹H NMR (400 MHz, CDCl₃) of **6k**, ● = water, grease.

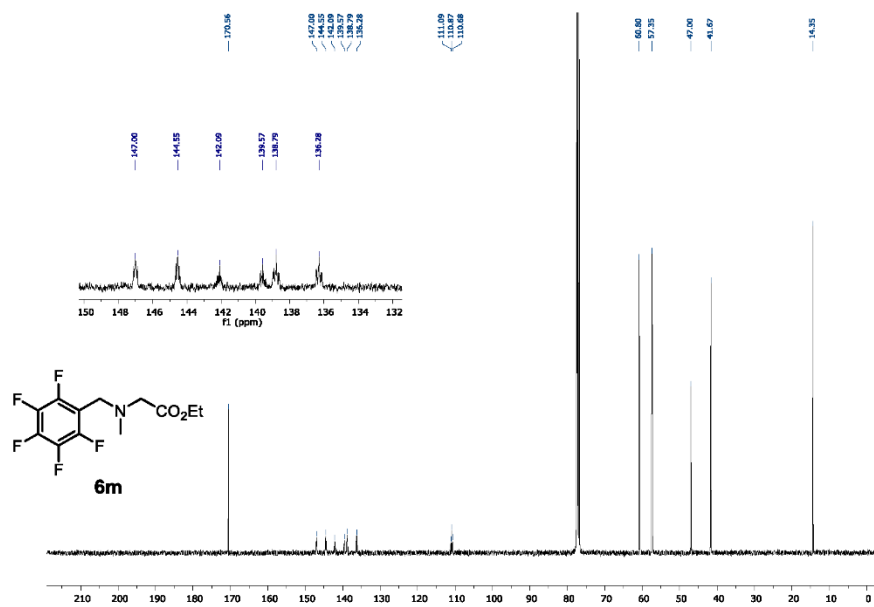
92

Figure S59: ¹³C NMR (126 MHz, CDCl₃) of **6k**.

93

Figure S62: ¹H NMR (400 MHz, CDCl₃) of **6m**, ● = water, grease.

96

Figure S63: ¹³C NMR (101 MHz, CDCl₃) of **6m**.

97

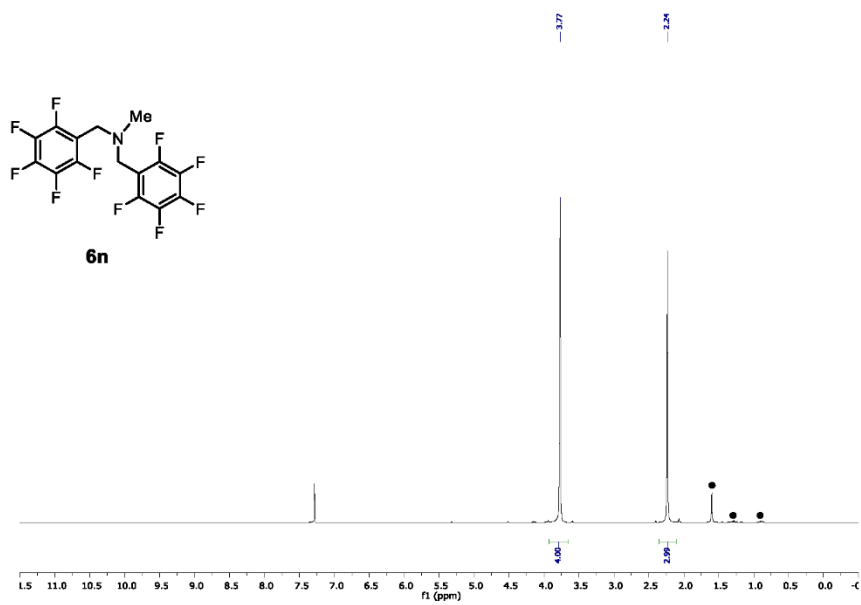


Figure S64: ¹H NMR (400 MHz, CDCl₃) of **6n**, ● = water, grease.

98

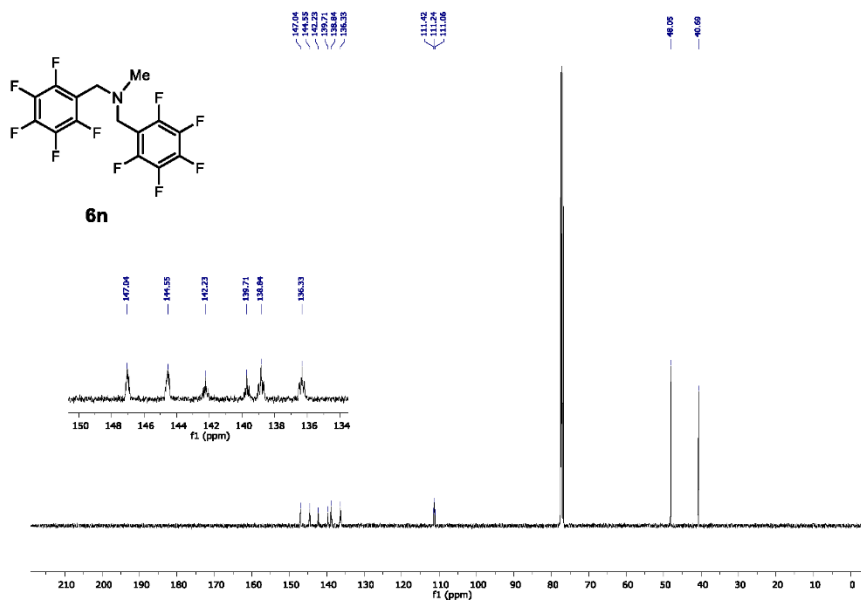


Figure S65: ¹³C NMR (101 MHz, CDCl₃) of **6n**.

99

References

- [1] *APEX suite of crystallographic software, APEX 2, version 2008.4.*, Bruker AXS Inc., Madison, Wisconsin, USA (2008).
- [2] *SAINT, version 7.56a, SADABS, version 2008.1*, Bruker AXS Inc., Madison, Wisconsin, USA (2008).
- [3] Hübschle, C. B.; Sheldrick, G. M.; Dittrich, B., *SHELXLE, J. Appl. Crystallogr.* **2011**, *44*, 1281-1284.
- [4] Sheldrick, G. M., *SHELXL-2014*, University of Göttingen, Göttingen, Germany (2014).
- [5] Sheldrick, G. M., *SHELXL-97*, University of Göttingen, Göttingen, Germany (1998).
- [6] Wilson, A. J. C., *International Tables for Crystallography*, Dordrecht, The Netherlands, Kluwer Academic Publishers (1992).
- [7] Spek, A. L., *J. Appl. Cryst.* **2003**, *36*, 7-13.
- [8] Spek, A. L., *Acta Cryst.* **2009**, *D65*, 148-155.
- [9] F. Neese, Version 3.0.3 ed., Max Plank Institute for Bioinorganic Chemistry, Mülheim an der Ruhr, Germany, **Jan 2012**.
- [10] J. P. Perdew, W. Yue, *Phys. Rev. B* **1986**, *33*, 8800.
- [11] J. P. Perdew, *Phys. Rev. B* **1986**, *33*, 8822.
- [12] A. D. Becke, *J. Chem. Phys.* **1986**, *84*, 4524.
- [13] A. D. Becke, *J. Chem. Phys.* **1993**, *98*, 5648.
- [14] C. T. Lee, W. T. Yang, R. G. Parr, *Phys. Rev. B* **1988**, *37*, 785.
- [15] A. Schäfer, H. Horn, R. Ahlrichs, *J. Chem. Phys.* **1992**, *97*, 2571.
- [16] A. Schäfer, C. Huber, R. Ahlrichs, *J. Chem. Phys.* **1994**, *100*, 5829.
- [17] K. Eichkorn, O. Treutler, H. Ohm, M. Häser, R. Ahlrichs, *Chem. Phys. Lett.* **1995**, *240*, 283.
- [18] K. Eichkorn, O. Treutler, H. Ohm, M. Häser, R. Ahlrichs, *Chem. Phys. Lett.* **1995**, *242*, 652.
- [19] R. Dennington, T. Keith, J. Milliam, Version 5.0 ed., Semichem Inc., Shawnee Mission KS, **2009**.
- [20] F. Neese, F. Wennmohs, A. Hansen and U. Becker, *Chem. Phys.*, **2009**, *356*, 98.
- [21] K. Eichkorn, F. Weigend, O. Treutler and R. Ahlrichs, *Theor. Chem. Acc.*, **1997**, *97*, 119.

- [22] C. J. van Wüllen, *J. Chem. Phys.*, **1998**, *109*, 392.
- [23] a) D. Rackel, V. Kais, P. Kreitmeier, O. Reiser, *Beilstein J. Org. Chem.* **2014**, *10*, 2157-2165; b) D. Lenhart, A. Pöthig, T. Bach, *Chem. Eur. J.* **2016**, *22*, 6519-6523
- [24] J. W. Tucker, J. M. R. Narayanam, S.W. Krabbe, C. R. J. Stephenson, *Org. Lett.* **2010**, *12*, 2, 368-371
- [25] Q. Lei, Y. Wei, D. Talwar, C. Wang, D. Xue, J. Xiao, *Chem. Eur. J.*, **2013**, *19*, 4021-4029
- [26] R. Feng, J. Yao, Z. Liang, Z. Liu, Y. Zhang, *J. Org. Chem.* **2013**, *78*(8), 3688
- [27] J. P. Barham, M. P. John, J. A. Murphy, *J. Am. Chem. Soc.* **2016**, *138*, 15482-15487
- [28] J. Michalak, H. B. Zhai, M. S. Platz, *J. Phys. Chem.* **1996**, *100*, 14028-14036
- [29] D. Lenhardt, A. Bauer, A. Pöthig, T. Bach, *Chem. Eur. J.* **2016**, *22*, 6519–6523
- [30] S. L. Murov, I. Carmichael, G. L. Hug, “*Handbook of Photochemistry*” , 2nd edition, Marcel Dekker, New York, 1993.
- [31] H. J. Kuhn, S. E. Braslavsky, R. Schmidt, *Pure Appl. Chem.* 2004, **76**, 2105–2146.
- [32] J. N. Demas, W. D. Bowman, E. F. Zalewski, R. A. Velapoldi, *J. Phys. Chem.* 1981, **85**, 2766–2771.
- [33] Y. Kaneko, Y. Nishimura, T. Arai, H. Sakuragi, K. Tokumaru, D. Matsunaga, *J. Photochem. Photobiol.* **1995**, *89*, 37
- [34] H.-C. Ku, C.-C. Wang, C.-H. Tu, *J. Chem. Eng. Data*, **2008**, *53*, 566–573
- [35] X.-H. Fan, Y.-P. Chen, C.-S. Su, *J. Chem. Eng. Data*, **2016**, *61*, 920–927
- [36] Hatchard, C. G.; Parker, C. A. *Proc. Roy. Soc. (London)* **1956**, *A235*, 518–536

Supporting Information Synthesis of Tetrahydroisoquinolines by Visible Light-mediated 6-exo-trig Cyclization of α -Aminoalkyl Radicals

Supporting Information
for DOI: 10.1055/s-0039-1690006

© 2019, Thieme. All rights reserved.

Georg Thieme Verlag KG, Rüdigerstraße 14, 70469 Stuttgart, Germany

Supporting Information for

Synthesis of Tetrahydroisoquinolines by Visible-light Mediated 6-*exo*-trig Cyclization of α -Aminoalkyl Radicals

Michael Grübel^a, Christian Jandl^a, Thorsten Bach^{*a}

^aDepartment Chemie and Catalysis Research Center (CRC), Technische Universität München,
Lichtenbergstraße 4, D-85748 Garching

Thosten.bach@ch.tum.de

Table of contents

Experimental	2
<i>Materials</i>	2
<i>Physical Measurements</i>	2
<i>Single crystal X-Ray Crystallography</i>	3
<i>Photochemical experiments</i>	4
<i>Optimization studies</i>	5
Table S1: Optimization studies.....	5
Syntheses	6
Molecular Structure	65
<i>Molecular Structure of 6</i>	65
Table S2: Sample and crystal data for 6	66
Table S3: Data collection and structure refinement of 6	67
Cyclic Voltammometry	68
NMR Spectra	76
References	132

Experimental

Materials

Chemicals were purchased from *Sigma Aldrich* and used without further purification, unless otherwise mentioned. Iridium catalysts were prepared according to literature¹ or purchased from *Sigma Aldrich*. Moisture or air sensitive reactions were conducted in flame-dried glass vessels under argon atmosphere. Dry solvents (MeOH, DMF) were purchased from *Acros Organics*. Dry CH₂Cl₂ and THF were taken from a MB-SPS-800 apparatus (*M. Braun*).

All solvents were deoxygenized via freeze-pump-thaw procedure prior to use. Dimethylformamide (DMF; 99.8% stored over molecular sieves). Tetrabutylammonium hexafluorophosphate was recrystallized four times from EtOH before use.

Physical Measurements

Solution state NMR spectra were recorded at room temperature on a *Bruker* AVA 400, *Bruker* AVA 500 or *Bruker* AVA 500cryo. ¹H-NMR spectra were calibrated to the residual solvent signal of chloroform-*d*₁ (CHCl₃ δ = 7.26 ppm), benzene-*d*₆ (C₆H₆ δ = 7.16 ppm) or methanol-*d*₄ (MeOD δ = 3.31 ppm). ¹³C-NMR spectra were calibrated to the ¹³C-D triplet of CDCl₃ (δ = 77.16 ppm), benzene-*d*₆ (C₆H₆ δ = 128.06 ppm) or methanol-*d*₄ (MeOD δ = 49.0 ppm). The following abbreviations for single multiplicities were used: s-singlet, d-doublet, t-triplet, q-quartet, quin-quintet.

HRMS measurements were performed on a Thermo Scientific DFS-HRMS spectrometer (EI, 70 eV), a Finnigan LCQ classic (ESI) and a ThermoFinnigan LTQ FT (HRMS-ESI) ESI mass spectra were measured on a Thermo Scientific™ UltiMate™ 3000 HPLC System using loop mode. Electrochemical measurements were carried out with an EmStat³⁺ potentiostat using a three-electrode cell equipped with glassy carbon working and counter electrode and a Ag/AgNO₃ as reference electrode. Potentials are reported with reference to AgNO₃. Melting points were measured on a Kofler melting point apparatus (Reichert) and are uncorrected. Infrared spectra were recorded on a PerkinElmer IR 4100 spectrometer directly measuring in substance via a total reflection method (ATR). Intensities are assigned as: w = weak, m = medium, s = strong. GC analysis was performed on an Agilent 7890B instrument (FID) with a HP 5 column (30 mm × 320 μm, 0.25 μm).

Single crystal X-Ray Crystallography

Data were collected on an X-ray single crystal diffractometer equipped with a CMOS detector (Bruker Photon-100), a IMS microsource with MoK α radiation ($\lambda = 0.71073 \text{ \AA}$) and a Helios mirror optic by using the APEX III software package.² The measurements were performed on a single crystal coated with perfluorinated ether. The crystal was fixed on top of a microsampler, transferred to the diffractometer and frozen under a stream of cold nitrogen. A matrix scan was used to determine the initial lattice parameters. Reflections were merged and corrected for Lorentz and polarization effects, scan speed, and background using SAINT.³ Absorption corrections, including odd and even ordered spherical harmonics, were performed using SADABS.³ Space group assignments were based upon systematic absences, E statistics, and successful refinement of the structures. Structures were solved by direct methods with the aid of successive difference Fourier maps, and were refined against all data using SHELXLE⁴ in conjunction with SHELXL-2014.⁵ Hydrogen atoms were assigned to ideal positions and refined using a riding model with an isotropic thermal parameter 1.2 times that of the attached carbon atom (1.5 times for methyl hydrogen atoms). If not mentioned otherwise, non-hydrogen atoms were refined with anisotropic displacement parameters. Full-matrix least-squares refinements were carried out by minimizing $\sum w(F_o^2 - F_c^2)^2$ with SHELXL-97⁶ weighting scheme. Neutral atom scattering factors for all atoms and anomalous dispersion corrections for the non-hydrogen atoms were taken from International Tables for Crystallography.⁷ Images of the crystal structures were generated by PLATON.^{8,9} CCDC 1915022 contains the supplementary crystallographic data for this paper. These data are provided free of charge by The Cambridge Crystallographic Data Centre.

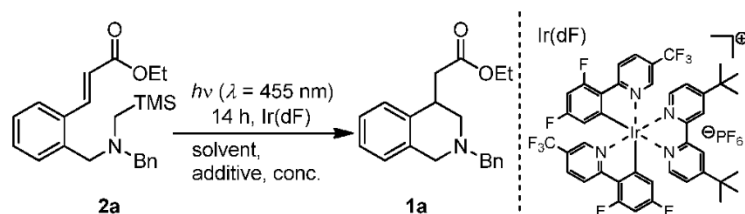
Photochemical experiments

All photochemical experiments were carried out using an individually built photoreactor. The interior of the photoreactor is lined with high performance mirrors. The lid and the LED with heat sink are exchangeable. The installed LEDs (10) are *Cree XLamp XP-G3* (3 W, Royal blue) lamps with a wavelength distribution of $\lambda = 455 \text{ nm} \pm 10 \text{ nm}$ at a working temperature of 25 °C (for the LED datasheet see: <https://www.cree.com/led-components/media/documents/dsXPG3.pdf>). The reactor chamber is cooled with two fans from each side for optimal air circulation. The LEDs are mounted on an aluminum heat sink with additional fans on top to guarantee working temperature of 25 °C.

All reaction tubes were flame-dried before usage. The photocatalytic reactions were conducted in 10 mL reactions tubes and are deoxygenated by three *freeze-pump-thaw* cycles before irradiation.

Optimization studies

Table S1: Optimization studies



entry	Ir-cat [mol%]	solvent	Conc [mM]	additive	Yield [%]	rsm. [%]
1	5	MeOH	50	-	7	-
2	5	EtOAc	50	-	3	-
3	5	DMSO	50	-	9	-
4	1	DMF	50	-	18	-
5	5	DMF	150	-	22	2
6	5	DMF	50	H ₂ O 2.0 eq	38	-
7	5	DMF	50	H ₂ O 10 eq	34	-
8	5	DMF	50	H ₂ O 100 eq	28	-
9	5	DMF	50	H ₂ O/Cs ₂ CO ₃ ; 1.0 eq/10 eq	29	27
10	5	DMF	50	H ₂ O/K ₃ PO ₄ ; 1.0 eq/1.0 eq	33	12
11	5	DMF	50	H ₂ O/KOAc; 1.0 eq/1.0 eq	45	-
12	5	DMF	50	H ₂ O/Na ₂ CO ₃ ; 1.0 eq/1.0 eq	33	-
13	5	DMF	50	H ₂ O/CsOPiv; 1.0 eq/1.0 eq	23	30
14	5	DMF	50	H ₂ O/KF; 1.0 eq/1.0 eq	44	-
15	5	DMF	50	H ₂ O/CsF; 1.0 eq/1.0 eq	38	-

Syntheses

General procedures

General procedure for *Wohl-Ziegler* bromination reactions **GP1**

1.00 eq. of the corresponding alkene substrate and 1.20 eq. *N*-bromosuccinimide (NBS) were dissolved in anhydrous chloroform (ca. 50 mM). 0.05 eq. of dibenzoyl peroxide (DBP) were added to the solution. The reaction mixture was heated to reflux until reaction monitoring by TLC showed full conversion. Afterwards, the reaction mixture was allowed to cool to room temperature, diluted with CH₂Cl₂ and washed with water (3 × 10 mL/mmol). The aqueous layer was re-extracted with CH₂Cl₂ (3 × 15 mL/mmol). The combined organic layers were washed with brine (1 × 20 mL/mmol), dried over Na₂SO₄, filtrated and the solvents were removed under reduced pressure.

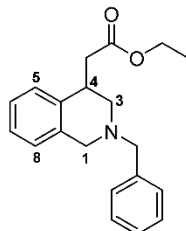
General procedure for substrates synthesis **GP2**

1.00 eq. of the brominated substrate was dissolved in acetone (30 mM) and 5.00 eq. K₂CO₃ were suspended in this solution. 1.10 eq. of the corresponding amine were added dropwise to the mixture which was subsequently heated under reflux (85 °C) over night with continuous stirring. The reaction mixture was allowed to cool to room temperature and remaining K₂CO₃ was removed by filtration at reduced pressure over celite. Residual organic solvents were removed under reduced pressure and the crude product was purified by column chromatography to obtain the desired amine.

General procedure for photocatalytic cyclization reactions **GP3**

1.00 eq. substrate, 1.00 eq. Cs₂CO₃, 1.00 eq. of H₂O and 0.05 eq. photoredox catalyst [Ir{dF(CF₃)ppy}₂(dtbpy)]PF₆ [Ir(dF)] were dissolved in dry DMF (ca. 2 ml per 0.10 mmol substrate). The yellow mixture was degassed by repeating three times a freeze-pump-thaw cycle and it was irradiated 14 hours with 30 W blue LED (λ = 455 nm) at room temperature in the previously described photoreactor while continuously stirring under argon atmosphere. After the indicated reaction time, water (ca. 5 ml/0.10 mmol substrate) was added. The phases were separated and the water layer was extracted with diethyl ether (3 × ca. 6 mL/0.10 mmol). The organic layers were washed with brine and dried over Na₂SO₄. After filtration, residual solvent was removed under reduced pressure. The crude product was purified by column chromatography to obtain the photoproduct.

Ethyl 2-(2-Benzyl-1,2,3,4-tetrahydroisoquinolin-4-yl) acetate (1a)



$C_{20}H_{23}NO_2$
Mw: 309.40 g/mol

According to **GP 3** 50.9 mg (133 μ mol, 1.00 eq.) of substrate **2a**, 7.48 mg (6.67 μ mol, 0.05 eq) of **[Ir(dF)]**, 2.40 mg (133 μ mol, 1.00 eq.) H_2O and 43.5 mg (133 μ mol, 1.00 eq.) Cs_2CO_3 in anhydrous dimethylformamide (3.00 mL) were irradiated for 14 hours. After purification by column chromatography (silica, pentane/EtOAc = 20/1) 21.3 mg (69.0 μ mol, 52 %) of product **1a** were isolated as a yellow oil.

TLC: R_f = 0.32 (pentane/EtOAc = 20/1), [UV/ $KMnO_4$].

IR (ATR): $\tilde{\nu}$ (cm^{-1}) = 3060 (w, C_{Ar-H}), 3027 (w C_{Ar-H}), 2980 (w, C-H), 2799 (w, C-H), 1731 (vs, C=O), 1494 (w), 1454 (m, C-H), 1370 (m, C-H), 1345 (w, C-N), 1260 (m), 1158 (m, C-O, ester), 1096 (w, C-N), 1029 (m) 748 (m, C_{Ar-H}).

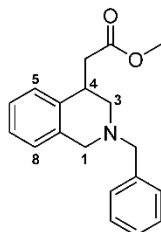
1H NMR (400 MHz, $CDCl_3$): δ (ppm) = 7.40 – 7.34 (m, 2H, 2 \times *meta*- C_{Ph-H}), 7.34 – 7.28 (m, 2H, 2 \times *ortho*- C_{Ph-H}), 7.27 – 7.21 (m, 1H, *para*- C_{Ph-H}), 7.17 – 7.07 (m, 3H, H-6, H-7, H-8), 7.00 – 6.94 (m, 1H, H-5), 4.13 – 3.99 (m, 2H, CH_2CH_3), 3.80 (d, 2J = 14.9 Hz, 1H, *CHH*-1), 3.71 (d, 2J = 13.1 Hz, 1H, Ph-*CHH*), 3.58 (d, 2J = 13.1 Hz, 1H, Ph-*CHH*), 3.42 (d, 2J = 14.9 Hz, 1H, *CHH*-1), 3.38 – 3.31 (m, 1H, H-4), 2.88 (dd, 2J = 16.0 Hz, 3J = 9.7 Hz, 1H, *CHHCO*₂Et), 2.80 (ddd, 3J = 11.7 Hz, 4J = 3.2 Hz, 4J = 1.3 Hz, 1H, *CHH*-3), 2.61 – 2.58 (m, 2H, *CHH*-3, *CHHCO*₂Et), 1.20 (t, 3J = 7.1 Hz, 3H, CH_2CH_3).

^{13}C -NMR (101 MHz, $CDCl_3$): δ (ppm) = 172.9 (s, CO_2Et), 138.7 (s, CH_2-C_{Ph}), 137.6 (s, C-4a), 135.3 (s, C-8a), 129.1 (d, *meta*- CH_{Ph}), 128.4 (d, C-8), 128.4 (d, *ortho*- CH_{Ph}), 127.2 (d, *para*- CH_{Ph}), 126.7 (d, C-6*), 126.5 (d, C-7*), 126.2 (d, C-5), 62.8 (t, CH_2-C_{Ph}), 60.4 (t, CH_2CH_3), 56.5 (t, C-1), 54.7 (t, C-3), 41.2 (t, CH_2CO_2Et), 35.8 (d, C-4), 14.3 (q, CH_2CH_3).

*Assignment is interconvertible

HRMS (ESI): m/z = calc. $[M+H]^+$: 310.1802; found: 310.1803.

GC-MS (EI, 70 eV): t_R = 16.9 min m/z (%) = 308 (12), 280 (7) $[M-C_2H_5]^+$, 264 (19) $[M-C_2H_5O]^+$, 218 (100) $[M-C_7H_7]^+$, 144 (10), 130 (26), 117 (20) $[C_9H_9]^+$, 91 (60) $[C_7H_7]^+$.

Methyl-2-(2-benzyl-1,2,3,4-tetrahydroisoquinolin-4-yl) acetate (1b)

C₁₉H₂₁NO₂
Mw: 295.38 g/mol

According to **GP 3** 48.8 mg (133 μ mol, 1.00 eq.) of substrate **2b**, 7.45 mg (6.64 μ mol, 0.05 eq) of **[Ir(dF)]**, 2.39 mg (133 μ mol, 1.00 eq.) H₂O and 43.3 mg (133 μ mol, 1.00 eq.) Cs₂CO₃ in anhydrous dimethylformamide (3.00 mL) were irradiated for 14 hours. After purification by column chromatography (silica, pentane/EtOAc = 20/1) 24.2 mg (82.0 μ mol, 62%) of **1b** could be isolated as a yellow oil.

TLC: R_f = 0.30 (pentane/EtOAc = 20/1), [UV/KMnO₄].

IR (ATR): $\tilde{\nu}$ (cm⁻¹) = 2925 (m, C_{Ar}-H), 2854 (w, C_{Al}-H), 1735 (s, C=O), 1653 (s, C=C), 1454 (m), 1257 (m), 1166 (m C-O, ester), 749 (m, C_{Ar}-H), 700 (m, C_{Ar}-H).

¹H NMR (400 MHz, CDCl₃): δ (ppm) = 7.41 – 7.36 (m, 2H, 2 \times *meta*-C_{Ph}-H), 7.35 – 7.29 (m, 2H, 2 \times *ortho*-C_{Ph}-H), 7.29 – 7.24 (m, 1H, *para*-C_{Ph}-H), 7.18 – 7.10 (m, 3H, H-6, H-7, H-8), 7.00 (d, ³ J = 6.5 Hz, 1H, H-5), 3.83 (d, ² J = 14.9 Hz, 1H, CHH-1), 3.74 (d, ² J = 13.1 Hz, 1H, Ph-CHH), 3.63 – 3.56 (m, 4H, CO₂CH₃, Ph-HH), 3.43 (d, ² J = 14.9 Hz, 1H, CHH-1), 3.37 – 3.30 (m, 1H, H-4), 2.93 (dd, ² J = 16.0 Hz, ³ J = 9.8 Hz, 1H, CHHCO₂CH₃), 2.85 – 2.78 (m, 1H, H-3), 2.67 – 2.54 (m, 2H, H-3, CHHCO₂CH₃).

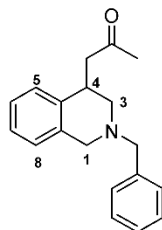
¹³C NMR (126 MHz, CDCl₃, 298 K): δ = 173.4 (s, CO₂CH₃), 138.7 (s, CH₂-C_{Ph}), 137.6 (s, C-4a), 135.3 (s, C-8a), 129.1 (d, *meta*-CH_{Ph}), 128.4 (d, C-8), 128.4 (d, *ortho*-CH_{Ph}), 127.2 (d, *para*-C_{Ph}), 126.7 (d, C-5), 126.5 (d, C-7), 126.3 (d, C-6), 62.8 (t, CH₂-C_{Ph}), 56.5 (t, C-1), 54.5 (t, C-3), 51.6 (q, CO₂CH₃), 41.0 (t, CH₂CO₂CH₃), 35.8 (d, C-4).

HRMS (ESI): m/z = calc. [C₁₉H₂₁NO₂+H]⁺: 296.1645; found: 296.1644.

GC-MS (EI, 70 eV): t_R = 17.8 min; m/z (%) = 294 (10), 264 (7) [M-OCH₃]⁺, 204 (100) [M-C₇H₇]⁺, 145 (5), 91 (51) [C₇H₇]⁺.

The analytical data obtained matched those reported in the literature.²¹

1-(2-Benzyl-1,2,3,4-tetrahydroisoquinolin-4-yl)propan-2-one (1c)



C₁₉H₂₁NO
Mw 279.38 g/mol

According to **GP 3** 51.0 mg (145 μ mol, 1.00 eq.) of substrate **2c**, 8.14 mg (7.25 μ mol, 0.05 eq) of **[Ir(dF)]**, 2.61 mg (145 μ mol, 1.00 eq.) H₂O and 47.3 mg (145 μ mol, 1.00 eq.) Cs₂CO₃ in anhydrous dimethylformamide (3.00 mL) were irradiated for 14 hours. After purification by column chromatography (silica, pentane/EtOAc = 50/1) 21.0 mg (75.2 μ mol, 52%) of **1c** were isolated as a yellow oil.

TLC: R_f = 0.20 (pentane/EtOAc = 15/1), [UV/KMnO₄].

IR (ATR): $\tilde{\nu}$ (cm⁻¹) = 3062 (w, C_{Ar}-H), 3026 (w C_{Ar}-H), 2924 (w, C-H), 1713 (vs, C=O), 1493 (w), 1453 (m, C-H), 1362 (m, C-H), 1258 (w), 1158 (m, C-O), 1094 (w), 1029 (w) 746 (s, C_{Ar}-H).

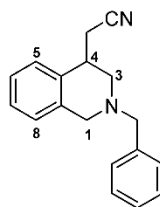
¹H NMR (400 MHz, CDCl₃): δ (ppm) = 7.38 – 7.35 (m, 2H, 2 \times *meta*-C_{Ph}-H), 7.35 – 7.30 (m, 2H, 2 \times *ortho*-C_{Ph}-H), 7.28 – 7.24 (m, 1H, *para*-C_{Ph}-H), 7.17 – 7.08 (m, 3H, H-6, H-7, H-8), 7.00 (d, ³J = 7.0 Hz, 1H, H-5), 3.84 (d, ²J = 14.9 Hz, 1H, CHH-1), 3.73 (d, ²J = 13.0 Hz, 1H, Ph-CHH), 3.55 (d, ²J = 13.0 Hz, 1H, Ph-CHH), 3.44 (d, ²J = 14.9 Hz, 1H, CHH-1), 3.42 – 3.37 (m, 1H, H-4), 3.15 (dd, ²J = 17.7 Hz, ³J = 9.6 Hz, 1H, CHHCOCH₃), 2.72 (d, ²J = 11.7 Hz, 1H, CHH-3), 2.63 (dd, ²J = 17.7 Hz, ⁴J = 3.3 Hz, 1H, CHHCOCH₃), 2.54 (dd, ²J = 11.7 Hz, ³J = 3.3 Hz, 1H, CHH-3), 2.01 (s, 3H, CH₃).

¹³C NMR (101 MHz, CDCl₃): δ (ppm) = 208.2 (s, CO), 138.1 (s, CH₂-C_{Ph}), 134.6 (s, C-4a), 129.9 (s, C-8a), 129.2 (d, *meta*-CH_{Ph}), 128.4 (d, *ortho*-CH_{Ph}, C-8), 127.3 (d, *para*-CH_{Ph}), 126.7 (d, C-5), 126.6 (d, C-6*), 126.1 (d, C-7*), 62.6 (t, CH₂-C_{Ph}), 56.5 (t, C-1), 54.3 (t, C-3), 50.5 (t, CH₂COCH₃), 34.2 (d, C-4), 30.7 (q, CH₃).

*Assignment is interconvertible

HRMS (ESI): calc. [C₁₉H₂₁NO+H]⁺: 280.1696; found: 280.1695.

GC-MS (EI, 70 eV): t_R = 16.4 min; m/z (%) = 278 (5), 220 (100) [M-C₃H₇O]⁺, 188 (95) [M-C₇H₇]⁺, 144 (5), 117 (35) [C₉H₉]⁺, 91 (80) [C₇H₇]⁺.

2-(2-Benzyl-1,2,3,4-tetrahydroisoquinolin-4-yl)acetonitrile (1d)

$C_{18}H_{18}N_2$
Mw 262.35 g/mol

According to **GP 3** 50.2 mg (150 μ mol, 1.00 eq.) of substrate **2d**, 8.42 mg (7.50 μ mol, 0.05 eq) of **[Ir(dF)]**, 2.70 mg (150 μ mol, 1.00 eq.) H_2O and 49.0 mg (150 μ mol, 1.00 eq.) CS_2CO_3 in anhydrous dimethylformamide (3.00 mL) were irradiated for 14 hours. After purification by column chromatography (silica, pentane/EtOAc = 30/1) 16.0 mg (61.0 μ mol, 41%) of **1d** were isolated as a yellow oil.

TLC: R_f = 0.17 (pentane/EtOAc = 15/1), [UV/ $KMnO_4$].

IR (ATR): $\tilde{\nu}$ (cm^{-1}) = 3063 (w, C_{Ar} -H), 3028 (w, C_{Ar} -H), 2923 (w, C-H), 2806 (w, C-H), 2762 (w, C-H), 2245 (w, $C\equiv N$), 1658 (m), 1454 (m, C-H), 1421 (m, C-H), 1369 (m), 1276 (m), 1145 (m, C-N), 1095 (m, C-N), 1028 (m, C-N), 748 (vs, C_{Ar} -H), 701 (vs, C_{Ar} -H).

1H NMR (400 MHz, $CDCl_3$): δ (ppm) = 7.40 – 7.33 (m, 4H, 2 \times *meta*- C_{Ph} -H, 2 \times *ortho*- C_{Ph} -H), 7.32 – 7.27 (m, 1H, *para*- C_{Ph} -H), 7.23 – 7.15 (m, 3H, H-6, H-7, H-8), 7.04 – 6.98 (m, 1H, H-5), 3.85 (d, 2J = 15.1 Hz, 1H, *CHH*-1), 3.77 – 3.63 (m, 2H, Ph- CH_2), 3.43 (d, 2J = 15.1 Hz, 1H, *CHH*-1), 3.23 – 3.13 (m, 1H, H-4), 3.01 – 2.98 (m, 1H, *CHH*-3), 2.89 (dd, 2J = 16.7, 3J = 9.0 Hz, 1H, *CHHCN*), 2.74 – 2.60 (m, 2H, *CHHCN*, *CHH*-3).

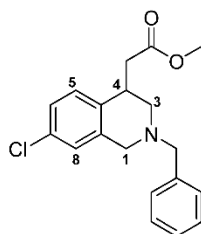
^{13}C NMR (101 MHz, $CDCl_3$): δ (ppm) = 138.4 (s, CH_2 - C_{Ph}), 135.5 (s, C-4a), 135.5 (s, C-8a), 129.4 (d, *meta*- CH_{Ph}), 128.9 (d, C-8), 128.9 (d, *ortho*- CH_{Ph}), 127.9 (d, *para*- CH_{Ph}), 127.5 (d, C-5), 127.3 (d, C-6*), 127.1 (d, C-7*), 119.6 (s, CN), 63.1 (t, CH_2 - C_{Ph}), 56.5 (t, C-1), 54.4 (t, C-3), 36.9 (d, C-4), 24.7 (t, CH_2CN).

*Assignment is interconvertible

HRMS (ESI): calc. $[C_{18}H_{18}N_2+H]^+$: 263.1543; found: 263.1542.

GC-MS (EI, 70 eV): t_R = 16.5 min; m/z (%) = 261 (2), 220 (50), 185 (20) $[M-C_6H_6]^+$, 171 (90) $[M-C_7H_7]^+$, 144 (10), 130 (25), 116 (48), 91 (100) $[C_7H_7]^+$.

The analytical data obtained matched those reported in the literature.²¹

Methyl 2-(2-benzyl-7-chloro-1,2,3,4-tetrahydroisoquinolin-4-yl)acetate (1e)

C₁₉H₂₀ClNO₂
Mw: 329.82 g/mol

According to **GP 3** 47.7 mg (119 μmol, 1.00 eq.) of substrate **2e**, 6.66 mg (5.93 μmol, 0.05 eq) of **[Ir(dF)]**, 2.14 mg (119 μmol, 1.00 eq.) H₂O and 38.7 mg (119 μmol, 1.00 eq.) Cs₂CO₃ in anhydrous dimethylformamide (3.00 mL) were irradiated for 14 hours. After purification by column chromatography (silica, pentane/EtOAc = 20/1) 26.0 mg (78.8 μmol, 66%) of **1e** could be isolated as a yellow oil.

TLC: *R_f* = 0.23 (pentane/EtOAc = 20/1) [UV/KMnO₄].

IR (ATR): $\tilde{\nu}$ (cm⁻¹) = 3026(w) 2926 (m, C_{Ar}-H), 2793 (w, C_{Al}-H), 1736 (s, C=O), 1486 (m), 1436 (m), 1364 (m), 1259 (m), 1165 (s, C-O, ester), 1086 (w).

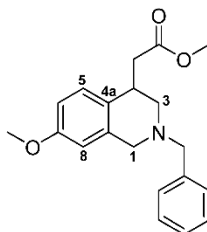
¹H NMR (400 MHz, CDCl₃): δ (ppm) = 7.39 – 7.35 (m, 2H, 2 × *meta*-C_{Ph}-H), 7.35 – 7.30 (m, 2H, 2 × *ortho*-C_{Ph}-H), 7.29 – 7.25 (m, 1H, *para*-C_{Ph}-H), 7.15 – 7.06 (m, 2H, H-6, H-8), 7.00 – 6.97 (m, 1H, H-5), 3.82 – 3.70 (m, 2H, *CHH*-1, Ph-*CHH*), 3.62 – 3.57 (m, 4H, CO₂CH₃, Ph-*CHH*), 3.39 (d, ²*J* = 14.9 Hz, 1H, *CHH*-1), 3.33 – 3.27 (m, 1H, H-4), 2.88 (dd, ²*J* = 16.1 Hz, ³*J* = 9.5 Hz, 1H, *CHHCO*₂CH₃), 2.81 (d, ²*J* = 10.9 Hz, 1H, *CHH*-3), 2.62 – 2.53 (m, 2H, *CHH*-3, *CHHCO*₂CH₃).

¹³C NMR (101 MHz, CDCl₃): δ (ppm) = 173.1 (s, CO₂CH₃), 138.2 (s, CH₂-C_{Ph}), 137.1 (s, C-8a), 136.0 (s, C-4a), 131.9 (s, C-7), 129.8 (d, C-6), 129.1 (d, *meta*-CH_{Ph}), 128.4 (d, *ortho*-CH_{Ph}), 127.3 (d, *para*-CH_{Ph}), 126.7 (d, C-8), 126.6 (d, C-5), 62.6 (t, CH₂-C_{Ph}), 56.0 (t, C-1), 54.3 (t, C-3), 51.7 (q, CO₂CH₃), 40.8 (t, CH₂CO₂CH₃), 35.2 (d, C-4).

HRMS (ESI): *m/z* = calc. [C₁₉H₂₀³⁵ClNO₂+H]⁺: 330.1255 found: 330.1255

GC-MS (EI, 70 eV): *t_R* = 18.56 min *m/z* (%) = 328 (5), 298 (5) [M-OCH₃]⁺, 254 (5), 238 (100) [M-C₇H₇]⁺, 164 (10), 91 (33) [C₇H₇]⁺.

Methyl 2-(2-benzyl-7-methoxy-1,2,3,4-tetrahydroisoquinolin-4-yl)acetate (1f)



$C_{20}H_{23}NO_3$
Mw: 325.40 g/mol

According to **GP 3** 52.3 mg (132 μ mol, 1.00 eq.) of substrate **2f**, 7.38 mg (6.58 μ mol, 0.05 eq) of **[Ir(dF)]**, 2.37 mg (132 μ mol, 1.00 eq.) H_2O and 42.9 mg (132 μ mol, 1.00 eq.) Cs_2CO_3 in anhydrous dimethylformamide (3.00 mL) were irradiated for 14 hours. After purification by column chromatography (silica, pentane/EtOAc = 50/1) 25.0 mg (76.8 μ mol, 59%) of **1f** could be isolated as a yellow oil.

TLC: R_f = 0.23 (pentane/EtOAc = 20/1), [UV/ $KMnO_4$].

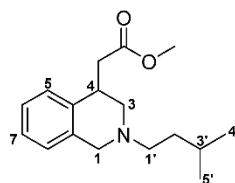
IR (ATR): $\tilde{\nu}$ (cm^{-1}) = 3026(w) 2926 (m, $C_{Ar}-H$), 2852 (w, $C_{Ar}-H$), 1735 (s, C=O), 1612 (m, C=C, conjugated), 1503 (s), 1435 (m), 1276 (m), 1246 (s), 1163 (s, C-O, ester), 1099 (w), 1038 (w).

1H NMR (400 MHz, $CDCl_3$): δ (ppm) = 7.41 – 7.36 (m, 2H, 2 \times *meta*- $C_{Ph}-H$), 7.35 – 7.30 (m, 2H, 2 \times *ortho*- $C_{Ph}-H$), 7.29 – 7.24 (m, 1H, *para*- $C_{Ph}-H$), 7.07 (d, 3J = 8.5 Hz, 1H, H-5), 6.73 (dd, 3J = 8.5 Hz, 4J = 2.7 Hz, 1H, H-6), 6.52 (d, 4J = 2.7 Hz, 1H, H-8), 3.82 – 3.69 (m, 5H, OCH_3 , *CHH*-1, *Ph-CHH*), 3.63 – 3.56 (m, 4H, CO_2CH_3 , *Ph-CHH*), 3.40 (d, 2J = 15.0 Hz, 1H, *CHH*-1), 3.32 – 3.25 (m, 1H, H-4), 2.88 (dd, 2J = 15.9 Hz, 3J = 9.6 Hz, 1H, *CHHCO* $_2$ CH_3), 2.83 – 2.77 (m, 1H, *CHH*-3), 2.64 – 2.55 (m, 2H, *CHH*-3, *CHHCO* $_2$ CH_3).

^{13}C NMR (101 MHz, $CDCl_3$): δ (ppm) = 173.5 (s, CO_2CH_3), 158.0 (s, C-7), 138.6 (s, CH_2-C_{Ph}), 136.4 (s, C-8a), 129.6 (s, C-4a), 129.3 (d, C-8), 129.1 (d, *meta*- CH_{Ph}), 128.4 (d, *ortho*- CH_{Ph}), 127.2 (d, *para*- CH_{Ph}), 113.0 (d, C-6), 111.1 (d, C-5), 62.7 (t, CH_2-C_{Ph}), 56.6 (t, C-1), 55.3 (q, OCH_3), 54.8 (t, C-3), 51.6 (q, CO_2CH_3), 41.0 (t, $CH_2CO_2CH_3$), 35.0 (C-4).

HRMS (ESI): m/z = calc. $[C_{20}H_{23}NO_3+H]^+$: 326.1751 found: 326.1752

GC-MS (EI, 70 eV): t_R = 19.14 min m/z (%) = 324 (5), 310 (5) $[M-CH_3]^+$, 250 (5), 234 (100) $[M-C_7H_7]^+$, 175.1 (20), 91 (30) $[C_7H_7]^+$.

Methyl 2-(2-isopentyl-1,2,3,4-tetrahydroisoquinolin-4-yl)acetate (1g)

$C_{17}H_{25}NO_2$
Mw: 275.39 g/mol

According to **GP 3** 51.0 mg (146 μ mol, 1.00 eq.) of substrate **2g**, 8.23 mg (7.34 μ mol, 0.05 eq) of **[Ir(dF)]**, 2.64 mg (146 μ mol, 1.00 eq.) H_2O and 47.8 mg (146 μ mol, 1.00 eq.) Cs_2CO_3 in anhydrous dimethylformamide (3.00 mL) were irradiated for 14 hours. After purification by column chromatography (silica, pentane/EtOAc = 50/1) 16.5 mg (60.0 μ mol, 41%) of **1g** were isolated as a yellow oil.

TLC: R_f = 0.23 (pentane/EtOAc = 20/1), [UV/ $KMnO_4$].

IR (ATR): $\tilde{\nu}$ (cm^{-1}) = 2953 (s, C-H), 2926 (m, C-H), 2868 (w), 2804 (w), 1737 (vs, C=O), 1466 (m, C-H), 1437 (m, C-H), 1360 (m), 1249 (m, C-N), 1165 (s, C-O, ester), 1100 (w), 749 (vs, C_{Ar} -H, 1,2-disubst.), 728 (w).

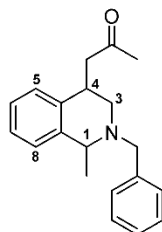
1H -NMR (400 MHz, $CDCl_3$): δ (ppm) = 7.17 – 7.09 (m, 3H, H-5, H-6, H-7), 7.05 – 7.00 (m, 1H, H-8), 3.78 (d, 2J = 15.1 Hz, 1H, CHH-1), 3.71 (s, 3H, CO_2CH_3), 3.40 (d, 2J = 15.1 Hz, 1H, CHH-1), 3.36 – 3.30 (m, 1H, H-4), 2.92 – 2.73 (m, 2H, CHH-3, CHH CO_2CH_3), 2.68 – 2.37 (m, 4H, CHH CO_2CH_3 , CHH-3, H-1'), 1.66 (h, 6.6 Hz, 1H, H-3'), 1.43 (q, 3J = 7.1 Hz, 2H, H-2'), 0.92 (d, 3J = 6.6 Hz, 6H, H-4', H-5').

^{13}C -NMR (101 MHz, $CDCl_3$): δ (ppm) = 173.6 (s, CO), 137.6 (s, C-4a), 135.5 (s, C-8a), 128.3 (d, C-5), 126.7 (d, C-6), 126.5 (d, C-7), 126.2 (d, C-8), 56.8 (t, C-1), 56.5 (t, C-1'), 55.1 (t, $CH_2CO_2CH_3$), 51.7 (q, CO_2CH_3), 40.9 (t, C-3), 36.2 (t, C-2'), 35.8 (d, C-4), 26.4 (d, C-3'), 22.9 (q, C-4'), 22.8 (q, C-5').

HRMS (ESI): m/z = calc. $[C_{17}H_{25}NO_2+H]^+$: 276.1958; found: 276.1957.

GC-MS (EI, 70 eV): t_R = 14.4 min; m/z (%) = 275 (11) $[M]^+$, 244 (8) $[M-OCH_3]^+$, 218 (100) $[M-CO_2CH_3+2H]^+$, 204 (53) $[M-C_5H_{11}]^+$, 144 (8), 115 (20), 91 (5) $[C_7H_7]^+$.

1-(2-Benzyl-1-methyl-1,2,3,4-tetrahydroisoquinolin-4-yl)propan-2-one (1h)



C₂₀H₂₃NO
Mw 293.41 g/mol

According to **GP 3** 90.4 mg (247 μ mol, 1.00 eq.) of substrate **2h**, 13.9 mg (12.4 μ mol, 0.05 eq) of **[Ir(dF)]**, 4.45 mg (247 μ mol, 1.00 eq.) H₂O and 80.6 mg (247 μ mol, 1.00 eq.) Cs₂CO₃ in 5.00 ml anhydrous DMF were irradiated for 14 hours. After purification by column chromatography (silica, pentane/EtOAc = 100/1) 41.0 mg (140 μ mol, 57%, d.r. = 80/20) of **1h** were isolated as a yellow oil.

IR (ATR): $\tilde{\nu}$ (cm⁻¹) = 3062 (w, C_{Ar}-H), 3027 (w, C_{Ar}-H), 2928 (w, C-H), 2799 (w, C-H), 1715 (vs, C=O), 1493 (m), 1453 (m, C-H), 1363 (m), 1158 (m, C-O), 760 (m, C_{Ar}-H), 701 (m, C_{Ar}-H).

Major diastereoisomer

TLC: R_f = 0.21 (pentane/EtOAc = 15/1), [UV/KMnO₄].

¹H NMR (400 MHz, CDCl₃): δ (ppm) = 7.38 – 7.34 (m, 2H, 2 \times *meta*-C_{Ph}-H), 7.34 – 7.30 (m, 2H, 2 \times *ortho*-C_{Ph}-H), 7.28 – 7.23 (m, 1H, *para*-C_{Ph}-H), 7.21 – 7.12 (m, 3H, H-6, H-7, H-8), 7.10 (d, ³J = 7.3 Hz, 1H, H-5), 4.08 (d, ²J = 13.6 Hz, 1H, Ph-CHH), 3.74 (q, ³J = 6.0 Hz, 1H, H-1), 3.36 (d, ²J = 13.6 Hz, 1H, Ph-CHH), 3.34 – 3.29 (m, 1H, H-4), 3.04 (dd, ²J = 17.6 Hz, ³J = 9.0 Hz, 1H, CHHCOCH₃), 2.80 – 2.71 (m, 1H, CHH-3), 2.65 (dd, ²J = 17.6, ⁴J = 3.9 Hz, 1H, CHHCOCH₃), 2.61 – 2.53 (m, 1H, CHH-3), 1.97 (s, 3H, COCH₃), 1.54 (d, ³J = 6.0 Hz, 3H, CH₃).

¹³C NMR (101 MHz, CDCl₃): δ (ppm) = 208.1 (s, CO), 140.4 (s, CH₂-C_{Ph}), 139.7 (s, C-4a), 138.3 (s, C-8a), 129.0 (d, *meta*-CH_{Ph}), 128.3 (d, *ortho*-CH_{Ph}), 128.2 (d, C-5), 127.2 (d, C-6*), 127.1 (d, *para*-C_{Ph}), 126.2 (d, C-7*), 126.1 (d, C-8), 58.7 (t, CH₂-C_{Ph}), 57.7 (d, C-1), 51.0 (t, C-3), 49.4 (t, CH₂COCH₃), 33.8 (d, C-4), 30.6 (q, COCH₃), 22.0 (q, CH₃).

*Assignment is interconvertible

Minor diastereoisomer

TLC: $R_f = 0.17$ (pentane/EtOAc = 15/1), [UV/KMnO₄].

¹H NMR (400 MHz, CDCl₃): δ (ppm) = 7.37 – 7.33 (m, 2H, 2 × *meta*-C_{Ph}-H), 7.33 – 7.28 (m, 2H, 2 × *ortho*-C_{Ph}-H), 7.26 – 7.22 (m, 1H, *para*-C_{Ph}-H), 7.16 – 7.11 (m, 2H, H-5, H-8), 7.08 – 7.02 (m, 2H, H-6, H-7), 4.14 (t, ³*J* = 6.8 Hz, 1H, H-1), 3.81 (d, ²*J* = 13.0 Hz, 1H, Ph-CHH), 3.55 (d, ²*J* = 13.0 Hz, 1H, Ph-CHH), 3.30 – 3.21 (m, 1H, H-4), 3.09 (dd, ²*J* = 17.8 Hz, ³*J* = 10.1 Hz, 1H, CHHCOCH₃), 2.94 (d, ²*J* = 12.3 Hz, 1H, CHH-3), 2.43 (d, ²*J* = 17.8 Hz, 1H, CHHCOCH₃), 2.36 (d, ²*J* = 12.3 Hz, 1H, CHH-3), 1.82 (s, 3H, COCH₃), 1.28 (d, ³*J* = 6.7 Hz, 3H, CH₃).

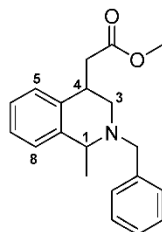
¹³C NMR (101 MHz, CDCl₃): δ (ppm) = 208.3 (s, CO), 141.5 (s, CH₂-C_{Ph}), 139.7 (s, C-4a), 138.1 (s, C-8a), 129.3 (d, *meta*-CH_{Ph}), 128.8 (d, *ortho*-CH_{Ph}), 128.3 (d, C-8), 127.3 (d, *para*-CH_{Ph}), 127.1 (d, C-5*), 126.4 (d, C-6*), 125.9 (d, C-7*), 58.4 (t, CH₂-C_{Ph}), 56.7 (d, C-1), 50.7 (d, CH₂COCH₃), 45.1 (t, C-3), 34.3 (d, C-4), 30.5 (q, COCH₃), 14.8 (q, CH₃).

*Assignment is interconvertible

HRMS (ESI): calc. [C₂₀H₂₃NO+H]⁺: 294.1852; found: 294.1852.

GC-MS (EI, 70 eV): $t_R = 16.8$ min; m/z (%) = 278 (100) [M-CH₃]⁺, 220 (10), 186 (2), 131 (7), 91 (80) [C₇H₇]⁺.

Methyl (Z)-2-(2-benzyl-1-methyl-2,3-dihydroisoquinolin-4(1H)-ylidene)acetate (1i)



$C_{20}H_{23}NO_2$
Mw: 309.40 g/mol

According to **GP 3** 49.0 mg (128 μ mol, 1.00 eq.) of substrate **2i**, 7.20 mg (6.42 μ mol, 0.05 eq) of **[Ir(dF)]**, 2.31 mg (128 μ mol, 1.00 eq.) H_2O and 41.8 mg (128 μ mol, 1.00 eq.) Cs_2CO_3 in anhydrous dimethylformamide (3.00 mL) were irradiated for 14 hours. After purification by column chromatography (silica, pentane/EtOAc = 50/1) 33.0 mg (107 μ mol, 83%, d.r. 82/18) of **1i** could be isolated as a yellow oil.

IR (ATR): $\tilde{\nu}$ (cm^{-1}) = 2949 (w, $C_{Ar}-H$), 2799 (w, C-H), 1734 (vs, C=O), 1492 (w), 1435 (m, C-H), 1364 (m, C-H), 1296 (m), 1157 (s, C-O, ester), 1099 (w, C-N), 764 (m, $C_{Ar}-H$, 1,2-disubst.).

Major diastereoisomer

TLC: R_f = 0.49 (P/EtOAc = 10/1), [UV/ $KMnO_4$].

1H NMR (400 MHz, $CDCl_3$): δ (ppm) = 7.39 – 7.36 (m, 2H, 2 \times meta- $C_{Ph}-H$), 7.33 – 7.29 (m, 2H, 2 \times ortho- $C_{Ph}-H$), 7.27 – 7.22 (m, 1H, para- $C_{Ph}-H$), 7.22 – 7.13 (m, 4H, H-5, H-6, H-7, H-8), 4.10 (d, 2J = 13.6 Hz, 1H, Ph-CHH), 3.75 (q, 3J = 6.3 Hz, 1H, H-1), 3.55 (s, 3H, CO_2CH_3), 3.40 (d, 2J = 13.6 Hz, 1H, Ph-CHH), 3.26 (dq, 3J = 9.0 Hz, 3J = 5.0 Hz, 1H, H-4), 2.90 – 2.80 (m, 2H, CHH-3, CHHCO $_2$ CH $_3$), 2.66 (dd, 2J = 16.0 Hz, 3J = 5.0 Hz, 1H, CHHCO $_2$ CH $_3$), 2.62 – 2.56 (m, 1H, CHH-3), 1.53 (d, 3J = 6.3 Hz, 3H, CH $_3$).

^{13}C NMR (101 MHz, $CDCl_3$): δ (ppm) = 173.2 (s, CO), 140.4 (s, C-8a), 139.6 (s, CH_2-C_{Ph}), 137.7 (s, C-4a), 128.9 (d, meta- CH_{Ph}), 128.3 (d, ortho- CH_{Ph}), 128.1 (d, C-8*), 127.3 (d, C-5*), 127.0 (d, para- CH_{Ph}), 126.4 (d, C-6**), 126.1 (d, C-7**), 58.9 (t, CH_2-C_{Ph}), 57.8 (d, C-1), 51.5 (q, CO_2CH_3), 50.9 (t, C-3), 39.9 (t, $CH_2CO_2H_3$), 35.1 (d, C-4), 21.9 (q, CH $_3$).

*/**Assignment is interconvertible

Minor diastereoisomer

TLC: $R_f = 0.38$ (pentane/EtOAc = 10/1), [UV/KMnO₄].

¹H NMR (400 MHz, CDCl₃): δ (ppm) = 7.39 – 7.35 (m, 2H, 2 × *meta*-C_{Ph}-H), 7.33 – 7.28 (m, 2H, 2 × *ortho*-C_{Ph}-H), 7.27 – 7.22 (m, 1H, *para*-C_{Ph}-H), 7.17 – 7.09 (m, 3H, H-6, H-7, H-8), 7.06 – 7.00 (m, 1H, H-5), 4.10 (q, ³*J* = 6.6 Hz, 1H, H-1), 3.83 (d, ²*J* = 13.1 Hz, 1H, Ph-CHH), 3.63 (d, ²*J* = 13.1 Hz, 1H, Ph-CHH), 3.52 (s, 3H, CO₂CH₃), 3.23 – 3.17 (m, 1H, H-4), 3.00 (d, ²*J* = 10.6 Hz, 1H, CHH-3), 2.88 (dd, ²*J* = 16.2 Hz, ³*J* = 10.1 Hz, 1H, CHHCO₂CH₃), 2.55 – 2.45 (m, 2H, CHH-3, CHHCO₂CH₃), 1.28 (d, ³*J* = 6.6 Hz, 3H, CH₃).

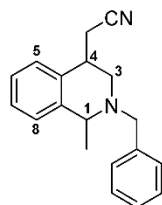
¹³C NMR (101 MHz, CDCl₃): δ (ppm) = 173.5 (s, CO), 141.4 (s, C-8a), 139.4 (s, CH₂-C_{Ph}), 137.5 (s, C-4a), 129.2 (d, *meta*-CH_{Ph}), 128.8 (d, C-8), 128.3 (d, *ortho*-CH_{Ph}), 127.4 (d, *para*-CH_{Ph}), 127.0 (d, C-5), 126.4 (d, C-6*), 126.2 (d, C-7*), 58.4 (t, CH₂-C_{Ph}), 56.0 (d, C-1), 51.5 (q, CO₂CH₃), 45.8 (t, C-3), 41.1 (t, CH₂CO₂CH₃), 35.9 (d, C-4), 14.8 (q, CH₃).

*Assignment is interconvertible

HRMS (ESI): $m/z = \text{calc. } [C_{20}H_{23}NO_2+H]^+$: 310.1802 found: 310.1803

GC-MS (EI, 70 eV): $t_R = 16.8$ min m/z (%) = 294 (100) [M-CH₃]⁺, 278 (5) [M-OCH₃]⁺, 218 (5) [M-C₇H₇]⁺, 144 (2), 91 (60) [C₇H₇]⁺.

2-(2-Benzyl-1-methyl-1,2,3,4-tetrahydroisoquinolin-4-yl)-acetonitrile (1j)



$C_{19}H_{20}N_2$
Mw 276.38 g/mol

According to **GP 3** 44.0 mg (126 μ mol, 1.00 eq.) of substrate **2j**, 7.08 mg (6.31 μ mol, 0.05 eq) of **[Ir(dF)]**, 2.27 mg (126 μ mol, 1.00 eq.) H_2O and 41.1 mg (126 μ mol, 1.00 eq.) Cs_2CO_3 in anhydrous dimethylformamide (3.00 mL) were irradiated for 14 hours. After purification by column chromatography (silica, pentane/EtOAc = 100/1) 15.0 mg (54.3 μ mol, 43%, d.r. = 73/27) of **1j** were isolated as a yellow oil.

IR (ATR): $\tilde{\nu}$ (cm^{-1}) = 3028 (w, C_{Ar-H}), 2974 (m, C-H), 2804 (w, C-H), 2245 (w, $C\equiv N$), 1493 (s) 1453 (s, C-H), 1370 (m), 1326 (w), 1276 (m), 1156 (m, C-N), 1099 (m, C-N), 1028 (m, C-N), 755 (vs, C_{Ar-H}), 70 (vs, C_{Ar-H}).

Major diastereoisomer

TLC: R_f = 0.26 (pentane/EtOAc = 15/1), [UV/ $KMnO_4$].

1H NMR (400 MHz, $CDCl_3$): δ (ppm) = 7.40 – 7.33 (m, 4H, 2 \times *meta*- C_{Ph-H} , 2 \times *ortho*- C_{Ph-H}), 7.32 – 7.23 (m, 2H, *para*- C_{Ph-H} , H-5), 7.22 – 7.17 (m, 3H, H-6, H-7, H-8), 4.14 (d, 2J = 13.6 Hz, 1H, Ph-CHH), 3.79 (q, 3J = 6.1 Hz, 1H, H-1), 3.43 (d, 2J = 13.6 Hz, 1H, Ph-CHH), 3.12 – 3.01 (m, 1H, H-4), 2.99 – 2.91 (m, 1H, CHH-3), 2.73 (dd, 3J = 7.0 Hz, 4J = 3.3 Hz, 2H, CH_2CN), 2.70 – 2.61 (m, 1H, CHH-3), 1.55 (d, 3J = 6.1 Hz, 3H, CH_3).

^{13}C NMR (101 MHz, $CDCl_3$): δ (ppm) = 140.3 (s, C-8a), 138.9 (s, CH_2-C_{Ph}), 135.1 (s, C-4a), 128.9 (d, *meta*- CH_{Ph}), 128.5 (d, *ortho*- CH_{Ph}), 128.4 (d, C-5*, C-8*), 127.5 (d, *para*- CH_{Ph}), 127.4 (d, C-6**), 126.3 (d, C-7**), 119.1 (s, CN), 58.7 (t, CH_2-C_{Ph}), 57.8 (d, C-1), 50.8 (t, C-3), 36.0 (d, C-4), 23.5 (t, CH_2CN), 21.8 (q, CH_3).

*/**Assignment is interconvertible

Minor diastereoisomer

TLC: R_f = 0.16 (pentane/EtOAc = 15/1), [UV/KMnO₄].

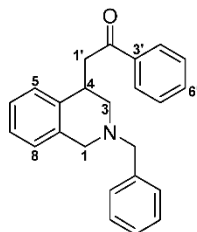
¹H NMR (400 MHz, CDCl₃): δ (ppm) = 7.39 – 7.32 (m, 4H, 2 × *meta*-C_{Ph}-H, 2 × *ortho*-C_{Ph}-H), 7.31 – 7.26 (m, 1H, *para*-C_{Ph}-H), 7.23 – 7.15 (m, 3H, H-6, H-7, H-8), 7.07 – 7.02 (m, 1H, H-5), 4.11 (q, ³*J* = 6.8 Hz, 1H, H-1), 3.86 (d, ²*J* = 13.1 Hz, 1H, Ph-CHH), 3.68 (d, ²*J* = 13.1 Hz, 1H, Ph-CHH), 3.09 (dd, ²*J* = 12.4 Hz, ⁴*J* = 3.0 Hz, 1H, H-3), 3.06 – 3.01 (m, 1H, H-4), 2.78 (dd, ²*J* = 16.7 Hz, ³*J* = 9.1 Hz, 1H, CHHCN), 2.66 (d, ²*J* = 12.4 Hz, 1H, H-3), 2.56 (dd, ²*J* = 16.7 Hz, ⁴*J* = 5.4 Hz, 1H, CHHCN), 1.27 (d, ³*J* = 6.8 Hz, 3H, CH₃).

¹³C NMR (101 MHz, CDCl₃): δ (ppm) = 141.3 (s, C-8a), 138.9 (s, CH₂-C_{Ph}), 134.9 (s, C-4a), 129.1 (d, 2 × *meta*-C_{Ph}), 129.0 (d, C-8*), 128.6 (d, 2 × *ortho*-C_{Ph}), 127.7 (d, C-5), 127.5 (d, *para*-C_{Ph}), 127.1 (d, C-6*), 126.6 (d, C-7*), 119.4 (d, CN), 58.3 (t, CH₂-C_{Ph}), 55.8 (d, C-1), 45.7 (t, C-3), 36.8 (d, C-4), 24.7 (t, CH₂CN), 14.6 (q, CH₃).

*Assignment is interconvertible

HRMS (ESI): calc. [C₁₉H₂₀N₂+H]⁺: 277.1699; found: 277.1699.

GC-MS (EI, 70 eV): t_R = 17.2 min; m/z (%) = 261 (100) [M-CH₃]⁺, 220 (5) [M-HCN-CH₃]⁺, 185 (2), 144 (7), 91 (75) [C₇H₇]⁺.

2-(2-Benzyl-1,2,3,4-tetrahydroisoquinolin-4-yl)-1-phenylethan-1-one (1k)

$C_{24}H_{23}NO$
Mw: 341,45 g/mol

According to **GP 3** 51.0 mg (123 μ mol, 1.00 eq.) of substrate **2k**, 6.92 mg (6.16 μ mol, 0.05 eq) of **[Ir(dF)]**, 2.22 mg (123 μ mol, 1.00 eq.) H_2O and 40.2 mg (123 μ mol, 1.00 eq.) Cs_2CO_3 in anhydrous dimethylformamide (3.00 mL) were irradiated for 14 hours. After purification by column chromatography (silica, pentane/EtOAc = 20/1) 23.0 mg (67.4 μ mol, 55 %) of **1k** could be isolated as a yellow oil.

TLC: R_f = 0.53 (pentane/EtOAc = 10/1) [UV/KMnO₄].

IR (ATR): $\tilde{\nu}$ (cm⁻¹) = 3062 (w), 2924 (s, C_{Ar}-H), 2854 (w, C_{Al}-H), 1683 (s, C=O), 1597 (w, C=C), 1494 (m), 1449 (s), 1362 (m), 1205 (m), 1140 (s, C-O), 1104 (m), 1028 (m), 751 (s, C_{Ar}-H), 699 (s).

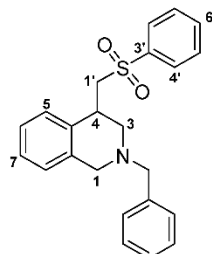
¹H NMR (400 MHz, CDCl₃): δ (ppm) = 7.95 (d, ³ J = 7.7 Hz, 2H, H-4', H-8'), 7.56 (t, ³ J = 7.4 Hz, 1H, H-6'), 7.45 (t, J = 7.7 Hz, 2H, H-5', H-7'), 7.34 – 7.28 (m, 2H, C_{Ar}-H), 7.21 – 7.11 (m, 6H, C_{Ar}-H), 7.02 (d, ³ J = 7.2 Hz, 1H, H-5), 3.91 – 3.81 (m, 2H, CHH-1', CHH-1), 3.68 (d, ² J = 13.0 Hz, 1H, Ph-CHH), 3.66 – 3.60 (m, 1H, H-4), 3.59 – 3.52 (m, 1H, Ph-CHH), 3.43 (d, ² J = 15.0 Hz, 1H, CHH-1), 3.08 (d, ² J = 17.3 Hz, 1H, CHH-1'), 2.84 (d, ² J = 11.4 Hz, 1H, CHH-3), 2.60 (d, ² J = 11.4 Hz, 1H, CHH-3).

¹³C NMR (101 MHz, CDCl₃): δ (ppm) = 199.5 (s, CO), 138.5 (s, CH₂-C_{Ph}), 137.4 (s, C-4a), 135.4 (s, C-8a), 133.1 (d, C-6'), 128.9 (d, C_{Ar}), 128.6 (d, C-5', C-7'), 128.6 (s, C-3'), 128.3 (d, C_{Ar}), 128.2 (d, C-3', C-8'), 127.1 (d, C_{Ar}), 126.7 (d, C_{Ar}), 126.6 (d, C_{Ar}), 126.1 (d, C_{Ar}), 62.8 (t, CH₂-C_{Ph}), 56.5 (t, C-1), 54.6 (t, C-3), 45.6 (t, C-1'), 34.8 (d, C-4).

HRMS (ESI): m/z = calc. [C₂₄H₂₃NO+H]⁺: 342.1852 found: 342.1854

GC-MS (EI, 70 eV): t_R = 23.29 min m/z (%) = 340 (2), 250 (15) [M-C₇H₇]⁺, 221 (100) [M-C₈H₆O]⁺, 130 (20), 91 (45) [C₇H₇]⁺.

2-Benzyl-4-((phenylsulfonyl)methyl)-1,2,3,4-tetrahydroisoquinoline (11)



$C_{23}H_{23}NO_2S$
Mw: 377.50 g/mol

According to **GP 3** 60.3 mg (134 μ mol, 1.00 eq.) of substrate **21**, 7.52 mg (6.70 μ mol, 0.05 eq) of **[Ir(dF)]**, 2.42 mg (134 μ mol, 1.00 eq.) H_2O and 43.7 mg (134 μ mol, 1.00 eq.) CS_2CO_3 in anhydrous dimethylformamide (3.00 mL) were irradiated for 14 hours. After purification by column chromatography (silica, pentane/EtOAc = 20/1) 18.0 mg (47.7 μ mol, 36 %) of **11** could be isolated as a yellow oil.

TLC: R_f = 0.52 (pentane/EtOAc = 5/1), [UV/ $KMnO_4$].

IR (ATR): $\tilde{\nu}$ (cm^{-1}) = 3028 (w, $C_{Ar}-H$), 2925 (s, C-H), 2854 (m, C-H), 2808 (w, C-H), 1495 (w), 1447 (m, C-H), 1369 (w), 1305 (vs, S=O), 1147 (vs, S=O), 1087 (s, C-N), 1026 (w), 742 (vs, $C_{Ar}-H$), 721 (w), 701 (w), 689 (w).

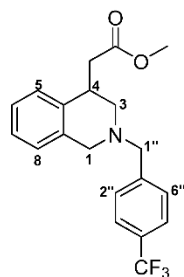
1H NMR (400 MHz, $CDCl_3$): δ (ppm) = 7.90 – 7.78 (m, 2H, H-4', H-8'), 7.67 – 7.58 (m, 1H, H-6'), 7.57 – 7.50 (m, 2H, H-5', H-7'), 7.41 – 7.28 (m, 5H, 2 \times meta- $C_{Ph}-H$, 2 \times ortho- $C_{Ph}-H$, para- $C_{Ph}-H$), 7.17 – 7.06 (m, 2H, H-6, H-7), 7.02 – 6.96 (m, 1H, H-8), 6.96 – 6.90 (m, 1H, H-5), 3.89 (dd, 2J = 14.4, 3J = 9.5 Hz, 1H, CHH-3), 3.78 (d, 2J = 15.1 Hz, 1H, CHH-1), 3.61 (s, 2H, H-1'), 3.45 – 3.43 (m, 1H, H-4), 3.34 (d, 2J = 15.1 Hz, 1H, CHH-1), 3.20 – 3.08 (m, 2H, CHH-3, Ph-CHH), 2.53 (dd, 2J = 11.8 Hz, 4J = 2.2 Hz, 1H, Ph-CHH).

^{13}C NMR (101 MHz, $CDCl_3$): δ (ppm) = 140.0 (s, C-3'), 138.4 (s, CH_2-C_{Ph}), 136.2 (s, C-8a), 135.5 (s, C-4a), 133.7 (d, C-6'), 129.5 (d, C-5', C-7'), 129.2 (d, ortho- CH_{Ph}), 128.5 (d, meta- CH_{Ph} , C-8), 128.1 (d, C-4', C-8'), 127.4 (d, para- CH_{Ph}), 127.0 (d, C-7), 126.8 (d, C-5, C6), 62.7 (t, CH_2-C_{Ph}), 61.8 (t, C-3), 55.7 (t, C-1), 53.9 (t, C-1'), 34.5 (d, C-4).

HRMS (ESI): m/z = calc. $[C_{23}H_{23}NO_2S+H]^+$: 378.1522; found: 378.1520.

GC-MS (EI, 70 eV): t_R = 21.9 min; m/z (%) = 376 (5), 286 (100) $[M-C_7H_7]^+$, 236 (54) $[M-SO_2Ph]^+$, 144 (19), 117 (54) $[C_9H_9]^+$, 91 (59) $[C_7H_7]^+$, 77 (9) $[C_6H_5]^+$.

Methyl 2-(2-(4-(trifluoromethyl)benzyl)-1,2,3,4-tetrahydroisoquinolin-4-yl)acetate (1m)



$C_{20}H_{20}F_3NO_2$
Mw: 363,38 g/mol

According to **GP 3** 53.0 mg (122 μ mol, 1.00 eq.) of substrate **2m**, 6.83 mg (6.67 μ mol, 0.05 eq) of **[Ir(dF)]**, 2.19 mg (122 μ mol, 1.00 eq.) H_2O and 39.7 mg (122 μ mol, 1.00 eq.) Cs_2CO_3 in 3.00 ml anhydrous DMF were irradiated for 14 hours. After purification by column chromatography (silica, pentane/EtOAc = 20/1) 26.0 mg (71.6 μ mol, 59 %) of **1m** could be isolated as a yellow oil.

TLC: R_f = 0.28 (pentane/EtOAc = 20/1), [UV/KMnO₄].

IR (ATR): $\tilde{\nu}$ (cm⁻¹) = 2953 (w, C-H), 2925 (w, C-H), 2800 (w, C-H), 2760 (w, C-H), 1735 (s, C=O), 1437 (w, C-H), 1418 (w, C-H), 1325 (vs, CF), 1161 (s, C-O), 1123 (s, CF₃), 1066 (s, CF₃), 1018 (m), 839 (w, C_{Ar}-H), 749 (w, C_{Ar}-H).

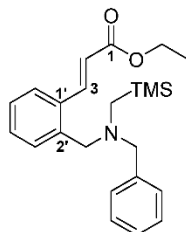
¹H NMR (400 MHz, CDCl₃): δ (ppm) = 7.58 (d, ³J = 8.1 Hz, 2H, 2 × *meta*-C_{Ph}-H), 7.50 (d, ³J = 8.1 Hz, 2H, 2 × *ortho*-C_{Ph}-H), 7.15 (d, ³J = 6.8 Hz, 3H, H-6, H-7, H-8), 7.00 (d, ³J = 6.8 Hz, 1H, H-5), 3.84 (d, ²J = 14.9 Hz, 1H, CHH-1), 3.79 (d, ²J = 13.5 Hz, 1H, Ph-CHH), 3.61 (d, ²J = 13.5 Hz, 1H, Ph-CHH), 3.57 (s, 3H, CO₂CH₃), 3.46 (d, ²J = 14.9 Hz, 1H, CHH-1), 3.37 – 3.28 (m, 1H, H-4), 2.91 (dd, ²J = 16.1 Hz, ³J = 10.1 Hz, 1H, CHHCO₂CH₃), 2.77 (d, ²J = 11.7 Hz, 1H, CHH-3), 2.65 – 2.55 (m, 2H, CHH-3, CHHCO₂CH₃).

¹³C NMR (101 MHz, CDCl₃): δ (ppm) = 173.3 (s, CO), 142.9 (s, CH₂-C_{Ph}), 137.4 (s, C-4a), 134.9 (s, C-8a), 129.7 (s, *para*-CH_{Ph}), 129.4 (s, CF₃), 129.3 (d, *ortho*-CH_{Ph}), 128.5 (d, C-8), 126.7 (d, C-5), 126.4 (d, C-6*, C-7*), 125.3 (q, ⁴J = 3.8 Hz, *meta*-CH_{Ph}), 62.2 (t, CH₂-C_{Ph}), 56.6 (t, C-1), 54.3 (t, C-3), 51.5 (q, CH₃), 40.9 (t, CH₂CO₂CH₃), 35.8 (d, C-4).

*Assignment is interconvertible

HRMS (ESI): m/z = calc. [C₂₀H₂₀F₃NO₂+H]⁺: 364.1519; found: 364.1517.

GC-MS (EI, 70 eV): t_R = 16.3 min; m/z (%) = 376 (14), 332 (14) [M-OCH₃]⁺, 288 (25) [M-C₆H₅]⁺, 204 (100) [M-C₈H₆F₃]⁺, 159 (41) [C₈H₆F₃]⁺, 145 (13), 130 (23).

Ethyl-(*E*)-3-[2'-((benzyl((trimethylsilyl)-methyl)-amino)-methyl)-phenyl]-acrylate (**2a**)

$C_{23}H_{31}NO_2Si$
MW: 381.59 g/mol

According to **GP2**, 3.29 g (12.2 mmol, 1.00 eq.) of bromide **5a**, 3.08 g (15.9 mmol, 1.20 eq.) of amine **8a** and 9.00 g (61.1 mmol, 5.00 eq.) K_2CO_3 were converted in acetone (150 mL). After purification by column chromatography (silica, pentane/EtOAc = 20/1) 3.76 g (9.85 mmol, 81%) of **2a** were isolated as a yellow oil.

TLC: R_f = 0.82 (pentane/EtOAc = 10/1), [UV/KMnO₄].

IR (ATR): $\tilde{\nu}$ (cm⁻¹) = 3063 (w, C_{Ar}-H), 3028 (w, C_{Ar}-H), 2955 (m, C-H), 2899 (w, C-H), 2789 (m, C-H), 1714 (s, C=O), 1634 (m, C=C, conjugated), 1601 (w), 1485 (w), 1454 (m, C-H), 1420 (w, C-H), 1366 (m, C-H), 1310 (s, C-N), 1273 (m), 1249 (m), 1174 (s, C-O, ester), 1096 (w, C-N), 1039 (m), 980 (m, C=C, disubst. trans), 856 (s, Si-CH₃), 765 (m, Si-CH₃), 747 (m, C_{Ar}-H, 1,2-disubst.), 700 (m, C_{Ar}-H, monosubst.).

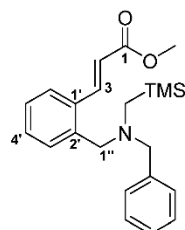
¹H NMR (400 MHz, CDCl₃): δ (ppm) = 8.23 (d, ³*J* = 16.0 Hz, 1H, H-3), 7.49 (dd, ³*J* = 7.69 Hz, ⁵*J* = 1.40 Hz, 1H, H-6'), 7.41 (dd, ³*J* = 7.69 Hz, ⁵*J* = 1.40 Hz, 1H, H-3'), 7.37 – 7.31 (m, 2H, 2 × *ortho*-C_{Ph}-H), 7.30 – 7.23 (m, 3H, 2 × *meta*-C_{Ph}-H, H-4', 7.23 – 7.16 (m, 2H, *para*-C_{Ph}-H, H-5'), 6.27 (d, ³*J* = 15.9 Hz, 1H, H-2), 4.26 (q, ³*J* = 7.1 Hz, 2H, CH₂CH₃), 3.52 (s, 2H, Ar-CH₂), 3.45 (s, 2H, Ph-CH₂), 1.85 (s, 2H, CH₂TMS), 1.32 (t, ³*J* = 7.1 Hz, 3H, CH₂CH₃), –0.01 (s, 9H, Si(CH₃)₃).

¹³C NMR (101 MHz, CDCl₃): δ (ppm) = 167.1 (s, C-1), 143.0 (d, C-3), 139.9 (s, CH₂-C_{Ph}), 139.3 (s, C-2'), 134.4 (s, C-1'), 130.8 (d, C-3'), 129.8 (d, C-4'), 129.0 (d, *ortho*-CH_{Ph}), 128.4 (d, *meta*-CH_{Ph}), 127.4 (d, *para*-CH_{Ph}), 127.0 (d, C-5'), 126.7 (d, C-6'), 119.5 (d, C-2), 62.8 (t, CH₂-C_{Ph}), 60.5 (t, CH₂CH₃), 60.5 (t, Ar-CH₂), 46.4 (t, CH₂TMS), 14.6 (q, CH₂CH₃), –1.04 (q, Si(CH₃)₃).

HRMS (ESI): m/z = calc. [C₂₃H₃₁NO₂Si+H]⁺: 382.2197; found: 382.2198.

GC-MS (EI, 70 eV): t_R = 17.8 min; m/z (%) = 381 (10) [M]⁺, 336 (7) [M-C₂H₅O]⁺, 308 (100) [M-C₃H₅O₂]⁺, 290 (7) [M-C₇H₇]⁺, 189 (8), 132 (6) [C₉H₁₀N]⁺, 117 (26), 91 (51) [C₇H₇]⁺, 73 (6) [Si(CH₃)₃]⁺.

Methyl (E)-3-[2'-{(benzyl((trimethylsilyl)methyl)amino)methyl}phenyl]acrylate (2b)



C₂₂H₂₉NO₂Si
Mw: 367.56 g/mol

According to **GP2** 378 mg (1.48 mmol, 1.00 eq.) bromide **5b**, 0.35 mL (315 mg, 1.63 mmol, 1.10 eq.) amine **8a** and 1.02 g (7.40 mmol, 5.00 eq.) K₂CO₃ were converted in acetone (40 mL). After purification by column chromatography (silica, pentane/EtOAc = 20/1) 406 mg (1.10 mmol, 75%) of **2b** were isolated as slightly yellow oil.

TLC: R_f = 0.56 (pentane/EtOAc = 20:1), [KMnO₄/UV].

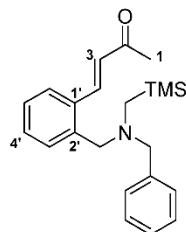
IR (ATR): $\tilde{\nu}$ (cm⁻¹) = 3063 (w, C_{Ar}-H), 3028 (w, C_{Ar}-H), 2951 (m, C_{Ar}-H), 2788 (w, C_{Alkyl}-H), 1718 (vs, C=O), 1633 (m, C=C, conjugated), 1435 (m, C-H), 1317 (s, C-N), 1274 (m), 1249 (m, Si-CH₃), 1192 (m, C-N), 1169 (vs, C-O, ester), 1040 (w), 1016 (w), 979 (m, C=C, disubst. trans), 853 (vs, Si-CH₃), 765 (s, Si-CH₃), 747 (vs, C_{Ar}-H, 1,2-disubst.), 700 (s, C_{Ar}-H, monosubst.).

¹H NMR (500 MHz, CDCl₃): δ (ppm) = 8.28 (d, ³J = 16.0 Hz, 1H, H-3), 7.54 (d, ³J = 7.7 Hz, 1H, H-6'), 7.44 (d, ³J = 7.4 Hz, 1H, H-3'), 7.39 (d, ³J = 7.4 Hz, 2H, 2 × *ortho*-C_{Ph}-H), 7.35 – 7.28 (m, 3H, 2 × *meta*-C_{Ph}-H, H-4'), 7.27 – 7.19 (m, 2H, *para*-C_{Ph}-H, H-5'), 6.32 (d, ³J = 16.0 Hz, 1H, H-2), 3.84 (s, 3H, CO₂CH₃), 3.56 (s, 2H, Ar-CH₂), 3.48 (s, 2H, Ph-CH₂), 1.89 (s, 2H, CH₂TMS), 0.03 [s, 9H, Si(CH₃)₃].

¹³C NMR (101 MHz, CDCl₃): δ (ppm) = 167.6 (s, C-1), 143.2 (d, C-3), 139.9 (s, CH₂-C_{Ph}), 139.3 (s, C-2'), 134.4 (s, C-1'), 130.9 (d, C-3'), 129.9 (d, C-4'), 129.1 (d, *ortho*-CH_{Ph}), 128.4 (d, *meta*-CH_{Ph}), 127.5 (d, *para*-CH_{Ph}), 127.0 (d, C-5'), 126.7 (d, C-6'), 118.9 (d, C-2), 62.8 (t, CH₂-C_{Ph}), 60.6 (t, Ar-CH₂), 51.7 (q, CO₂CH₃), 46.4 (t, CH₂TMS), -1.1 [q, Si(CH₃)₃].

HRMS (ESI): m/z = calc. [C₂₂H₂₉NO₂Si+H]⁺: 368.2040; found: 368.2038.

GC-MS (EI, 70 eV): t_R = 17.5 min; m/z (%) = 367 (8) [M]⁺, 336 (3) [M-OCH₃]⁺, 294 (100) [M-Si(CH₃)₃]⁺, 276 (5) [M-C₇H₇]⁺, 131 (10), 91 (41) [C₇H₇]⁺, 73 (8) [Si(CH₃)₃]⁺, 59 (6) [CO₂CH₃]⁺.

(E)-4-[2'-((Benzyl((trimethylsilyl)methyl)amino)methyl)phenyl]-but-3-en-2-one (2c)

C₂₂H₂₉NOSi
Mw: 351.56 g/mol

According to **GP2** 400 mg (1.67 mmol, 1.00 eq.) bromide **5c**, 1.16 g (8.36 mmol, 5.00 eq.) K₂CO₃ and 0.40 mL (356 mg, 1.84 mmol, 1.10 eq.) *N*-(trimethylsilylmethyl)benzylamine (**8a**) were converted in 30 mL acetone. After purification by column chromatography (silica, pentane/EtOAc = 10/1) 447 mg of **2c** (1.27 mmol, 76%) was isolated as orange colored oil.

TLC: *R_f* = 0.51 (pentane/EtOAc = 10/1), [KMnO₄/UV].

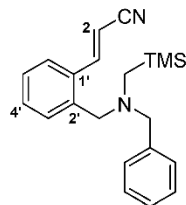
IR (ATR): $\tilde{\nu}$ (cm⁻¹) = 3062 (w, C_{Ar}-H), 3027 (w, C-H), 2954 (w, C_{Alk}-H), 1692 (m), 1672 (s, C=O), 1654 (m), 1609 (m, C=C, conjugated), 1598 (m, C_{Ar}=C_{Ar}), 1420 (m, C_{Alk}-H), 1359 (s), 1248 (s), 1175 (m, C-N), 973 (s, C=C, disubst. trans), 853 (vs, Si-CH₃), 838 (vs), 750 (vs, C_{Ar}-H, 1,2-disubst. trans), 700 (s, C_{Ar}-H).

¹H NMR (400 MHz, CDCl₃, 298 K): δ (ppm) = 8.04 (d, ³*J* = 16.2 Hz, 1H, H-4), 7.59 – 7.54 (m, 1H, H-3'), 7.47 – 7.41 (m, 1H, H-6'), 7.40 – 7.27 (m, 6H, H-4', C_{Ph}-H), 7.25 – 7.21 (m, 1H, H-5'), 6.58 (d, ³*J* = 16.2 Hz, 1H, H-3), 3.57 (s, 2H, Ar-CH₂), 3.50 (s, 2H, Ph-CH₂), 2.36 (s, 3H, COCH₃), 1.89 (s, 2H, CH₂TMS), 0.03 [s, 9H, Si(CH₃)₃].

¹³C NMR (101 MHz, CDCl₃, 298 K): δ (ppm) = 198.7 (s, C-2), 141.7 (d, C-4), 139.6 (s, CH₂-C_{Ph}), 139.5 (s, C-2'), 134.4 (s, C-1'), 131.2 (d, C-3'), 130.1 (d, C-4'), 129.2 (d, CH_{Ph}), 128.5 (d, CH_{Ph}), 128.3 (d, C-3), 127.6 (d, CH_{Ph}), 127.2 (d, C-5'), 126.7 (d, C-6'), 63.0 (d, Ar-CH₂), 60.7 (d, CH₂-C_{Ph}), 46.3 (t, CH₂TMS), 27.9 (q, COCH₃), -1.0 [q, Si(CH₃)₃].

HRMS (ESI): *m/z* = calc. [C₂₂H₂₉NOSi+H]⁺: 352.2091; found: 352.2092.

GC-MS (EI, 70 eV): *t_R* = 18.0 min; *m/z* (%) = 351 (5) [M]⁺, 308 (2) [M-C₂H₃O]⁺, 278 (100) [M-Si(CH₃)₃]⁺, 236 (6), 192 (5), 159 (15), 115 (16), 91 (60) [C₇H₇]⁺, 73 (14) [Si(CH₃)₃]⁺.

(E)-3-[2'-((Benzyl((trimethylsilyl)methyl)amino)methyl)phenyl]acrylonitrile (2d)

C₂₁H₂₆N₂Si
Mw 334.53 g/mol

According to **GP2** 300 mg (1.35 mmol, 1.00 eq.) bromide **5d**, 0.32 mL (287 mg, 1.49 mmol, 1.10 eq.) amine **8a** and 930 mg (6.75 mmol, 5.00 eq.) K₂CO₃ were converted in 25 mL Acetone. After purification by column chromatography (silica, pentane/EtOAc = 10/1) 363 mg (1.08 mmol, 80%) of **2d** could be isolated as white solid.

TLC: R_f = 0.82 (pentane/EtOAc = 10/1), [KMnO₄/UV].

IR (ATR): $\tilde{\nu}$ (cm⁻¹) = 3069 (w, C_{Ar}-H), 2218 (s, C≡N), 1617 (m, C=C, conjugated), 1485 (m, C_{Ar}=C_{Ar}), 1465 (w, C_{Alkyl}-H), 1228 (m), 1214 (m), 963 (s, C=C, 1,2-disubst. trans), 830 (w, Si-CH₃), 794 (m, Si-CH₃), 760 (vs, C_{Ar}-H, 1,2-disubst.), 739 (m, C_{Ar}-H, monosubst.).

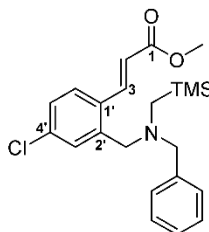
¹H NMR (400 MHz, CDCl₃, 298 K): δ (ppm) = 7.90 (d, ³J = 16.7 Hz, 1H, H-3), 7.47 – 7.36 (m, 5H, C_{Ar}-H), 7.36 – 7.27 (m, 4H, C_{Ar}-H), 5.72 (d, ³J = 16.7 Hz, 1H, H-2), 3.48 (s, 2H, Aryl-CH₂), 3.43 (s, 2H, Ph-CH₂), 1.84 (s, 2H, CH₂TMS), 0.01 [s, 9H, Si(CH₃)₃].

¹³C NMR (101 MHz, CDCl₃, 298 K): δ (ppm) = 149.6 (d, C-3), 139.3 (s, CH₂-C_{Ph}), 138.9 (s, C-2'), 133.7 (s, C-1'), 131.8 (d, C-3'), 130.5 (d, C-4'), 129.4 (d, ortho-CH_{Ph}), 128.8 (d, meta-CH_{Ph}), 127.9 (d, para-CH_{Ph}), 127.5 (d, C-5'), 125.8 (d, C-6'), 118.5 (s, CN), 96.1 (d, C-2), 63.1 (t, Aryl-CH₂), 60.9 (t, CH₂-C_{Ph}), 46.0 (t, CH₂TMS), -1.1 [q, Si(CH₃)₃].

HRMS (ESI): *m/z* = calc. [C₂₁H₂₆N₂Si+H]⁺: 335.1938; found: 335.1937.

GC-MS (EI, 70 eV): *t_R* = 17.6 min; *m/z* (%) = 334 (5) [M]⁺, 319 (9), 261 (100) [M-Si(CH₃)₃]⁺, 243 (3) [M-C₇H₇]⁺, 192 (3), 91 (73) [C₇H₇]⁺, 73 (10) [Si(CH₃)₃]⁺.

Methyl-(E)-3-(2'-((benzyl((trimethylsilyl)methyl)amino)methyl)-4'-chlorophenyl)acrylate (2e)



C₂₂H₂₈ClNO₂Si
Mw: 402.01 g/mol

According to **GP2**, 200 mg (0.69 mmol, 1.00 eq.) of bromide **5e**, 167 mg (0.86 mmol, 1.10 eq.) of amine **8a** and 477 mg (3.54 mmol, 5.00 eq.) K₂CO₃ were converted in acetone (15 mL). After purification by column chromatography (silica, pentane/EtOAc = 50/1) 200 mg (0.49 mmol, 72%) of **2e** were isolated as a yellow oil.

TLC: *R_f* = 0.43 (pentane/EtOAc = 20/1), [UV/KMnO₄].

IR (ATR): $\tilde{\nu}$ (cm⁻¹) = 2951 (w, C_{Ar}-H), 1721 (vs, C=O), 1634 (m, C=C, conjugated), 1592 (m), 1435 (m, C-H), 1316 (s, C-N), 1249 (m,), 1171 (s, C-O, ester), 977 (w, C=C, disubst. trans), 854 (s, Si-CH₃), 700 (m, C_{Ar}-H, monosubst).

¹H NMR (400 MHz, CDCl₃): δ (ppm) = 8.14 (d, ³*J* = 16.0 Hz, 1H, H-3), 7.49 – 7.43 (m, 2H, H-3', H-6'), 7.40 – 7.36 (m, 2H, 2 × *ortho*-C_{Ph}-H), 7.35 – 7.29 (m, 2H, 2 × *meta*-C_{Ph}-H), 7.26 – 7.19 (m, 2H, H-5', *para*-C_{Ph}-H), 6.28 (d, ³*J* = 16.0 Hz, 1H, H-2), 3.83 (s, 3H, CO₂CH₃), 3.62 – 3.40 (m, 4H, Ar-CH₂, Ph-CH₂), 1.90 (s, 2H, CH₂TMS), 0.05 (s, 9H, Si(CH₃)₃).

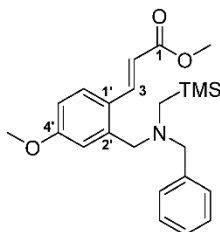
¹³C NMR (101 MHz, CDCl₃): δ (ppm) = 167.3 (s, C-1), 141.8 (d, C-3), 141.2 (s, C-4'), 139.5 (s, CH₂-C_{Ph}), 135.8 (s, C-2'), 132.7 (s, C-1'), 130.5 (d, C-3'), 129.0 (d, *ortho*-CH_{Ph}), 128.5 (d, *meta*-CH_{Ph}), 128.0 (d, *para*-CH_{Ph}), 127.6 (d, C-5'), 127.2 (d, C-6'), 119.4 (d, C-2), 62.9 (t, CH₂-C_{Ph}), 60.0 (t, Ar-CH₂), 51.8 (q, CO₂CH₃), 46.6 (t, CH₂TMS), -1.1 (q, Si(CH₃)₃).

HRMS (ESI): *m/z* = calc. [C₂₂H₂₈³⁵ClNO₂+H]⁺: 402.1651; found: 402.1652.

m/z = calc. [C₂₂H₂₈³⁷ClNO₂+H]⁺: 404.1621; found: 404.1623.

GC-MS (EI, 70 eV): *t_R* = 19.83 min *m/z* (%) = 401 (2) [M]⁺, 370 (5) [M-OCH₃]⁺, 328 (100) [M-Si(CH₃)₃]⁺, 281 (2).

Methyl-(*E*)-3-[2'-((benzyl[(trimethylsilyl)methyl]amino)methyl)-4'-methoxyphenyl]acrylate (2f)



$C_{23}H_{31}NO_3Si$
Mw: 397.59 g/mol

According to **GP2**, 250 mg (0.88 mmol, 1.00 eq.) of bromide **5f**, 220 mg (1.14 mmol, 1.30 eq.) of amine **8a** and 606 mg (4.38 mmol, 5.00 eq.) K_2CO_3 were converted in acetone (20 mL). After purification by column chromatography (silica, pentane/EtOAc = 50/1) 315 mg (0.79 mmol, 90%) of **2f** were isolated as a yellow oil.

TLC: R_f = 0.65 (pentane/EtOAc = 10/1), [UV/ $KMnO_4$].

IR (ATR): $\tilde{\nu}$ (cm^{-1}) = 2950 (w, C_{Ar-H}), 2837 (w, C_{Ar-H}), 1717 (s, C=O), 1602 (s, C=C, conjugated), 1495 (m), 1435 (m), 1258 (s), 1159 (s, C-O, ester), 1041 (m), 854 (s, C-Si).

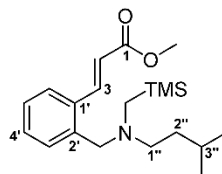
1H NMR (400 MHz, $CDCl_3$): δ (ppm) 8.19 (d, 3J = 15.9 Hz, 1H, H-3), 7.52 (d, 3J = 8.7 Hz, 1H, H-6'), 7.42 – 7.36 (m, 2H, 2 \times *ortho*- C_{Ph-H}), 7.34 – 7.27 (m, 2H, 2 \times *meta*- C_{Ph-H}), 7.25 – 7.19 (m, 1H, *para*- C_{Ph-H}), 7.07 (d, 4J = 2.7 Hz, 1H, H-3'), 6.78 (dd, 3J = 8.7 Hz, 4J = 2.7 Hz, 1H, H-5'), 6.23 (d, 3J = 15.9 Hz, 1H, H-2), 3.84 (s, 3H, OCH_3), 3.82 (s, 3H, CO_2CH_3), 3.55 (s, 2H, Ar- CH_2), 3.50 (s, 2H, Ph- CH_2), 1.92 (s, 2H, CH_2TMS), 0.04 (s, 9H, $Si(CH_3)_3$).

^{13}C NMR (101 MHz, $CDCl_3$): δ (ppm) = 167.9 (s, C-1), 161.1 (s, C-4'), 142.5 (d, C-3), 141.5 (s, C-2'), 139.9 (s, CH_2-C_{Ph}), 129.0 (d, *meta*- CH_{Ph}), 128.4 (d, *ortho*- CH_{Ph}), 128.2 (d, C-6'), 127.0 (d, *para*- CH_{Ph}), 126.7 (s, C-1'), 116.5 (d, C-2), 115.6 (d, C-3'), 113.1 (d, C-5'), 62.8 (t, Ph- CH_2), 60.3 (t, Ar- CH_2), 55.4 (q, OCH_3), 51.6 (q, CO_2CH_3), 46.5 (t, CH_2TMS), -1.0 (q, $Si(CH_3)_3$).

HRMS (ESI): m/z = calc. [$C_{23}H_{31}NO_3Si+H$] $^+$: 398.2146; found: 398.2146.

GC-MS (EI, 70 eV): t_R = 21.03 min m/z (%) = 397 (5) [M] $^+$, 366 (2) [$M-OCH_3$] $^+$, 324 (100) [$M-Si(CH_3)_3$] $^+$, 205 (5) [$M-C_{11}H_{18}NSi$] $^+$, 145 (20).

Methyl (E)-3-[2-((isopentyl(trimethylsilyl)methyl)amino)methyl]phenyl]acrylate (2g)



$C_{20}H_{33}NO_2Si$
Mw: 347.57 g/mol

According to **GP2**, 154 mg (602 μ mol, 1.00 eq.) of bromide **5b**, 115 mg (662 μ mol, 1.10 eq.) of amine **8b** and 416 mg (3.01 mmol, 5.00 eq.) K_2CO_3 were converted in acetone (20 mL). After purification by column chromatography (silica, pentane/EtOAc = 20/1) 117 mg (336 μ mol, 56%) of **2g** were isolated as a yellow oil.

TLC: R_f = 0.48 (pentane/EtOAc = 20/1), [UV/ $KMnO_4$].

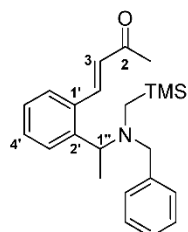
IR (ATR): $\tilde{\nu}$ (cm^{-1}) = 2953 (m, C–H), 2870 (w, C–H), 2793 (w, C–H), 1721 (vs, C=O), 1634 (m, C=C, conjugated), 1467 (w), 1435 (m), 1366 (w), 1314 (m, C–N), 1272 (m), 1248 (s, Si–CH₃), 1218 (m), 1192 (m, C–N), 1168 (vs, C–O, ester), 1042 (w), 978 (w, C=C, disubst. trans), 852 (vs, Si–CH₃), 765 (s, Si–CH₃), 743 (w, C_{Ar} –H, 1,2-disubst.), 700 (w).

1H NMR (400 MHz, $CDCl_3$): δ (ppm) = 8.30 (d, 3J = 16.0 Hz, 1H, H-3), 7.56 (d, 3J = 7.4 Hz, 1H, H-6'), 7.36 (d, 3J = 7.1 Hz, 1H, H-3'), 7.33 – 7.28 (m, 1H, H-4'), 7.28 – 7.23 (m, 1H, H-5'), 6.32 (d, 3J = 16.0 Hz, 1H, H-2), 3.80 (s, 3H, CO_2CH_3), 3.58 (s, 2H, Ar-CH₂), 2.40 – 2.32 (m, 2H, H-1''), 1.88 (s, 2H, CH_2TMS), 1.57 – 1.47 (m, 1H, H-3''), 1.43 – 1.38 (m, 2H, H-2''), 0.84 (d, 3J = 6.5 Hz, 6H, 2 \times CH₃), –0.01 (s, 9H, $Si(CH_3)_3$).

^{13}C NMR (101 MHz, $CDCl_3$): δ (ppm) = 167.6 (s, C-1), 143.4 (d, C-3), 139.7 (s, C-2'), 134.5 (s, C-1'), 130.9 (d, C-3'), 129.7 (d, C-4'), 127.4 (d, C-5'), 126.6 (d, C-6'), 118.6 (d, C-2), 60.7 (t, Ar-CH₂), 55.7 (t, C-1''), 51.7 (q, CO_2CH_3), 46.1 (t, CH_2TMS), 35.6 (t, C-2''), 26.5 (d, C-3''), 23.0 (q, 2 \times CH₃), –1.2 (q, $Si(CH_3)_3$).

HRMS (ESI): m/z = calc. $[C_{20}H_{33}NO_2Si+H]^+$: 348.2353; found: 348.2351.

GC-MS (EI, 70 eV): t_R = 15.6 min; m/z (%) = 347 (8) $[M]^+$, 332 (3) $[M-CH_3]^+$, 316 (3) $[M-OCH_3]^+$, 290 (33) $[M-C_4H_9]^+$, 274 (100) $[M-Si(CH_3)_3]^+$, 218 (15), 175 (5), 131 (12) $[C_9H_9N]^+$, 115 (52), 91 (7) $[C_7H_7]^+$, 73 (7) $[Si(CH_3)_3]^+$, 59 (6) $[CO_2CH_3]^+$.

(E)-4-(2'-(1''-(Benzyl((trimethylsilyl)methyl)amino)ethyl)phenyl)but-3-en-2-one (2h)

C₂₃H₃₁NOSi
Mw 365.59 g/mol

According to **GP2** 300 mg (1.19 mmol, 1.00 eq.) bromide **5h**, 0.28 mL (252 mg, 1.30 mmol, 1.10 eq.) amine **8a** and 0.82 g (5.93 mmol, 5.00 eq.) K₂CO₃ were converted in 25 ml Acetone. After purification by column chromatography (silica, pentane/EtOAc = 10/1) 253 mg (0.69 mmol, 58%) of **2h** could be isolated as orange oil.

TLC: R_f = 0.46 (pentane/EtOAc = 10/1), [KMnO₄/UV].

IR (ATR): $\tilde{\nu}$ (cm⁻¹) = 2953 (m, C_{Alkyl}-H), 1692 (m, C=C, conjugated), 1672 (vs, C=O), 1607 (s, C_{Ar}=C_{Ar}), 1452 (w, C_{Alkyl}-H), 1358 (m), 1248 (s), 972 (w, C=C, disubst. trans), 856 (vs, Si-CH₃), 749 (s, C_{Ar}-H).

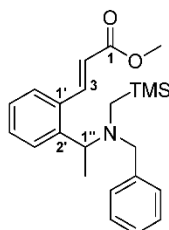
¹H NMR (500 MHz, CDCl₃, 298 K): δ (ppm) = 7.94 (d, *J* = 16.1 Hz, 1H, H-4), 7.54 – 7.46 (m, 2H, 2 × *meta*-C_{Ph}-H), 7.39 – 7.35 (m, 3H, H-5', 2 × *ortho*-C_{Ph}-H), 7.34 – 7.29 (m, 2H, H-4', H-3'), 7.26 – 7.21 (m, 2H, *para*-C_{Ph}-H, H-6'), 6.54 (d, ³*J* = 16.1 Hz, 1H, H-3), 4.12 (q, ³*J* = 6.7 Hz, 1H, H-1''), 3.66 – 3.57 (m, 2H, Ph-CH₂), 2.24 (s, 3H, COCH₃), 2.03 (d, ²*J* = 14.6 Hz, 1H, CHHTMS), 1.95 (d, ²*J* = 14.7 Hz, 1H, CHHTMS), 1.33 (d, ³*J* = 6.7 Hz, 3H, H-2''), -0.07 [s, 9H, Si(CH₃)₃].

¹³C NMR (126 MHz, CDCl₃, 298 K): δ (ppm) = 198.7 (s, C-2), 143.6 (s, C-2'), 142.4 (d, C-4), 140.1 (s, CH₂-C_{Ph}), 134.5 (s, C-1'), 129.7 (d, *para*-CH_{Ph}), 128.9 (d, *ortho*-CH_{Ph}), 128.8 (d, *meta*-CH_{Ph}), 128.4 (d, C-3), 128.3 (d, C-5'), 127.2 (d, C-3'), 127.2 (d, C-4'), 127.0 (d, C-6'), 58.9 (t, CH₂-C_{Ph}), 57.9 (d, C-1''), 41.8 (t, CH₂TMS), 27.9 (q, COCH₃), 15.5 (q, C-2''), -1.1 [q, Si(CH₃)₃].

HRMS (ESI): *m/z* = calc. [C₂₃H₃₁NOSi+H]⁺: 366.2248; found: 366.2246.

GC-MS (EI, 70 eV): *t_R* = 19.1 min; *m/z* (%) = 350 (5) [M-CH₃]⁺, 322 (2) [M-COCH₃]⁺, 292 (100) [M-Si(CH₃)₃]⁺, 248 (2), 91 (90) [C₇H₇]⁺.

Methyl (*E*)-3-[2'-{1''-(benzyl((trimethylsilyl)methyl)amino)ethyl}phenyl]acrylate (2i**)**



$C_{23}H_{31}NO_2Si$
Mw: 381.59 g/mol

According to **GP2**, 0.52 g (1.91 mmol, 1.00 eq.) of bromide **5i**, 0.44 mg (2.30 mmol, 1.20 eq.) of amine **8a** and 1.32 g (9.57 mmol, 5.00 eq.) K_2CO_3 were converted in acetone (60 mL). After purification by column chromatography (silica, pentane/EtOAc = 50/1) 0.53 mg (1.38 mmol, 72%) of **2i** could be isolated as a yellow oil.

TLC: R_f = 0.53 (pentane/EtOAc = 10/1), [UV/ $KMnO_4$].

IR (ATR): $\tilde{\nu}$ (cm^{-1}) = 2950 (w, C_{Ar-H}), 2898 (w, C_{Ar-H}), 1719 (s, C=O), 1631 (s, C=C, conjugated), 1435 (m), 1316 (s), 1270 (m), 1169 (s, C-O, ester), 855 (s, C-Si).

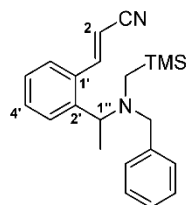
1H NMR (400 MHz, $CDCl_3$): δ (ppm) = 8.28 (d, 3J = 15.9 Hz, 1H, H-3), 7.51 (d, 3J = 7.7 Hz, 1H, H-6'), 7.47 – 7.38 (m, 3H, 2 \times *ortho*- C_{Ph-H} , H-3'), 7.36 – 7.28 (m, 3H, 2 \times *meta*- C_{Ph-H} , H-4'), 7.26 – 7.19 (m, 2H, *para*- C_{Ph-H} , H-5'), 6.29 (d, 3J = 15.9 Hz, 1H, H-2), 4.08 (q, 3J = 6.8 Hz, 1H, H-1''), 3.83 (s, 3H, CO_2CH_3), 3.66 (d, 2J = 14.1 Hz, 1H, Ph-*CHH*), 3.56 (d, 2J = 14.1 Hz, 1H, Ph-*CHH*), 1.94 (s, 2H, CH_2TMS), 1.29 (d, 3J = 6.8 Hz, 3H, H-2''), –0.08 (s, 9H, $Si(CH_3)_3$).

^{13}C NMR (101 MHz, $CDCl_3$): δ (ppm) = 167.5 (s, C-1), 144.1 (d, C-3), 143.7 (s, C-2'), 140.2 (s, $C-CH_2-C_{Ph}$), 134.5 (s, C-1'), 129.5 (d, C-4'), 129.0 (d, *ortho*- CH_{Ph}), 128.3 (d, *meta*- CH_{Ph}), 128.3 (d, C-3'), 127.1 (d, C-6'), 127.1 (d, *para*- CH_{Ph}), 126.8 (d, C-5'), 119.2 (d, C-2), 59.2 (t, CH_2-C_{Ph}), 58.5 (d, C-1''), 51.7 (q, CO_2CH_3), 42.2 (t, CH_2TMS), 14.5 (q, C-2''), –1.2 (q, $Si(CH_3)_3$).

HRMS (EI): m/z = calc. $[C_{23}H_{31}NO_2Si+H]^+$: 382.2197; found: 382.2197.

GC-MS (EI, 70 eV): t_R = 21.03 min m/z (%) = 381 (5) $[M]^+$, 366 (2) $[M-CH_3]^+$, 308 (95) $[M-Si(CH_3)_3]^+$, 189 (5), 129 (100) $[C_{10}H_9]^+$.

3-[2'-{1''-(Benzyl((trimethylsilyl)methyl)amino)ethyl}phenyl]acrylonitrile (2j)



C₂₂H₂₈N₂Si
Mw: 348.56 g/mol

According to **GP2** 141 mg (597 μ mol, 1.00 eq.) bromide **5j**, 139 mg (719 μ mol, 1.20 eq.) amine **8a** and 413 mg (2.98 mmol, 5.00 eq.) K₂CO₃ were converted in acetone (30 mL). After purification by column chromatography (silica, pentane/EtOAc = 20/1) 150 mg (430 μ mol, 71%, 73/27 mixture of E/Z isomers) of **2j** were isolated as yellowish oil.

IR (ATR): $\tilde{\nu}$ (cm⁻¹) = 3065 (w, C_{Ar}-H), 3030 (w, C-H, conjugated), 2953 (w, C_{Alkyl}-H), 2216 (m, C \equiv N), 1614 (m, C=C, conjugated), 1599 (m, C_{Ar}=C_{Ar}), 1452 (m, C_{Alkyl}-H), 1372 (m), 1247 (s), 1122 (w, C-N), 1081 (w), 957 (m, C=C, disubst. trans), 854 (vs, Si-CH₃), 837 (vs), 779 (m, Si-CH₃), 749 (vs, C_{Ar}-H, 1,2-disubst.), 703 (s, C_{Ar}-H, monosubst.)

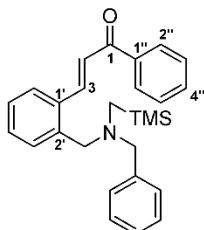
E-isomer:

TLC: *R*_f = 0.71 (pentane/EtOAc = 10/1), [KMnO₄/UV].

¹H NMR (400 MHz, C₆D₆, 298 K): δ (ppm) = 7.69 (d, ³*J* = 16.6 Hz, 1H, H-3), 7.60 – 7.42 (m, 3H, C_{Ar}-H), 7.29 – 7.19 (m, 2H, C_{Ar}-H), 7.13 – 7.05 (m, 1H, C_{Ar}-H), 7.04 – 6.94 (m, 2H, C_{Ar}-H), 6.89 – 6.83 (m, 1H, C_{Ar}-H), 5.07 (d, ³*J* = 16.6 Hz, 1H, H-2), 3.77 (q, ³*J* = 6.6 Hz, 1H, H-1''), 3.66 (d, ²*J* = 13.0 Hz, 1H, Ph-CHH), 3.21 (d, ²*J* = 13.0 Hz, 1H, Ph-CHH), 1.71 (d, ²*J* = 14.6 Hz, 1H, CHHTMS), 1.59 (d, ²*J* = 14.6 Hz, 1H, CHHTMS), 1.03 (d, ³*J* = 6.6 Hz, 3H, H-2''), -0.14 [s, 9H, Si(CH₃)₃].

¹³C NMR (101 MHz, C₆D₆, 298 K): δ (ppm) = 149.1 (d, C-3), 142.8 (s, CH₂-C_{Ph}), 138.9 (s, C-2'), 134.3 (s, C-1'), 129.8 (d, *ortho*-CH_{Ph}), 129.7 (d, *meta*-CH_{Ph}), 129.3 (d, C_{Ar}), 127.2 (d, *para*-CH_{Ph}), 126.1 (d, C_{Ar}), 118.4 (s, CN), 96.6 (d, C-2), 59.0 (t, CH₂-C_{Ph}), 54.5 (d, C-1''), 39.6 (t, CH₂TMS), 8.2 (q, C-2''), -1.4 [q, Si(CH₃)₃].

**(E)-3-[2-((Benzyl((trimethylsilyl)methyl)amino)methyl)phenyl]-1-phenylprop-2-en-1-one
(2k)**



C₂₇H₃₁NOSi
Mw: 413.63 g/mol

According to **GP2**, 150 mg (498 μmol, 1.00 eq.) of bromide **5k**, 116 mg (598 μmol, 1.20 eq.) of amine **8a** and 344 mg (2.49 mmol, 5.00 eq.) K₂CO₃ were converted in acetone (7 mL). After purification by column chromatography (silica, pentane/EtOAc = 20/1) 185 mg (447 μmol, 90%) of **2k** were isolated as a yellow oil.

TLC: R_f = 0.54 (pentane/EtOAc = 10/1), [UV/KMnO₄].

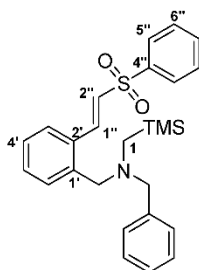
IR (ATR): $\tilde{\nu}$ (cm⁻¹) = 3062 (w, C_{Ar}-H), 2952 (w, C-H), 2788 (w), 1765 (w), 1663 (vs, C=O), 1605 (s, C_{Ar}=C_{Ar}), 1594 (s, C_{Ar}=C_{Ar}), 1482 (w, C_{Ar}=C_{Ar}), 1448 (w, C_{Ar}=C_{Ar}), 1328 (w), 1247 (m), 1211 (s), 1016 (s), 976 (m, C=C, disubst. trans), 855 (s), 839 (s), 765 (m, Si-CH₃).

¹H NMR (400 MHz, CDCl₃): δ (ppm) = 8.34 (d, ³J = 15.6 Hz, 1H, H-3), 8.07 – 8.02 (m, 2H, H-2'', H-6''), 7.69 – 7.65 (m, 1H, C_{Ar}-H), 7.62 – 7.57 (m, 1H, C_{Ar}-H), 7.55 – 7.48 (m, 3H, H-3'', H-5'', H-3'), 7.42 – 7.34 (m, 4H, H-2, C_{Ar}-H), 7.32 – 7.24 (m, 3H, C_{Ar}-H), 7.23 – 7.17 (m, 1H, H-6'), 3.60 (s, 2H, Ar-CH₂), 3.50 (s, 2H, Ph-CH₂), 1.91 (s, 2H, CH₂TMS), 0.02 (s, 9H, Si(CH₃)₃).

¹³C NMR (101 MHz, CDCl₃): δ (ppm) = 190.6 (s, C-1), 143.1 (d, C-3), 140.0 (s, C-3'), 139.8 (s, CH₂-C_{Ph}), 138.6 (s, C-1''), 135.0 (s, C-1'), 132.8 (d, C_{Ar}), 130.8 (d, C_{Ar}), 130.1 (d, C_{Ar}), 129.1 (d, C_{Ar}), 128.8 (d, C_{Ar}), 128.7 (d, C_{Ar}), 128.4 (d, C_{Ar}), 127.4 (d, C_{Ar}), 127.0 (d, C-6'), 126.7 (d, C_{Ar}), 123.5 (d, C-2), 62.8 (t, CH₂-C_{Ph}), 60.2 (t, Ar-CH₂), 46.4 (t, CH₂TMS), -1.0 (q, Si(CH₃)₃).

HRMS (ESI): *m/z* = calc. [C₂₇H₃₁NOSi+H]⁺: 414.2248; found: 414.2251.

GC-MS (EI, 70 eV): *t*_R = 24.6 min; *m/z* (%) = 413 (3) [M]⁺, 340 (75) [M-Si(CH₃)₃]⁺, 221 (5), 105 (100) [C₇H₅O]⁺.

(E)-N-Benzyl-N-[2'-(2''-(phenylsulfonyl)vinyl)benzyl]-1-(trimethylsilyl)methanamine (2I)

C₂₆H₃₁NO₂SSi
Mw: 449.68 g/mol

According to **GP2**, 102 mg (302 μ mol, 1.00 eq.) bromide **5I**, 0.07 mL (63.0 mg, 326 μ mol, 1.10 eq.) amine **8a** and 207 mg (1.50 mmol, 5.00 eq.) K₂CO₃ were converted in of acetone (15 mL). After purification by column chromatography (silica, pentane/EtOAc = 20/1) 128 mg (285 μ mol, 95%) of **2I** were isolated as slightly yellow oil.

TLC: *R*_f = 0.33 (*n*-hexane/EtOAc = 5/1) [UV].

IR (ATR): $\tilde{\nu}$ (cm⁻¹) = 3061 (w, C_{Ar}-H), 3029 (w, C_{Ar}-H), 2953 (w, C-H), 2790 (w, C-H), 1699 (w), 1612 (m, C=C, conjugated), 1447 (m, C-H), 1364 (w), 1307 (s, S=O), 1248 (m, Si-CH₃), 1146 (vs, S=O), 1085 (s, C-N), 972 (w, C=C), 852 (vs, Si-CH₃), 788 (m, Si-CH₃), 748 (vs, C_{Ar}-H, 1,2-disubst.), 701 (s, C_{Ar}-H, monosubst.), 688 (s, C_{Ar}-H, monosubst.).

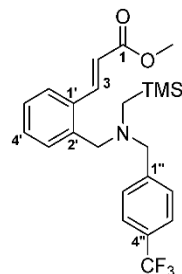
¹H NMR (500 MHz, CDCl₃): δ (ppm) = 8.30 (d, ³*J* = 15.3 Hz, 1H, H-1''), 7.94 (d, ³*J* = 7.4 Hz, 2H, H-5'', H-9''), 7.61 (t, ³*J* = 7.4 Hz, 1H, H-7''), 7.54 (t, ³*J* = 7.4 Hz, 2H, H-6'', H-8''), 7.44 – 7.42 (m, 4H, 2 \times *meta*-C_{Ph}-H, 2 \times *ortho*-C_{Ph}-H), 7.38 – 7.30 (m, 3H, H-3', H-4', H-5'), 7.26 – 7.17 (m, 2H, H-6', *para*-C_{Ph}-H), 6.76 (d, ³*J* = 15.3 Hz, 1H, H-2''), 3.56 (s, 2H, Ph-CH₂), 3.53 (s, 2H, Ar-CH₂), 1.88 (s, 2H, CH₂TMS), 0.03 (s, 9H, Si(CH₃)₃).

¹³C NMR (126 MHz, CDCl₃): δ (ppm) = 141.1 (s, C-4''), 140.6 (d, C-1''), 140.0 (s, CH₂-C_{Ph}), 139.5 (s, C-1'), 133.4 (d, C-7''), 132.1 (s, C-2'), 131.4 (d, C_{Ar}), 130.8 (d, C-3'), 129.4 (d, C-5''), 129.2 (d, *ortho*-CH_{Ph}), 128.6 (d, *meta*-CH_{Ph}), 128.0 (d, C-2''), 127.8 (d, C-9''), 127.6 (d, C_{Ar}), 127.2 (d, C_{Ar}), 127.0 (d, C_{Ar}), 63.0 (t, Ar-CH₂), 60.6 (t, CH₂-C_{Ph}), 46.3 (t, CH₂TMS), - 1.0 (q, Si(CH₃)₃).

HRMS (ESI): *m/z* = calc. [C₂₆H₃₁NO₂SSi+H]⁺: 450.1918; found: 450.1915.

GC-MS (EI, 70 eV): *t*_R = 22.9 min; *m/z* (%) = 434 (5) [M-CH₃]⁺, 376 (100) [M-Si(CH₃)₃]⁺, 308 (14) [M-SO₂Ph]⁺, 141 (14) [SO₂Ph]⁺, 115 (10), 91 (72) [C₇H₇]⁺, 73 (18) [Si(CH₃)₃]⁺.

Methyl (E)-3-[2'-{(4''-[trifluoromethyl]benzyl)((trimethylsilyl)methyl)amino)methyl}phenyl]acrylate (2m)



$C_{23}H_{28}F_3NO_2Si$
Mw: 435.56 g/mol

First *N*-(4-(trifluoromethyl)benzyl)-1-(trimethylsilyl)methylamine (**8c**) was synthesized according to a literature procedure.¹⁵ 0.68 mL (0.83 g, 4.76 mmol, 1.20 eq.) 4-(trifluoromethyl)benzylamine and 1.12 g (8.07 mmol, 2.00 eq.) K_2CO_3 were suspended in acetonitrile (40 mL). 0.60 mL (0.86 g, 4.04 mmol, 1.00 eq.) (trimethylsilyl)methyl iodide were added dropwise. After 20 h at 85 °C the mixture was concentrated under reduced pressure. The residue was dissolved in water (25 mL) and extracted with dichloromethane (3 × 25 mL). The combined organic layers were dried over Na_2SO_4 , filtrated and concentrated under reduced pressure. The compound was used without further purification in the next synthesis step. According to **GP2**, 149 mg (585 μ mol, 1.00 eq.) of bromide **5b**, 191 mg (732 μ mol, 1.25 eq.) *N*-(4-(trifluoromethyl)benzyl)-1-(trimethylsilyl)methylamine and 405 mg (2.93 mmol, 5.00 eq.) K_2CO_3 were converted in acetone (20 mL). After purification by column chromatography (silica, pentane/EtOAc = 50/1) 83.1 mg (191 μ mol, 33%) of **2m** could be isolated as slightly yellow oil.

TLC: R_f = 0.58 (pentane/EtOAc = 20/1) [UV].

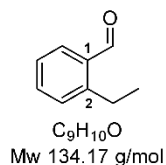
IR (ATR): $\tilde{\nu}$ (cm^{-1}) = 2952 (w, C–H), 2899 (w, C–H), 2798 (w, C–H), 1719 (s, C=O), 1634 (m, C=C, conjugated), 1485 (w), 1436 (w), 1417 (w), 1324 (vs, C–F), 1275 (m), 1250 (m, Si–CH₃), 1193 (m, C–N), 1165 (vs, C–O, ester), 1123 (vs, CF₃), 1066 (s, CF₃), 1018 (m), 980 (w, C=C, disubst. trans), 890 (w), 855 (s, Si–CH₃), 840 (s, Si–CH₃), 823 (m), 765 (m, Si–CH₃), 745 (w, C_{Ar}–H, 1,2-disubst.), 700 (w, C_{Ar}–H, monosubst.).

¹H NMR (400 MHz, CDCl₃): δ (ppm) = 8.27 (d, ³*J* = 15.9 Hz, 1H, H-3), 7.58 – 7.53 (m, 3H, 2 × *meta*-C_{Ph}-H, H-6'), 7.49 (d, ³*J* = 8.0 Hz, 2H, 2 × *ortho*-C_{Ph}-H), 7.42 (d, ³*J* = 7.4 Hz, 1H, H-3'), 7.33 (t, ³*J* = 7.4 Hz, 1H, H-4'), 7.26 (t, ³*J* = 7.4 Hz, 1H, H-5'), 6.33 (d, ³*J* = 15.9 Hz, 1H, H-2), 3.84 (s, 3H, CO₂CH₃), 3.59 (s, 2H, Ph-CH₂), 3.51 (s, 2H, Ar-CH₂), 1.91 (s, 2H, CH₂TMS), 0.04 (s, 9H, Si(CH₃)₃).

¹³C NMR (101 MHz, CDCl₃): δ (ppm) = 167.5 (s, C-1), 144.1 (s, C-1''), 143.0 (d, C-3), 138.8 (s, C-2'), 134.4 (s, C-1'), 130.9 (d, C-3'), 129.9 (d, C-4'), 129.1 (q, ³J_{C-F} = 31.1 Hz, C-4''), 129.1 (d, *ortho*-CH_{Ph}), 127.7 (d, C-5'), 126.8 (d, C-6'), 125.3 (q, ³J_{C-F} = 3.7 Hz, *meta*-CH_{Ph}), 124.3 (q, ¹J_{C-F} = 270 Hz, CF₃), 119.1 (d, C-2), 62.3 (t, CH₂-C_{Ph}), 60.8 (t, Ar-CH₂), 51.8 (q, CO₂CH₃), 46.8 (t, CH₂TMS), -1.1 (q, Si(CH₃)₃).

HRMS (ESI): *m/z* = calc. [C₂₃H₂₈F₃NO₂Si+H]⁺: 436.1914; found: 436.1913.

GC-MS (EI, 70 eV): *t_R* = 17.1 min; *m/z* (%) = 435 (2) [M]⁺, 404 (5) [M-OCH₃]⁺, 362 (100) [M-Si(CH₃)₃]⁺, 304 (6), 260 (9)⁺, 175 (9) [C₉H₇]⁺, 159 (20) [C₈H₆F₃]⁺, 115 (63), 91 (13) [C₇H₇]⁺.

2-Ethylbenzaldehyde (3a)

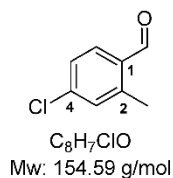
For the synthesis of 2-ethylbenzaldehyde (**3a**), a literature procedure was adapted.¹² 5.15 mL (7.00 g, 41.6 mmol, 1.00 eq.) 1-bromo-2-ethylbenzene were dissolved in 100 mL anhydrous tetrahydrofuran and cooled to $-78\text{ }^{\circ}\text{C}$. Then 18.1 mL (2.67 g, 1.10 eq.) *n*-butyllithium solution (2.3 M) in hexane were added slowly. After stirring the mixture at $-78\text{ }^{\circ}\text{C}$ for three hours, 3.50 mL (3.32 g, 45.4 mmol, 1.20 eq.) dimethylformamide were added and the solution was stirred for another 30 minutes at $-78\text{ }^{\circ}\text{C}$. The cooling was removed and stirring was continued for 30 minutes. Subsequently an ammonium chloride solution (70 mL) was added, the layers were separated and the organic layer was washed with brine (70 mL). The combined aqueous layers were extracted with ethyl acetate ($2 \times 100\text{ mL}$). The combined organic layers were dried over Na₂SO₄, filtered and the solvent was removed under reduced pressure. Purification by column chromatography (silica, pentane/EtOAc = 10/1) gave 4.32 g (32.2 mmol, 85%) of **3a** as yellow oil.

TLC: $R_f = 0.77$ (pentane/EtOAc = 10/1), [KMnO₄/UV].

¹H NMR (400 MHz, CDCl₃, 298 K): δ (ppm) = 10.3 (s, 1H, CHO), 7.83 (dd, ³ $J = 7.6\text{ Hz}$, ⁴ $J = 1.5\text{ Hz}$, 1H, H-6), 7.52 (td, ³ $J = 7.5\text{ Hz}$, ⁴ $J = 1.5\text{ Hz}$, 1H, H-4), 7.36 (td, ³ $J = 7.6\text{ Hz}$, ⁴ $J = 1.1\text{ Hz}$, 1H, H-5), 7.30 (dd, ³ $J = 7.6\text{ Hz}$, ⁴ $J = 1.1\text{ Hz}$, 1H, H-3), 3.08 (q, ³ $J = 7.6\text{ Hz}$, 2H, CH₂CH₃), 1.28 (t, ³ $J = 7.6\text{ Hz}$, 3H, CH₂CH₃).

¹³C NMR (101 MHz, CDCl₃, 298 K): δ (ppm) = 192.5 (d, CHO), 147.2 (s, C-1), 134.1 (d, C-6), 133.7 (s, C-2), 131.9 (d, C-5), 130.4 (d, C-4), 126.5 (d, C-3), 25.9 (t, CH₂CH₃), 16.5 (q, CH₂CH₃).

The analytical data obtained matched those reported in the literature.¹²

4-Chloro-2-methylbenzaldehyde (3e)

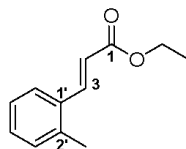
For the synthesis of **3e**, a literature procedure was adapted.¹⁶ A solution of 1.61 mL (1.50 g, 14.9 mmol, 1.00 eq.) *N*-methylpiperazine in anhydrous benzene (15 mL) was cooled to 0 °C. Then 7.16 mL (1.06 g, 16.5 mmol, 1.10 eq.) of a 2.3 M *n*-butyllithium in hexane solution were added and the mixture was stirred for one hour at room temperature. 2.00 g (14.2 mmol, 0.94 eq.) of 4-chlorobenzaldehyde were added to the mixture at 0 °C which was then allowed to warm to room temperature. Additional 9.28 mL (1.37 g, 21.3 mmol, 1.42 eq.) *n*-butyllithium solution (2.3 M) in hexane were transferred to the reaction and the mixture was stored in the freezer for 16 h. 5.31 mL (12.1 g, 85.5 mmol, 6.00 eq.) iodomethane were added to the reaction mixture at -78 °C which was allowed to warm to room temperature. Residual *n*-butyllithium was hydrolyzed by addition of 1 M HCl-solution (30 ml) and the aqueous layer was extracted with dichloromethane (3 × 20 ml). The combined organic layers were dried over Na₂SO₄ and the solvent were removed under reduced pressure. After purification by column chromatography (silica, pentane/EtOAc = 20/1) 0.68 g (4.40 mmol, 30%) of **3e** were isolated as a white solid.

TLC: *R_f* = 0.62 (pentane/EtOAc = 20/1), [UV/KMnO₄].

¹H NMR (400 MHz, CDCl₃): δ (ppm) = 10.22 (s, 1H, CHO), 7.73 (d, ³*J* = 8.3, Hz, 1H, H-6), 7.34 (d, ³*J* = 8.3 Hz, 1H, H-5), 7.26 (s, 1H, H-2), 2.65 (s, 3H, CH₃).

¹³C NMR (101 MHz, CDCl₃): δ (ppm) = 191.5 (d, CHO), 142.5 (s, C-1), 140.1 (s, C-4), 133.4 (d, C-6), 132.7 (s, C-3), 131.9 (d, C-5), 126.8 (d, C-2), 19.5 (q, CH₃).

The analytic results match with the literature data.¹⁶

Ethyl (*E*)-3-(*o*-tolyl)acrylate (4a**)**

$C_{12}H_{14}O_2$
Mw: 190.24 g/mol

For the synthesis of **4a**, a literature procedure was adapted.¹³ 7.00 g (43.2 mmol, 1.00 eq.) 2-methylcinnamic acid was dissolved with 1.50 mL (3.51 g, 23.1 mmol, 1.20 eq.) DBU in anhydrous dimethylformamide (40 mL) and stirred for 15 min at roomtemperature. 4.16 mL (8.08 g, 51.8 mmol, 1.20 eq.) ethyl iodide was added dropwise and the solution stirred for 48 h at roomtemperature. The reaction mixture was diluted with diethylether (50 mL) and the combined organic layers were washed with 10% aqueous HCl (25 mL), water (20 mL) and brine (50 mL), dried over Na_2SO_4 and the solvents were removed under reduced pressure. After purification by column chromatography (silica, pentane/EtOAc = 10/1) 8.20 g (43.1 mmol, 99%) of **4a** were obtained as a yellow oil.

TLC: R_f = 0.84 (pentane/EtOAc = 10/1), [UV/KMnO₄].

IR (ATR): $\tilde{\nu}$ (cm⁻¹) = 3063 (w, C_{Ar}-H), 2981 (s, C-H), 1709 (vs, C=O), 1633 (m, C=C, conjugated), 1602 (m, C=C, arom), 1573 (w, C=C, arom), 1486 (m, C=C, arom), 1462 (m, C=C, arom), 1390 (m), 1366 (s), 1312 (s), 1269 (s), 1249 (s), 1220 (s), 1167 (vs, C-O, ester), 1096 (m), 1035 (s), 980 (s, C=C, disubst. trans), 864 (m), 762 (s, CH, arom), 731 (s, C-H, arom), 695 (w).

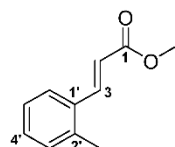
¹H NMR (400 MHz, CDCl₃): δ (ppm) = 7.98 (d, ³*J* = 15.9 Hz, 1H, H-3), 7.59 – 7.52 (m, 1H, H-6'), 7.33 – 7.23 (m, 1H, H-3'), 7.25 – 7.16 (m, 2H, H-4', H-5'), 6.36 (d, ³*J* = 15.9 Hz, 1H, H-2), 4.27 (q, ³*J* = 7.1 Hz, 2H, CH₂CH₃), 2.44 (s, 3H, CH₃), 1.35 (t, ³*J* = 7.1 Hz, 3H, CH₂CH₃).

¹³C NMR (101 MHz, CDCl₃): δ (ppm) = 167.2 (s, C-4), 142.4 (d, C-6), 137.8 (s, C-10a), 133.6 (s, C-6a), 130.9 (d, C-10), 130.1 (d, C-8), 126.5 (d, C-9), 126.5 (d, C-7), 119.5 (d, C-5), 60.6 (t, C-2), 20.0 (q, C-11), 14.5 (q, C-1).

HRMS (ESI): m/z = calc. [C₁₂H₁₄O₂+H]⁺: 191.1067; found: 191.1067.

GC-MS (EI, 70 eV): t_R = 11.4 min; m/z (%) = 190 (33) [M]⁺, 175 (11) [M-CH₃]⁺, 145 (100) [M-C₂H₅O]⁺, 115 (81), 91 (25) [C₇H₇]⁺.

The analytical data obtained matched those reported in the literature.²⁰

Methyl (*E*)-3-(*o*-tolyl)acrylate (4b**)**

$C_{11}H_{12}O_2$
Mw: 176.22 g/mol

For the synthesis of Methyl (*E*)-3-(*o*-tolyl)acrylate (**4b**), a literature procedure was adapted.¹³ 3.12 g (19.2 mmol, 1.00 eq.) 2-methylcinnamic acid was dissolved with 1.50 mL (3.51 g, 23.1 mmol, 1.20 eq.) 1,8-diazabicyclo[5.4.0]undec-7-ene (DBU) in anhydrous dimethylformamide (40 mL) and stirred at room temperature for 15 min. 4.00 mL (4.10 g, 28.9 mmol, 1.50 eq.) methyl iodide was added dropwise and the solution stirred at room temperature for 14 h. The reaction mixture was diluted with diethylether (40 mL). The organic layers were washed with 10% aqueous HCl (20 mL), water (2 × 20 mL), brine (20 mL) and dried over Na_2SO_4 . The combined organic layers were removed under reduced pressure. After purification by column chromatography (silica, pentane/EtOAc = 20/1) 2.57 g (14.6 mmol, 76%) of **4b** were isolated as colorless oil.

TLC: R_f = 0.62 (pentane/EtOAc = 10/1), [KMnO₄/UV].

IR (ATR): $\tilde{\nu}$ (cm⁻¹) = 3022 (w, C_{Ar}-H), 2951 (s, C-H), 1714 (vs, C=O), 1633 (m, C=C, conjugated), 1602 (w), 1461 (w), 1435 (m, C-H), 1316 (s), 1273 (s), 1220 (m), 1193 (s), 1169 (vs, C-O), 1037 (w), 980 (m, C=C, disubst. trans), 862 (w), 763 (s, C_{Ar}-H, 1,2-disubst.), 710 (w).

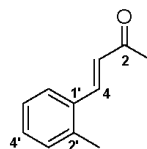
¹H NMR (400 MHz, CDCl₃): δ (ppm) = 7.99 (d, ³*J* = 15.9 Hz, 1H, H-3), 7.58 – 7.48 (m, 1H, H-6'), 7.31 – 7.27 (m, 1H, H-3'), 7.24 – 7.17 (m, 2H, H-4', H-5'), 6.36 (d, ³*J* = 15.9 Hz, 1H, H-2), 3.81 (s, 3H, CO₂CH₃), 2.44 (s, 3H, CH₃).

¹³C NMR (126 MHz, CDCl₃): δ (ppm) = 167.7 (s, C-1), 142.7 (d, C-3), 137.8 (s, C-2'), 133.5 (s, C-1'), 130.9 (d, C-4'), 130.2 (d, C-3'), 126.5 (d, C-6'), 126.5 (d, C-5'), 119.0 (d, C-2), 51.9 (q, CO₂CH₃), 20.0 (q, CH₃).

HRMS (ESI): m/z = calc. [C₁₁H₁₂O₂+H]⁺: 177.2225; found: 177.2225.

GC-MS (EI, 70 eV): t_R = 10.7 min; m/z (%) = 176 (41) [M]⁺, 161 (32) [M-CH₃]⁺, 145 (100) [M-OCH₃]⁺, 115 (92), 91 (26) [C₇H₇]⁺.

The analytical data obtained matched those reported in the literature.¹³

(E)-4-(o-Tolyl)but-3-en-2-one (4c)

$C_{11}H_{12}O$
Mw 160.22 g/mol

For the synthesis of **4c** a literature procedure was adapted.¹⁰ 1.94 mL (2.00 g, 16.7 mmol, 1.00 eq.) 2-methylbenzaldehyde were added dropwise to a mixture of acetone (36 mL) and 7.20 mL NaOH solution (20.0 mmol, 1.20 eq., 10%). The reaction mixture was stirred at room temperature until reaction monitoring by TLC showed only traces of starting material remaining after three hours. The reaction was neutralized using HCl (2 M) and extracted with Et₂O (3 × 30 mL). The organic layers were dried over Na₂SO₄, filtered and the solvent was removed under reduced pressure. Purification by column chromatography (silica, pentane/EtOAc = 10/1→4/1) gave 1.96 g of **4c** (12.2 mmol, 74%) as yellow oil.

TLC: *R_f* = 0.51 (pentane/EtOAc = 10/1), [KMnO₄/UV].

IR (ATR): $\tilde{\nu}$ (cm⁻¹) = 1670 (s, C=O), 1646 (s, C=O), 1608 (m, C=C), 1596 (s, C=C), 1484 (m, CH), 1455 (m, CH), 1357 (m, CH₃), 1209 (brm, C-O-C), 971 (s, C=C trans), 756 (s, C_{Ar}-H).

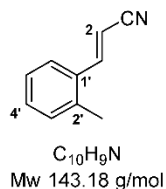
¹H NMR (400 MHz, CDCl₃, 298 K): δ (ppm) = 7.82 (d, ³*J* = 16.1 Hz, 1H, H-4), 7.62 – 7.51 (m, 1H, H-6'), 7.32 – 7.27 (m, 1H, H-3'), 7.25 – 7.19 (m, 2H, H-4', H-5'), 6.65 (d, ³*J* = 16.1 Hz, 1H, H-3), 2.45 (s, 3H, Ar-CH₃), 2.39 (s, 3H, COCH₃).

¹³C NMR (101 MHz, CDCl₃, 298 K): δ (ppm) = 198.5 (s, C-2), 141.0 (d, C-4), 138.0 (s, C-2'), 133.5 (s, C-1'), 131.0 (d, C-4'), 130.4 (d, C-3'), 128.3 (d, C-3), 126.6 (d, C-6'), 126.6 (d, C-5'), 28.0 (q, COCH₃), 19.9 (q, Ar-CH₃).

HRMS (ESI): *m/z* = calc.[C₁₁H₁₂O+H]⁺: 161.0961; found: 161.0961.

GC-MS (EI, 70 eV): *t_R* = 10.53 min *m/z* (%) = 160 (10) [M]⁺, 145 (100) [M-CH₃]⁺, 115 (70) [M-C₂H₅O]⁺, 91 (15) [C₇H₇]⁺.

The analytical data obtained matched those reported in the literature.¹⁰

3-(*o*-Tolyl)acrylonitrile (4d)

For the synthesis of **4d**, a literature procedure was adapted.¹¹ 1.10 g (19.6 mmol, 1.18 eq.) powdered KOH were suspended in acetonitrile (10 mL). Then 1.94 mL (2.00 g, 16.7 mmol, 1.00 eq.) 2-methylbenzaldehyde were dissolved in acetonitrile (10 mL) and added to the suspension. The mixture was heated to reflux until reaction monitoring by TLC showed only traces of starting material remaining after 15 min. The red suspension was poured into 100 mL cold water and extracted with CH₂Cl₂ (3 × 75 mL). The organic layers were dried over Na₂SO₄, filtered and the solvent was removed under reduced pressure. Purification by column chromatography (silica, pentane/EtOAc = 10/1) gave 1.08 g of **4d** (7.56 mmol, 45%, 81/19 mixture of *E/Z* isomers) as off-white crystals.

M.p.: 34 °C.

IR (ATR): $\tilde{\nu}$ (cm⁻¹) = 3058 (w, C_{Ar}=C_{Ar}), 2216 (w), (s, C=N), 1614 (m, C=C), 1599 (m), 1484 (m, C_{Alk}-H), 963 (s; C=C, disubst. trans), 749 (vs).

E-isomer:

TLC: *R*_f = 0.72 (pentane/EtOAc = 10/1), [KMnO₄/UV].

¹H NMR (400 MHz, CDCl₃, 298 K): δ (ppm) = 7.70 (d, ³*J* = 16.6 Hz, 1H, H-3), 7.49 – 7.44 (m, 1H, C_{Ar}-H), 7.35 – 7.28 (m, 1H, C_{Ar}-H), 7.25 – 7.20 (m, 2H, C_{Ar}-H), 5.80 (d, ³*J* = 16.6 Hz, 1H, H-2), 2.41 (s, 3H, CH₃).

¹³C NMR (101 MHz, CDCl₃, 298 K): δ (ppm) = 148.6 (d, C-3), 137.4 (s, C-1'), 132.7 (s, C-2'), 131.2 (d, C-3'), 131.1 (d, C-4'), 126.7 (d, C-5'), 125.7 (d, C-6'), 118.5 (s, CN), 97.3 (d, C-2), 19.8 (q, CH₃).

Z-isomer:

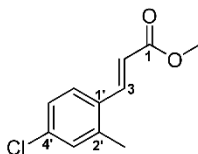
TLC: *R*_f = 0.62 (pentane/EtOAc = 10/1), [KMnO₄/UV].

¹H NMR (400 MHz, CDCl₃, 298 K): δ (ppm) = 7.92 (dd, ³*J* = 7.5 Hz, ⁴*J* = 1.4 Hz, 1H, C_{Ar}-H), 7.44 – 7.39 (m, 1H, C_{Ar}-H), 7.41 (d, ³*J* = 12.0 Hz, 1H, H-3), 7.25 – 7.20 (m, 2H, C_{Ar}-H), 5.52 (d, ³*J* = 12.0 Hz, 1H, H-2), 2.35 (s, 3H, CH₃).

¹³C NMR (101 MHz, CDCl₃, 298 K): δ (ppm) = 147.7 (d, C-3), 137.2 (s, C-1'), 132.8 (s, C-2'), 130.7 (d, C-3'), 130.7 (d, C-4'), 127.8 (d, C-5'), 126.6 (d, C-6'), 117.3 (s, CN), 97.1 (d, C-2), 19.8 (q, CH₃).

HRMS (ESI): *m/z* = calc. [C₁₀H₉N+H]⁺: 144.0808; found: 144.0809.

GC-MS (EI, 70 eV): *t*_R = 18.0 min; *m/z* (%) = 143 (75) [M]⁺, 116 (2) [M-HCN]⁺, 91 (100) [C₇H₇]⁺, 89 (5).

Methyl (E)-3-(4'-chloro-2'-methylphenyl)acrylate (4e)

$C_{11}H_{11}ClO_2$
Mw: 210.65 g/mol

To a suspension of 142 mg (3.56 mmol, 1.10 eq.) NaH (60 w%) in anhydrous tetrahydrofuran (20 mL) 565 μ l (648 mg, 3.56 mmol, 1.10 eq.) trimethylphosphonoacetate were added at 0 °C and the mixture was stirred for 20 minutes at 0 °C. 500 mg (3.23 mmol, 1.00 eq.) of **3e** in anhydrous tetrahydrofuran (5 mL) were added to the reaction and the mixture was heated to 80 °C for 16 h. Residual NaH was hydrolyzed with 20 mL water and the mixture was extracted with diethylether (3 \times 20 mL). The combined organic layers were washed with brine (20 mL), dried over Na_2SO_4 and the solvents were removed under reduced pressure. After purification by column chromatography chromatography (silica, pentane/EtOAc = 20/1) 641 mg (3.09 mmol, 96%) of **4e** could be obtained as white powder.

M.p.: 34 °C.

TLC: R_f = 0.56 (pentane/EtOAc = 20/1), [UV/KMnO₄].

IR (ATR): $\tilde{\nu}$ (cm⁻¹) = 2951 (w, C_{Ar}-H), 1718 (vs, C=O), 1634 (m), 1593 (m), 1481 (m, C=C), 1316 (s), 1194 (m), 1171 (s, C-O, ester), 980 (m, C=C, disubst. trans), 818 (w).

¹H NMR (400 MHz, CDCl₃): δ (ppm) = 7.89 (d, ³J = 15.9 Hz, 1H, H-3), 7.47 – 7.43 (m, 1H, H-6'), 7.19 – 7.15 (m, 2H, H-3', H-5'), 6.34 (d, ³J = 15.9 Hz, 1H, H-2), 3.81 (s, 3H, CO₂CH₃), 2.41 (s, 3H, CH₃).

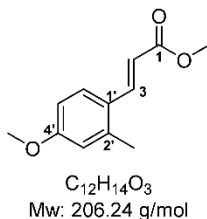
¹³C NMR (101 MHz, CDCl₃): δ (ppm) = 167.4 (s, C-1), 141.4 (d, C-3), 139.5 (s, C-2'), 135.8 (s, C-4'), 132.0 (s, C-1'), 130.8 (d, C-5'), 127.8 (d, C-6'), 126.7 (d, C-3'), 119.5 (d, C-2), 51.9 (q, CO₂CH₃), 19.8 (q, CH₃).

HRMS (ESI): m/z = calc. [$C_{11}H_{11}^{35}ClO_2+H$]⁺: 211.0520; found: 211.0521.

m/z = calc. [$C_{11}H_{11}^{37}ClO_2+H$]⁺: 213.0491; found: 213.0492.

GC-MS (EI, 70 eV): t_R = 12.2 min, m/z (%) = 210 (25) [M]⁺, 195 (5) [M-CH₃]⁺, 179 (80) [M-OCH₃]⁺, 150 (30), 115 (100) [M-CO₂CH₃-HCl]⁺, 89 (5).

The analytic results match with the literature data.¹⁷

Methyl-(E)-3-(4'-methoxy-2'-methylphenyl)acrylate (4f)

To a suspension of 0.44 g (10.9 mmol, 1.10 eq.) NaH (60 w%) in anhydrous tetrahydrofuran (100 mL), 1.77 mL (2.00 g, 10.9 mmol, 1.10 eq.) trimethylphosphonoacetat were added at 0 °C and the mixture was stirred for 20 minutes at 0 °C. 1.50 g (9.99 mmol, 1.00 eq.) of 4-methoxy-2-methylbenzaldehyde in anhydrous tetrahydrofuran (20 mL) were added to the reaction and the mixture was heated to 80 °C for 16 h. Residual NaH was hydrolyzed with water (100 mL) and the mixture was extracted with diethylether (3 × 100 mL). The combined organic layers were washed with brine (150 mL), dried over Na₂SO₄ and the solvents were removed under reduced pressure. After purification by column chromatography (silica, pentane/EtOAc = 50/1) 2.03 g (9.84 mmol, 99%) of **4f** were obtained as colorless viscous oil.

TLC: R_f = 0.61 (pentane/EtOAc = 20/1), [UV/KMnO₄].

IR (ATR): $\tilde{\nu}$ (cm⁻¹) = 2950 (w, C_{Ar}-H), 2839 (w, C_{Al}-H), 1712 (s, C=O), 1602 (s, C=C, conjugated), 1499 (m), 1435 (m), 1256 (s), 1161 (s, C-O, ester), 1104 (m), 1042 (m), 981 (w), 813 (w).

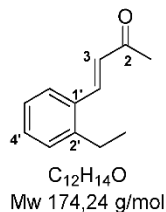
¹H NMR (400 MHz, CDCl₃): δ (ppm) 7.93 (d, ³J = 15.8 Hz, 1H, H-3), 7.53 (d, ³J = 8.5 Hz, 1H, H-3'), 6.79 – 6.71 (m, 2H, H-5', H-6'), 6.27 (d, ³J = 15.8 Hz, 1H, H-2), 3.82 (s, 3H, CO₂CH₃), 3.80 (s, 3H, OCH₃), 2.43 (s, 3H, CH₃).

¹³C NMR (101 MHz, CDCl₃): δ (ppm) = 167.9 (s, C-1), 161.2 (s, C-4'), 142.2 (d, C-3), 139.9 (s, C-2'), 128.1 (d, C-6'), 126.1 (s, C-1'), 116.4 (d, C-2), 116.0 (d, C-5'), 112.3 (d, C-3'), 55.4 (q, CO₂CH₃), 51.7 (q, OCH₃), 20.2 (q, CH₃).

HRMS (ESI): m/z = calc. [C₁₂H₁₄O₃+H]⁺: 207.1016; found: 207.1016.

GC-MS (EI, 70 eV): t_R = 12.89 min m/z (%) = 206 (60) [M]⁺, 191 (5) [M-CH₃]⁺, 175 (100) [M-OCH₃]⁺, 160 (5), 146 (20), 131 (15).

The analytic results match with the literature data.¹⁸

(E)-4-(2'-Ethylphenyl)but-3-en-2-one (4h)

1.00 g (11.2 mmol, 1.00 eq.) 2-ethylbenzaldehyde (**3a**) was added dropwise to a mixture of acetone (25 mL) and 4.85 mL NaOH solution (13.4 mmol, 1.20 eq., 10%). The reaction mixture was stirred at room temperature until reaction monitoring by TLC showed only traces of starting material remaining after three hours. The reaction was neutralized using HCl (2 M) and extracted with diethyl ether (3 × 20 mL). The organic layer was washed with brine (30 mL) and dried over Na₂SO₄. After filtration the solvent was removed reduced pressure. Purification by column chromatography (silica, pentane/EtOAc = 10/1) gave 1.37 g (7.85 mmol, 70%) of **4h** as yellow solid.

M.p.: 39 °C.

TLC: *R_f* = 0.59 (pentane/EtOAc = 10/1), [KMnO₄/UV].

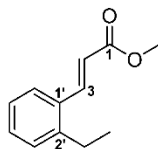
IR (ATR): $\tilde{\nu}$ (cm⁻¹) = 3061 (w, C_{Ar}-H), 2967 (m, C_{Ar}-H), 1691 (m, C=C, conjugated), 1669 (vs, C=O), 1609 (s, C_{Ar}=C_{Ar}), 1485 (m, C_{Ar}=C_{Ar}), 1454 (w, C_{Alkyl}-H), 1358 (m), 1255 (m), 1176 (m), 975 (s, C=C, disubst. trans), 760 (s, C_{Ar}-H).

¹H NMR (400 MHz, CDCl₃, 298 K): δ (ppm) = 7.87 (d, ³*J* = 16.0 Hz, 1H, H-4), 7.60 – 7.56 (m, 1H, H-6'), 7.36 – 7.31 (m, 1H, H-4'), 7.26 – 7.20 (m, 2H, H-3', H-5'), 6.66 (d, ³*J* = 16.0 Hz, 1H, H-3), 2.80 (q, ³*J* = 7.6 Hz, 2H, CH₂CH₃), 2.39 (s, 3H, COCH₃), 1.23 (t, ³*J* = 7.6 Hz, 3H, CH₂CH₃).

¹³C NMR (101 MHz, CDCl₃, 298 K): δ (ppm) = 198.5 (s, C-2), 144.2 (s, C-2'), 140.8 (d, C-4), 132.8 (s, C-1'), 130.6 (d, C-4'), 129.5 (d, C-3'), 128.4 (d, C-3), 126.7 (d, C-6'), 126.6 (d, C-5'), 28.0 (q, COCH₃), 26.6 (t, CH₂CH₃), 16.0 (q, CH₂CH₃).

HRMS (ESI): *m/z* = calc. [C₁₂H₁₄O+H]⁺: 175.1117; found: 175.1117.

GC-MS (EI, 70 eV): *t_R* = 11.2 min; *m/z* (%) = 174 (5) [M]⁺, 159 (15) [M-CH₃]⁺, 145 (100) [M-C₂H₅]⁺, 131 (15) [M-COCH₃]⁺, 115 (20), 91 (10) [C₇H₇]⁺.

Methyl-(E)-3-(2'-ethylphenyl)acrylate (4i)

$C_{12}H_{14}O_2$
Mw: 190.24 g/mol

To a suspension of 0.82 g (20.5 mmol, 1.10 eq.) NaH (60 w%) in anhydrous tetrahydrofuran (250 mL) 3.30 mL (3.73 g, 20.5 mmol, 1.10 eq.) trimethylphosphonoacetat were added at 0 °C and the mixture was stirred at 0 °C for 20 minutes. 2.50 g (18.6 mmol, 1.00 eq.) of **3a** in anhydrous tetrahydrofuran (50 mL) were added to the reaction and the mixture was heated to 80 °C for 16 h. Residual NaH was hydrolyzed with 200 mL water and the mixture was extracted with diethylether (3 × 150 mL). The combined organic layers were washed with brine (150 mL), dried over Na_2SO_4 and the solvents were removed under reduced pressure. After purification by column chromatography (silica, pentane/EtOAc = 50/1) 3.07 g (16.1 mmol, 87%) of **4i** were obtained as yellow oil.

TLC: R_f = 0.45 (pentane/EtOAc = 20/1), [UV/ $KMnO_4$].

IR (ATR): $\tilde{\nu}$ (cm^{-1}) = 3064 (w, C_{Ar-H}), 2967 (w, C_{Ar-H}), 2876 (w, C_{Ar-H}), 1717 (s, C=O), 1632 (m, C=C, conjugated), 1435 (m), 1317 (s), 1170 (s, C-O, ester), 981 (w), 764 (w).

1H NMR (400 MHz, $CDCl_3$): δ (ppm) 8.02 (d, 3J = 15.8 Hz, 1H, H-3), 7.56 (d, 3J = 7.6 Hz, 1H, H-6'), 7.36 – 7.29 (m, 1H, H-3'*), 7.25 – 7.18 (m, 2H, H-4'* , H-5'*), 6.37 (d, 3J = 15.8 Hz, 1H, H-2), 3.82 (s, 3H, CO_2CH_3), 2.79 (q, 3J = 7.6 Hz, 2H, CH_2CH_3), 1.22 (t, 3J = 7.6 Hz, 3H, CH_2CH_3).

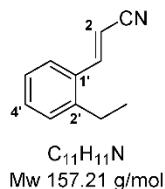
^{13}C NMR (101 MHz, $CDCl_3$): δ (ppm) = 167.6 (s, C-1), 144.0 (s, C-2'), 142.5 (d, C-3), 132.8, (s, C-1'), 130.3 (d, C-3'), 129.4 (d, C-5'), 126.6 (d, C-6'), 126.5 (d, C-4'), 119.1 (d, C-2), 51.8 (q, CO_2CH_3), 26.5 (t, CH_2CH_3), 16.0 (q, CH_2CH_3).

*Assignment is interconvertible.

HRMS (ESI): m/z = calc. [$C_{12}H_{14}O_2+H$] $^+$: 191.1067; found: 191.1067.

GC-MS (EI, 70 eV): t_R = 11.19 min m/z (%) = 190 (25) [M] $^+$, 175 (2) [$M-CH_3$] $^+$, 161 (50) [$M-C_2H_5$] $^+$, 130 (100) [$M-CO_2CH_3$] $^+$, 115 (75).

The analytic results match with the literature data.¹⁹

3-(2'-Ethylphenyl)acrylonitrile (4j)

0.99 g (17.6 mmol, 1.18 eq.) potassium hydroxide were suspended in 10 mL acetonitrile and heated to reflux. Then 1.00 g (14.9 mmol, 1.00 eq.) **3a**, dissolved in 10 mL acetonitrile was added. The reaction mixture was refluxed until reaction monitoring by TLC showed only traces of starting material remaining after 30 min. The orange suspension was poured into 100 mL cold water and extracted with CH₂Cl₂ (3 x 50 mL). The organic layer was dried over Na₂SO₄, filtered and the solvent was removed *in vacuo*. After purification by column chromatography (silica, pentane/EtOAc = 50/1) 1.21 g (82/18 mixture of *E/Z* isomers, 7.66 mmol, 51%) of **4j** could be obtained as a yellow oil.

IR (ATR): $\tilde{\nu}$ (cm⁻¹) = 3417 (w), 3059 (w, C_{Ar}-H), 2968 (m, C_{Alkyl}-H), 2934 (w), 2217 (s, C≡N), 1614 (m, C=C, conjugated), 1600 (m, C_{Ar}=C_{Ar}), 1483 (m, C_{Ar}=C_{Ar}), 1453 (m, C_{Alkyl}-H), 1265 (w), 1217 (w), 1055 (w), 965 (s, C=C, disubst. trans), 786 (w), 752 (s, C_{Ar}-H).

E-isomer:

TLC: *R_f* = 0.84 (pentane/EtOAc = 10/1), [KMnO₄/UV].

¹H NMR (400 MHz, CDCl₃, 298 K): δ (ppm) = 7.74 (d, ³*J* = 16.5 Hz, 1H, H-3), 7.55 – 7.44 (m, 1H, H-6'), 7.41 – 7.33 (m, 1H, H-3'), 7.26 – 7.21 (m, 2H, H-4', H-5'), 5.82 (d, ³*J* = 16.5 Hz, 1H, H-2), 2.74 (q, ³*J* = 7.6 Hz, 2H, CH₂CH₃), 1.22 (t, ³*J* = 7.6 Hz, 3H CH₂CH₃).

¹³C NMR (101 MHz, CDCl₃, 298 K): δ (ppm) = 148.4 (d, C-3), 143.6 (s, C-2'), 131.9 (s, C-1'), 131.3 (d, C-3'), 129.6 (d, C-4'), 126.7 (d, C-5'), 125.8 (d, C-6'), 118.6 (s, CN), 97.5 (d, C-2), 26.4 (t, CH₂CH₃), 15.9 (q, CH₂CH₃).

Z-isomer

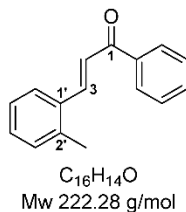
TLC: *R_f* = 0.75 (pentane/EtOAc = 10/1), [KMnO₄/UV].

¹H NMR (400 MHz, CDCl₃, 298 K): δ (ppm) = 7.93 – 7.89 (m, 1H, H-6'), 7.55 – 7.44 (m, 1H, H-3), 7.41 – 7.33 (m, 1H, H-3'), 7.33 – 7.28 (m, 2H, H-4', H-5'), 5.53 (d, ³*J* = 11.9 Hz, 1H, H-2), 2.69 (q, ³*J* = 7.6 Hz, 2H, CH₂CH₃), 1.21 (t, ³*J* = 7.6 Hz, 3H, CH₂CH₃).

¹³C NMR (101 MHz, CDCl₃, 298 K): δ (ppm) = 147.7 (d, C-3), 143.4 (s, C-2'), 132.1 (s, C-1'), 130.9 (d, C-3'), 129.1 (d, C-4'), 128.1 (d, C-6'), 126.6 (d, C-5'), 117.3 (s, CN), 97.3 (s, C-2), 26.6 (t, CH₂CH₃), 15.6 (q, CH₂CH₃).

HRMS (ESI): *m/z* = calc. [C₁₁H₁₁N+H]⁺: 158.2235; found: 158.2236.

GC-MS (EI, 70 eV): *t_R* = 10.6 min; *m/z* (%) = 157 (83) [M]⁺, 142 (30) [M-CH₃]⁺, 129 (41), 115 (100) [M-HCN-CH₃]⁺, 102 (9), 77 (11) [C₆H₅]⁺, 51 (10) [C₄H₃]⁺.

(E)-1-Phenyl-3-(o-tolyl)prop-2-en-1-one (4k)

5.00 mL (5.20 g, 43.3 mmol, 1.00 eq.) 2-methylbenzaldehyde were added dropwise at 0 °C to a mixture of ethanol (50 mL) and 2.60 g (64.9 mmol, 1.50 eq) NaOH in water (15 mL). The reaction mixture was stirred at room temperature for 16 h. The reaction was neutralized with HCl (2 M) and the aqueous layer was extracted with ethylacetate (3 × 50 mL). The combined organic layers were dried over Na₂SO₄, filtrated and the solvent was removed under reduced pressure. After purification by column chromatography (silica, pentane/EtOAc = 20/1) 8.69 g (39.1 mmol, 90%) of **4k** were isolated as yellow oil.

TLC: R_f = 0.61 (pentane/EtOAc = 10/1), [UV/KMnO₄].

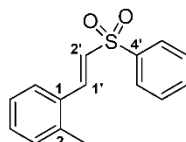
IR (ATR): $\tilde{\nu}$ (cm⁻¹) = 3058 (w, C_{Ar}-H), 1661 (s, C=O), 1594 (s, C=C, conjugated), 1577 (m, C=C, conjugated), 1447 (w, C-H), 1319 (m, C-H), 1279 (m), 1214 (s), 1015 (s), 977 (m, C=C, disubst. trans).

¹H NMR (400 MHz, CDCl₃): δ (ppm) = 8.13 (d, ³J = 15.6 Hz, 1H, H-3), 8.07 – 8.02 (m, 2H, 2 × *ortho*-C_{Ph}-H), 7.74 – 7.69 (m, 1H, H-3'), 7.63 – 7.56 (m, 1H, *para*-C_{Ph}-H), 7.55 – 7.49 (m, 2H, 2 × *meta*-C_{Ph}-H), 7.47 (d, ³J = 15.6 Hz, 1H, H-2), 7.35 – 7.29 (m, 1H, H-5'), 7.28 – 7.22 (m, 2H, H-6', H-4'), 2.49 (s, 3H, CH₃).

¹³C NMR (101 MHz, CDCl₃): δ (ppm) = 190.6 (s, C-1), 142.6 (d, C-3), 138.5 (s, C-2'), 138.4 (s, COC_{Ph}), 134.1 (s, C-1'), 132.9 (d, *para*-CH_{Ph}), 131.1 (d, C-4'), 130.4 (d, C-5'), 128.8 (d, *meta*-CH_{Ph}), 128.7 (d, *ortho*-CH_{Ph}), 126.6 (d, C-6'), 126.5 (d, C-3'), 123.3 (d, C-2), 20.0 (q, CH₃).

HRMS (ESI): m/z = calc. [C₁₆H₁₄O+H]⁺: 223.1117; found: 223.1118.

GC-MS (EI, 70 eV): t_R = 15.2 min; m/z (%) = 222 (25) [M]⁺, 207 (100) [M-CH₃]⁺, 145(10) [M-C₆H₅]⁺, 115 (30), 91 (5) [C₇H₇]⁺.

(E)-1-Methyl-2-[2'-(phenylsulfonyl)viny]benzene (4I)

C₁₅H₁₄O₂S
Mw: 258.33 g/mol

1.00 mL (0.92 g, 7.94 mmol, 1.00 eq.) of 1-ethynyl-2-methylbenzene was added to tetrahydrofuran (25 mL) in a pressure tube. 0.97 mL (1.05 g, 9.52 mmol, 1.20 eq.) benzenethiol, 425 mg (7.94 mmol, 1.00 eq.) NH₄Cl and 0.90 mL H₂O₂ (30% in water) were added successively to the reaction tube. The mixture was stirred at 50 °C for 48 h. The mixture was diluted with water (50 mL) the aqueous layer was separated and extracted with ethylacetate (3 × 20 mL). The organic layers were dried over Na₂SO₄ and concentrated under reduced pressure. After purification by column chromatography (silica, pentane/EtOAc = 5/1) 1.23 g (4.76 mmol, 60%) of **4I** were isolated as colorless crystals.

M.p.: 78 °C.

TLC: *R_f* = 0.56 (pentane/EtOAc = 5/1) [UV].

IR (ATR): $\tilde{\nu}$ (cm⁻¹) = 3059 (w, C_{Ar}-H), 1613 (w, C=C, conjugated), 1596 (w), 1446 (m, C-H), 1305 (s, S=O), 1143 (vs, S=O), 1085 (s), 972 (m, C=C, disubst. trans), 834 (m), 747 (s, C_{Ar}-H, 1,2-disubst.), 687 (s, C_{Ar}-H, monosubst.).

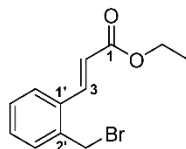
¹H NMR (500 MHz, CDCl₃): δ (ppm) = 7.97 – 7.94 (m, 3H, C_{Ar}-H), 7.66 – 7.53 (m, 3H, C_{Ar}-H), 7.46 – 7.42 (m, 1H, C_{Ar}-H), 7.30 – 7.28 (m, 1H, C_{Ar}-H), 7.24 – 7.16 (m, 2H, C_{Ar}-H), 6.79 (d, ³*J* = 15.3 Hz, 1H, C_{Ar}-H), 2.46 (s, 3H, CH₃).

¹³C NMR (126 MHz, CDCl₃): δ (ppm) = 140.8 (s, C-4'), 140.3 (d, C-1'), 138.4 (d, C-2), 133.5 (d, *para*-CH_{Ph}), 131.4 (s, C-1), 131.2 (d, C-4), 131.1 (d, C-3), 129.5 (d, C-2'), 128.2 (d, *meta*-CH_{Ph}), 127.8 (d, C-5), 127.0 (d, *ortho*-CH_{Ph}), 126.6 (d, C-6), 19.9 (q, CH₃).

HRMS (ESI): *m/z* = calc. [C₁₅H₁₄O₂S+H]⁺: 259.0787; found: 259.0787.

GC-MS (EI, 70 eV): *t_R* = 17.1 min; *m/z* (%) = 258 (40) [M]⁺, 241 (1), 116 (100) [M-HSO₂Ph]⁺.

The analytical data obtained matched those reported in the literature.¹⁴

Ethyl (E)-3-[2'-(bromomethyl)phenyl] acrylate (5a)

$C_{12}H_{13}BrO_2$
Mw: 269.14 g/mol

According to **GP1**, 8.09 g (42.5 mmol, 1.00 eq.) of **4a**, 9.71 g (54.5 mmol, 1.20 eq.) NBS and 0.55 g (2.27 mmol, 0.05 eq.) DBP were heated under reflux for 18 h in anhydrous chloroform (200 mL). After purification by column chromatography (silica, pentane/EtOAc = 10/1) 7.96 g (29.6 mmol, 70 %) of **5a** were isolated as yellow, viscous oil.

TLC: R_f = 0.55 (pentane/EtOAc = 10/1), [UV/KMnO₄].

IR (ATR): $\tilde{\nu}$ (cm⁻¹) = 3070, (vw, C_{Ar}-H), 2982 (w, C-H), 1765 (w), 1711 (vs, C=O), 1636 (m, C=C, conjugated), 1601 (w, C_{Ar}=C_{Ar}), 1573 (vw, C_{Ar}=C_{Ar}), 1487 (w, C_{Ar}=C_{Ar}), 1456 (w, C_{Ar}=C_{Ar}), 1392 (w), 1367 (w), 1316 (m), 1282 (m), 1253 (m), 1226 (m), 1179 (vs, C-O, ester), 1096 (w), 1035 (m), 977 (m, C=C, disubst. trans), 865 (w), 844 (w), 763 (m, C_{Ar}H), 705 (w).

¹H NMR (400 MHz, CDCl₃): δ (ppm) = 8.06 (d, ³J = 15.7 Hz, 1H, H-3), 7.64 – 7.54 (m, 1H, H-6'), 7.43 – 7.31 (m, 3H, H-3', H-4', H-5'), 6.44 (d, ³J = 15.7 Hz, 1H, H-2), 4.60 (s, 2H, CH₂Br), 4.29 (q, ³J = 7.1 Hz, 2H, CH₂CH₃), 1.35 (t, ³J = 7.1 Hz, 3H, CH₂CH₃).

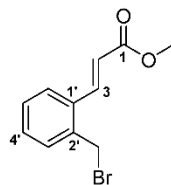
¹³C NMR (101 MHz, CDCl₃): δ (ppm) = 166.8 (s, C-1), 140.6 (d, C-3), 136.7 (s, C-2'), 133.9 (s, C-1'), 130.8 (d, C-5'), 130.4 (d, C-4'), 129.4 (d, C-3'), 127.4 (d, C-6'), 121.2 (d, C-2), 60.8 (t, CH₂CH₃), 30.7 (t, CH₂Br), 14.5 (q, CH₂CH₃).

HRMS (ESI): m/z = calc. [C₁₂H₁₃⁷⁹BrO₂+H]⁺: 269.0172; found: 269.0173.

m/z = calc. [C₁₂H₁₃⁸¹BrO₂+H]⁺: 271.0151; found: 271.0152.

GC-MS (EI, 70 eV): t_R = 13.6 min; m/z (%) = 223 (12) [M-C₃H₅O]⁺, 189 (83) [M-HBr]⁺, 175 (7), 145 (13), 115 (100) [M-C₃H₅O-HBr]⁺, 89 (13).

The analytical data obtained matched those reported in the literature.²⁰

Methyl (E)-3-(2'-(bromomethyl)phenyl)acrylate (5b)

$C_{11}H_{11}BrO_2$
Mw: 255.11 g/mol

According to **GP1** 2.00 g (11.4 mmol, 1.00 eq.) of **4b**, 2.42 g (13.6 mmol, 1.20 eq.) NBS and 140 mg (0.58 mmol, 0.05 eq.) DBP were heated under reflux in anhydrous chloroform (150 mL) for 30 h. After purification by column chromatography (silica, pentane/EtOAc = 20/1) 2.29 g (8.97 mmol, 80 %) of **5b** could be isolated as colorless crystals.

M.p.: 82 °C.

TLC: R_f = 0.46 (pentane/EtOAc = 10:1), [KMnO₄/UV].

IR (ATR): $\tilde{\nu}$ (cm⁻¹) = 3024 (w, C_{Ar}-H), 2950 (w, C-H), 1714 (vs, C=O), 1634 (m, C=C, conjugated), 1601 (w), 1487 (w), 1435 (m, C_{Ar}-H), 1320 (s), 1301 (m), 1281 (s), 1254 (m), 1227 (m), 1195 (s), 1173 (vs, C-O, ester), 1037 (w), 1014 (w), 976 (m, C=C, disubst. trans), 863 (w), 845 (w), 795 (w), 764 (s, C_{Ar}-H, 1,2-disubst.), 712 (w).

¹H NMR (500 MHz, CDCl₃): δ (ppm) = 8.07 (d, ³J = 15.8 Hz, 1H, H-3), 7.62 – 7.56 (m, 1H, H-6'), 7.40 – 7.32 (m, 3H, H-3', H-4', H-5'), 6.45 (d, ³J = 15.8 Hz, 1H, H-2), 4.60 (s, 2H, CH₂Br), 3.83 (s, 3H, CO₂CH₃).

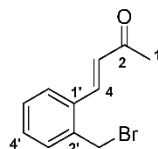
¹³C NMR (126 MHz, CDCl₃): δ (ppm) = 167.2 (s, C-1), 140.9 (d, C-3), 136.7 (s, C-2'), 133.8 (s, C-1'), 130.8 (d, C-4'), 130.5 (d, C-3'), 129.4 (d, C-6'), 127.4 (d, C-5'), 120.7 (d, C-2), 52.0 (q, CO₂CH₃), 30.7 (t, CH₂Br).

HRMS (ESI): m/z = calc. [C₁₁H₁₁⁷⁹BrO₂+H]⁺: 255.0015; found: 255.0015.

m/z = calc. [C₁₁H₁₁⁸¹BrO₂+H]⁺: 256.9995; found: 256.9994.

GC-MS (EI, 70 eV): t_R = 13.1 min; m/z (%) = 223 (5) [M-OCH₃]⁺, 175 (49) [M-HBr]⁺, 143 (10), 131 (9), 115 (100) [C₉H₇]⁺, 91 (13) [C₇H₇]⁺, 59 (10) [CO₂CH₃]⁺.

The analytical data obtained matched those reported in the literature.¹³

(E)-4-[2'-(Bromomethyl)phenyl]but-3-en-2-one (5c)

C₁₁H₁₁BrO
Mw 239.11 g/mol

According to **GP1** 1.00 g (6.24 mmol, 1.00 eq.) of (*E*)-4-(*o*-Tolyl)-but-3-en-2-one (**4c**), 1.33 g (7.49 mmol, 1.20 eq.) NBS and 75.6 mg (310 μmol, 0.05 eq.) DBP were heated under reflux for 16 h in anhydrous chloroform (45 mL). After purification by column chromatography (silica, pentane/EtOAc = 15/1) 494 mg of (2.06 mmol, 57%) **5c** was isolated as an off-white solid.

M.p.: 43 °C.

TLC: *R_f* = 0.21 (pentane/EtOAc = 15/1), [KMnO₄/UV].

IR (ATR): $\tilde{\nu}$ (cm⁻¹) = 1690 (m, C=O), 1666 (s, C=C), 1610 (s, C=C), 1596 (s, C=C), 1357 (m, CH₃), 1293 (m), 1254 (s), 1219 (m), 1175 (m), 971 (s, C=C, trans), 748 (vs, C-O), 1565 (w), 1014 (w), 976 (m, C=C, trans), 748 (s, C_{Ar}-H).

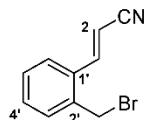
¹H-NMR (400 MHz, CDCl₃, 298 K): δ (ppm) = 7.93 (d, ³*J* = 16.1 Hz, 1H, H-3), 7.64 – 7.59 (m, 1H, H-6'), 7.42 – 7.33 (m, 3H, H-3', H-4', H-5'), 6.71 (d, ³*J* = 16.1 Hz, 1H, H-4), 4.61 (s, 2H, CH₂Br), 2.43 (s, 3H, COCH₃).

¹³C-NMR (126 MHz, CDCl₃, 298 K): δ (ppm) = 198.5 (s, C-2), 139.4 (d, C-4), 136.8 (s, C-2'), 134.0 (s, C-1'), 130.9 (d, C-5'), 130.6 (d, C-4'), 129.7 (d, C-3'), 129.6 (d, C-3), 127.4 (d, C-6'), 30.8 (t, Ar-CH₂Br), 27.8 (q, COCH₃).

HRMS (ESI): *m/z* = calc. [C₁₁H₁₁⁷⁹BrO+H]⁺: 239.0066; found: 239.0067.

m/z = calc. [C₁₁H₁₁⁸¹BrO+H]⁺: 241.0046; found: 241.0047

GC-MS (EI, 70 eV): 12.8 min; *m/z* (%) = 240 (2) [⁸¹BrM]⁺, 238 (2) [⁷⁹BrM]⁺, 223 (3) [M-CH₃]⁺, 159 (76) [M-Br]⁺, 145 (77), 115 (100) [M-C₂H₃O-HBr]⁺, 77 (3).

(E)-3-[2-(Bromomethyl)phenyl]acrylonitrile (5d)

C₁₀H₈BrN
Mw 222.08 g/mol

According to **GP1** 490 mg (3.42 mmol, 1.00 eq.) of 3-(*o*-Tolyl)acrylonitrile (**4d**) as *E/Z*-mixture, 731 mg (4.11 mmol, 1.20 eq.) NBS and 41.5 mg (0.17 mmol, 0.05 eq.) DBP were heated under reflux for 18 h in anhydrous chloroform (45 mL). After purification by column chromatography (silica, pentane/EtOAc = 15/1) 525 mg (2.36 mmol, 69%) of **5d** was isolated as an off-white solid.

M.p.: 93 °C.

IR (ATR): $\tilde{\nu}$ (cm⁻¹) = 3060 (w, C_{Ar}=C_{Ar}), 2214 (w), (s, C=N), 1615 (m, C=C), 1484 (m, CH₂), 1212 (m), 965 (s, C=C, disubst. trans), 737 (s), 599 (s, C-Br).

TLC: *R_f* = 0.21 (pentane/EtOAc = 15/1), [KMnO₄/UV].

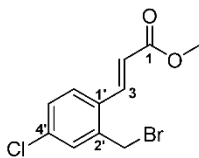
¹H NMR (400 MHz, CDCl₃, 298 K): δ (ppm) = 7.82 (d, ³*J* = 16.4 Hz, 1H, H-3), 7.54 – 7.49 (m, 1H, H-6'), 7.45 – 7.34 (m, 3H, H-3', H-4', H-5'), 5.92 (d, ³*J* = 16.4 Hz, 1H, H-2), 4.53 (s, 2H, CH₂Br).

¹³C NMR (101 MHz, CDCl₃, 298 K): δ (ppm) = 147.1 (d, C-3), 136.4 (s, C-1'), 133.0 (s, C-2'), 131.4 (d, C-3'), 131.0 (d, C-4'), 129.7 (d, C-5'), 126.7 (d, C-6'), 118.1 (s, CN), 99.3 (d, C-2), 30.2 (t, CH₂Br).

HRMS (ESI): *m/z* = calc. [C₁₀H₈⁷⁹BrN+H+MeCN]⁺: 263.0178; found: 263.0179.

GC-MS (EI, 70 eV): *t_R* = 18.0 min; *m/z* (%) = 221 (10), 141 (100) [M-HBr]⁺, 115 (95) [M-HBr-CN]⁺.

Methyl-(E)-3-(2'-(bromomethyl)-4'-chlorophenyl)acrylate (5e)



$C_{11}H_{10}BrClO_2$
Mw: 289.55 g/mol

According to **GP1**, 503 mg (2.39 mmol, 1.00 eq.) of **4e**, 510 mg (2.87 mmol, 1.20 eq.) NBS and 28.9 mg (0.12 mmol, 0.05 eq.) DBP were heated under reflux for 30 h in anhydrous chloroform (150 mL). After purification by column chromatography (silica, pentane/EtOAc = 50/1) 250 mg (0.86 mmol, 36%) of **5e** were isolated as colorless crystals.

M.p.: 52 °C.

TLC: R_f = 0.43 (pentane/EtOAc = 20/1), [UV/KMnO₄].

IR (ATR): $\tilde{\nu}$ (cm⁻¹) = 2950 (w, C_{Ar}-H), 1717 (vs, C=O), 1636 (m, C=C conjugated), 1593 (m), 1483 (m), 1318 (s), 1276 (m), 1174 (s, C-O, ester), 1109 (m), 900 (w).

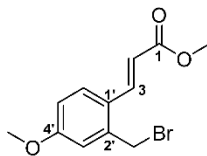
¹H NMR (400 MHz, CDCl₃): δ (ppm) = 7.97 (d, ³J = 15.8 Hz, 1H, H-3), 7.52 (d, ³J = 8.4 Hz, 1H, H-6'), 7.39 (d, ⁴J = 2.0 Hz, 1H, H-3'), 7.31 (dd, ³J = 8.4, ⁴J = 2.0 Hz, 1H, H-5'), 6.42 (d, ³J = 15.8 Hz, 1H, H-2), 4.52 (s, 2H, CH₂Br), 3.83 (s, 3H, CO₂CH₃).

¹³C NMR (101 MHz, CDCl₃): δ (ppm) = 166.9 (s, C-1), 139.7 (d, C-3), 138.3 (s, C-2'), 136.1 (s, C-4'), 132.3 (s, C-1'), 130.7 (d, C-5'), 129.6 (d, C-6'), 128.7 (d, C-3'), 121.2 (d, C-2), 52.1 (q, CO₂CH₃), 29.5 (t, CH₂Br).

HRMS (ESI): m/z = calc. [C₁₁H₁₀⁷⁹Br³⁵ClO₂+H]⁺: 288.9625; found: 288.9627.

m/z = calc. [C₁₁H₁₀⁸¹Br³⁵ClO₂+H]⁺: 290.9605; found: 290.9608.

GC-MS (EI, 70 eV): t_R = 14.29 min m/z (%) = 288 (5) [M]⁺, 256 (5) [M-OCH₃]⁺, 209 (50) [M-HBr]⁺, 179 (10), 149 (50), 130 (10), 115 (100) [M-CO₂CH₃-Cl-Br]⁺, 89 (5).

Methyl-(E)-3-(2'-(bromomethyl)-4'-methoxyphenyl)acrylate (5f)

$C_{12}H_{13}BrO_3$
Mw: 285.13 g/mol

According to **GP1**, 750 mg (3.64 mmol, 1.00 eq.) of **4f**, 776 mg (4.36 mmol, 1.20 eq.) NBS and 44.0 mg (0.18 mmol, 0.05 eq.) DBP were heated under reflux for 20 h in anhydrous chloroform (100 mL). After purification by column chromatography (silica, pentane/EtOAc = 20/1) 353 mg (1.24 mmol, 34%) of **5f** were isolated as colorless crystals.

M.p.: 80 °C.

TLC: R_f = 0.42 (pentane/EtOAc = 20/1), [UV/KMnO₄].

IR (ATR): $\tilde{\nu}$ (cm⁻¹) = 2950 (w, C_{Ar}-H), 2841 (w, C_{Al}-H), 1714 (s, C=O), 1603 (s, C=C, conjugated), 1499 (m), 1299 (m), 1262 (s), 1163 (s, C-O, ester), 1035 (m).

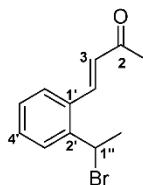
¹H NMR (400 MHz, CDCl₃): δ (ppm) 7.99 (d, ³J = 15.8 Hz, 1H, H-3), 7.57 (d, ³J = 8.3 Hz, 1H, H-6'), 6.93 – 6.83 (m, 2H, H-3', H-5'), 6.36 (d, ³J = 15.8 Hz, 1H, H-2), 4.57 (s, 2H, CH₂Br), 3.84 (s, 3H, OCH₃), 3.82 (s, 3H, CO₂CH₃).

¹³C NMR (101 MHz, CDCl₃): δ (ppm) = 167.5 (s, C-1), 161.2 (s, C-4'), 140.4 (d, C-3), 138.5 (s, C-2'), 129.0 (d, C-6'), 126.1 (s, C-1'), 118.2 (d, C-2), 115.8 (d, C-3'), 115.3 (d, C-5'), 55.6 (q, OCH₃), 51.9 (q, CO₂CH₃), 30.6 (t, CH₂Br).

HRMS (ESI): m/z = calc. [C₁₂H₁₃⁷⁹BrO₃+H]⁺: 285.0121; found: 285.0122.

m/z = calc. [C₁₂H₁₃⁸¹BrO₃+H]⁺: 287.0100; found: 287.0101.

GC-MS (EI, 70 eV): t_R = 14.903 min m/z (%) = 253 (5), 205 (90) [M-HBr]⁺, 175 (5) [M-Br-OCH₃]⁺, 145 (100) [M-HBr-CO₂CH₃]⁺, 131 (50).

(E)-4-[2'-(1''-Bromoethyl)phenyl]but-3-en-2-one (5h)

C₁₂H₁₃BrO
Mw 253.13 g/mol

According to **GP1** 500 mg (2.87 mmol, 1.00 eq.) of **4h**, 613 mg (3.44 mmol, 1.20 eq.) NBS and 34.8 mg (0.14 mmol, 0.05 eq.) DBP were heated under reflux for 18 h in anhydrous chloroform (45 mL). After purification by column chromatography (silica, pentane/EtOAc = 10/1) 521 mg (2.06 mmol, 72%) of **5h** could be isolated as brown oil.

TLC: *R_f* = 0.33 (pentane/EtOAc = 10/1), [KMnO₄/UV].

IR (ATR): $\tilde{\nu}$ (cm⁻¹) = 3061 (w, C_{Ar}-H), 3021 (w, C_{Ar}-H, conjugated), 2967 (m, C_{Alkyl}-H), 1692 (m, C=C, conjugated), 1670 (vs, C=O), 1609 (s, C_{Ar}=C_{Ar}), 1598 (s, C_{Ar}=C_{Ar}), 1454 (m, C_{Alkyl}-H), 1256 (s), 1177 (m), 975 (s, C=C, disubst. trans), 751 (s, C_{Ar}-H).

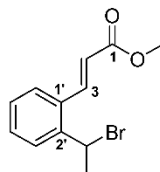
¹H NMR (400 MHz, CDCl₃, 298 K): δ (ppm) = 8.04 (d, ³*J* = 16.0 Hz, 1H, H-4), 7.64 (dd, ³*J* = 7.9 Hz, ⁴*J* = 1.3 Hz, 1H, H-3'), 7.55 (dd, ³*J* = 7.7 Hz, ⁴*J* = 1.5 Hz, 1H, H-6'), 7.45 (td, ³*J* = 7.6 Hz, ⁴*J* = 1.5 Hz, 1H, H-4'), 7.35 (td, ³*J* = 7.7 Hz, ⁴*J* = 1.3 Hz, 1H, H-5'), 6.67 (d, ³*J* = 16.0 Hz, 1H, H-3), 5.53 (q, ³*J* = 6.9 Hz, 1H, CHBr), 2.45 (s, 3H, COCH₃), 2.12 (d, ³*J* = 6.9 Hz, 3H, CHBrCH₃).

¹³C NMR (101 MHz, CDCl₃, 298 K): δ (ppm) = 198.3 (s, C-2), 141.6 (s, C-2'), 139.8 (d, C-4), 132.9 (s, C-1'), 130.7 (d, C-4'), 130.2 (d, C-3), 128.9 (d, C-5'), 127.5 (d, C-3'), 126.9 (d, C-6'), 44.8 (d, CHBr), 27.9 (q, COCH₃), 26.1 (q, CHBrCH₃).

HRMS (ESI): *m/z* = calc. [C₁₂H₁₃⁷⁹BrO+H]⁺: 253.0223; found: 253.0223.

m/z = calc. [C₁₂H₁₃⁸¹BrO+H]⁺: 255.0202; found: 255.0202.

GC-MS (EI, 70 eV): *t_R* = 13.1 min; *m/z* (%) = 209 (1) [M-COCH₃]⁺, 173 (100) [M-HBr]⁺, 145 (20) [C₁₀H₉O]⁺, 129 (86) [M-COCH₃-HBr]⁺, 115 (59), 102 (13) [C₉H₇]⁺, 77 (15)⁺.

Methyl (*E*)-3-[2'-(1''-bromoethyl)phenyl]acrylate (5i**)**

$C_{12}H_{13}BrO_2$
Mw: 269.13 g/mol

According to **GP1**, 1.57 g (8.25 mmol, 1.00 eq.) **4i**, 1.76 g (9.90 mmol, 1.20 eq.) NBS and 0.10 g (0.41 mmol, 0.05 eq.) DBP were heated under reflux for 20 h in 200 mL anhydrous chloroform. After purification by column chromatography (silica, pentane/EtOAc = 20/1) 1.89 g (7.01 mmol, 85%) of **5i** were isolated as yellow oil.

TLC: R_f = 0.65 (pentane/EtOAc = 20/1), [UV/KMnO₄].

IR (ATR): $\tilde{\nu}$ (cm⁻¹) = 2992 (w, C_{Ar}-H), 2950 (w, C_{Al}-H), 1717 (s, C=O), 1634 (s, C=C, conjugated), 1435 (m), 1317 (s), 1274 (m), 1172 (s, C-O, ester), 973 (w) 762 (m).

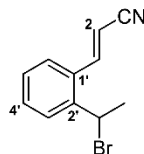
¹H NMR (400 MHz, CDCl₃): δ (ppm) = 8.14 (d, ³*J* = 15.7 Hz, 1H, H-3), 7.63 (d, ³*J* = 7.8 Hz, 1H, H-6'), 7.50 (d, ³*J* = 7.8 Hz, 1H, H-3'), 7.41 (t, ³*J* = 7.4 Hz, 1H, H-4'), 7.31 (t, ³*J* = 7.4 Hz, 1H, H-5'), 6.38 (d, ³*J* = 15.7 Hz, 1H, H-2), 5.52 (q, ³*J* = 6.9 Hz, 1H, CHBrCH₃), 3.83 (s, 3H, CO₂CH₃), 2.07 (d, ³*J* = 6.9 Hz, 3H, CHBrCH₃).

¹³C NMR (101 MHz, CDCl₃): δ (ppm) = 167.1 (s, C-1), 141.6 (s, C-2'), 141.3 (d, C-3), 132.6 (s, C-1'), 130.5 (d, C-4'), 128.8 (d, C-5'), 127.4 (d, C-3'), 127.0 (d, C-6'), 121.3 (d, C-2), 52.0 (q, CO₂CH₃), 44.6 (d, CHBrCH₃), 26.2 (q, CHBrCH₃).

HRMS (ESI): m/z = calc. [C₁₂H₁₃⁷⁹BrO₂+H]⁺: 269.0172; found: 269.0173.

m/z = calc. [C₁₂H₁₃⁸¹BrO₂+H]⁺: 271.0151; found: 271.0153.

GC-MS (EI, 70 eV): t_R = 13.28 min m/z (%) = 209 (5), 189 (20) [M-HBr]⁺, 157 (5) [M-HBr-OCH₃]⁺, 129 (100) [M-HBr-CO₂CH₃]⁺.

3-[2'-(1''-Bromoethyl)phenyl]acrylonitrile (**5j**)

$C_{11}H_{10}BrN$
Mw 236.11 g/mol

According to **GP1** 500 mg (3.17 mmol, 1.00 eq.) of **4j**, 679 mg (3.82 mmol, 1.20 eq.) NBS and 38.5 mg (0.16 mmol, 0.05 eq.) DBP were heated under reflux for 16 h in anhydrous chloroform (45 mL). After purification by column chromatography (silica, pentane/EtOAc = 20/1) 750 mg (3.17 mmol, *quant.*, 80/20 mixture of *E/Z* isomers) of **5j** were isolated as yellow solid.

M.p.: 89 °C.

IR (ATR): $\tilde{\nu}$ (cm⁻¹) = 3060 (w, C_{Ar}-H), 2981 (w, C_{Alkyl}-H), 2219 (s, C≡N), 1616 (m), 1485 (m, C_{Ar}=C_{Ar}), 1452 (m, C_{Alkyl}-H), 1378 (m, C_{Alkyl}-H), 1222 (m), 1197 (m), 1033 (m), 962 (s, C=C, disubst. trans), 761 (vs, C_{Ar}-H), 739 (m, disubst. cis).

E-isomer

TLC: *R_f* = 0.41 (pentane/EtOAc = 10/1), [KMnO₄/UV].

¹H NMR (400 MHz, CDCl₃, 298 K): δ (ppm) = 7.92 (d, ³*J* = 16.4 Hz, 1H, H-3), 7.63 – 7.59 (m, 1H, H-6'), 7.51 – 7.40 (m, 2H, H-3', H-4'), 7.39 – 7.31 (m, 1H, H-5'), 5.85 (d, ³*J* = 16.4 Hz, 1H, H-2), 5.37 (q, ³*J* = 6.9 Hz, 1H, CHBr), 2.09 (t, ³*J* = 6.9 Hz, 3H, CHBrCH₃).

¹³C NMR (126 MHz, CDCl₃, 298 K): δ (ppm) = 147.4 (d, C-3), 140.9 (s, C-2'), 131.9 (s, C-1'), 131.3 (d, C-4'), 128.9 (d, C-5'), 126.8 (d, C-3'), 126.7 (d, C-6'), 117.9 (s, CN), 99.5 (d, C-2), 44.0 (d, CHBr), 25.6 (q, CHBrCH₃).

Z-isomer:

TLC: *R_f* = 0.34 (pentane/EtOAc = 10/1), [KMnO₄/UV].

¹H NMR (400 MHz, CDCl₃, 298 K): δ (ppm) = 7.78 – 7.74 (m, 1H, H-6'), 7.70 (d, ³*J* = 11.8 Hz, 1H, H-3), 7.50 – 7.40 (m, 2H, H-3', H-4'), 7.39 – 7.31 (m, 1H, H-5'), 5.67 (d, ³*J* = 11.8 Hz, 1H, H-2), 5.26 (q, ³*J* = 6.9 Hz, 1H, CHBr), 2.09 (t, ³*J* = 6.9 Hz, 3H, CHBrCH₃).

¹³C NMR (126 MHz, CDCl₃, 298 K): δ (ppm) = 147.1 (d, C-3), 140.7 (s, C-2'), 131.9 (s, C-1'), 130.9 (d, C-4'), 128.8 (d, C-5'), 126.7 (d, C-3'), 126.4 (d, C-6'), 99.6 (d, C-2), 44.9 (d, CHBr), 25.5 (q, CHBrCH₃).

HRMS (ESI): *m/z* = calc. [C₁₁H₁₀⁷⁹BrN+H]⁺: 236.0069; found: 236.0070.

m/z = calc. [C₁₁H₁₀⁸¹BrN+H]⁺: 238.0049; found: 238.0051.

GC-MS (EI, 70 eV): *t_R* = 12.8 min; *m/z* (%) = 208 (1) [M-HCN]⁺, 156 (100) [M-HBr]⁺, 129 (92), 115 (36) [M-HCN-CH₃]⁺, 102 (7), 77 (11) [C₆H₅]⁺, 51 (10) [C₄H₃]⁺.

Z-isomer:

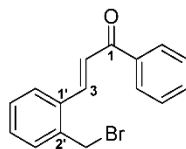
TLC: $R_f = 0.65$ (pentane/EtOAc = 10/1), [KMnO₄/UV].

¹H NMR (400 MHz, C₆D₆, 298 K): δ (ppm) = 8.05 – 8.01 (m, 1H, C_{Ar}-H), 7.60 – 7.42 (m, 3H, C_{Ar}-H), 7.29 – 7.19 (m, 1H, C_{Ar}-H), 7.13 – 7.05 (m, 2H, C_{Ar}-H, H-3), 7.04 – 6.94 (m, 2H, C_{Ar}-H), 6.89 – 6.83 (m, 1H, C_{Ar}-H), 4.75 (d, ³J = 12.0 Hz, 1H, H-2), 3.71 (q, ³J = 6.6 Hz, 1H, H-1''), 3.55 (d, ²J = 13.0 Hz, 1H, Ph-CHH), 3.21 (d, ²J = 13.0 Hz, 1H, Ph-CHH), 1.82 (d, ²J = 14.6 Hz, 1H, CHHTMS), 1.67 (d, ²J = 14.6 Hz, 1H, CHHTMS), 1.03 (d, ³J = 6.6 Hz, 3H, H-2''), –0.13 [s, 9H, Si(CH₃)₃].

¹³C NMR (101 MHz, C₆D₆, 298 K): δ (ppm) = 148.5 (d, C-3), 142.7 (s, CH₂-C_{Ph}), 139.5 (s, C-2'), 134.2 (s, C-1'), 129.9 (d, *ortho*-CH_{Ph}), 129.7 (d, *meta*-CH_{Ph}), 128.6 (d, C_{Ar}), 127.5 (d, *para*-CH_{Ph}), 117.4 (s, CN), 96.0 (d, C-2), 58.5 (t, CH₂-C_{Ph}), 54.9 (d, C-1''), 39.9 (t, CH₂TMS), 8.7 (q, C-2''), –1.4 [Si(CH₃)₃].

HRMS (ESI): $m/z = \text{calc. [C}_{22}\text{H}_{28}\text{N}_2\text{Si+H}]^+$: 349.2095; found: 349.2093.

GC-MS (EI, 70 eV): $t_R = 18.2$ min; m/z (%) = 348 (8) [M]⁺, 333 (14) [M-CH₃]⁺, 275 (100) [M-(SiCH₃)₃]⁺, 220 (2), 156 (54) [M-C₁₁H₁₈NSi]⁺, 120 (81), 91 (71) [C₇H₇]⁺, 73 (18) [(SiCH₃)₃]⁺.

(E)-3-[2'-(Bromomethyl)phenyl]-1-phenylprop-2-en-1-one (5k)

C₁₆H₁₃BrO
Mw: 301.18 g/mol

According to **GP1** 1.00 g (4.50 mmol, 1.00 eq.) of **4k**, 0.96 g (5.40 mmol, 1.20 eq.) NBS and 0.06 g (0.23 mmol, 0.05 eq.) DBP were heated under reflux for 18 h in anhydrous chloroform (75 mL). After purification by column chromatography (silica, pentane/EtOAc = 50/1) 0.39 g (1.29 mmol, 29%) of **5k** were isolated as yellow solid.

TLC: R_f = 0.75 (pentane/EtOAc = 10/1), [UV/KMnO₄].

IR (ATR): $\tilde{\nu}$ (cm⁻¹) = 3062, (vw, C_{Ar}-H), 1765 (w), 1663 (s, C=O), 1606 (s, C_{Ar}=C_{Ar}), 1596 (s, C_{Ar}=C_{Ar}), 1485 (w, C_{Ar}=C_{Ar}), 1329 (m), 1216 (s), 1015 (vs), 974 (m, C=C, disubst. trans), 756 (m, C_{Ar}H).

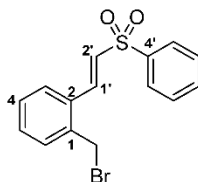
¹H NMR (400 MHz, CDCl₃): δ (ppm) = 8.16 (d, ³J = 15.6 Hz, 1H, H-3), 8.09 – 8.03 (m, 2H, 2 × *ortho*-C_{Ph}-H), 7.77 – 7.70 (m, 1H, H-3'), 7.64 – 7.57 (m, 1H, *para*-C_{Ph}-H), 7.56 – 7.49 (m, 3H, 2 × *meta*-C_{Ph}-H, H-2), 7.45 – 7.36 (m, 3H, H-4', H-5', H-6'), 4.64 (s, 2H, CH₂Br).

¹³C NMR (101 MHz, CDCl₃): δ (ppm) = 190.5 (s, C-1), 140.8 (d, C-3), 138.1 (s, C-2'), 137.3 (s, COC_{Ph}), 134.4 (s, C-1'), 133.1 (d, *para*-CH_{Ph}), 131.0 (d, C-4'), 130.6 (d, C-5'), 129.4 (d, C-3'), 128.8 (d, *ortho*-CH_{Ph}), 128.8 (d, *meta*-CH_{Ph}), 127.6 (d, C-6'), 125.0 (d, C-2), 30.8 (t, CH₂Br).

HRMS (ESI): m/z = calc. [C₁₆H₁₃⁷⁹BrO+H]⁺: 301.0223; found: 301.0224

m/z = calc. [C₁₆H₁₃⁸¹BrO+H]⁺: 303.0202; found: 303.0203.

GC-MS (EI, 70 eV): t_R = 17.4 min; m/z (%) = 221 (40) [M-HBr]⁺, 207 (95) [M-CH₂Br]⁺, 145 (2), 115 (100) [M-C₇H₅O-HBr]⁺.

(E)-1-(Bromomethyl)-2-(2'-(phenylsulfonyl)vinyl)benzene (5I)

C₁₅H₁₃BrO₂S
Mw 337.23 g/mol

According to **GP1**, 657 mg (2.54 mmol, 1.00 eq.) of **4I**, 550 mg (3.09 mmol, 1.20 eq.) NBS and 30.8 mg (0.13 mmol, 0.05 eq.) DBP were heated under reflux for six days in anhydrous chloroform (45 mL). After purification by column chromatography (silica, pentane/EtOAc = 10/1) 460 mg (1.36 mmol, 54%) of **5I** were isolated as colorless crystals.

M.p.: 139 °C.

TLC: R_f = 0.36 (pentane/EtOAc = 5/1) [UV].

IR (ATR): $\tilde{\nu}$ (cm⁻¹) = 3059 (w, C_{Ar}-H), 1712 (w), 1616 (w, C=C, conjugated), 1598 (w), 1482 (w), 1447 (m, C-H), 1306 (s, S=O), 1222 (m), 1144 (vs, S=O), 1084 (s), 968 (m, C=C, disubst. trans), 853 (m), 840 (m), 778 (m), 752 (s, C_{Ar}-H, 1,2-disubst.), 736 (s), 714 (m), 687 (s, C_{Ar}-H, monosubst.).

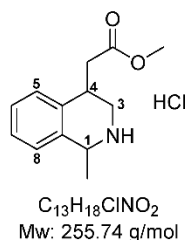
¹H NMR (500 MHz, CDCl₃): δ (ppm) = 8.05 (d, ³J = 15.2 Hz, 1H, H-1'), 8.02 – 7.96 (m, 2H, 2 × *ortho*-C_{Ph}-H), 7.67 – 7.60 (m, 1H, *para*-C_{Ph}-H), 7.56 (t, ³J = 7.6 Hz, 2H, 2 × *meta*-C_{Ph}-H), 7.51 – 7.47 (m, 1H, H-3), 7.40 – 7.37 (m, 2H, H-4, H-5), 7.36 – 7.31 (m, 1H, H-6), 6.88 (d, ³J = 15.2 Hz, 1H, H-2'), 4.60 (s, 2H, CH₂Br).

¹³C NMR (126 MHz, CDCl₃): δ (ppm) = 140.4 (s, C-4'), 138.9 (d, C-1'), 137.3 (s, C-1), 133.7 (d, *para*-CH_{Ph}), 131.9 (s, C-2), 131.3 (d, C-5), 130.9 (d, C-6), 130.1 (d, C-2'), 129.6 (d, *meta*-CH_{Ph}), 129.5 (d, C-4), 128.0 (d, *ortho*-CH_{Ph}), 127.9 (d, C-3), 30.4 (t, CH₂Br).

HRMS (ESI): m/z = calc. [C₁₅H₁₃⁷⁹BrO₂S+H]⁺: 336.9892; found: 336.9892.

m/z = calc. [C₁₅H₁₃⁸¹BrO₂S+H]⁺: 338.9822; found: 338.9871.

GC-MS (EI, 70 eV): t_R = 18.4 min; m/z (%) = 257 (39) [M-HBr]⁺, 195 (13), 141 (15) [SO₂Ph]⁺, 115 (100) [C₉H₇]⁺, 77 (27) [C₆H₅]⁺.

Methyl 2-(1-methyl-1,2,3,4-tetrahydroisoquinolin-4-yl)acetate hydrochloride (6)

To a reaction mixture of 40.0 mg (129 μ mol, 1.00 eq.) **1i** (major diastereoisomer) and 0.1 mL of conc. HCl in 1.0 mL methanol 45.9 mg (38.8 μ mol, 0.30 eq., 10 w%) Pd/C were added in one portion. The flask atmosphere was exchanged with Hydrogen and the reaction was stirred for 16 hours at room temperature under Hydrogen pressure (1 atm). The suspension was filtered through a celite plug and the organic solvents were removed under reduced pressure. After diffusion crystallization (MeOH/Et₂O) 29.0 mg (113 μ mol, 88%) of the ammonium salt **6** were isolated as off-white crystals.

M.p.: 159 °C.

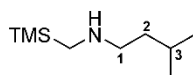
IR (ATR): $\tilde{\nu}$ (cm⁻¹) = 2963 (bm, NH), 2905 (bm, NH), 2766 (bs, NH), 2695(m), 2523 (w), 1735 (s, C=O), 1593 (w, C=C), 1492 (m), 1442 (s), 1385 (m), 1204 (m), 1160 (s, C-O), 1178 (s), 1103 (m), 1016 (m), 775 (s, C_{Ar}-H), 751 (s).

¹H-NMR (500 MHz, MeOD): δ (ppm) = 7.40 – 7.31 (m, 4H, H-5, H-6, H-7, H-8), 4.64 (q, ³J = 6.9 Hz, 1H, H-1), 3.70 (s, 3H, CO₂CH₃), 3.65 – 3.55 (m, 3H, H-3, H-4), 3.05 – 2.96 (m, 2H, CH₂CO₂CH₃), 1.75 (d, ³J = 6.9 Hz, 3H, CH₃).

¹³C-NMR (126 MHz, MeOD): δ (ppm) = 173.8 (s, CO₂CH₃), 134.8 (s, C-8a), 134.7 (s, C-4a), 129.6 (d, C-6), 128.8 (d, C-7), 128.6 (d, C-5), 127.5 (d, C-8), 52.6 (d, C-1), 52.5 (q, CO₂CH₃), 43.6 (t, C-3), 38.5 (t, CH₂CO₂CH₃), 32.4 (d, C-4), 19.4 (q, CH₃).

HRMS (ESI): m/z = calc. [C₁₃H₁₈ClNO₂-Cl+H]⁺: 220.1332 found: 220.1332.

GC-MS (EI, 70 eV): t_R = 12.89 min m/z (%) = 218 (5) [M-HCl]⁺, 204 (100) [M-Cl-CH₃]⁺, 144 (40), 130 (55) [M-Cl-C₃H₄O₂-CH₃]⁺.

3-Methyl-N-((trimethylsilyl)methyl)butan-1-amine (8b)

$C_9H_{23}NSi$
Mw: 173.37 g/mol

For the synthesis of 3-methyl-N-((trimethylsilyl)methyl)butan-1-amine (**8b**), a literature procedure was adapted.¹⁵ 0.46 mL (346 mg, 3.97 mmol, 1.20 eq.) *iso*-pentylamine and 930 mg (6.73 mmol, 2.00 eq.) K_2CO_3 were suspended in acetonitrile (40 mL). The mixture was cooled to 0 °C and 0.50 mL (720 mg, 3.36 mmol, 1.00 eq.) (trimethylsilyl)methyl iodide were added dropwise. After 19 h at room temperature, the mixture was concentrated under reduced pressure. The residue dissolved in water (10 mL) and extracted with dichloromethane (3 × 10 mL). The combined organic layers were dried over Na_2SO_4 , filtrated and concentrated under reduced pressure. Without further purification 281 mg (1.62 mmol, 49%) of **8b** were obtained as clear yellowish oil.

TLC: R_f = 0.32 ($CH_2Cl_2/MeOH$ = 9/1) [ninhydrin].

IR (ATR): $\tilde{\nu}$ (cm^{-1}) = 2955 (m, C–H), 2871 (w, C–H), 2764 (w), 1647 (w, N–H), 1467 (w), 1384 (w), 1368 (w), 1248 (s, Si–CH₃), 1126 (w, N–H), 841 (vs, Si–CH₃), 763 (m, Si–CH₃), 697 (m).

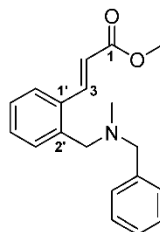
¹H NMR (400 MHz, $CDCl_3$): δ (ppm) = 2.69 – 2.56 (m, 2H, H-1), 2.08 (s, 2H, CH_2TMS), 1.59 (hept, 3J = 6.7 Hz, 1H, H-3), 1.44 – 1.31 (m, 2H, H-2), 0.89 (d, 3J = 6.7 Hz, 6H, 2 × CH_3), 0.05 (s, 9H, $Si(CH_3)_3$).

¹³C NMR (101 MHz, $CDCl_3$): δ (ppm) = 52.8 (t, C-1), 40.4 (t, CH_2TMS), 38.6 (t, C-2), 26.5 (d, C-3), 22.8 (q, 2 × CH_3), -2.3 (q, $Si(CH_3)_3$).

HRMS (ESI): m/z = calc. $[C_9H_{23}NSi+H]^+$: 174.1673; found: 174.1672.

GC-MS (EI, 70 eV): t_R = 13.7 min; m/z (%) = 172 (9), 158 (23) $[M-CH_3]^+$, 143 (100) $[M-C_2H_6]^+$, 130 (9) $[M-C_3H_7]^+$, 116 (5) $[M-C_4H_9]^+$, 86 (5) $[C_5H_{12}N]^+$, 73 (42) $[Si(CH_3)_3]^+$.

Methyl-(E)-3-[2'-{(benzyl(methyl)amino)methyl}phenyl]acrylate (10)



$C_{19}H_{21}NO_2$
Mw: 295.38 g/mol

According to **GP2** 360 mg (1.41 mmol, 1.00 eq.) of bromide **5b**, 205 mg (1.69 μ mol, 1.20 eq.) of benzyl-methyl-amine and 975 mg (7.06 mmol, 5.00 eq.) K_2CO_3 were converted in acetone (20 mL). After purification by column chromatography (silica, pentane/EtOAc = 20/1) 326 mg (1.10 mmol, 78%) of **10** were isolated as a yellow oil.

TLC: R_f = 0.62 (pentane/EtOAc = 10/1) [UV/ $KMnO_4$].

IR (ATR): $\tilde{\nu}$ (cm^{-1}) = 3062, (w, C_{Ar} -H), 2948 (w, C-H), 2788 (w), 1716 (vs, C=O), 1633 (m, $C_{Ar}=C_{Ar}$), 1434 (w, $C_{Ar}=C_{Ar}$), 1316 (m), 1169 (s), 1017 (s), 977 (w, C=C, disubst. trans), 854 (w), 748 (m), 699 (m).

1H NMR (400 MHz, $CDCl_3$): δ (ppm) = 8.33 (d, 3J = 16.0 Hz, 1H, H-3), 7.62 – 7.57 (m, 1H, H-3'), 7.39 – 7.27 (m, 7H, C_{Ar} -H), 7.25 – 7.20 (m, 1H, C_{Ar} -H), 6.38 (d, 3J = 16.0 Hz, 1H, H-2), 3.84 (s, 3H, CO_2CH_3), 3.63 (s, 2H, Ar- CH_2), 3.55 (s, 2H, Ph- CH_2), 2.09 (s, 3H, CH_3).

^{13}C NMR (101 MHz, $CDCl_3$): δ (ppm) = 167.7 (s, C-1), 143.3 (d, C-3), 139.3 (s, CH_2-C_{Ph}), 138.8 (s, C-2'), 134.6 (s, C-1'), 130.9 (d, C_{Ar}), 129.8 (d, C_{Ar}), 129.1 (d, *ortho*- CH_{Ph}), 128.4 (d, *meta*- CH_{Ph}), 127.8 (d, C_{Ar}), 127.1 (d, C_{Ar}), 126.8 (d, C_{Ar}), 118.7 (d, C-2), 62.6 (t, CH_2-C_{Ph}), 60.6 (t, Ar- CH_2), 51.8 (q, CO_2CH_3), 41.7 (q, CH_3).

HRMS (ESI): m/z = calc. [$C_{19}H_{21}NO_2+H$] $^+$: 296.1645; found: 296.1644.

GC-MS (EI, 70 eV): t_R = 16.2 min; m/z (%) = 294 (25), 280 (65) [$M-CH_3$] $^+$, 204 (95) [$M-C_7H_7$] $^+$, 174 (15) [$M-C_8H_{10}N$] $^+$, 144 (70), 115 (75), 91 (100) [C_7H_7] $^+$,

Molecular Structure

Molecular Structure of 6

A colorless fragment-like specimen of $C_{13}H_{18}ClNO_2$, approximate dimensions 0.044 mm x 0.134 mm x 0.214 mm, was used for the X-ray crystallographic analysis. The X-ray intensity data were measured on a Bruker D8 Venture Duo IMS system equipped with a Helios optic monochromator and a Mo IMS microsource ($\lambda = 0.71073 \text{ \AA}$).

A total of 3434 frames were collected. The total exposure time was 26.12 hours. The frames were integrated with the Bruker SAINT software package using a narrow-frame algorithm. The integration of the data using a monoclinic unit cell yielded a total of 62800 reflections to a maximum θ angle of 26.73° (0.79 \AA resolution), of which 2763 were independent (average redundancy 22.729, completeness = 100.0, $R_{\text{int}} = 4.85\%$, $R_{\text{sig}} = 1.43\%$) and 2599 (94.06%) were greater than $2\sigma(F^2)$. The final cell constants of $a = 15.5693(9) \text{ \AA}$, $b = 9.3104(5) \text{ \AA}$, $c = 9.3874(5) \text{ \AA}$, $\beta = 106.804(2)^\circ$, volume = $1302.66(12) \text{ \AA}^3$, are based upon the refinement of the XYZ-centroids of 166 reflections above $20 \sigma(I)$ with $5.171^\circ < 2\theta < 45.85^\circ$. Data were corrected for absorption effects using the Multi-Scan method (SADABS). The ratio of minimum to maximum apparent transmission was 0.964. The calculated minimum and maximum transmission coefficients (based on crystal size) are 0.9420 and 0.9880.

The final anisotropic full-matrix least-squares refinement of F^2 with 162 variables converged at $R_1 = 4.13\%$, for the observed data and $wR_2 = 8.48\%$ for all data. The goodness-of-fit was 1.203. The largest peak in the final difference electron density synthesis was $0.382 \text{ e}^-/\text{\AA}^3$ and the largest hole was $-0.226 \text{ e}^-/\text{\AA}^3$ with an RMS deviation of $0.050 \text{ e}^-/\text{\AA}^3$. On the basis of the final model, the calculated density was 1.304 g/cm^3 and $F(000)$, $544e^-$.

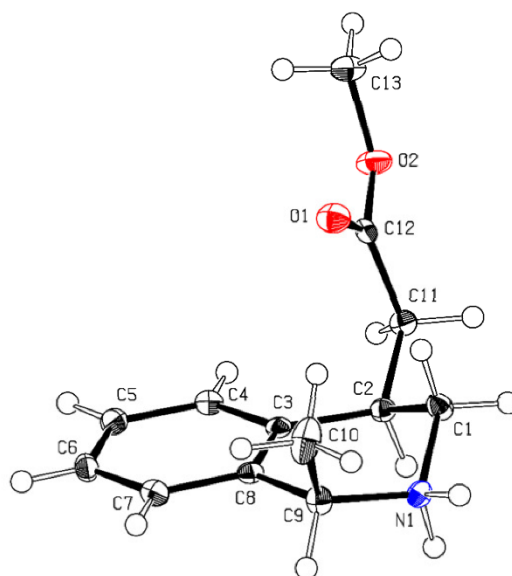


Figure S1: Molecular structure of 6.

Table S2: Sample and crystal data for 6.

Identification code	GruMi27	
Chemical formula	$C_{13}H_{18}ClNO_2$	
Formula weight	255.73	
Temperature	100 (2) K	
Wavelength	0.71073 Å	
Crystal size	0.044 x 0.134 x 0.214 mm	
Crystal habit	colorless fragment	
Crystal system	Monoclinic	
Space group	P 1 21/c 1	
Unit cell dimensions	a = 15.5693 (9) Å	$\alpha = 90^\circ$
	b = 9.3104 (5) Å	$\beta = 106.804 (2)$
	c = 9.3874 (5) Å	$\gamma = 90$
Volume	1302.66 (12) Å ³	
Z	4	
Density	1.304 g/cm ³	
Absorption	0.284 mm ⁻¹	
F (000)	544	

Table S3: Data collection and structure refinement of 6.

Diffractometer	Bruker D8 Venturo Duo IMS		
Radiation source	IMS microsource, Mo		
Theta range for data collection	2.58 to 26.73°		
Index ranges	-19<=h<=19, -11<=k<=11, -11<=l<=11		
Reflections collected	628000		
Independent reflections	2763 [R(int) = 0.0485]		
Coverage of independent reflections	100.0 %		
Absorption correction	Multi-Scan		
Max. and Min. transmission	0.9880 and 0.9420		
Refinement method	Full-matrix least-squares on F ²		
Refinement program	SHELXL-2014/7 (Sheldrick, 2014)		
Function minimized	$\sum w (F_o^2 - F_c^2)^2$		
Data/ restraints / parameters	2763 / 0 / 162		
Goodness-of-fit on F²	1.203		
Δ / σ_{\max}	0.001		
Final R indices	2599 data; >2 σ	R1 = 0.0413,	wR2 = 0.0835
	All data	R1 = 0.0446	wR2 = 0.0848
Weighting scheme	$w = 1/[\sigma^2/(F_o^2) + (0.0201P)^2 + 1.3271P]$		
	Where $P = (F_o^2 + 2F_c^2)/3$		
Largest diff. peak and hole	0.382 and -0.226 eÅ ⁻³		
R.M.S. deviation from mean	0.050 eÅ ⁻³		

Cyclic Voltammometry

The CV measurements were performed with the corresponding photosubstrates **2**, product **1a** and **7** (1 mM) in 0.1 M of $[N(n\text{-Bu})_4]PF_6$ in MeCN. Glassy carbon electrode was used as working and counter electrode, Ag/AgNO₃ (0.01 M in MeCN) as reference electrode, and a scan rate of 100 mV/s. The value of the potential at the inflexion point of each oxidation curve was selected as the oxidation potential of the given substrate or product. 300 mV were added to this value to give the corresponding oxidation potentials (E_{ox}) vs. the Saturated Calomel Electrode (SCE).²³

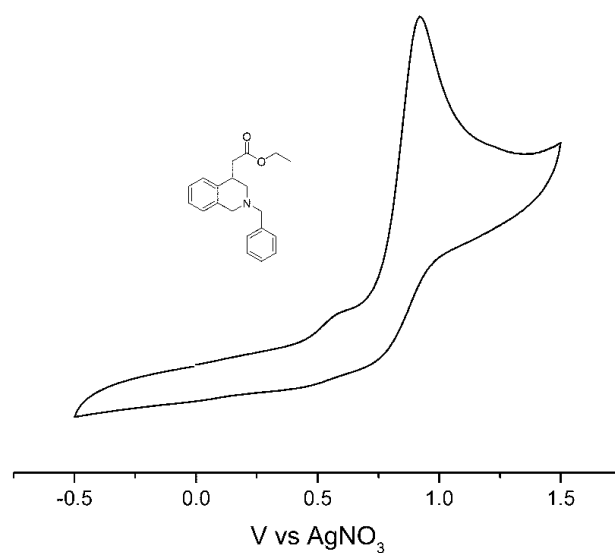


Figure S2: Cyclic voltammogram of **1a**.

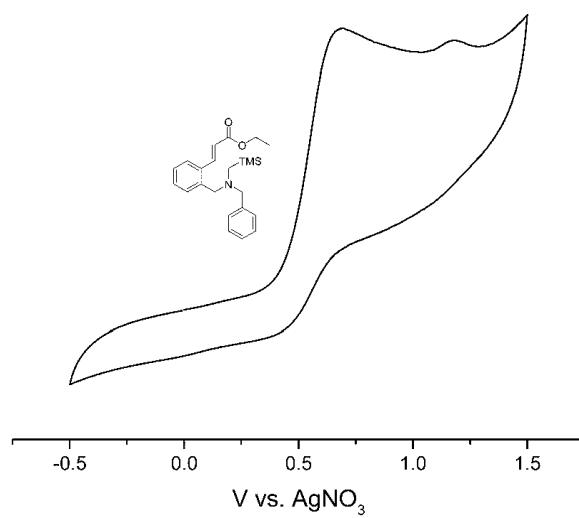


Figure S3: Cyclic voltammogram of **2a**.

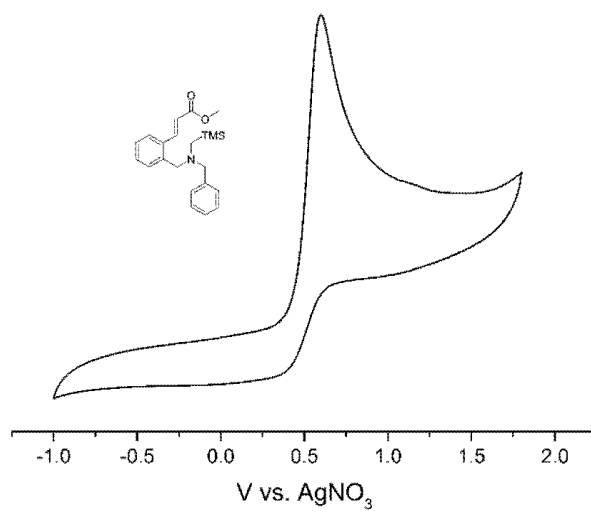


Figure S4: Cyclic voltammogram of **2b**.

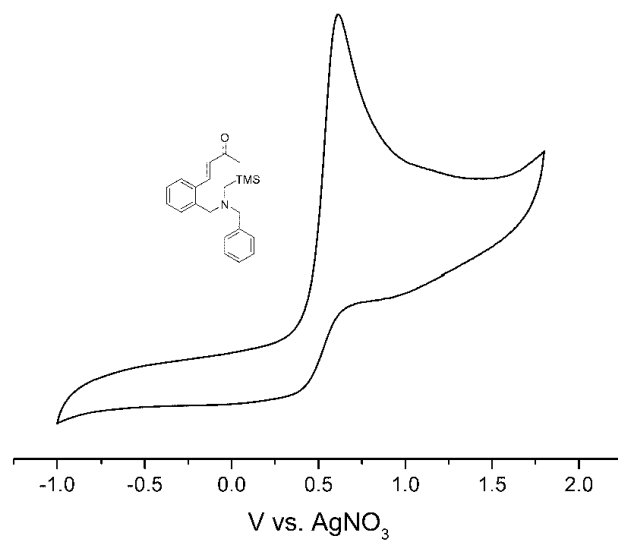


Figure S5: Cyclic voltammogram of 2c.

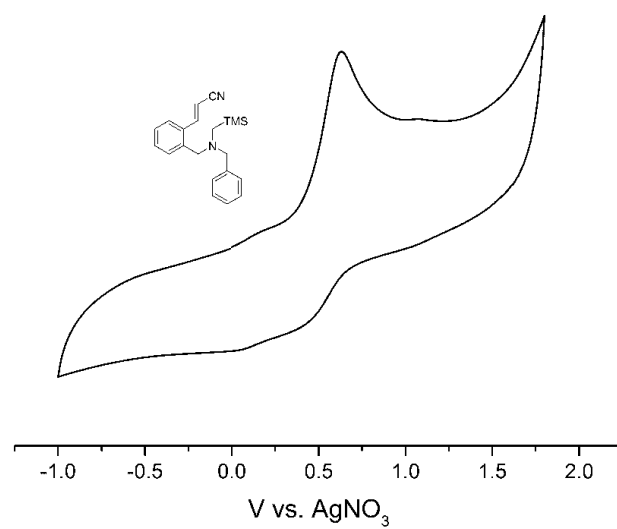


Figure S6: Cyclic voltammogram of 2d.

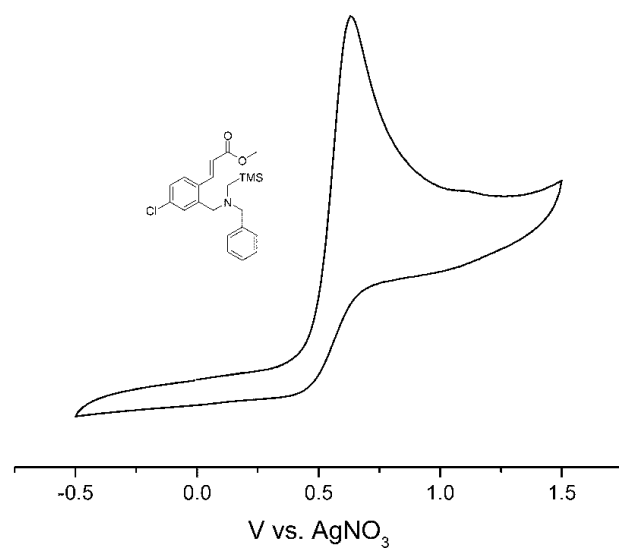


Figure S7: Cyclic voltammogram of 2e.

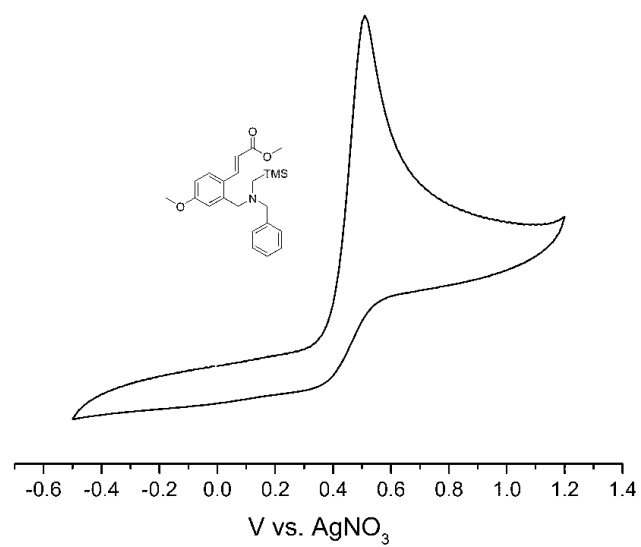


Figure S8: Cyclic voltammogram of 2f.

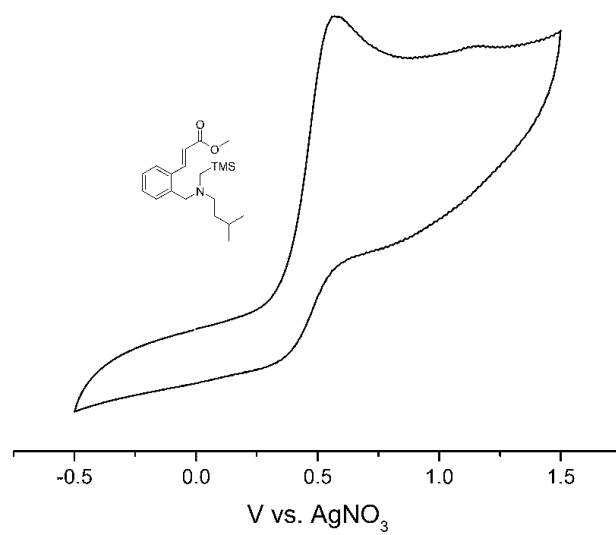


Figure S9: Cyclic voltammogram of 2g.

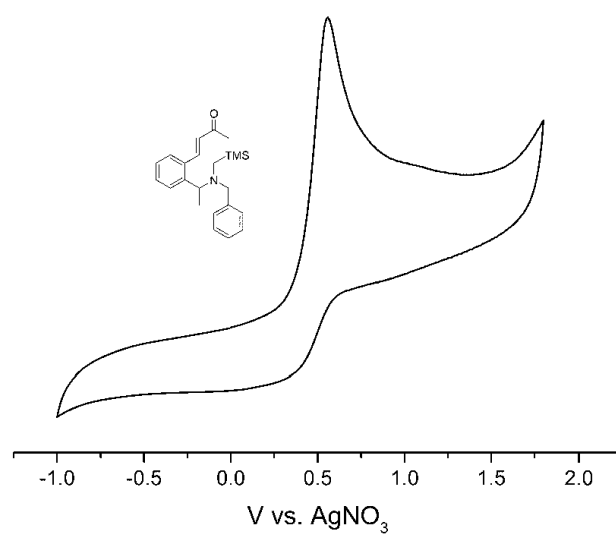


Figure S10: Cyclic voltammogram of 2h.

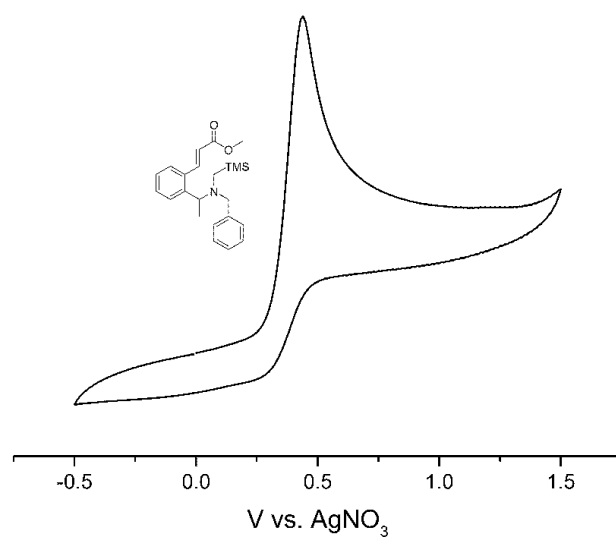


Figure S11: Cyclic voltammogram of 2i.

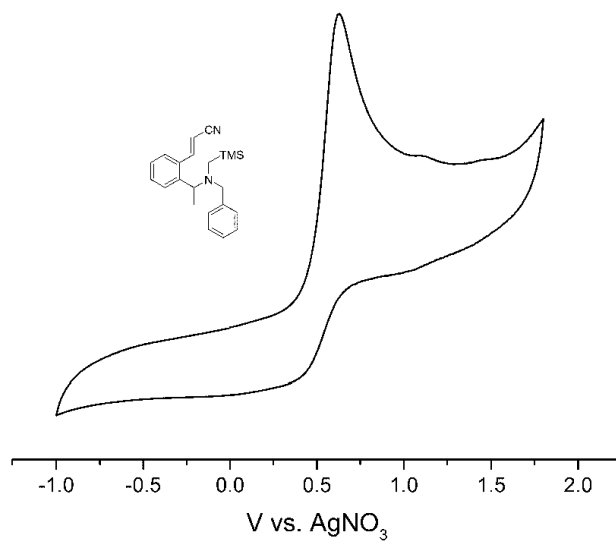


Figure S12: Cyclic voltammogram of 2j.

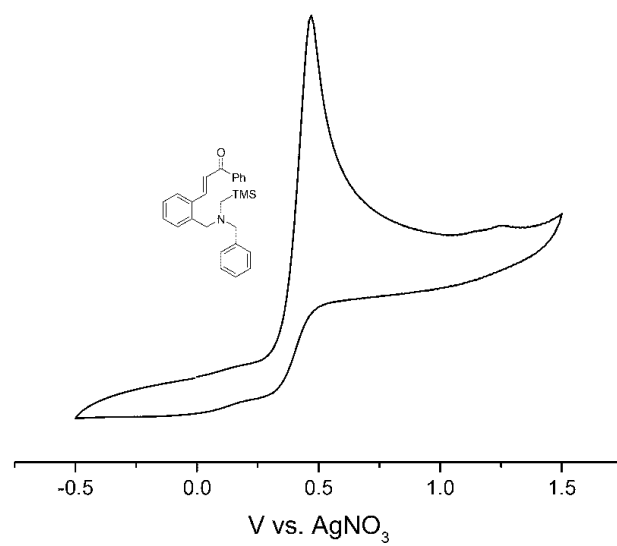


Figure S13: Cyclic voltammogram of **2k**.

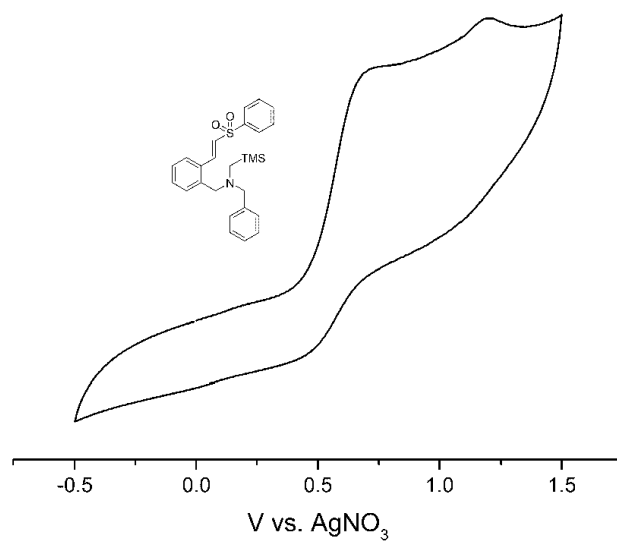


Figure S14: Cyclic voltammogram of **2l**.

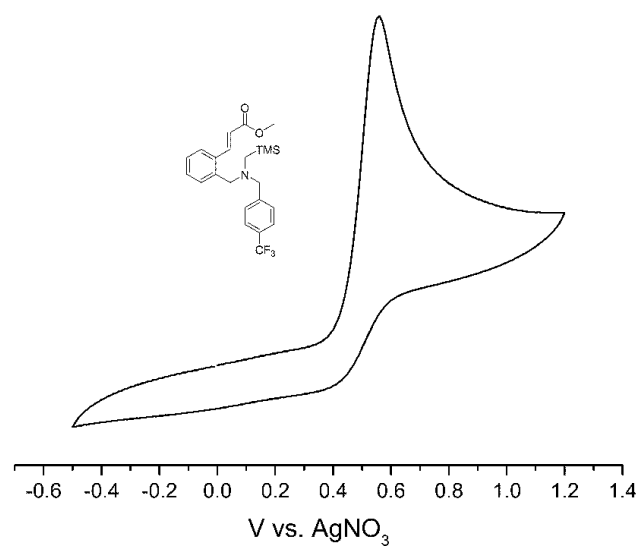


Figure S15: Cyclic voltammogram of 2m.

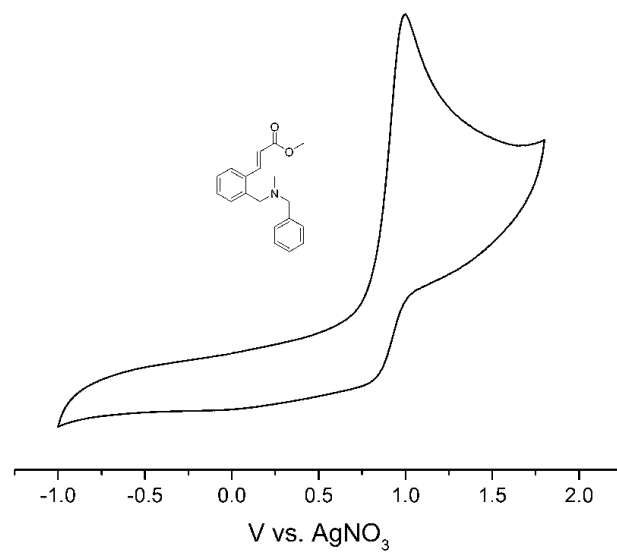
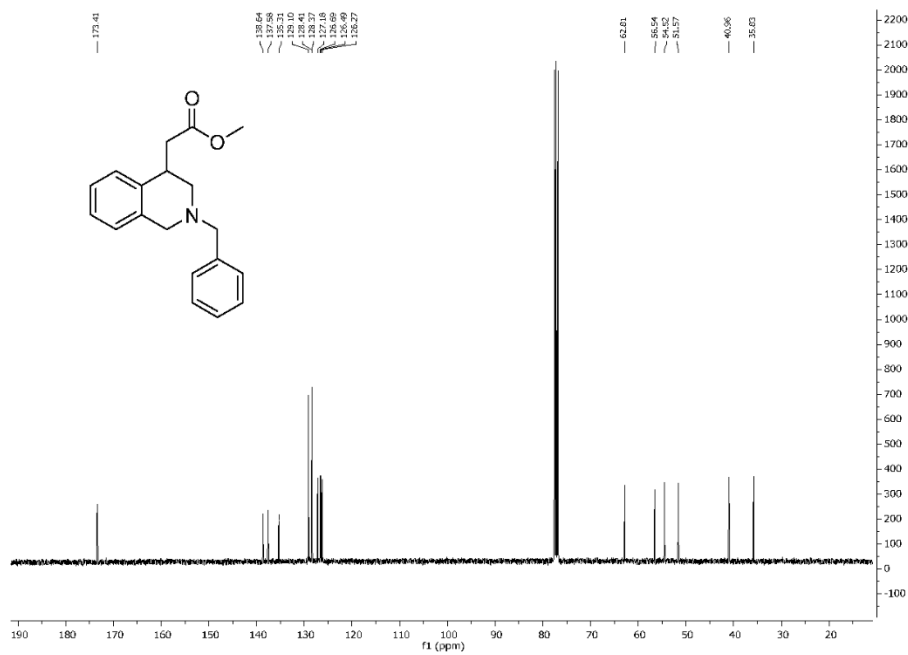
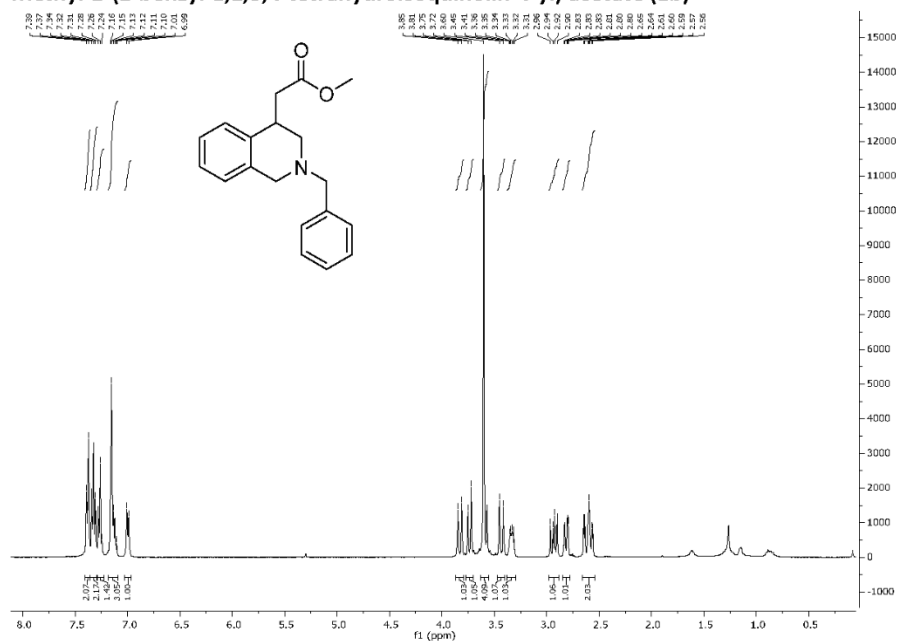
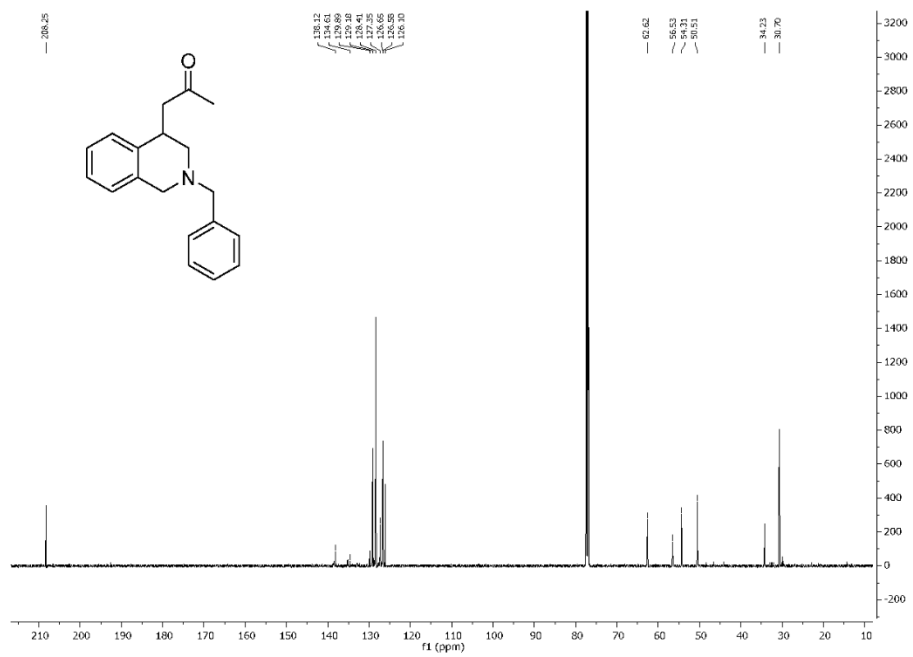
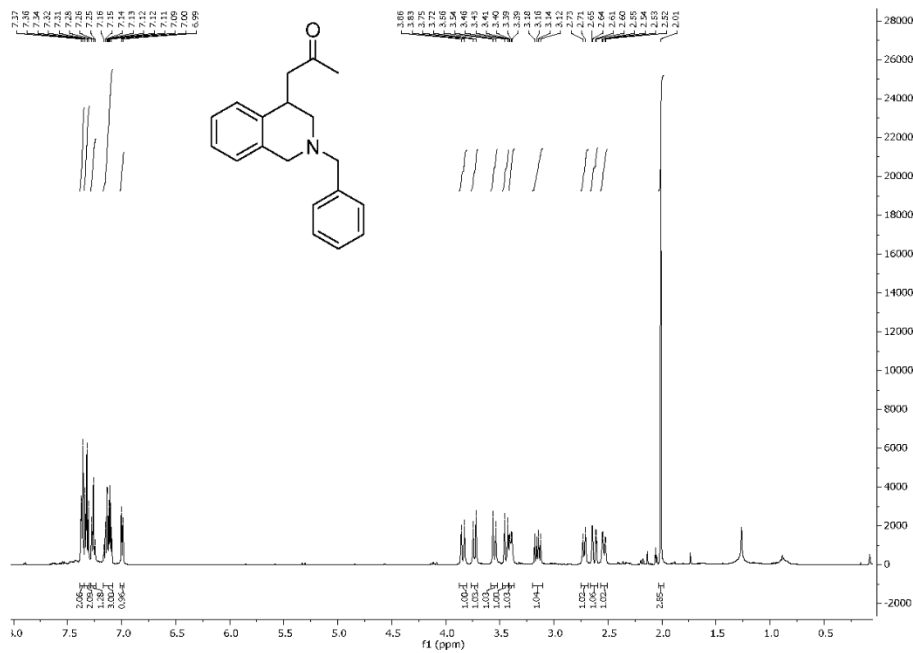


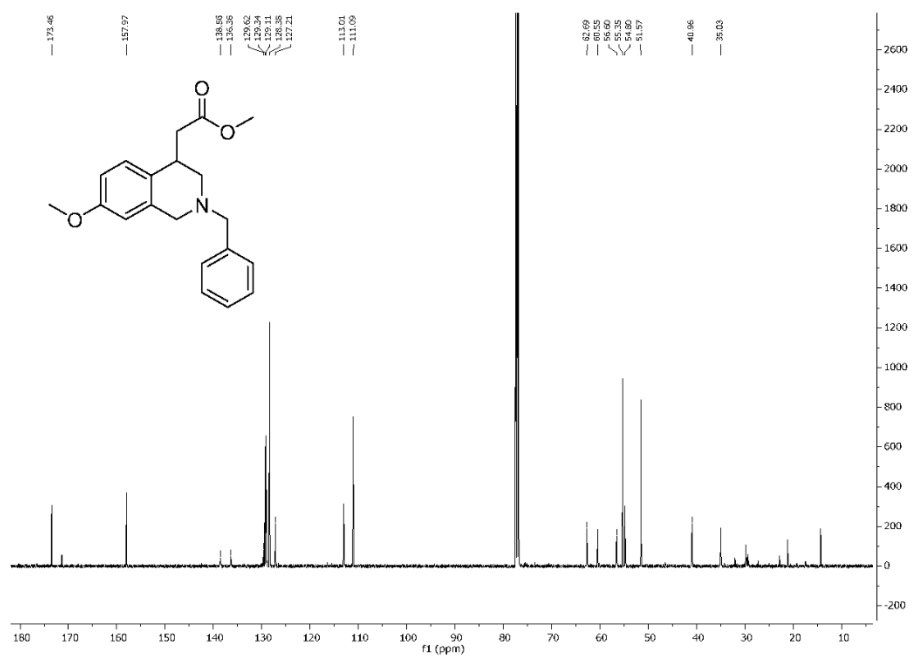
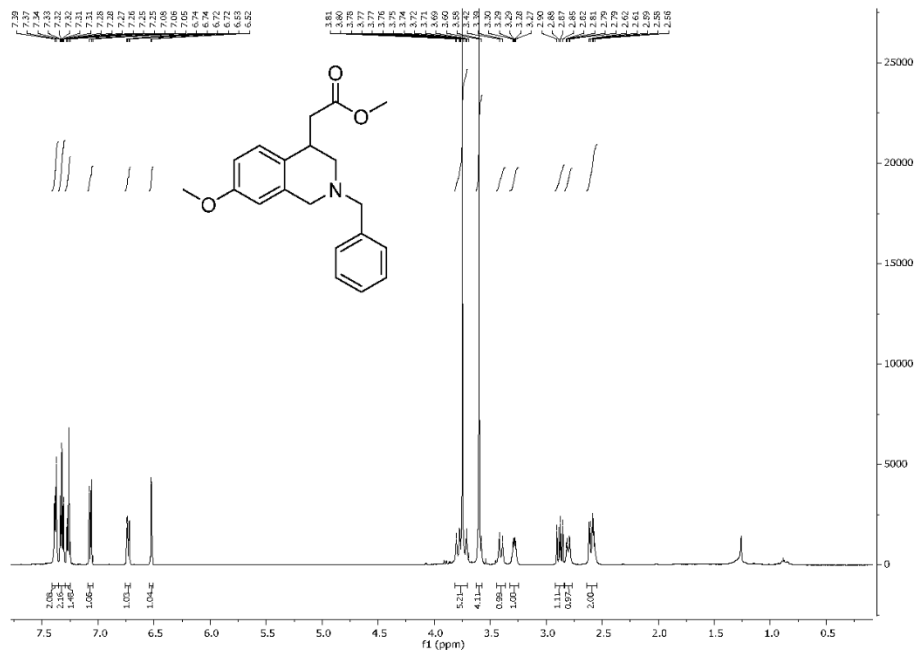
Figure S16: Cyclic voltammogram of 7.

Methyl-2-(2-benzyl-1,2,3,4-tetrahydroisoquinolin-4-yl) acetate (1b)

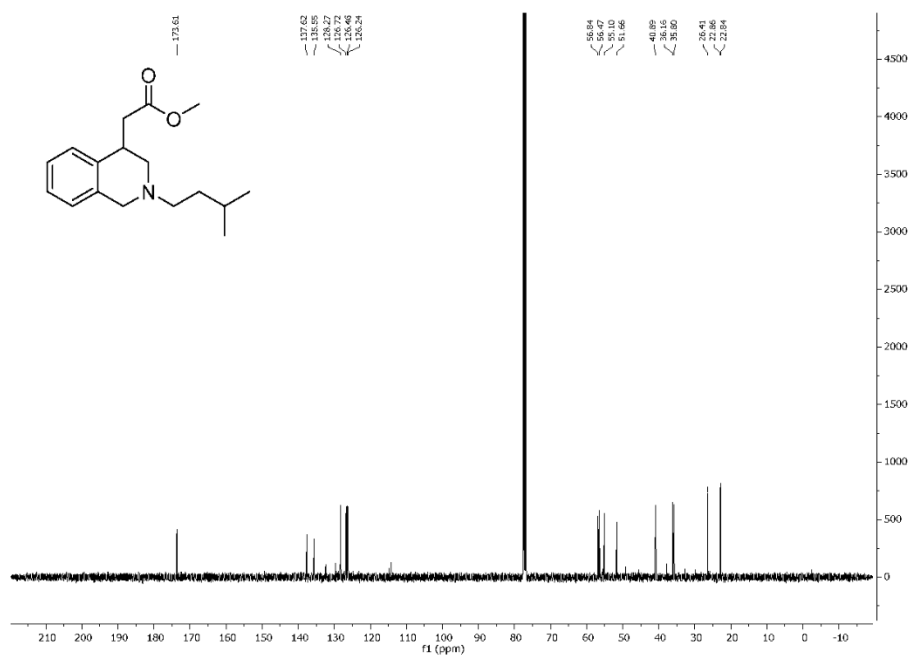
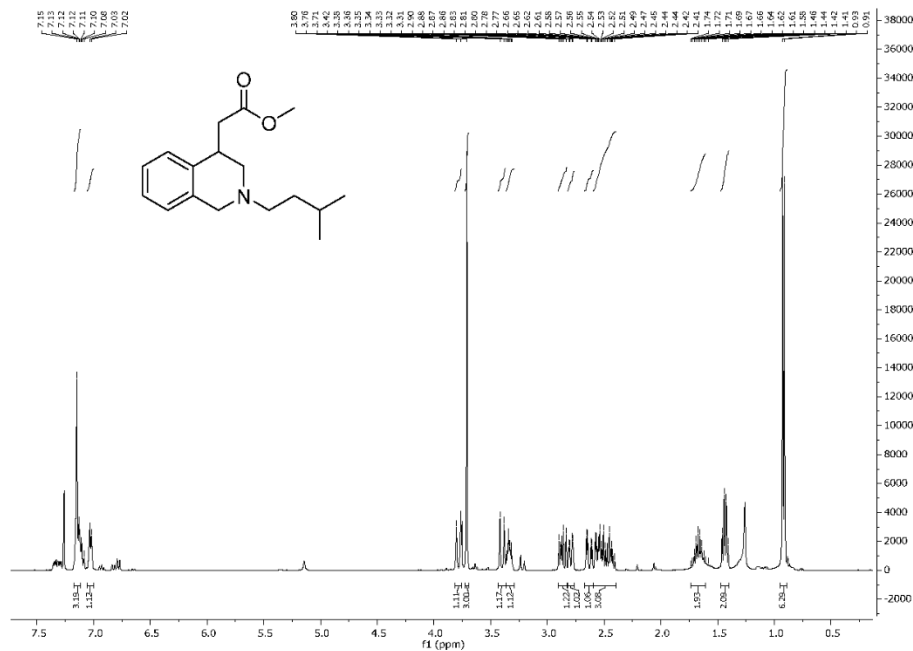
1-(2-Benzyl-1,2,3,4-tetrahydroisoquinolin-4-yl)propan-2-one (1c)



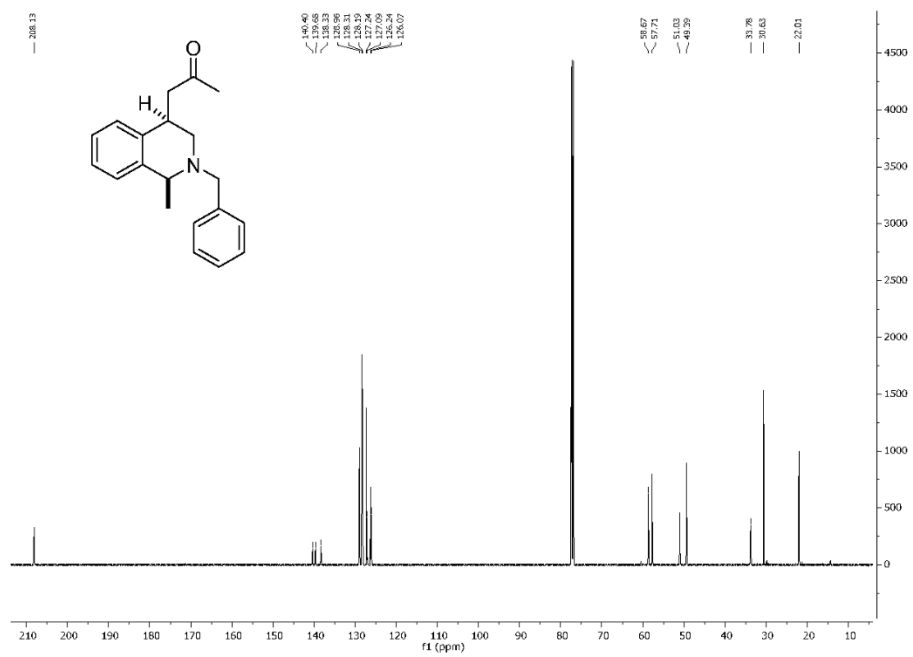
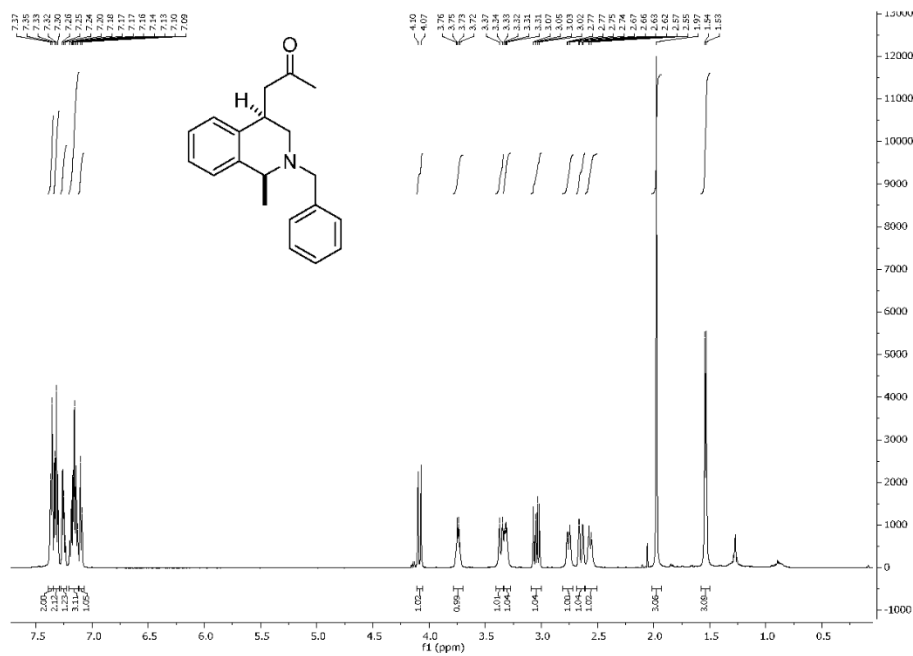
Methyl 2-(2-benzyl-7-methoxy-1,2,3,4-tetrahydroisoquinolin-4-yl)acetate(1f)



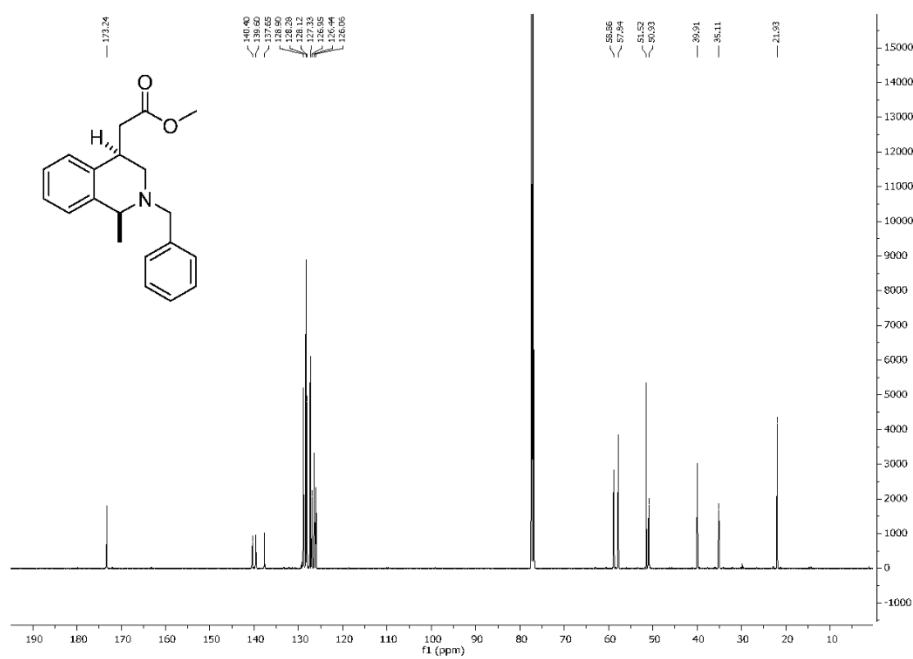
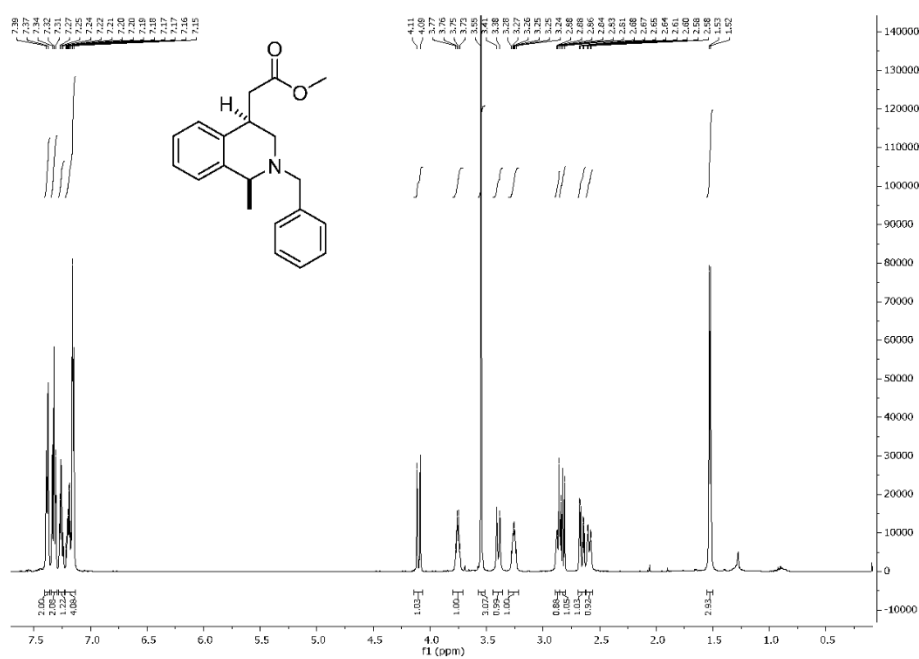
Methyl 2-(2-isopentyl-1,2,3,4-tetrahydroisoquinolin-4-yl)acetate(1g)



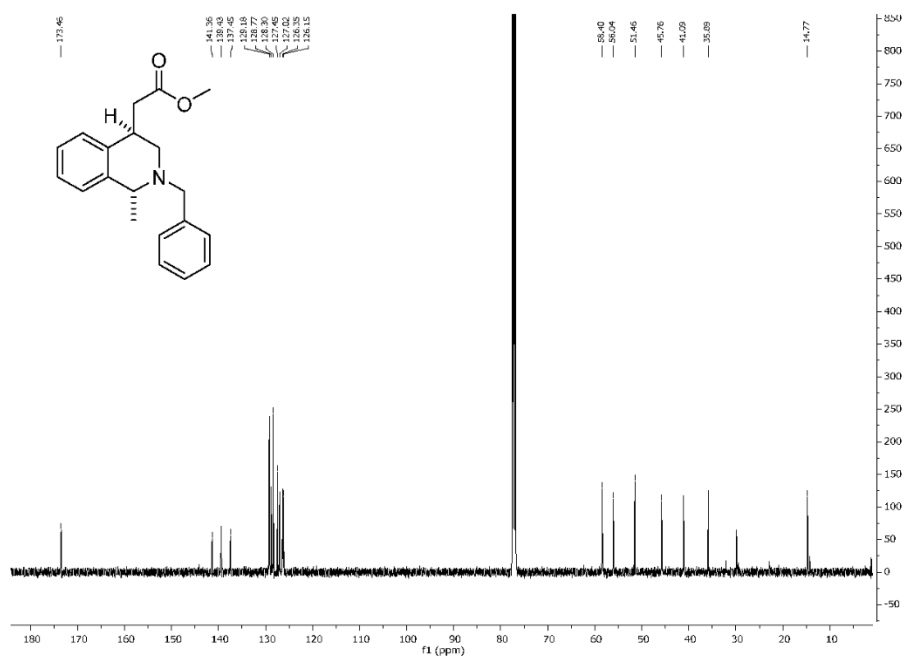
1-(2-Benzyl-1-methyl-1,2,3,4-tetrahydroisoquinolin-4-yl)propan-2-one (major) (1h)



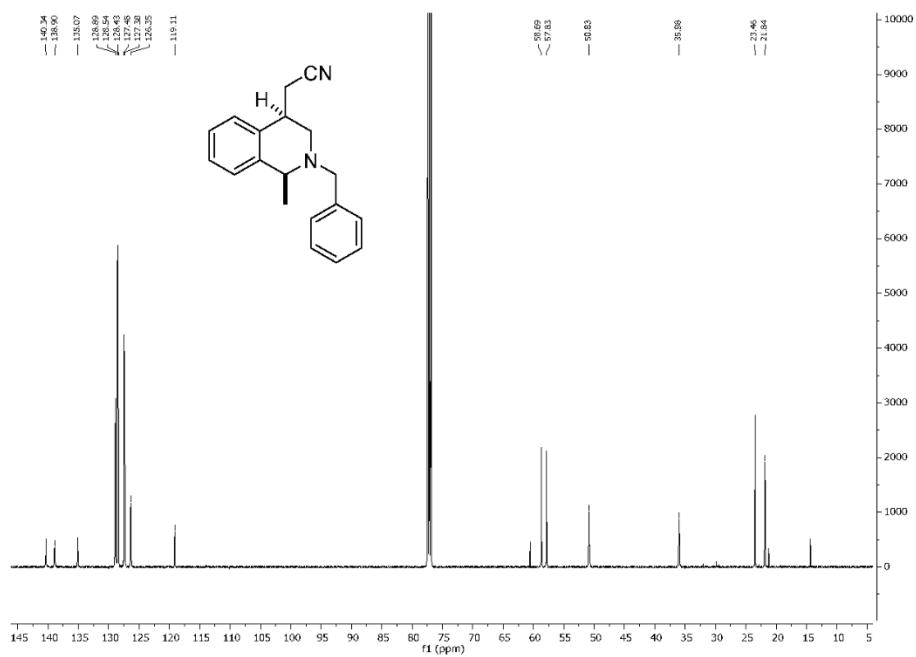
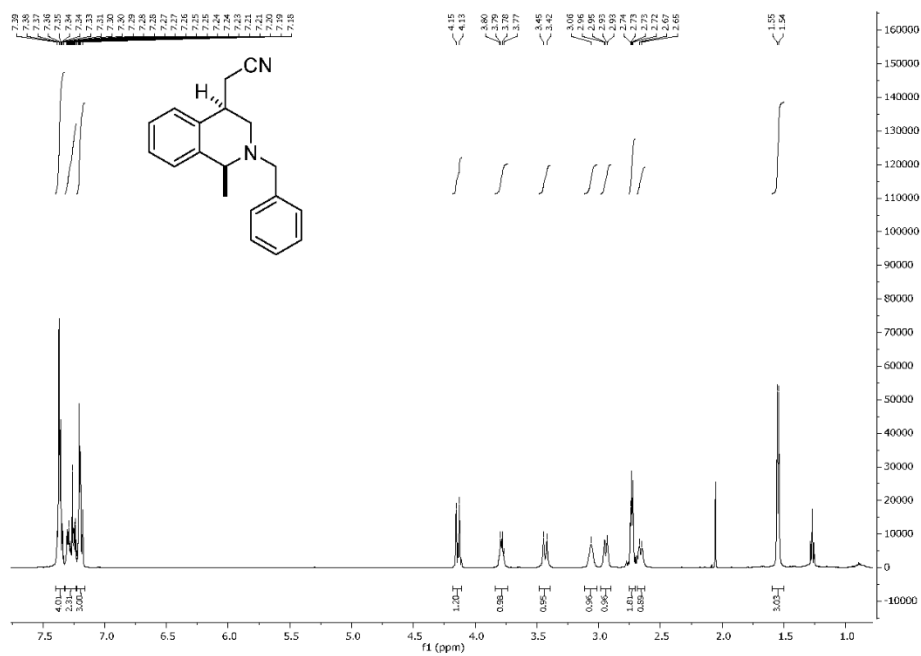
Methyl (Z)-2-(2-benzyl-1-methyl-2,3-dihydroisoquinolin-4(1H)-ylidene)acetate (major)(1i)



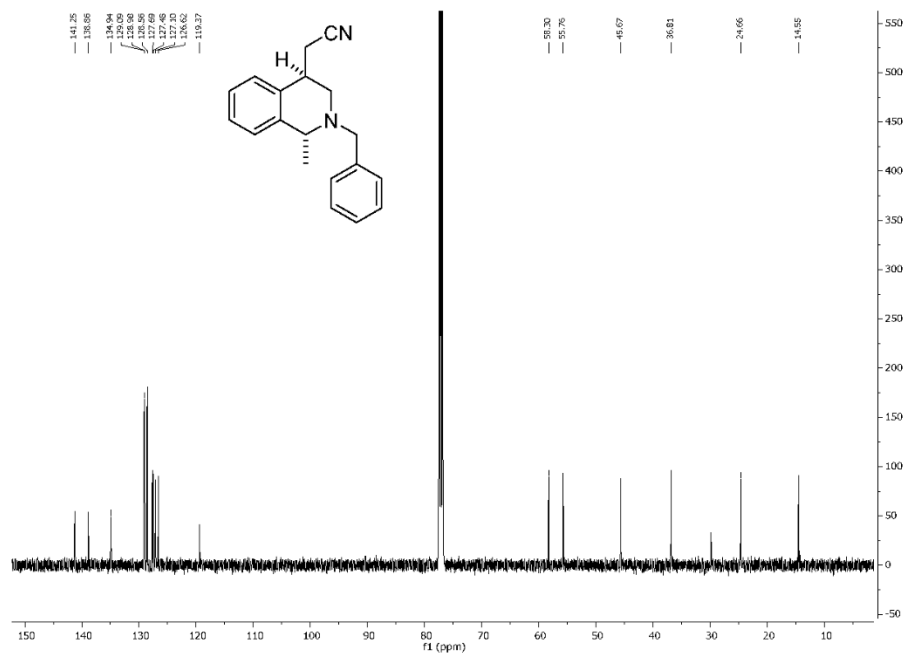
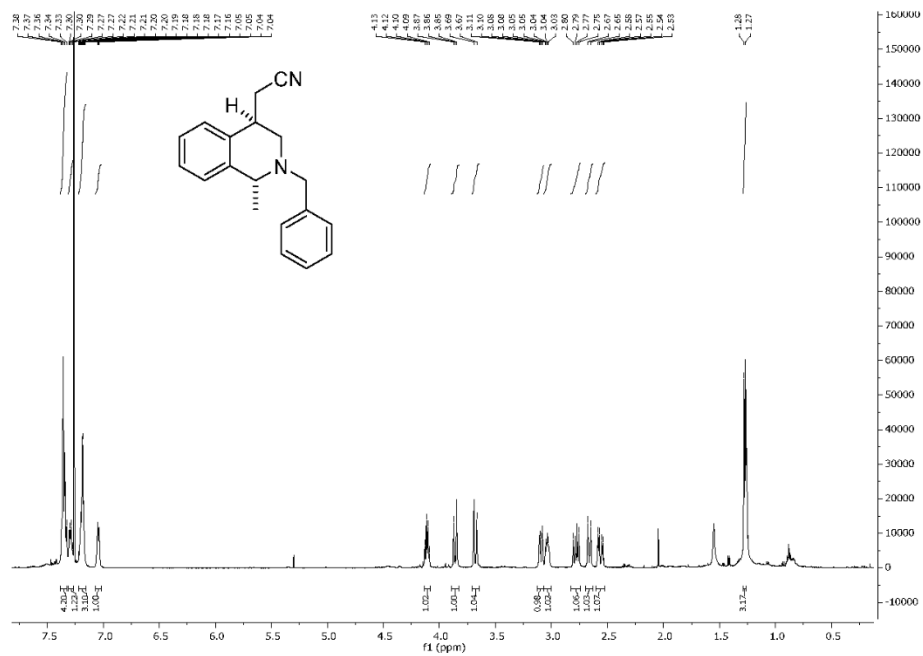
Methyl (Z)-2-(2-benzyl-1-methyl-2,3-dihydroisoquinolin-4(1H)-ylidene)acetate (minor)(1i)



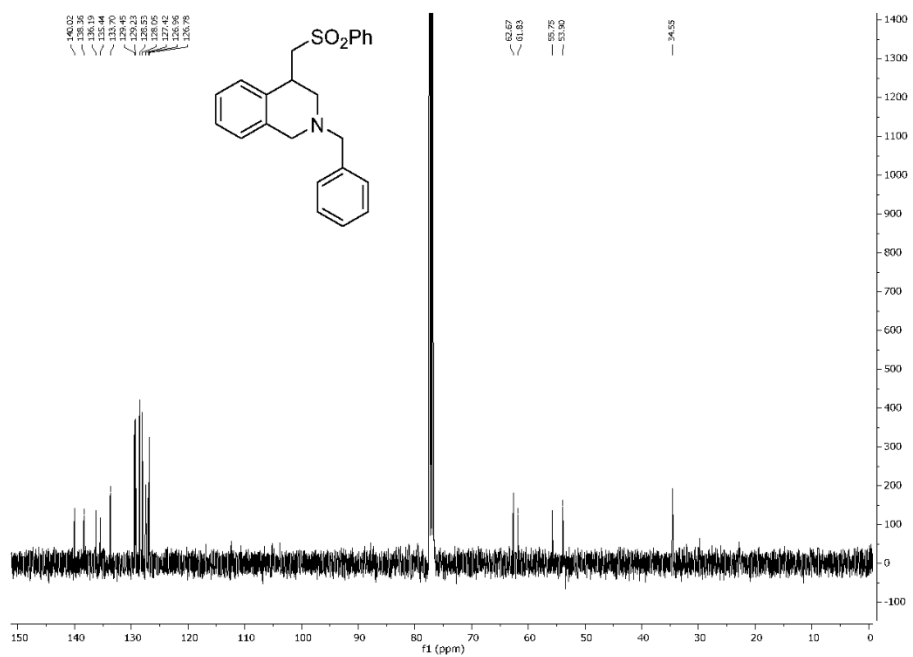
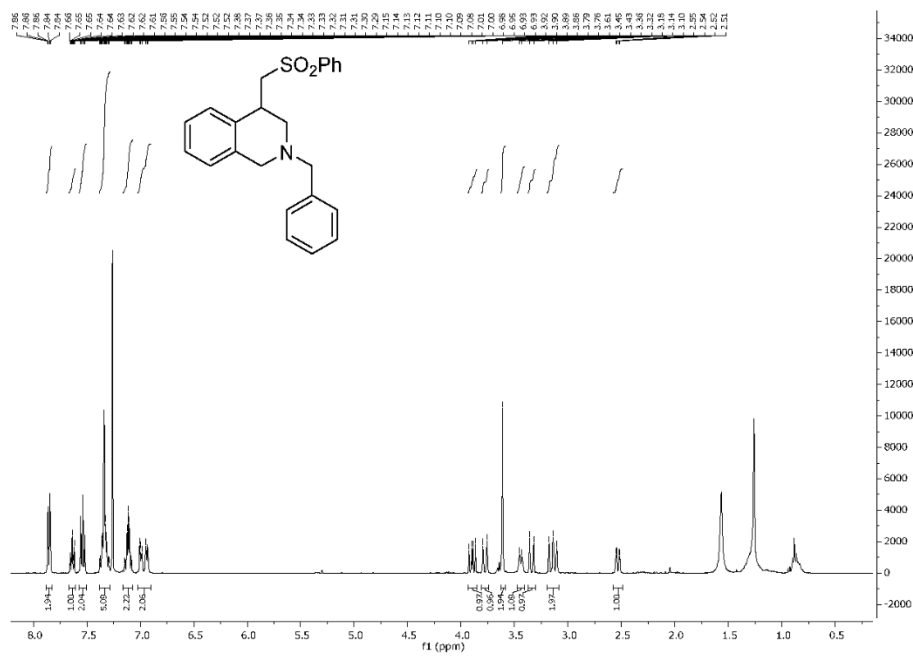
2-(2-Benzyl-1-methyl-1,2,3,4-tetrahydroisoquinolin-4-yl)-acetonitrile (major)(1j)

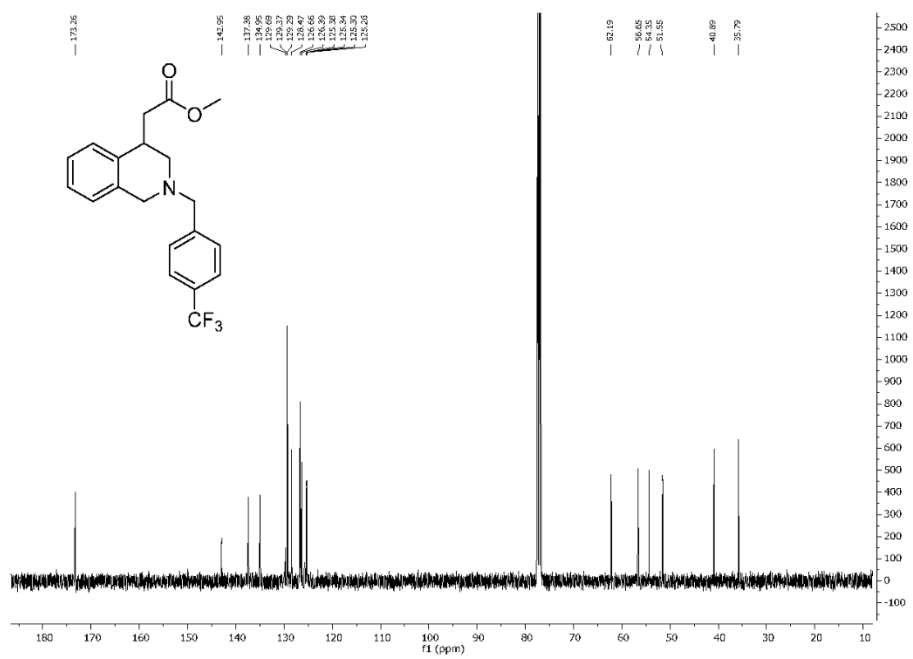
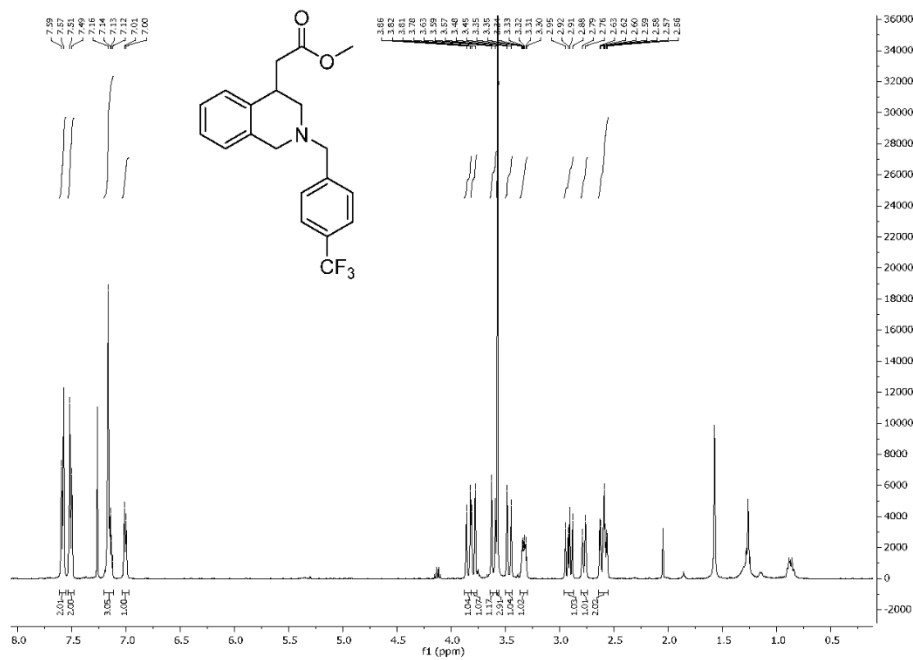


2-(2-Benzyl-1-methyl-1,2,3,4-tetrahydroisoquinolin-4-yl)-acetonitrile (minor) (1j)

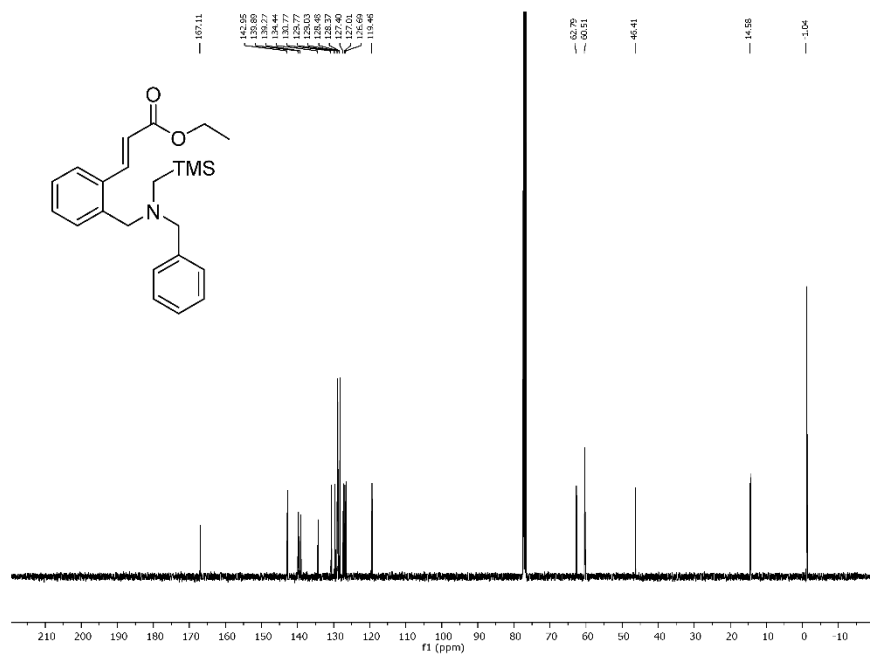
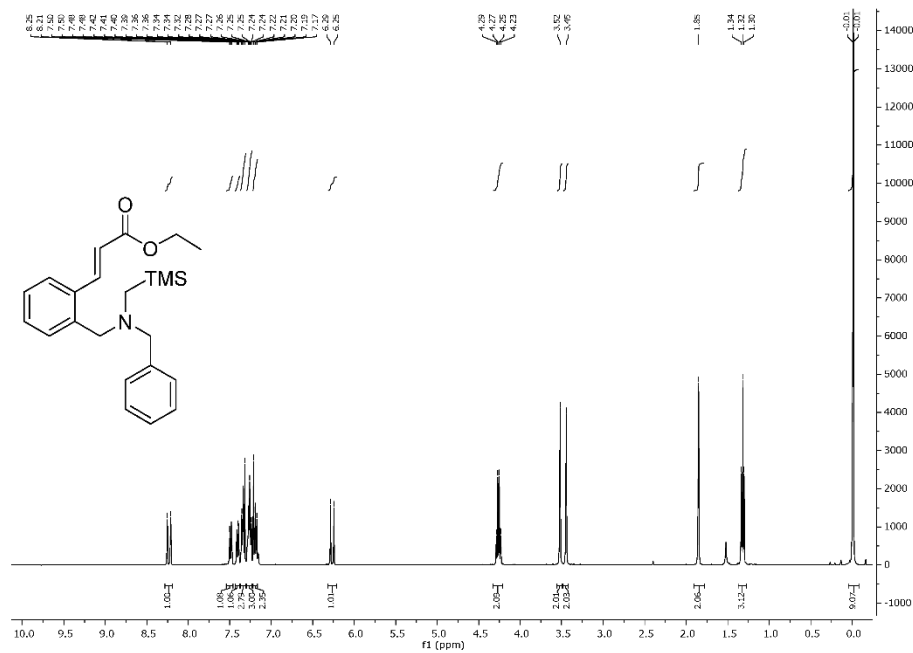


2-Benzyl-4-((phenylsulfonyl)methyl)-1,2,3,4-tetrahydroisoquinoline (11)

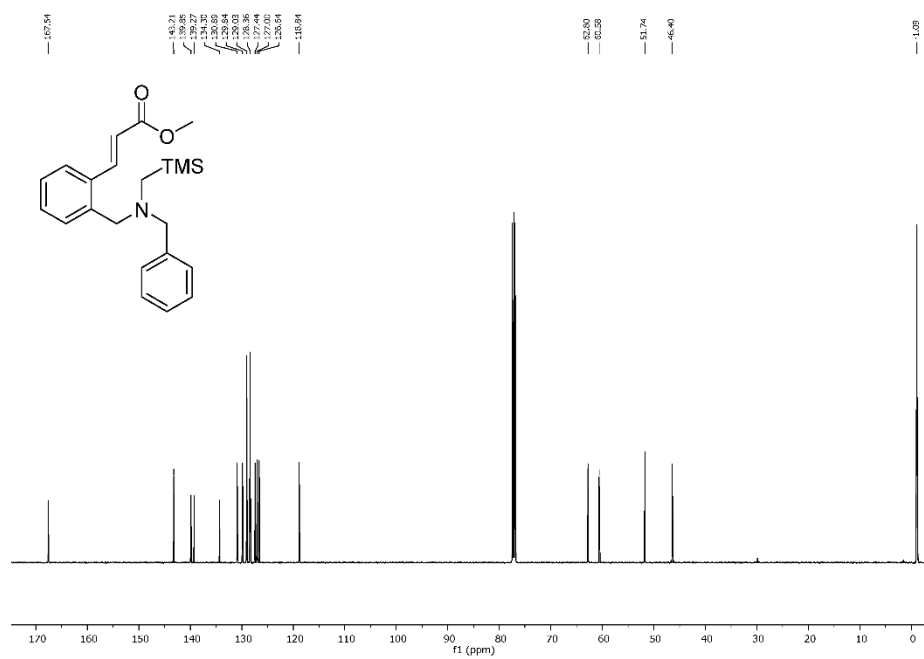
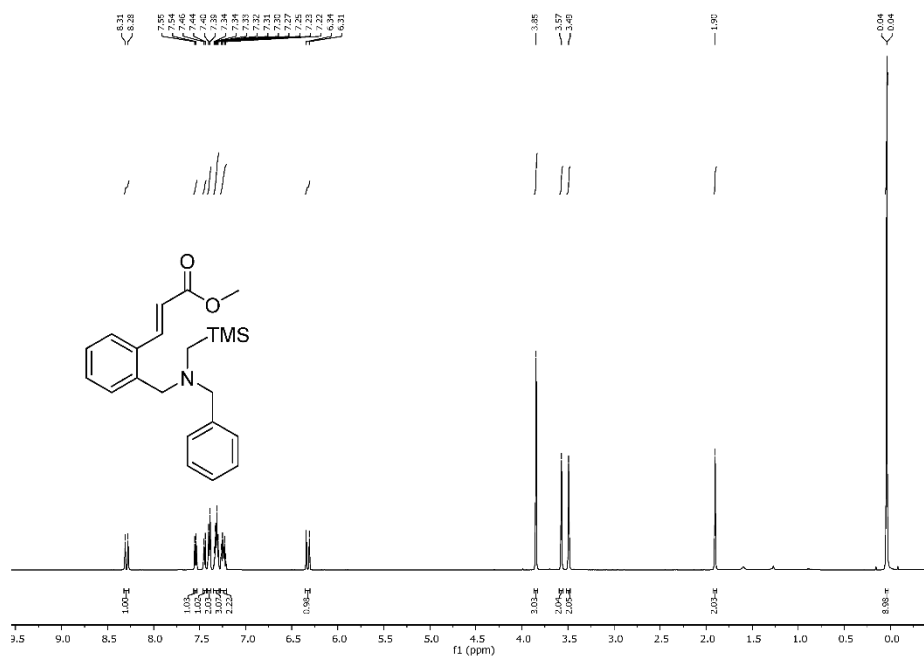


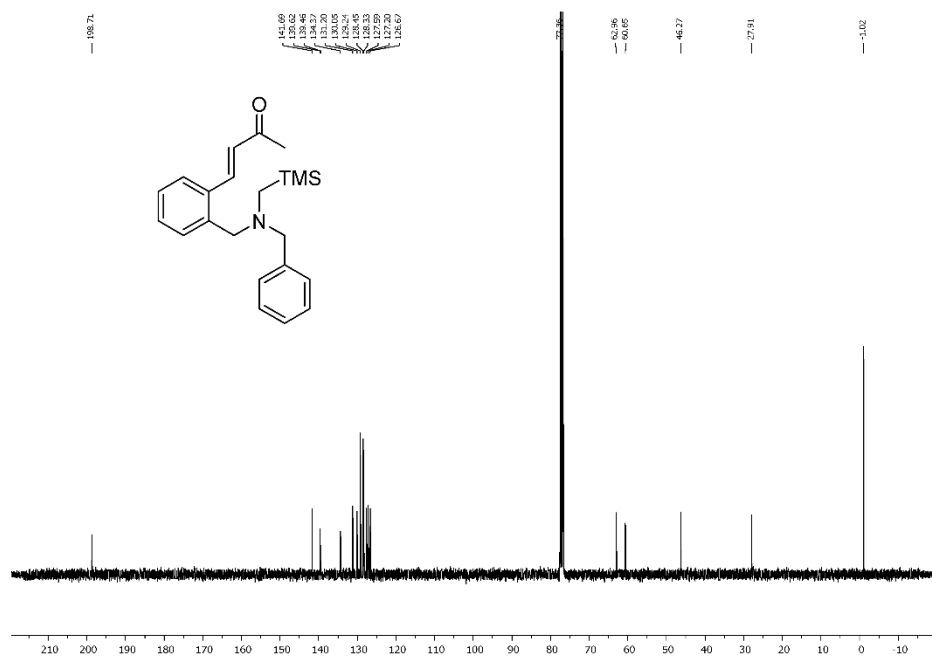
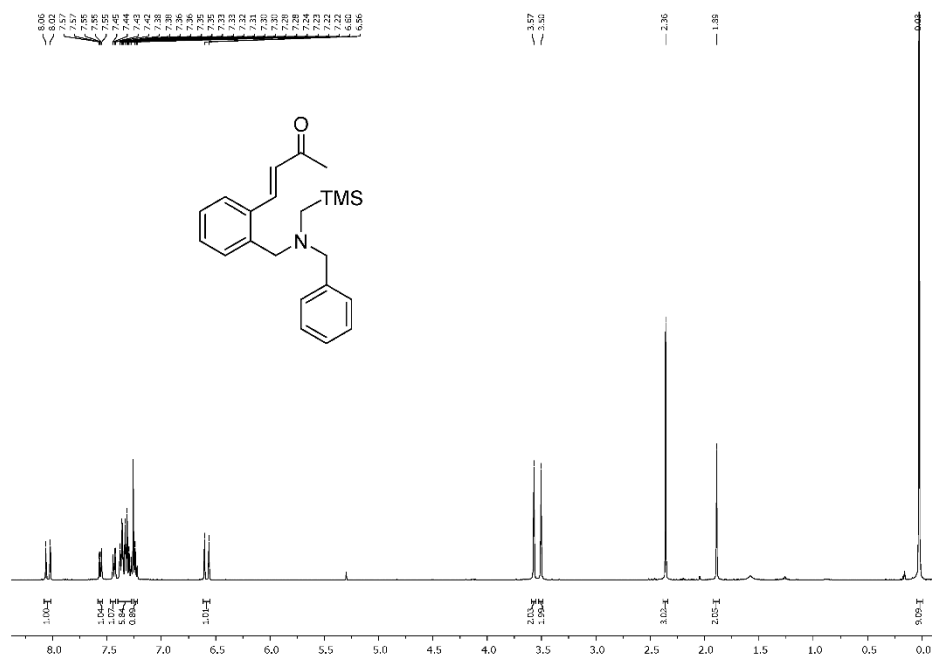
Methyl 2-(2-(4-(trifluoromethyl)benzyl)-1,2,3,4-tetrahydroisoquinolin-4-yl)acetate (1m)

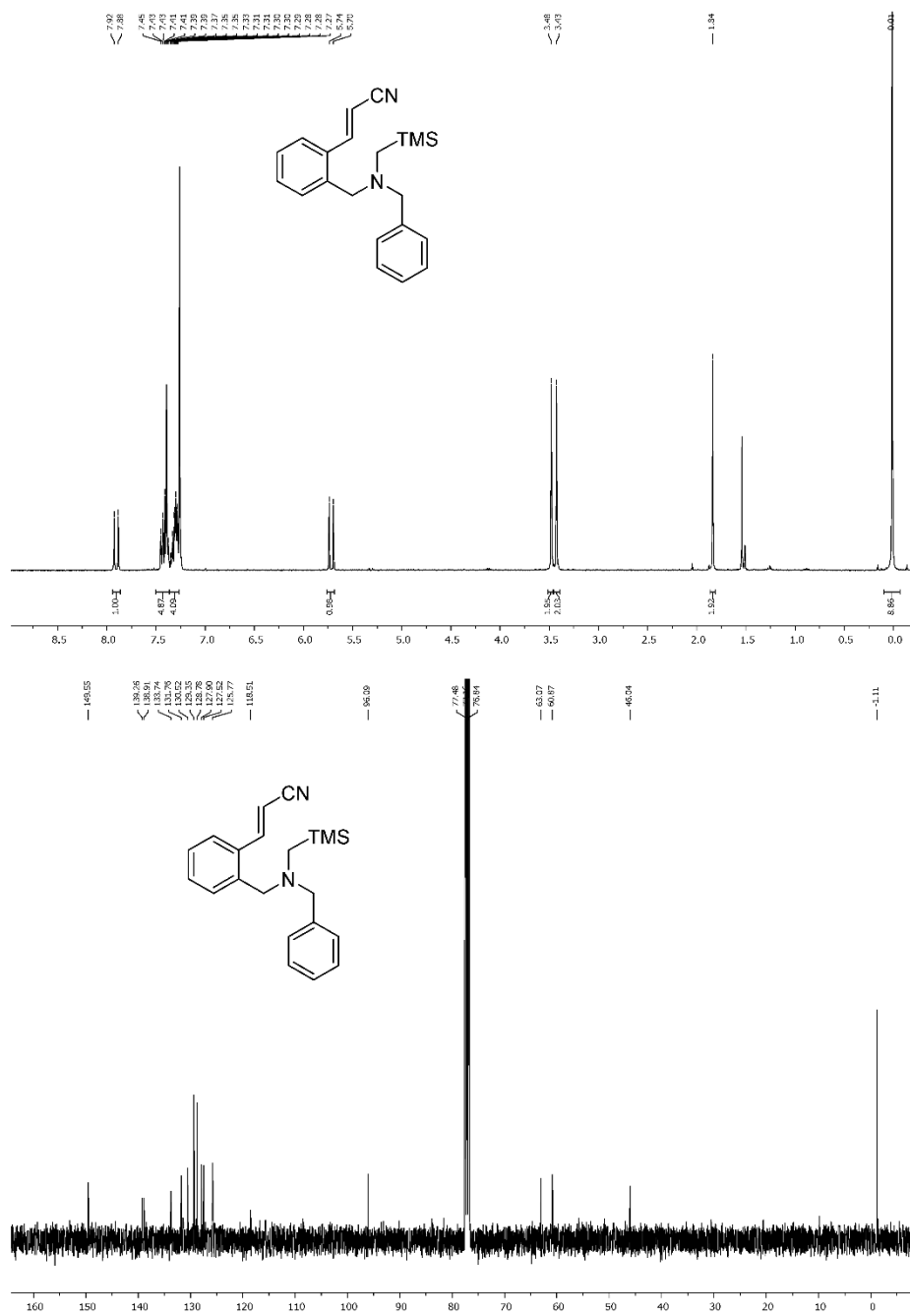
Ethyl-(E)-3-(2-((benzyl(trimethylsilyl)-methyl)-amino)-methyl)-phenyl)acrylate (2a)



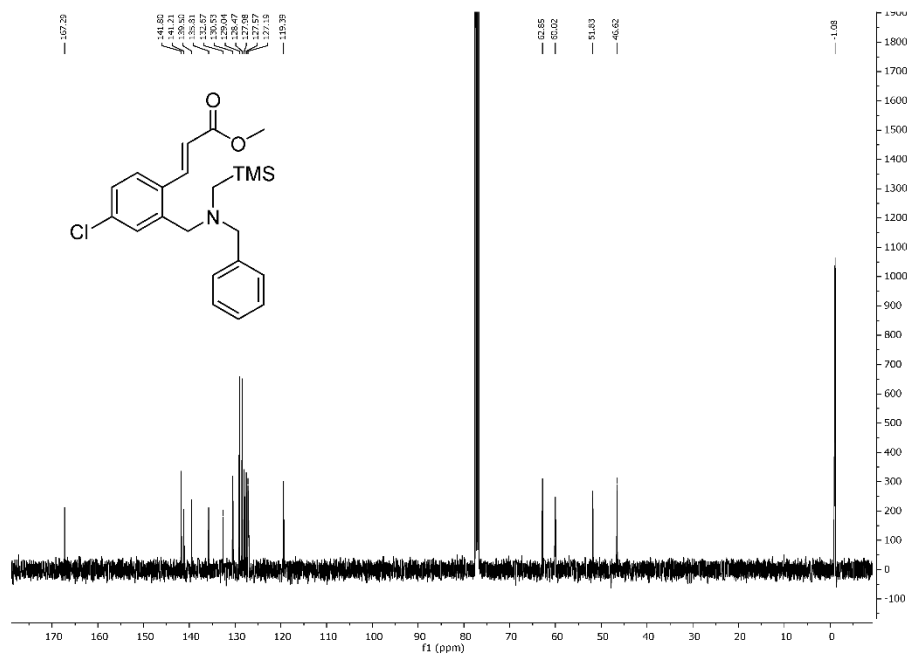
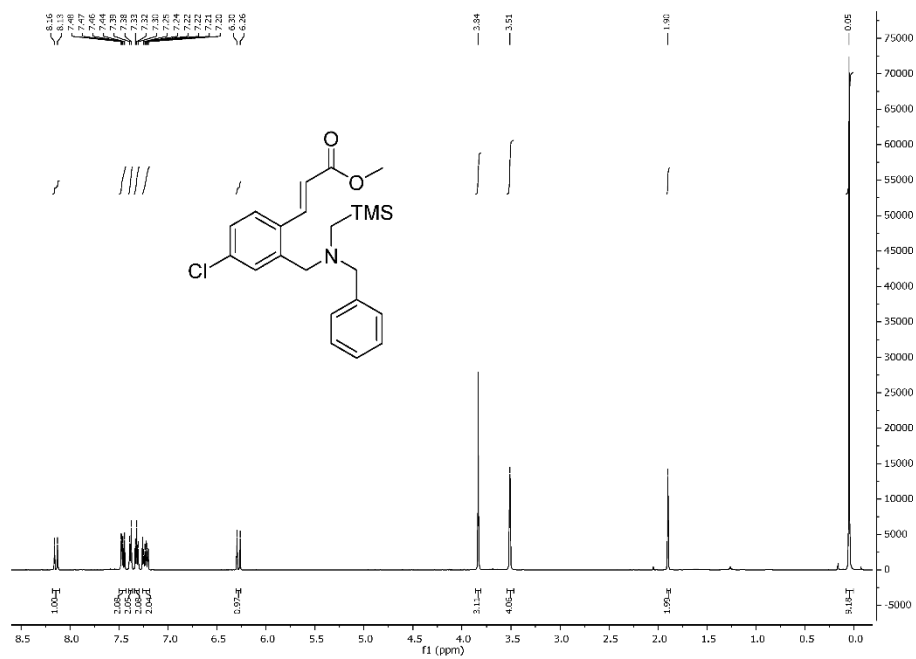
Methyl (E)-3-(2-((benzyl(trimethylsilyl)methyl)amino)methyl)phenyl)acrylate (2b)



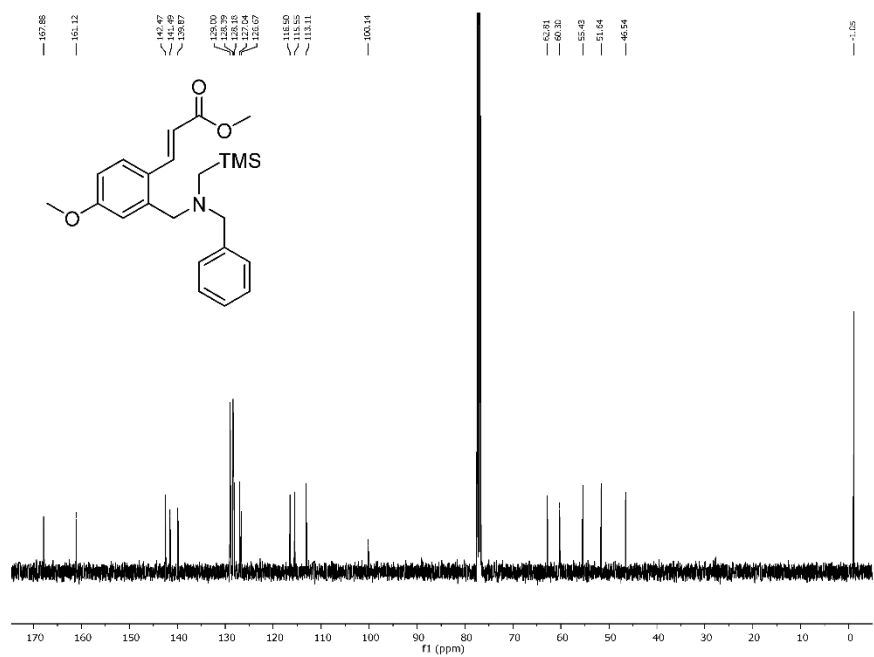
(E)-4-(2-((Benzyl(trimethylsilyl)methyl)amino)methyl)phenyl)but-3-en-2-one (2c)

(E)-3-(2-((Benzyl(trimethylsilyl)methyl)amino)methyl)phenyl)acrylonitrile (2d)

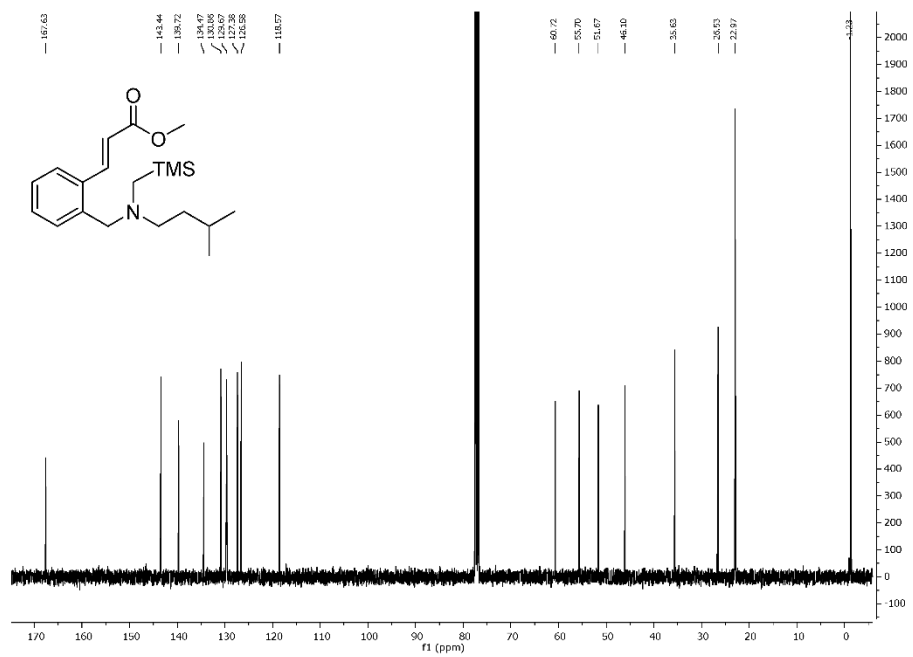
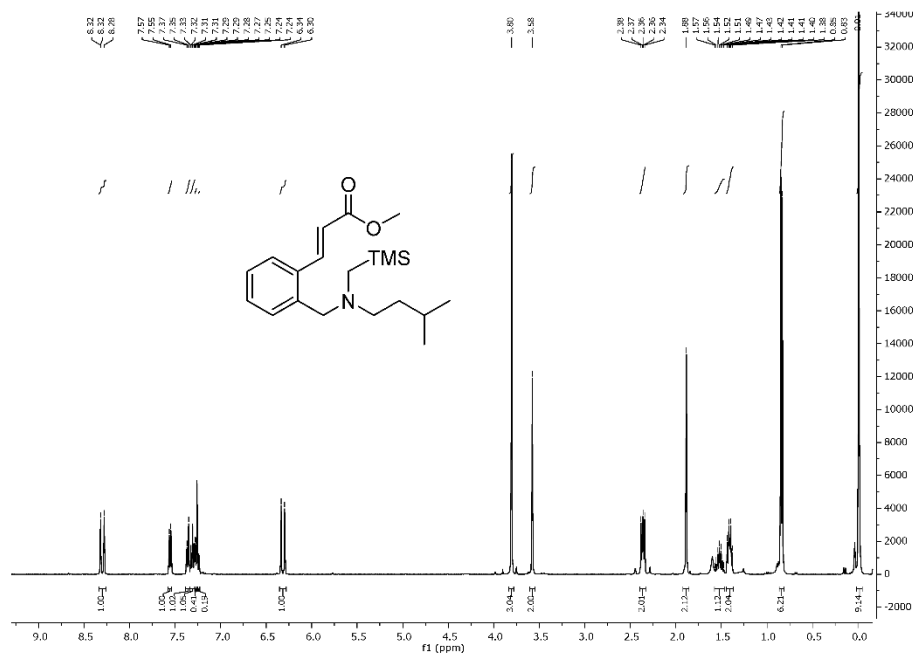
Methyl-(E)-3-(2-((benzyl(trimethylsilyl)amino)methyl)-4-chlorophenyl)acrylate (2e)

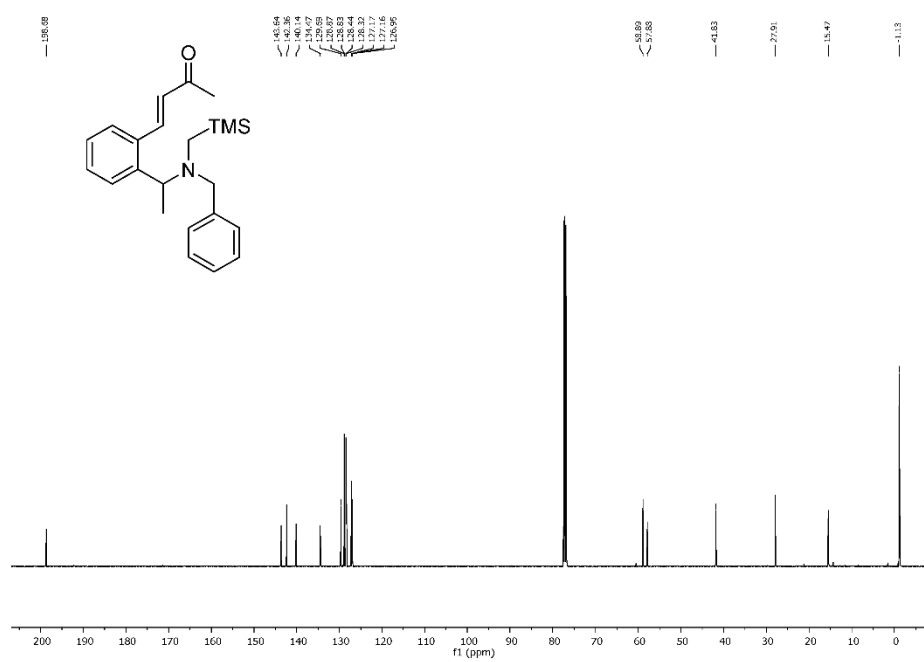
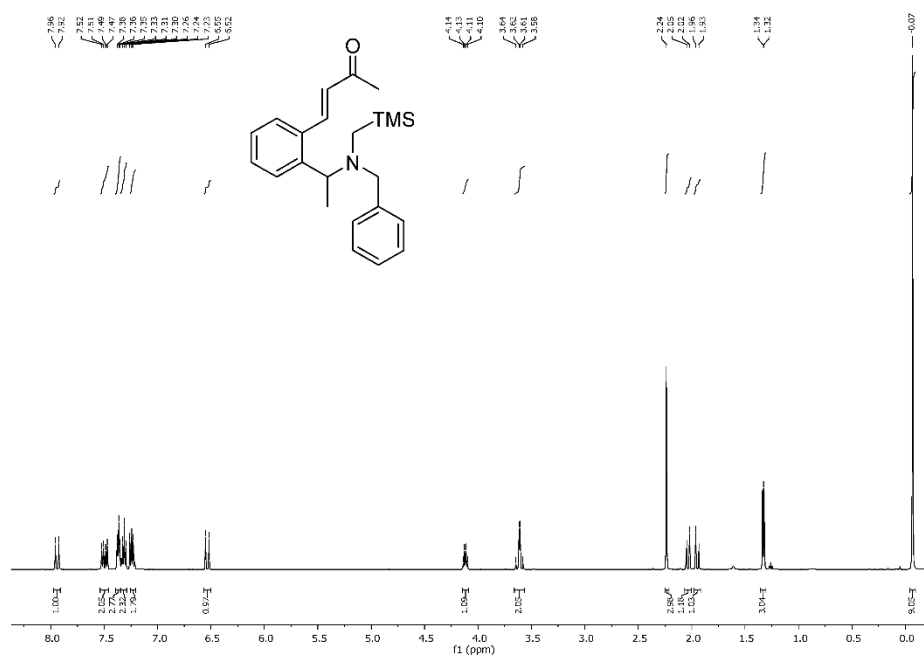


**Methyl-(E)-3-(2-((benzyl((trimethylsilyl)methyl)amino)methyl)-4-methoxyphenyl)acrylate
(2f)**

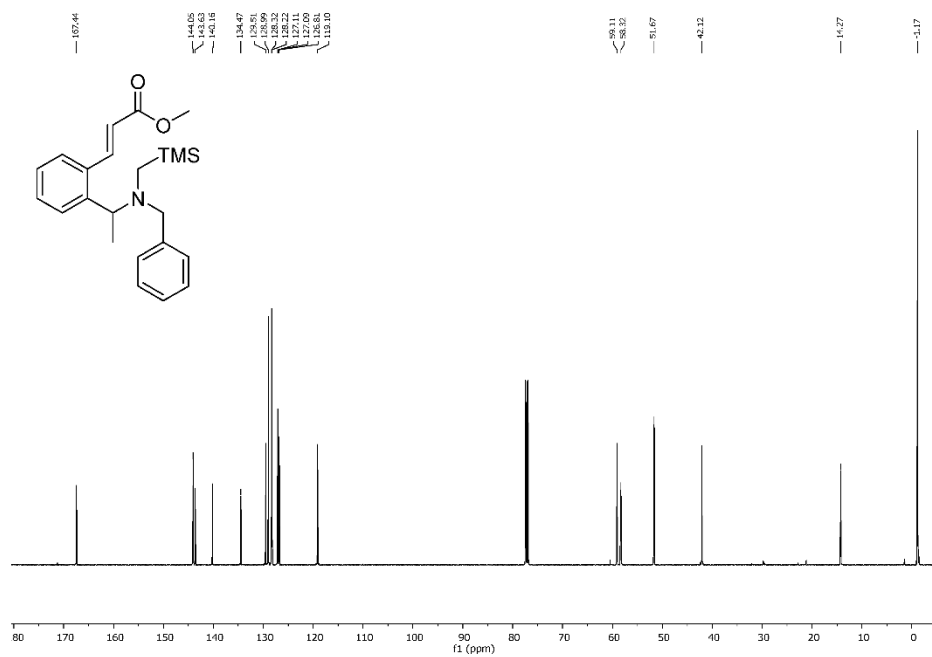
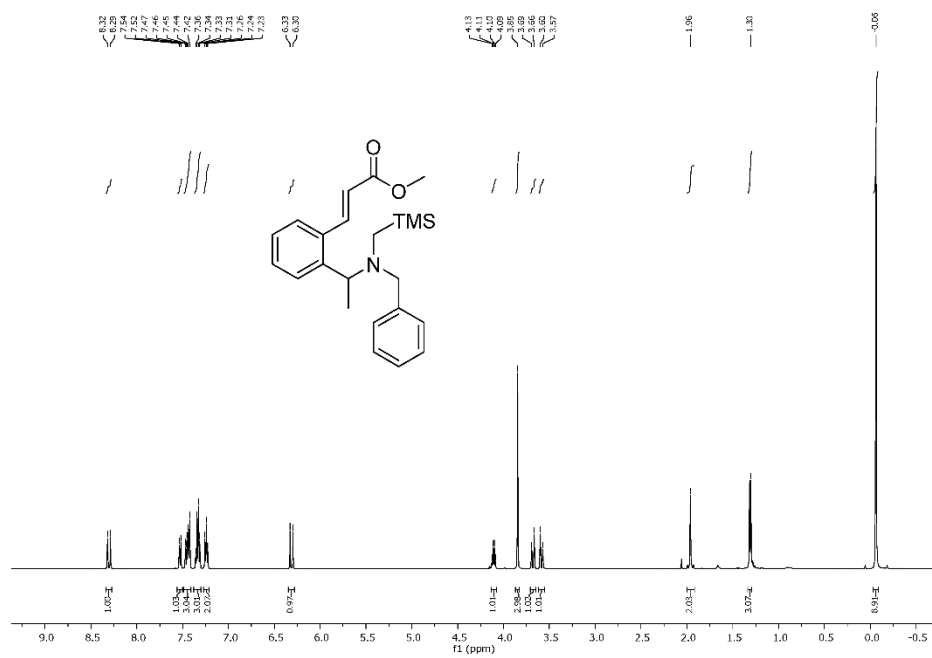


Methyl (E)-3-(2-((isopentyl(trimethylsilyl)methyl)amino)methyl)phenyl)acrylate (2g)

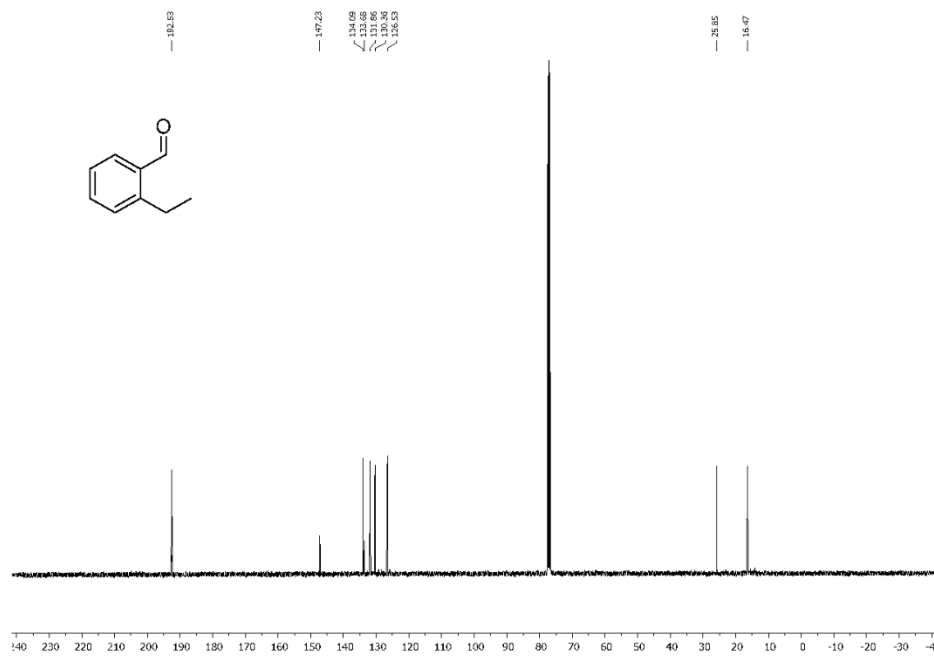
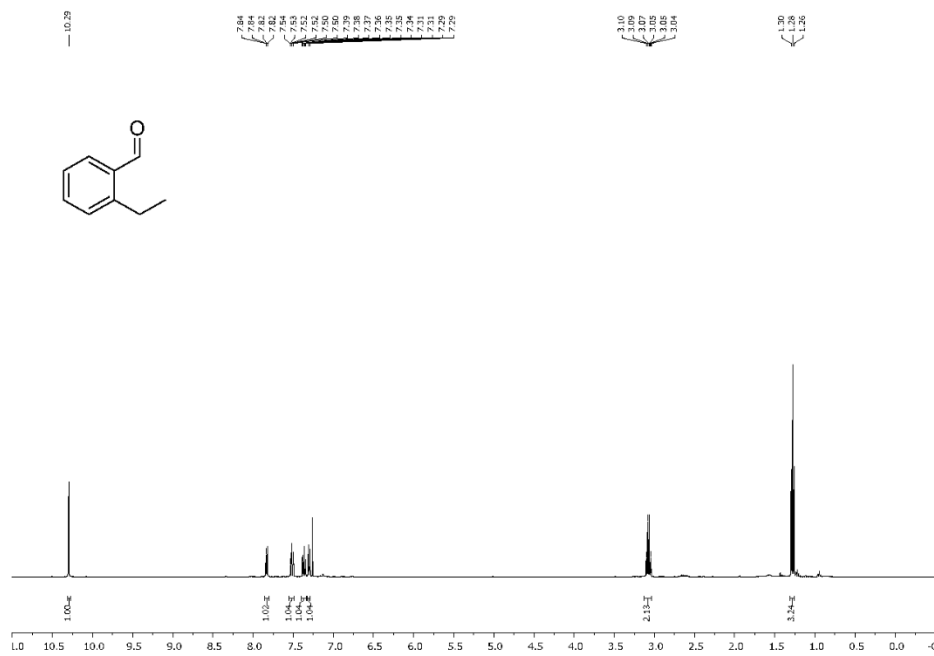


(E)-4-(2-(1-(Benzyl((trimethylsilyl)methyl)amino)ethyl)phenyl)but-3-en-2-one (2h)

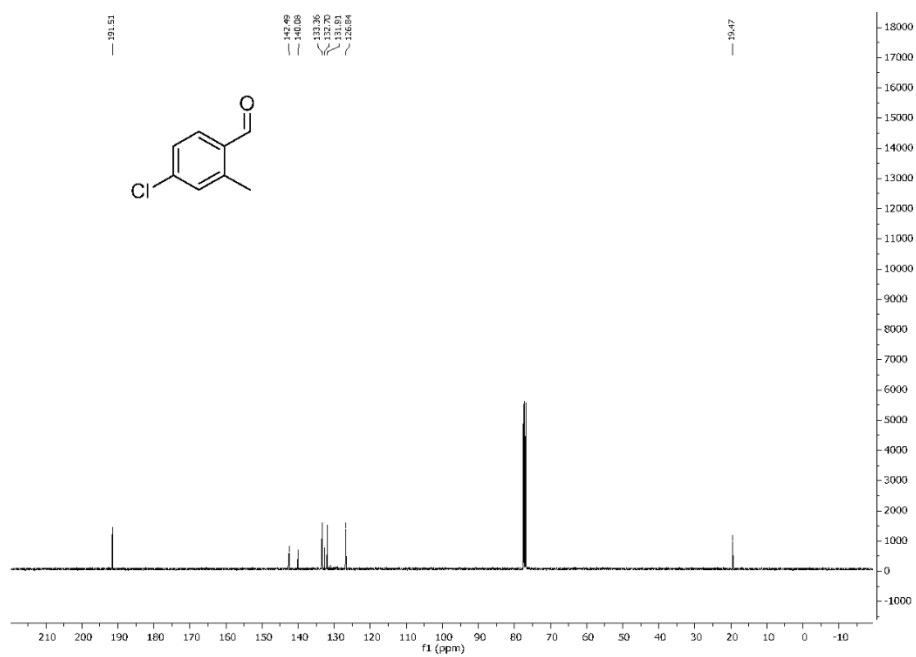
Methyl (E)-3-(2-(1-(benzyl(trimethylsilyl)methyl)amino)ethyl)phenyl)acrylate (2i)



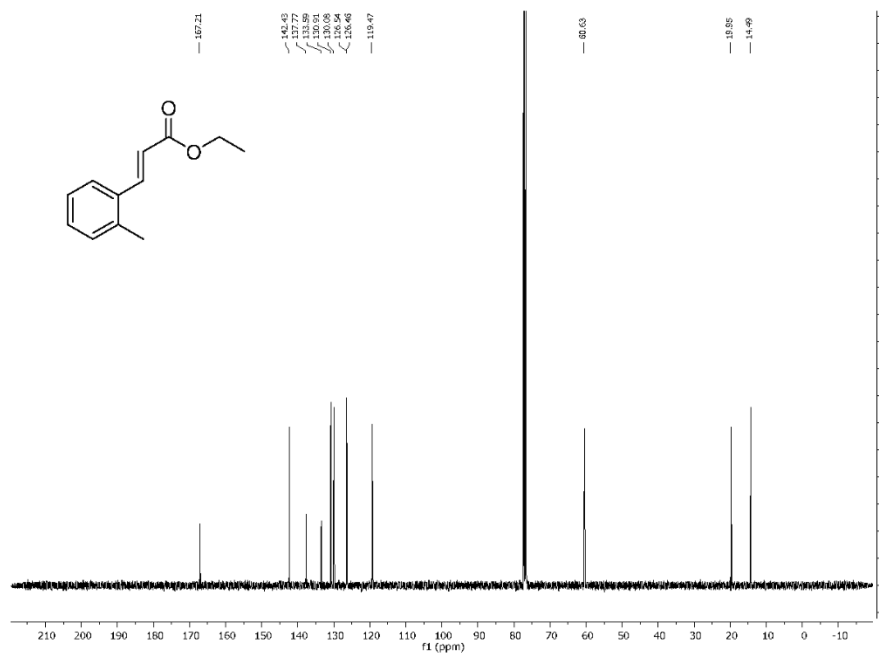
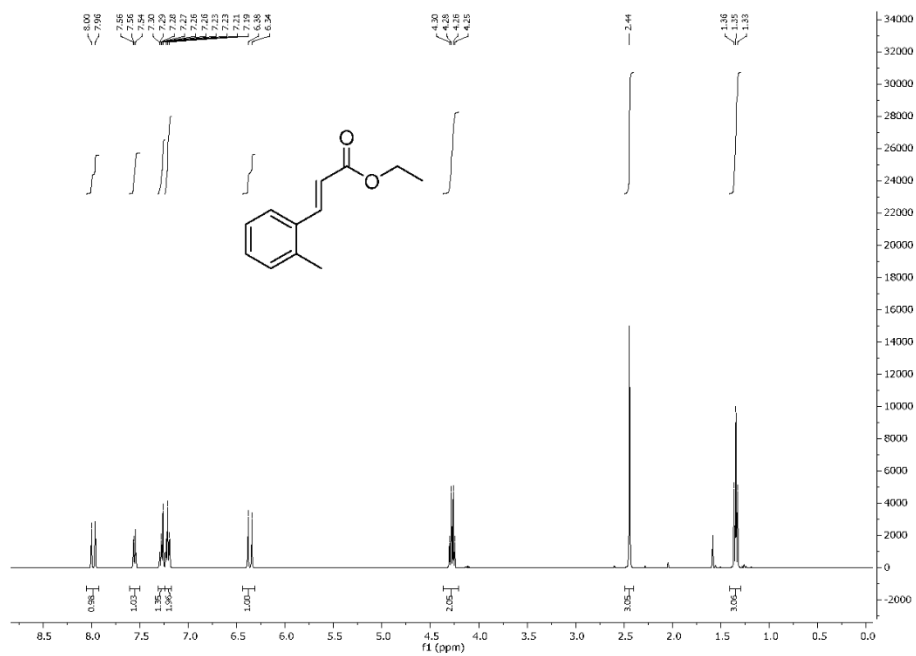
2-Ethylbenzaldehyde (3a)



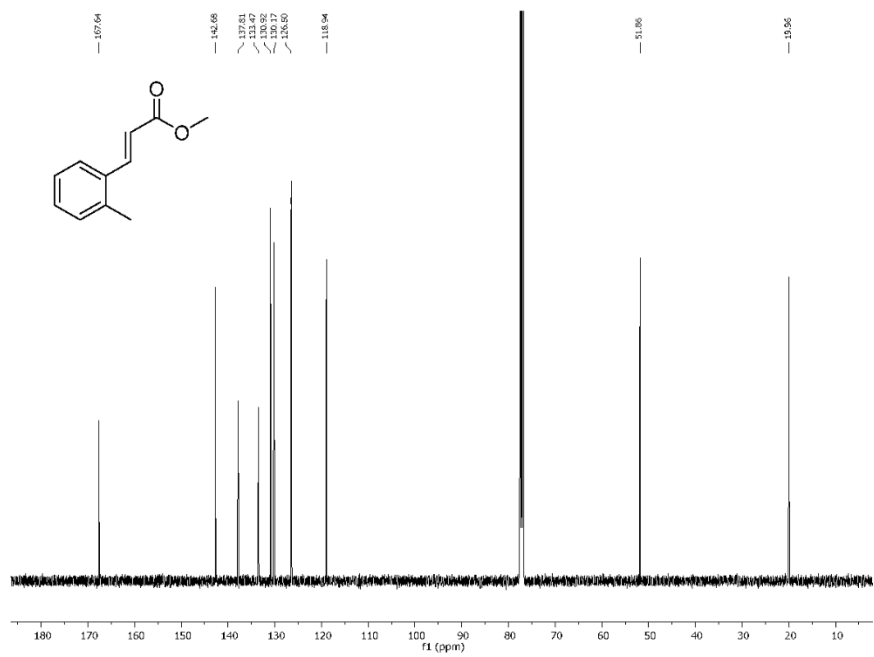
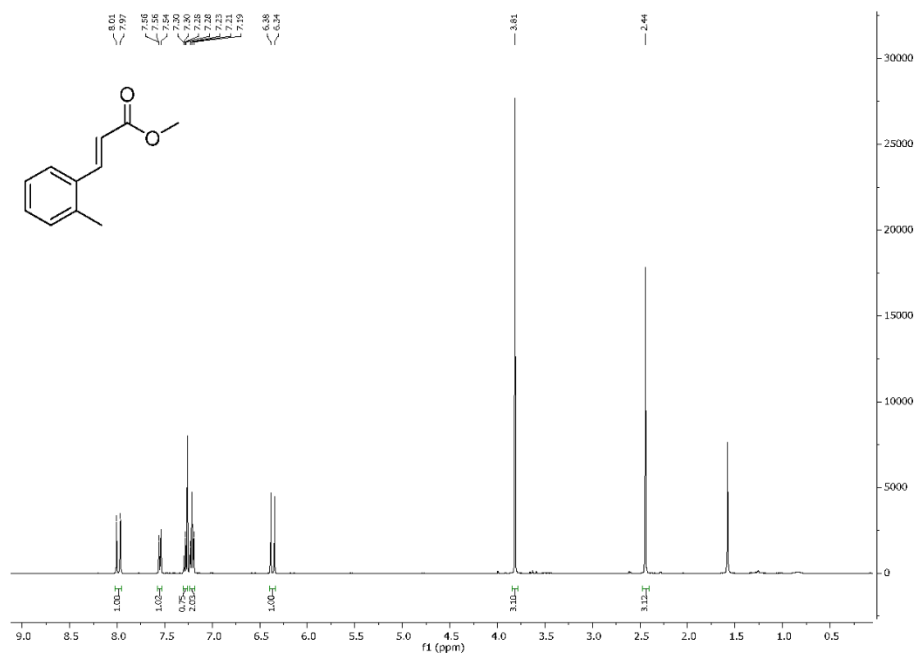
4-Chloro-2-methylbenzaldehyde (3e)

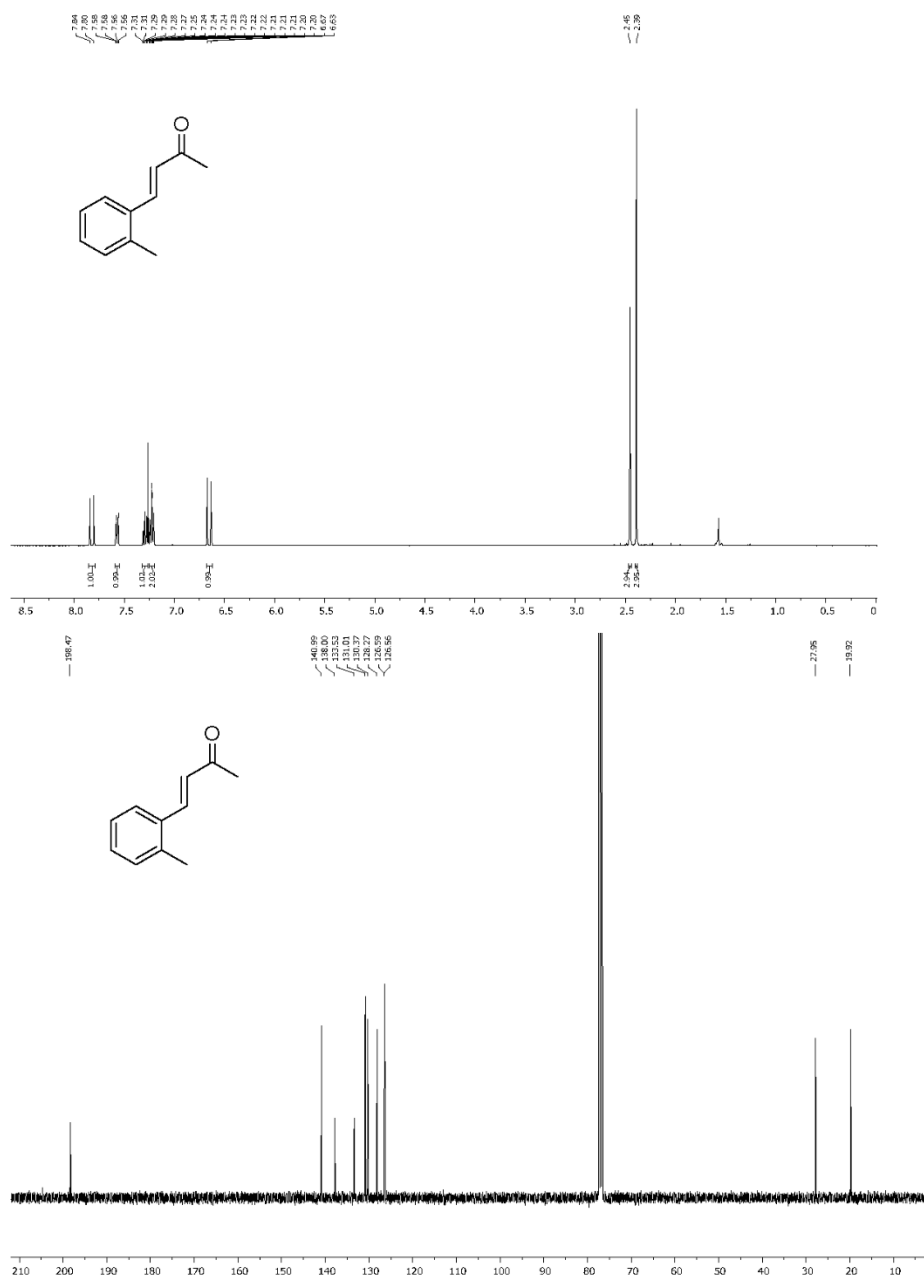


Ethyl-(E)-3-(o-tolyl)-acrylate (4a)

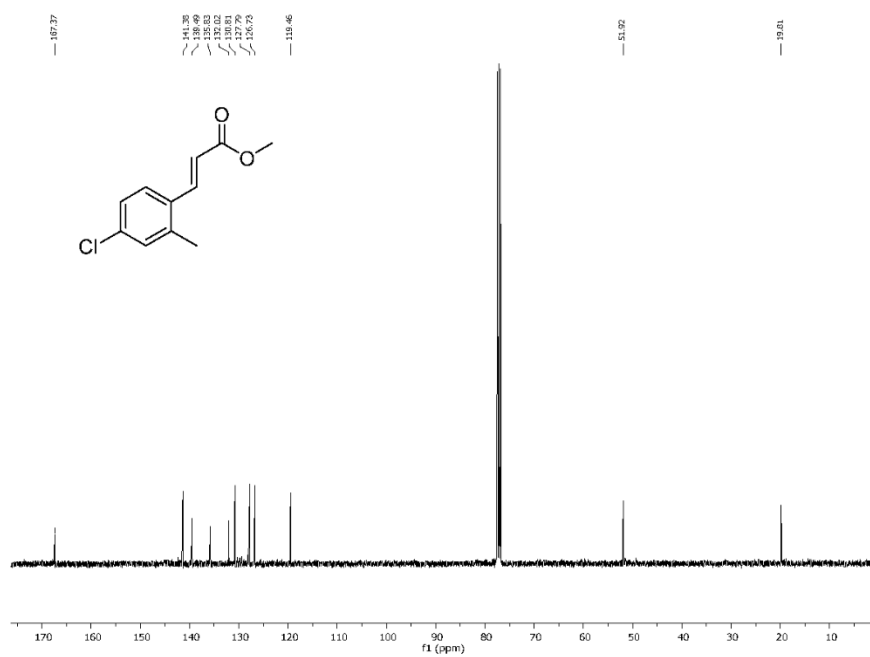


Methyl (E)-3-(o-tolyl)acrylate (4b)

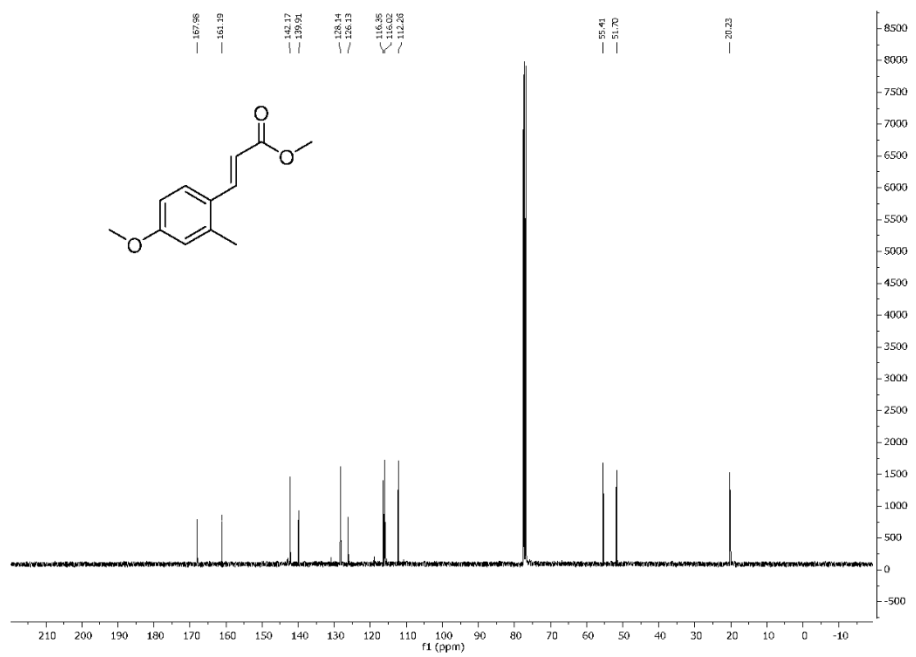
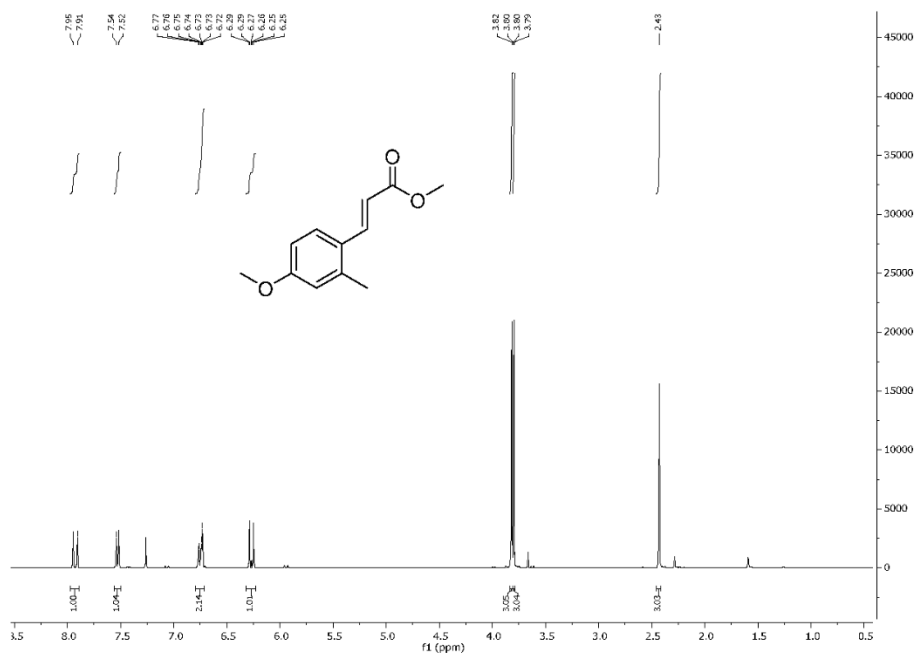


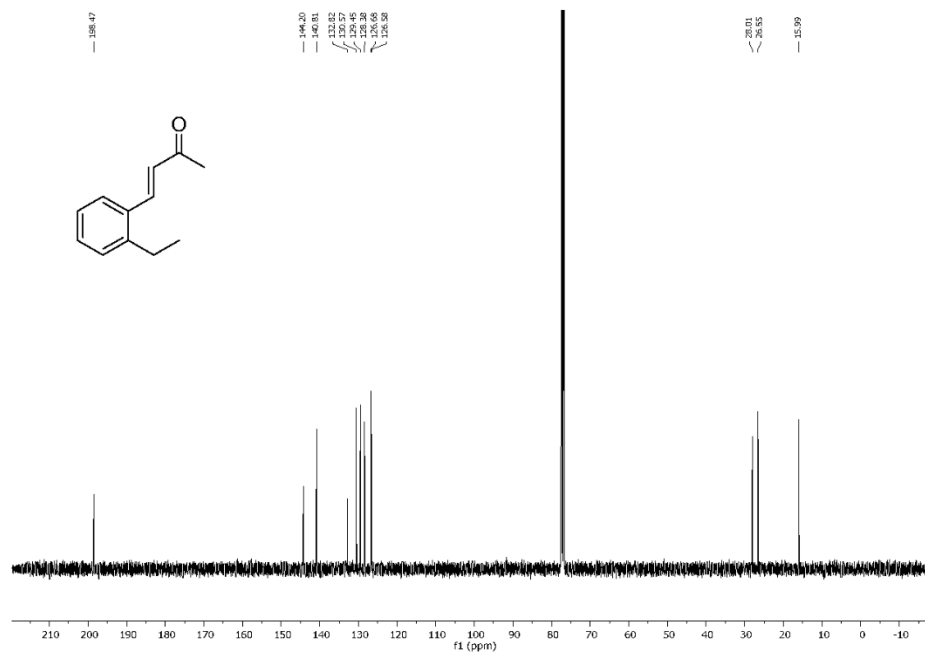
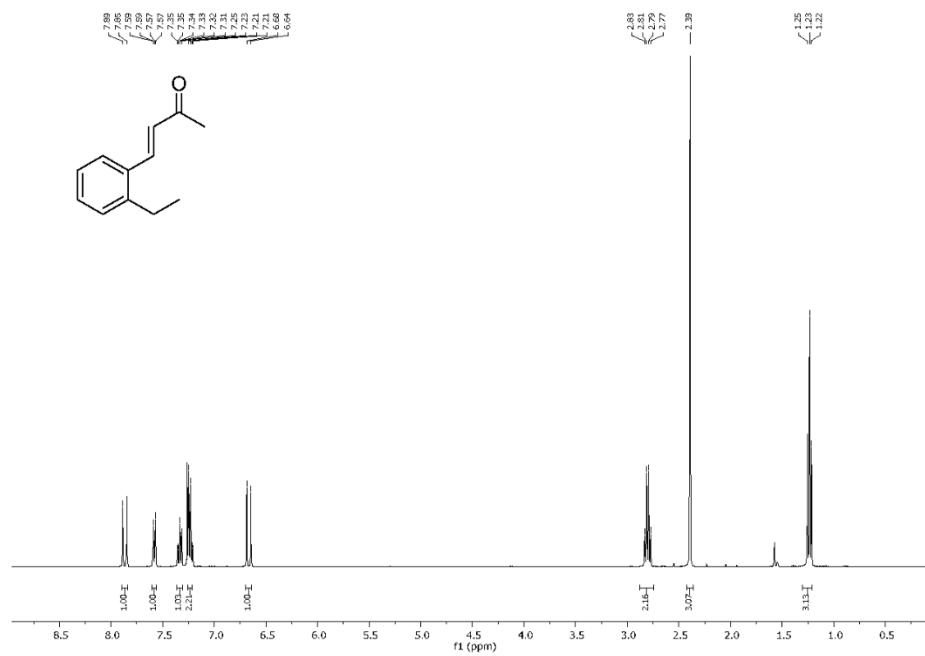
(E)-4-(*o*-Tolyl)but-3-en-2-one (4c)

Methyl (E)-3-(4-chloro-2-methylphenyl)acrylate (4e)

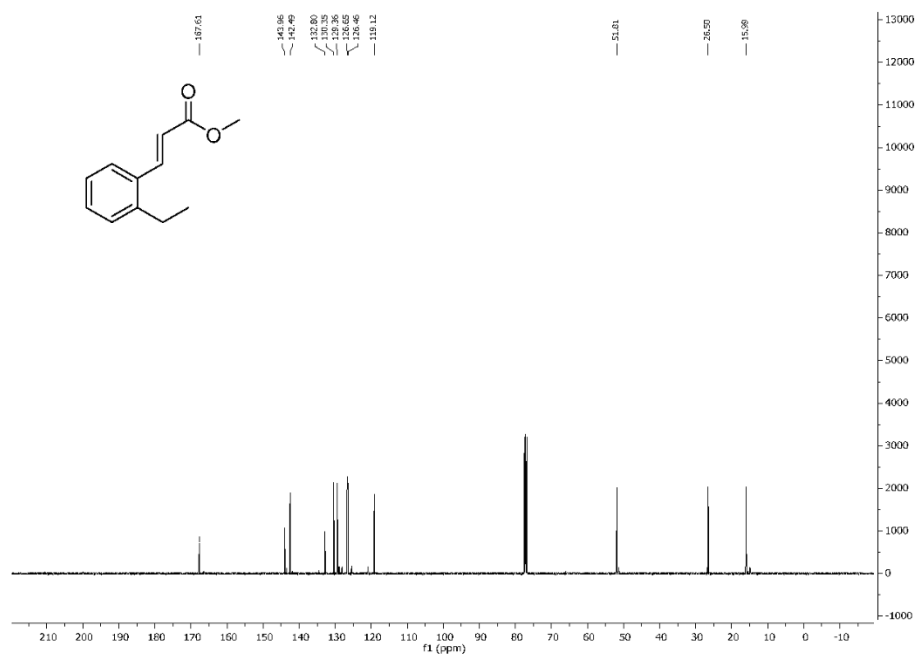
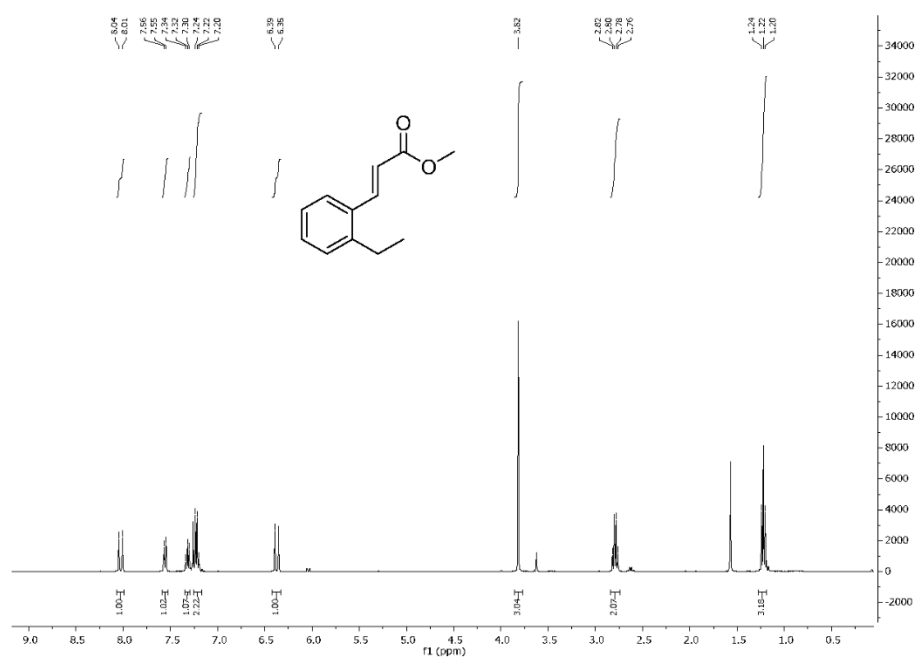


Methyl-(E)-3-(4-methoxy-2-methylphenyl)acrylate (4f)

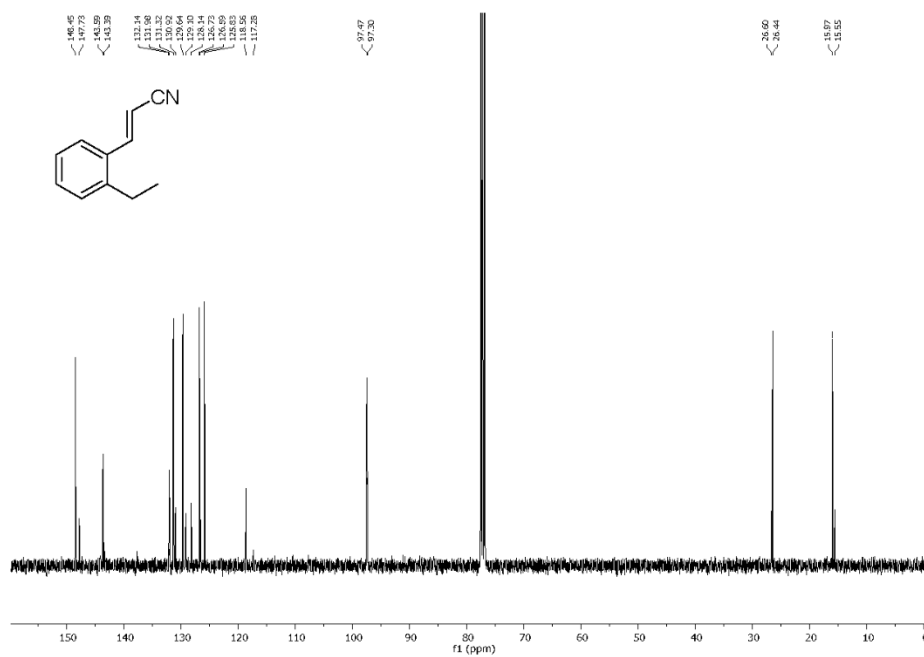
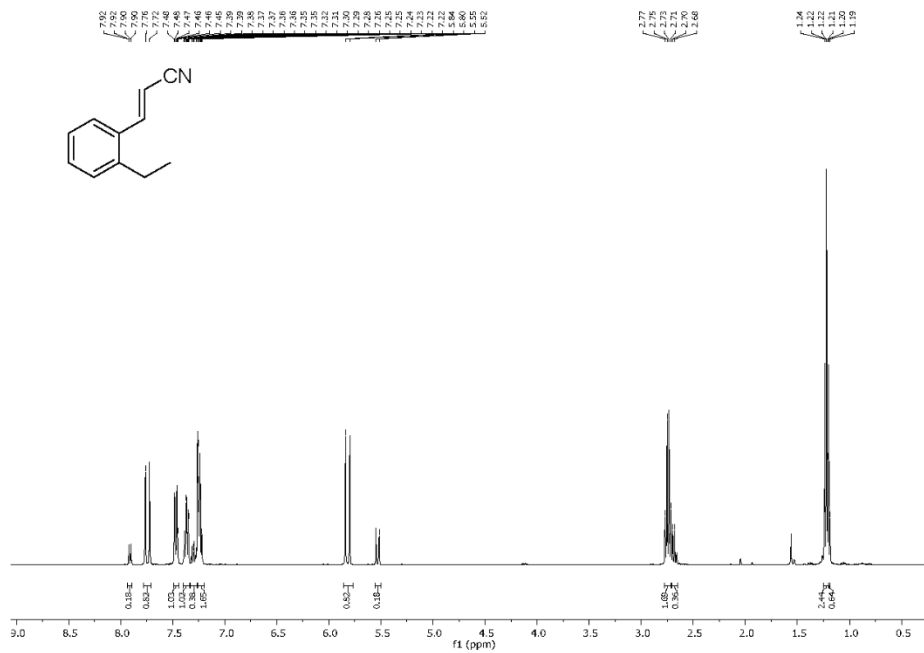


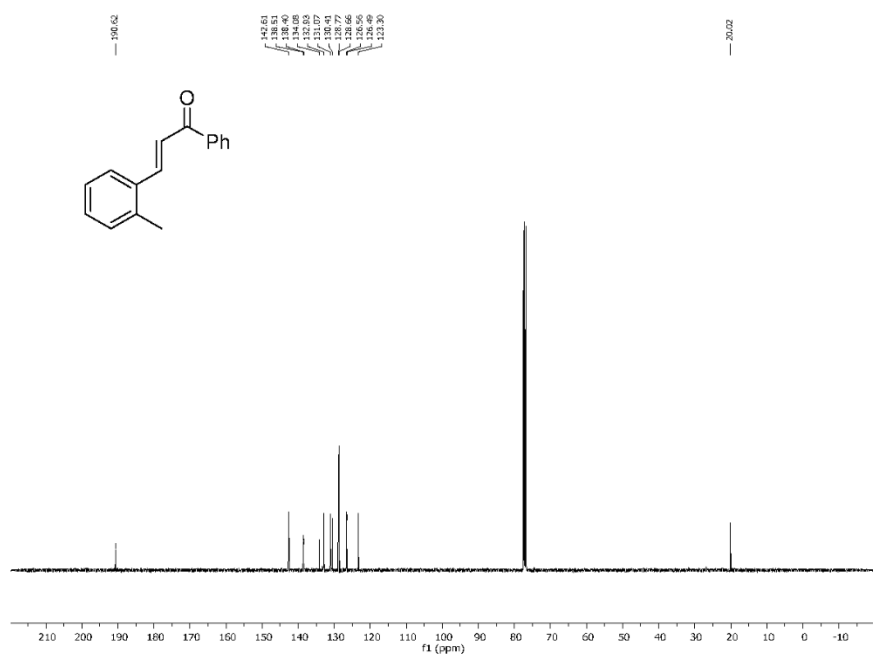
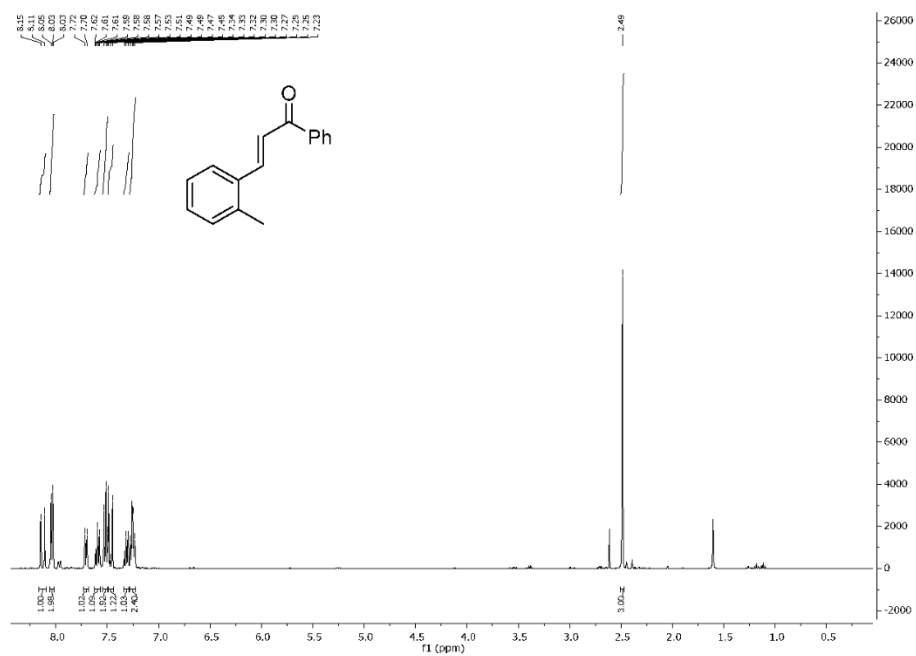
(E)-4-(2-Ethylphenyl)but-3-en-2-one (4h)

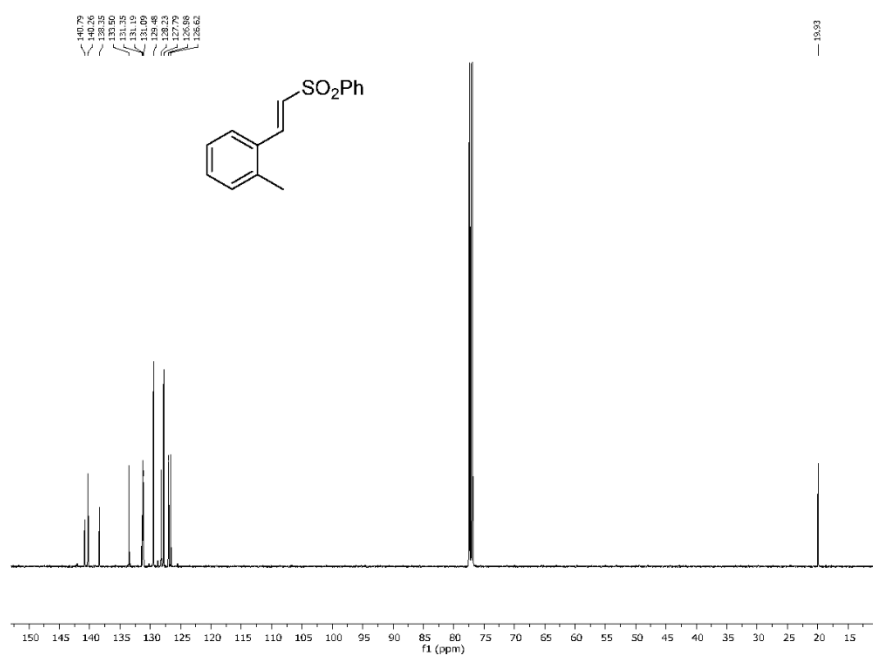
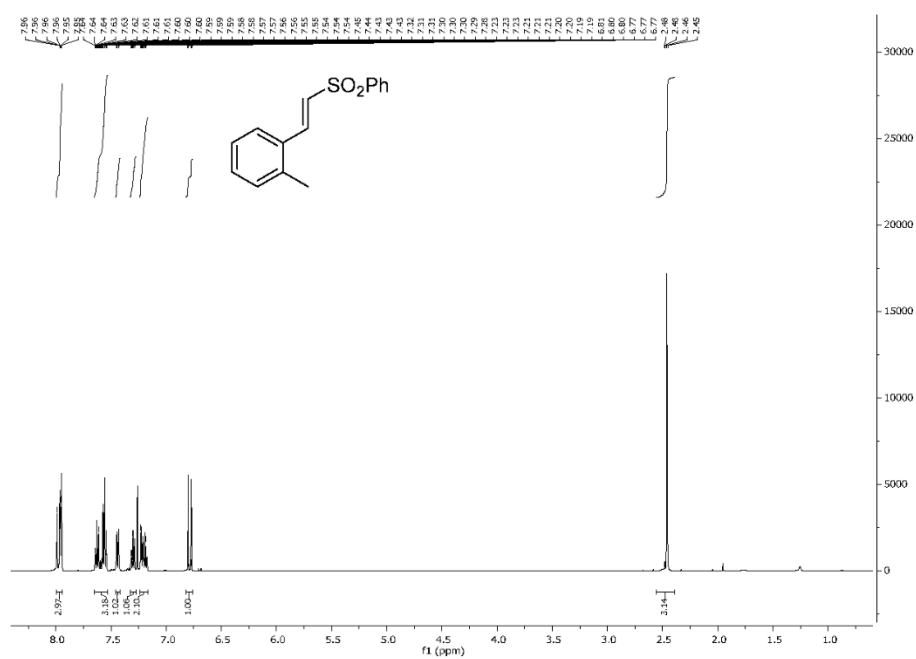
Methyl-(E)-3-(2-ethylphenyl)acrylate (4i)



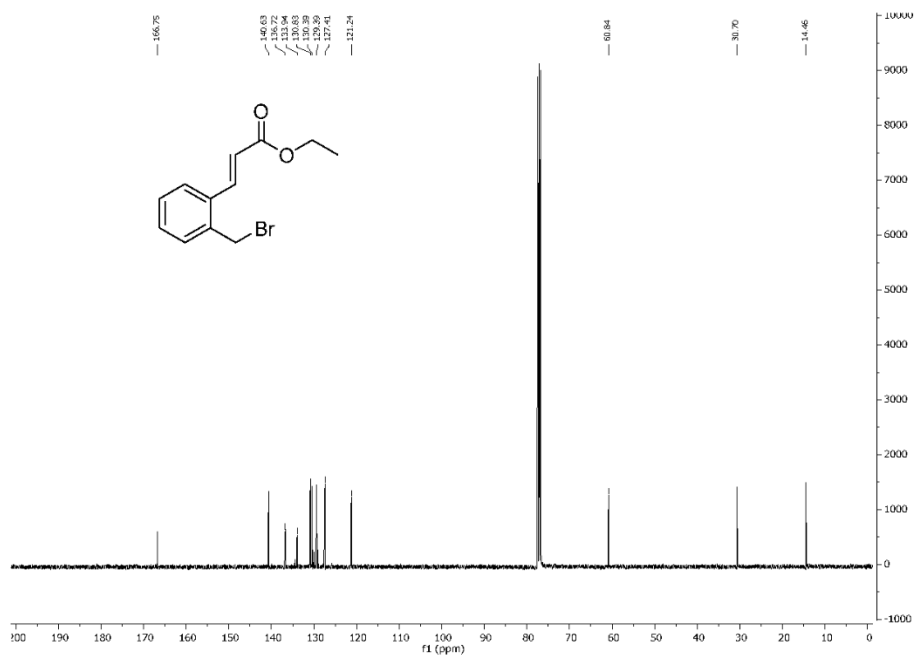
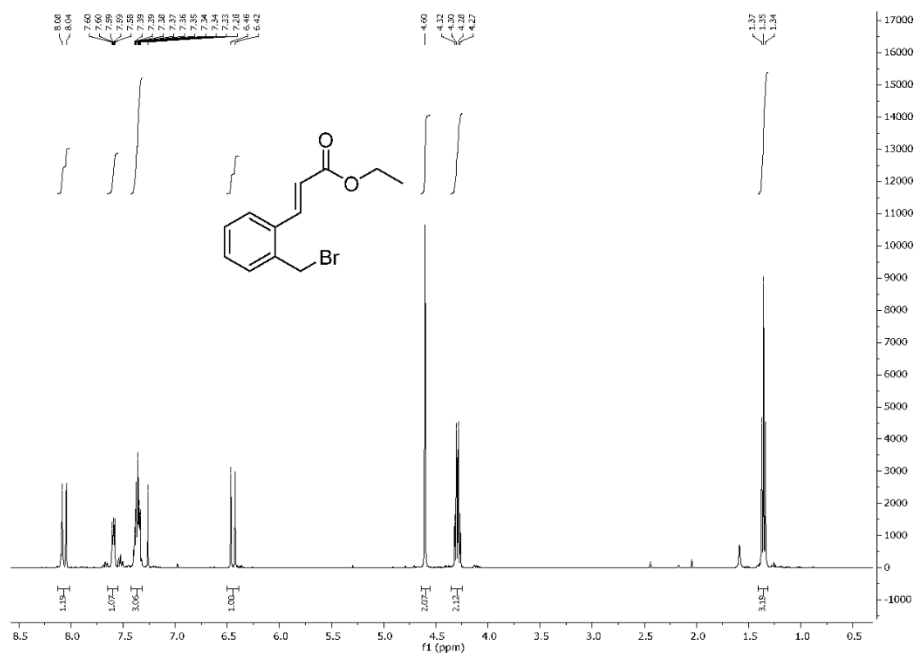
3-(2-Ethylphenyl)acrylonitrile (4j)



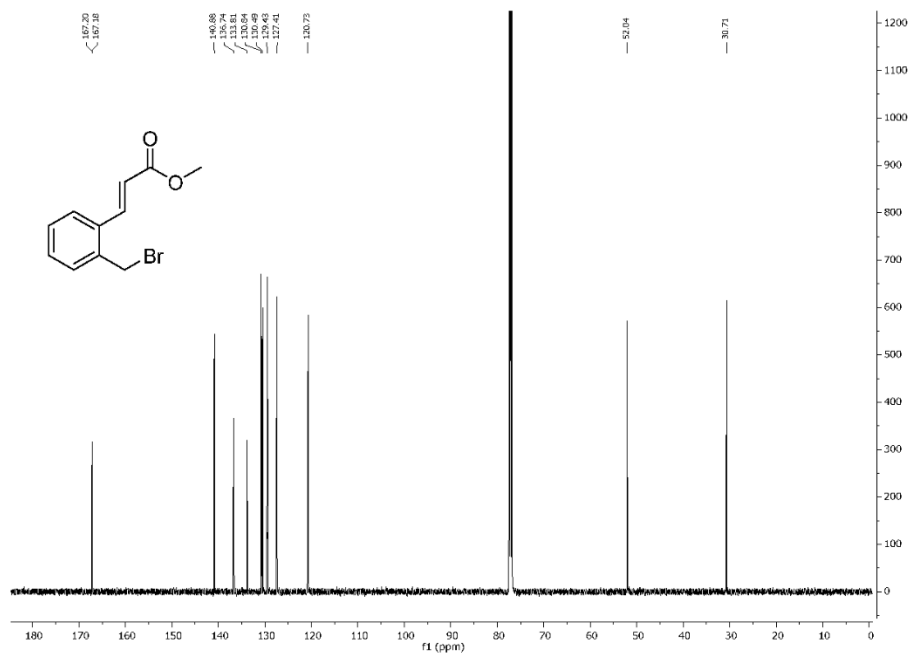
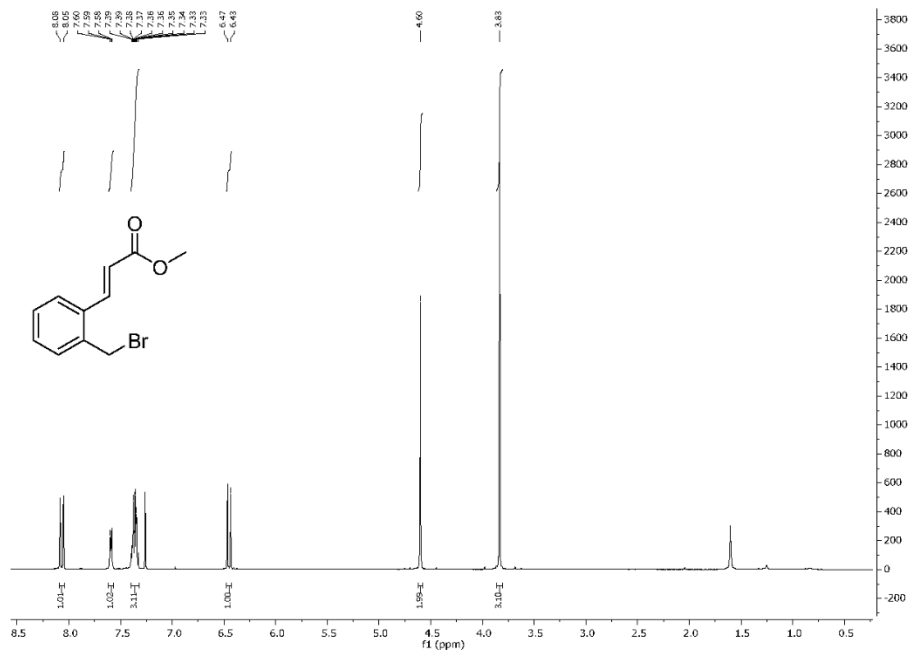
(E)-1-Phenyl-3-(o-tolyl)prop-2-en-1-one (4k)

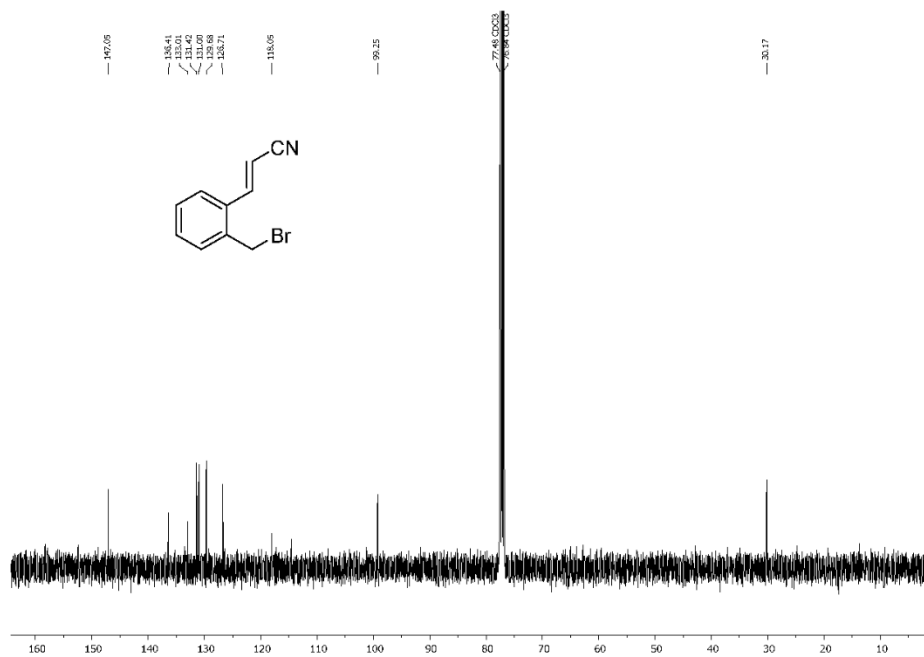
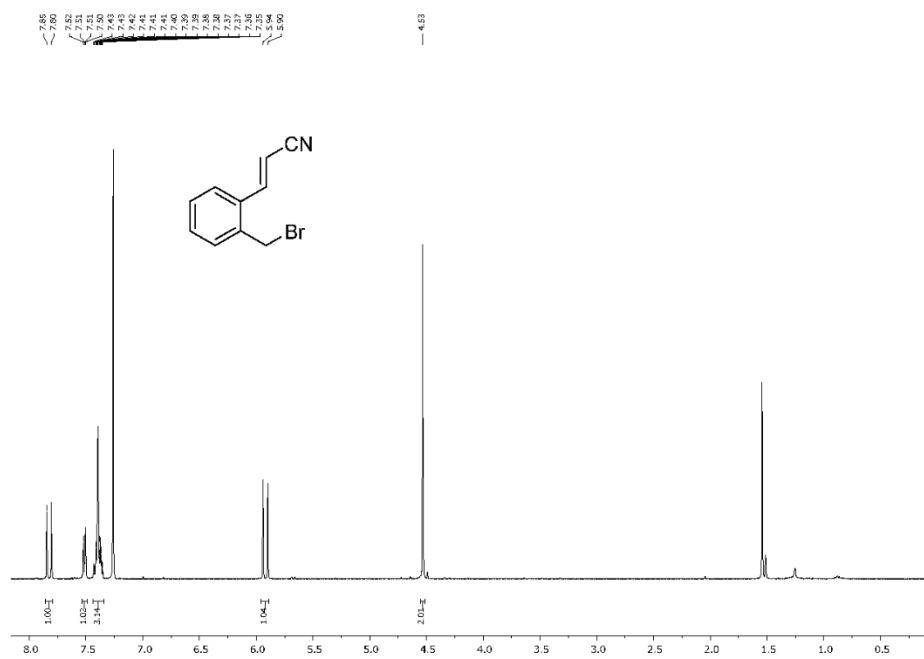
(E)-1-Methyl-2-(2-(phenylsulfonyl)vinyl)benzene (4I)

Ethyl-(E)-3-(2-(bromomethyl)phenyl) acrylate (5a)

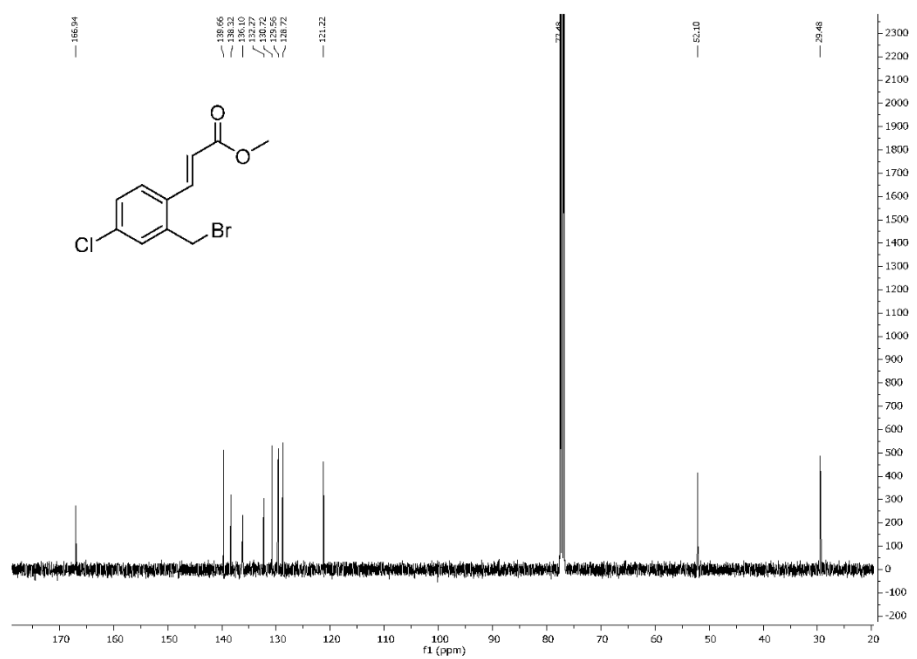
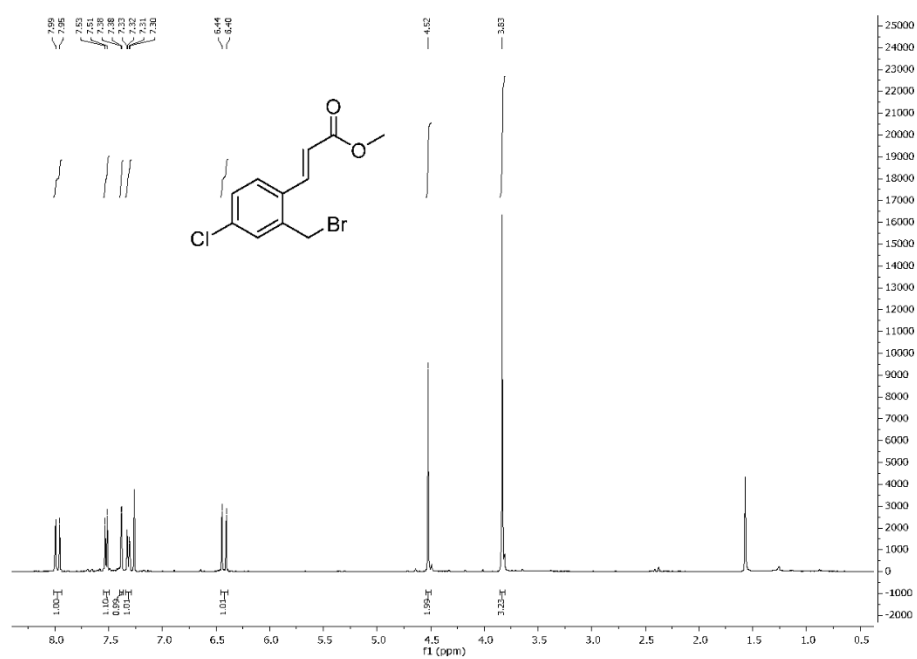


Methyl (E)-3-(2-(bromomethyl)phenyl)acrylate (5b)

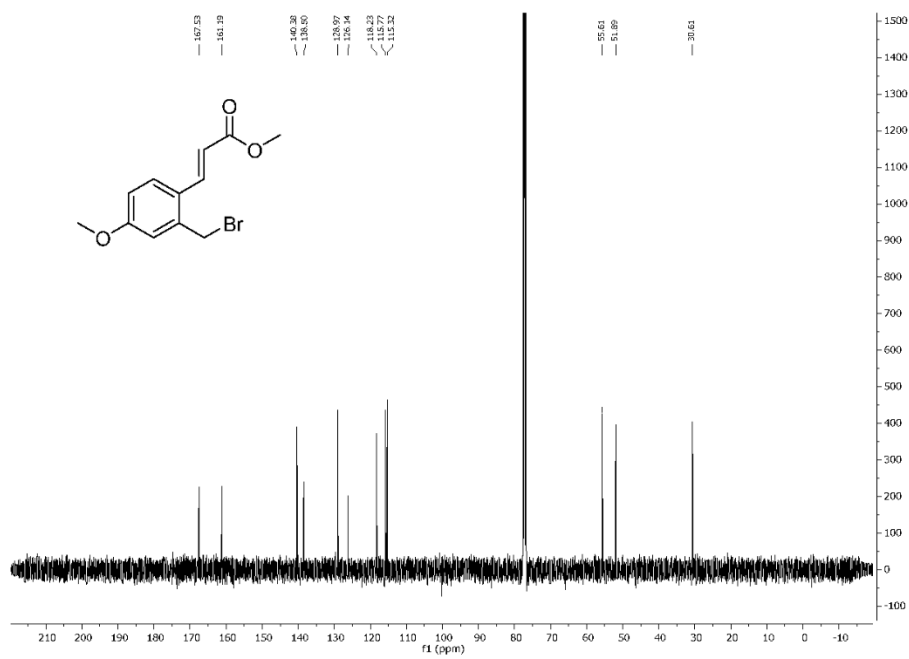
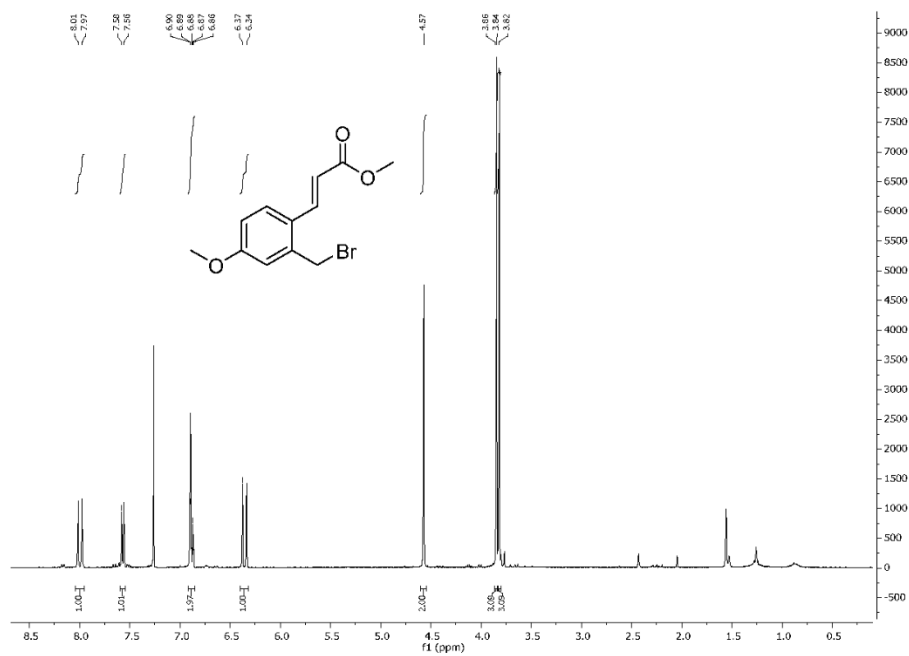


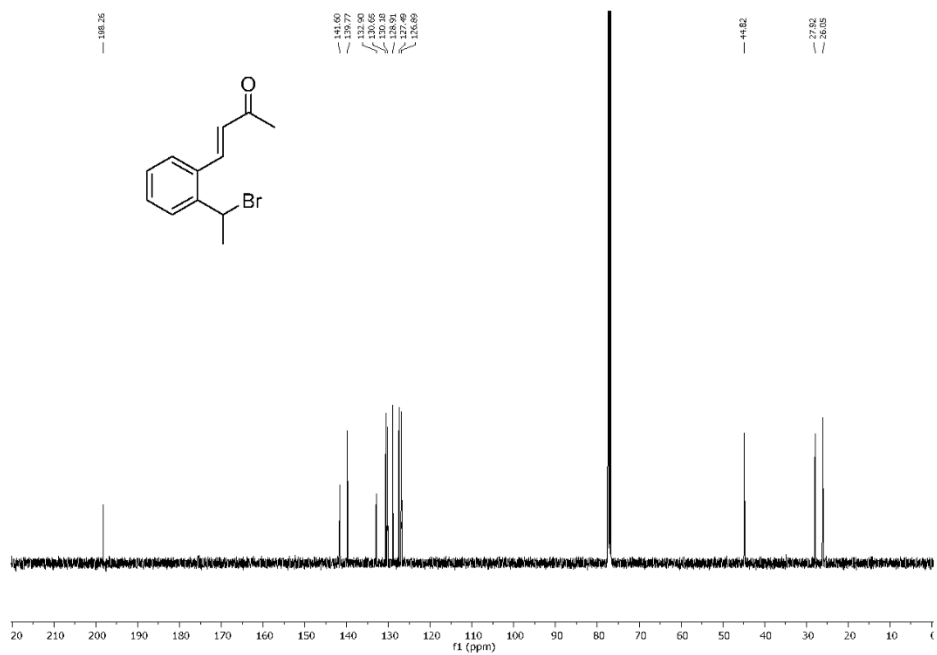
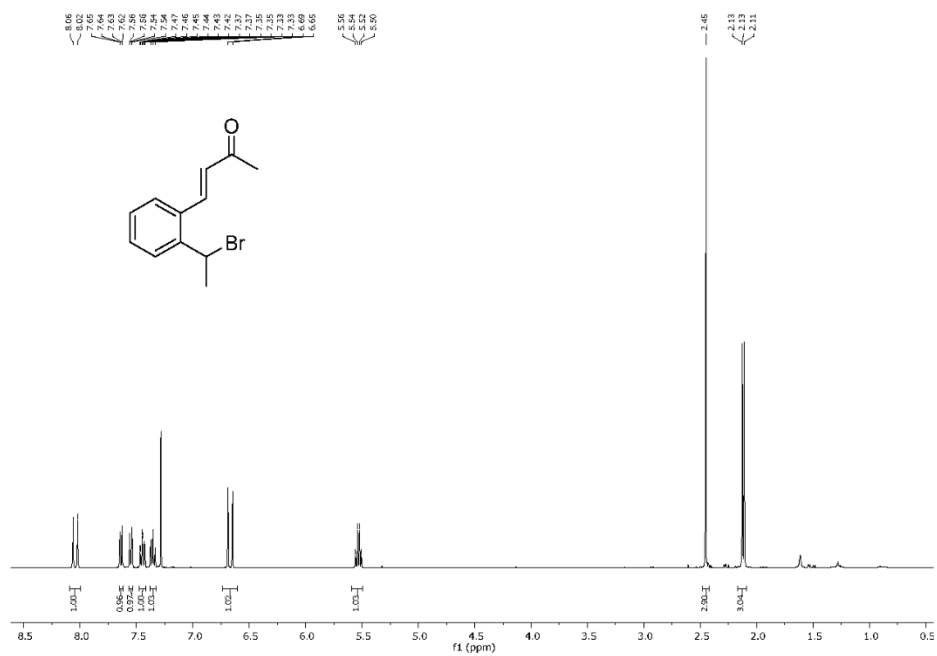
(E)-3-(2-(Bromomethyl)phenyl)acrylonitrile (5d)

Methyl (E)-3-(2-(bromomethyl)-4-chlorophenyl)acrylate (5e)

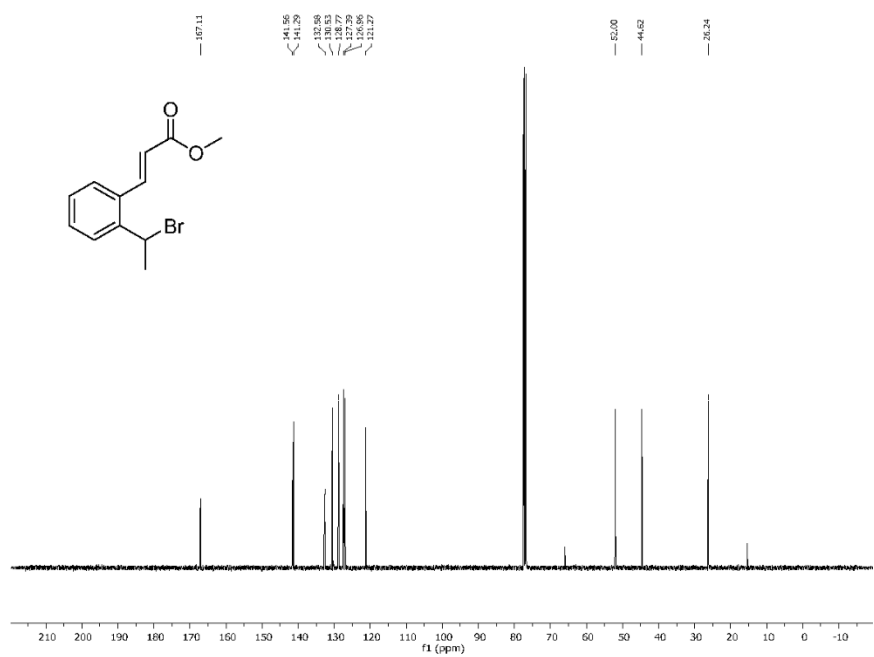
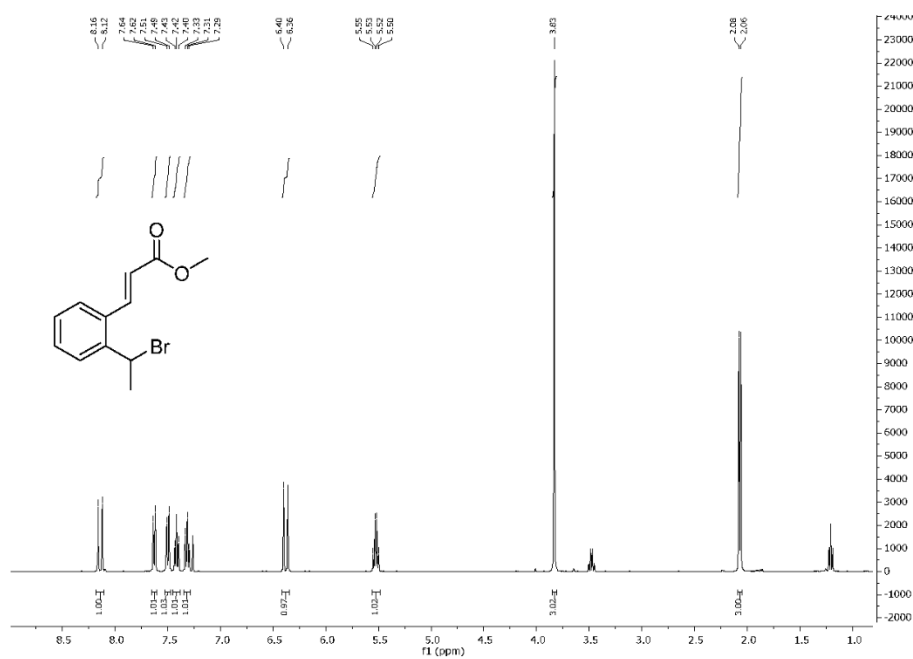


Methyl-(E)-3-(2-(bromomethyl)-4-methoxyphenyl)acrylate (5f)

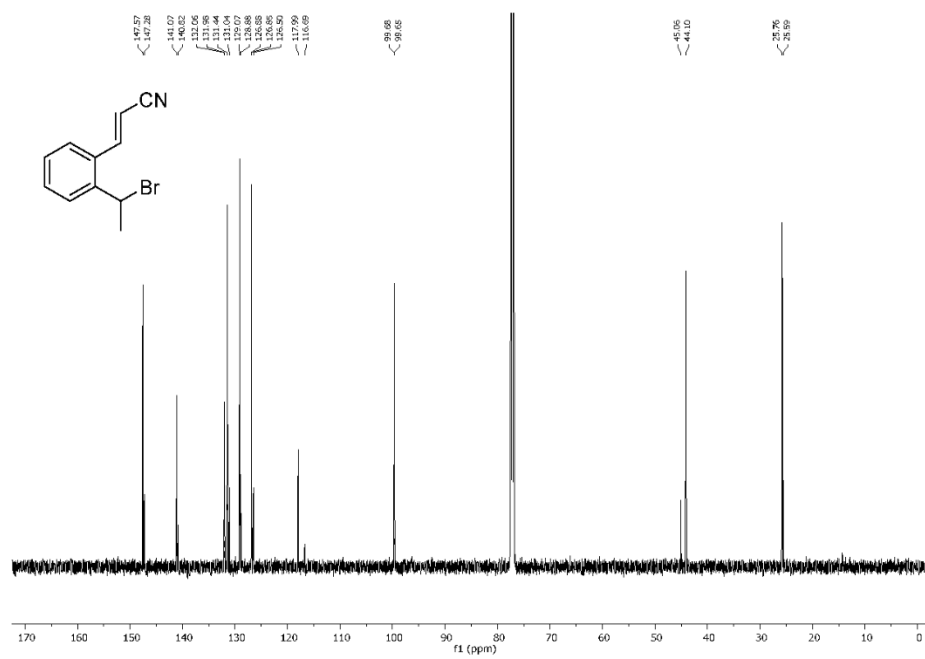
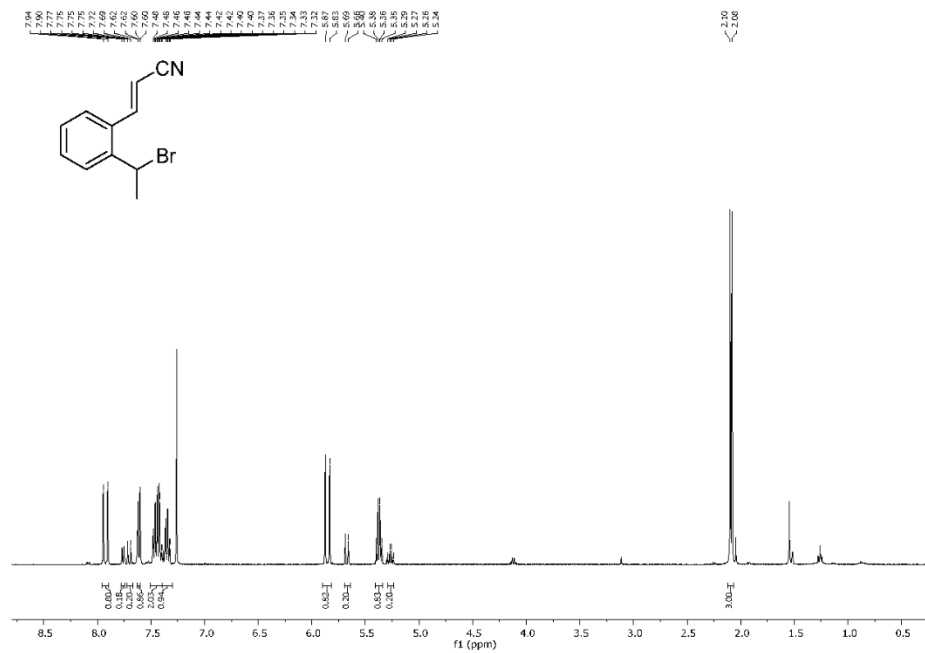


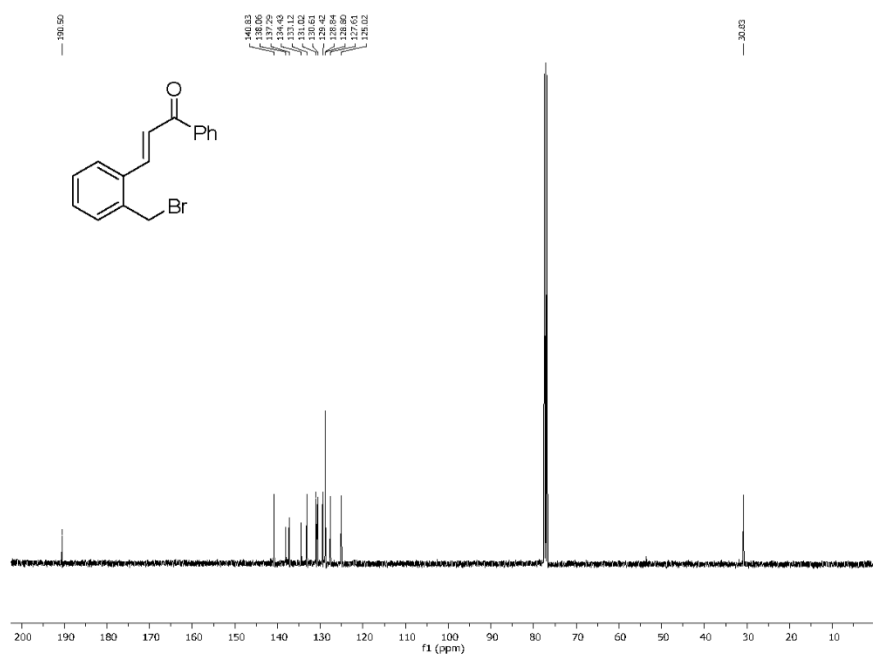
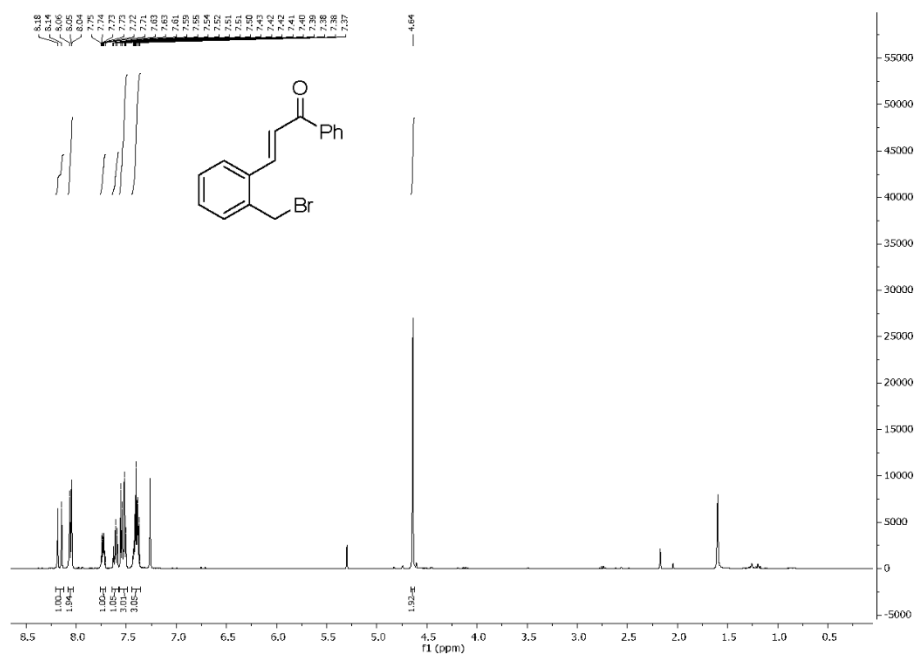
(E)-4-(2-(1-Bromoethyl)phenyl)but-3-en-2-one (5h)

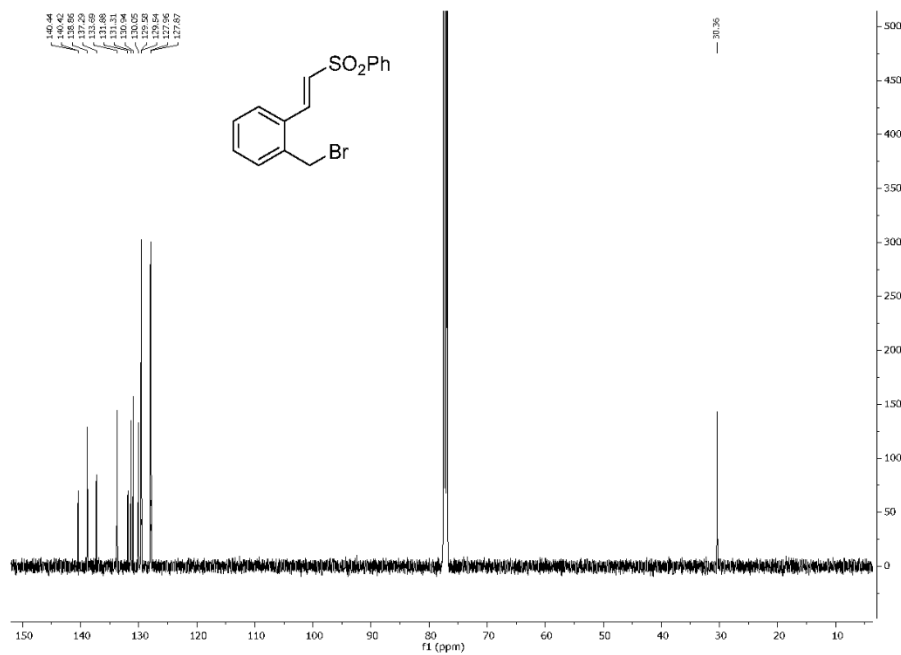
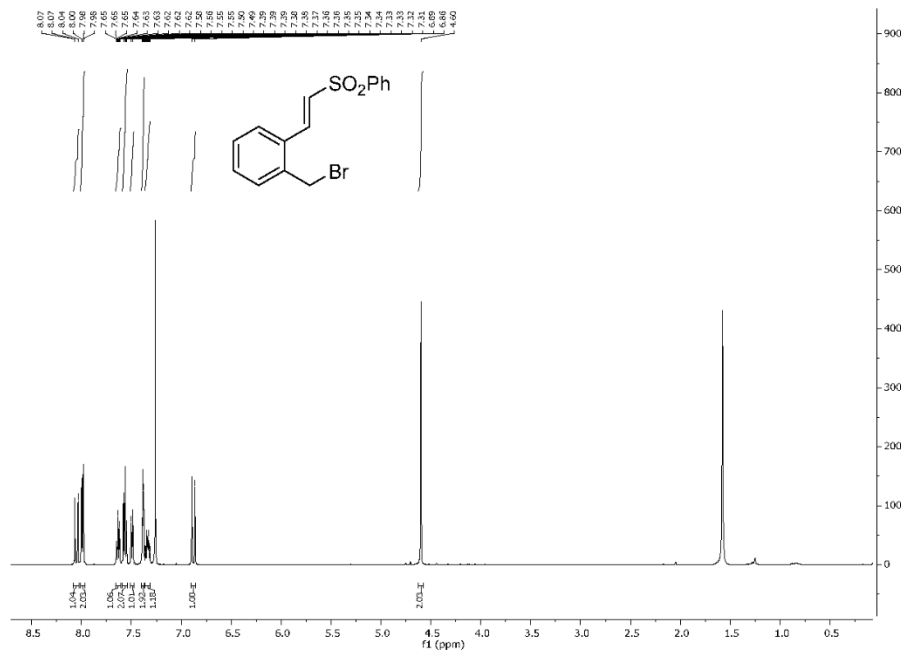
Methyl (E)-3-(2-(1-bromoethyl)phenyl)acrylate (5i)



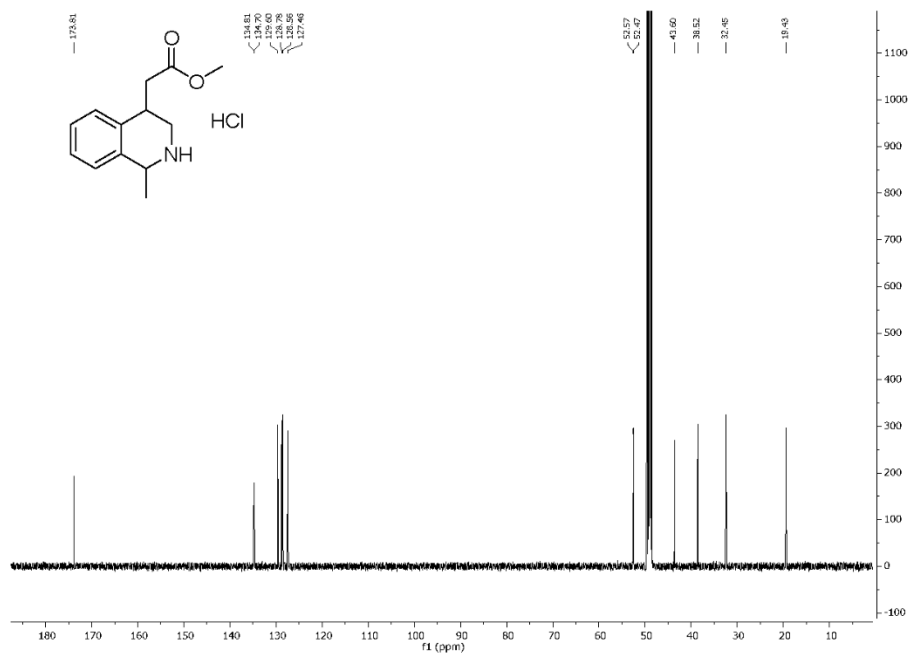
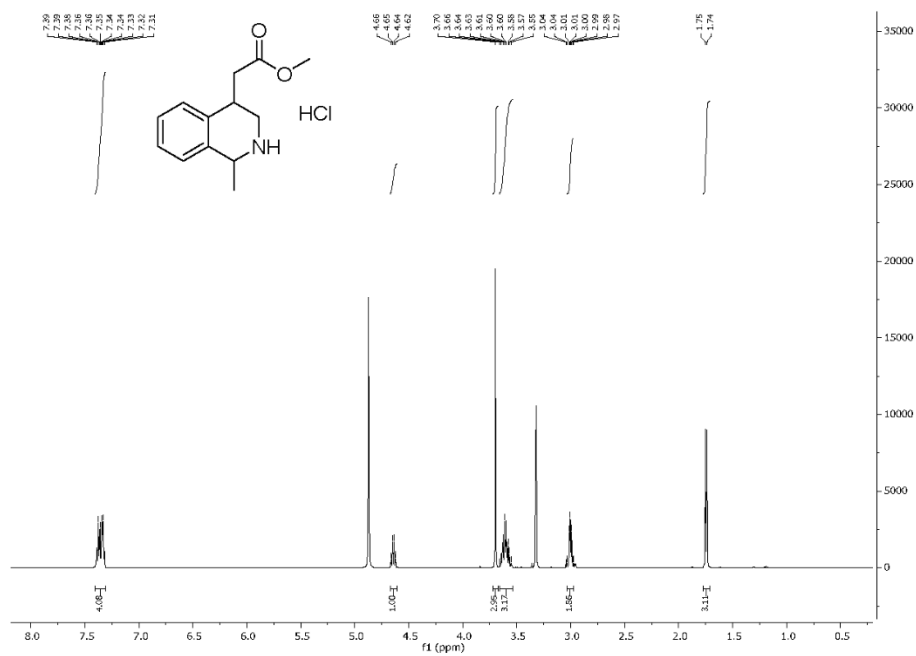
3-(2-(1-Bromoethyl)phenyl)acrylonitrile (5j)



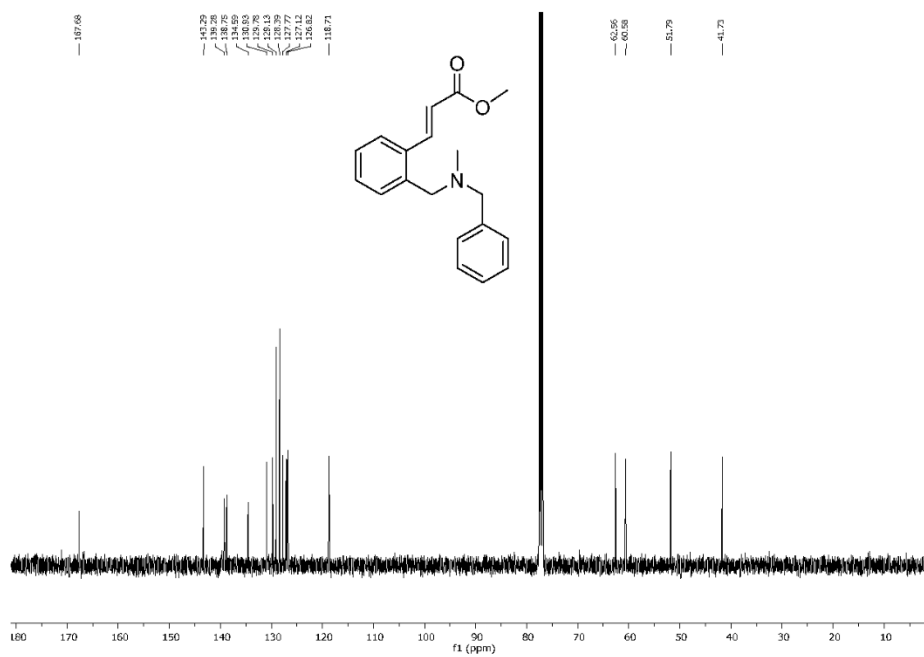
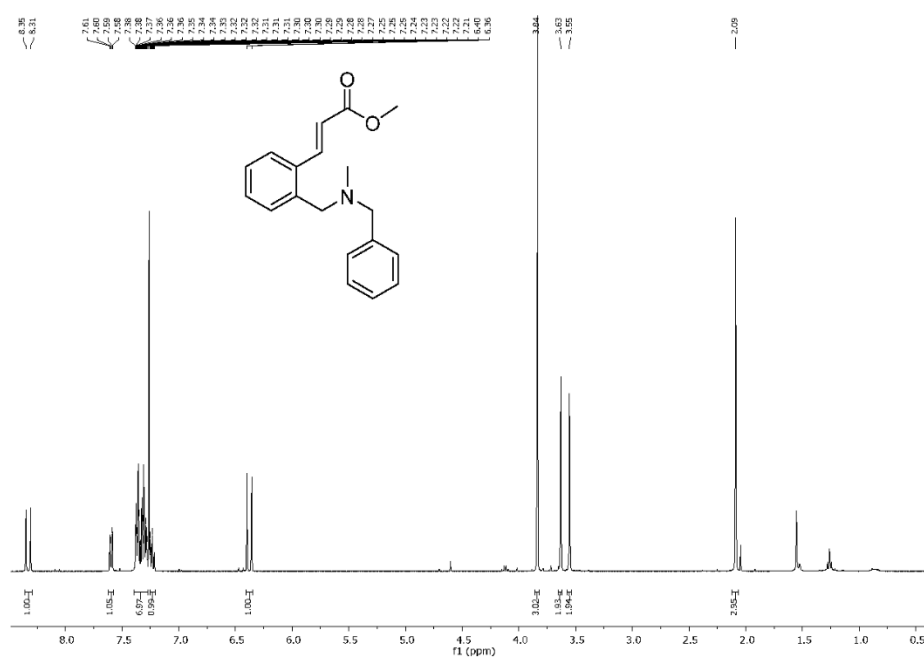
(E)-3-(2-(Bromomethyl)phenyl)-1-phenylprop-2-en-1-one (5k)

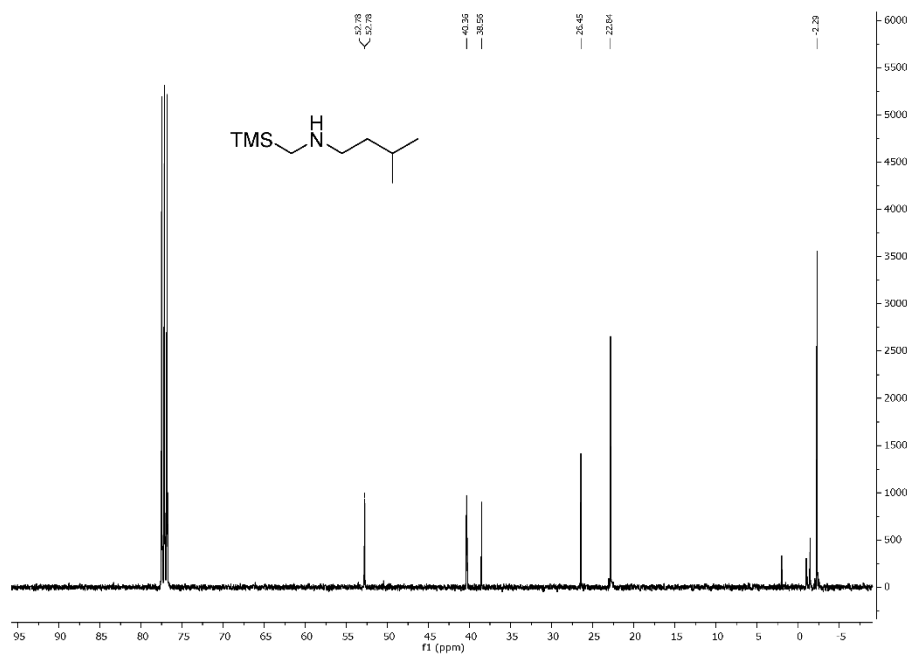
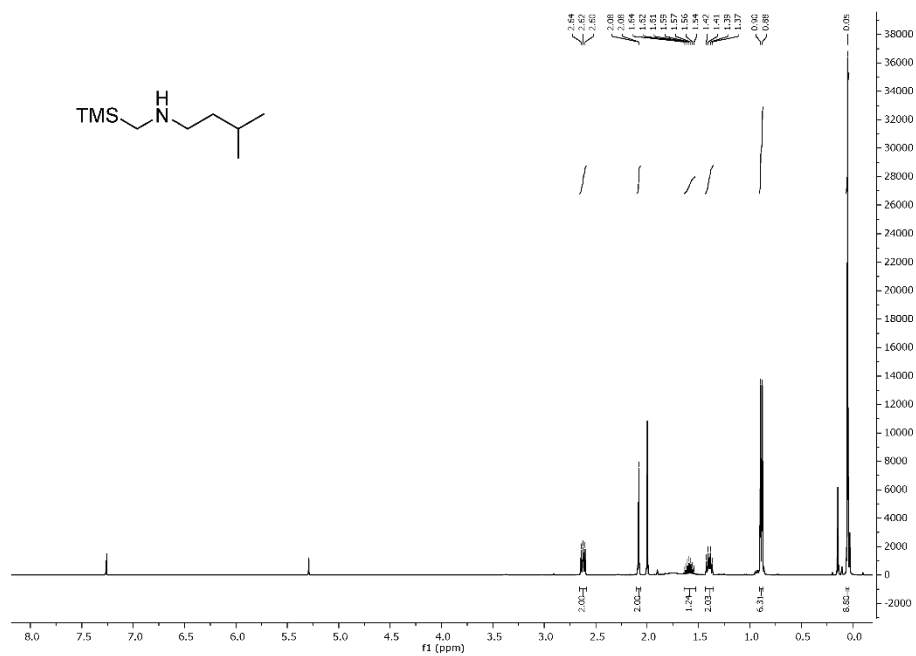
(E)-1-(Bromomethyl)-2-(2-(phenylsulfonyl)vinyl)benzene (5I)

Methyl 2-(1-methyl-1,2,3,4-tetrahydroisoquinolin-4-yl)acetate hydrochloride (6)



Methyl-(E)-3-(2-((benzyl(methyl)amino)methyl)phenyl)acrylate (7)



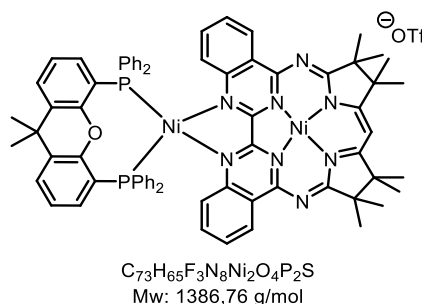
3-Methyl-N-((trimethylsilyl)methyl)butan-1-amine (8b)

References

- (1) Monos, T. M.; Sun, A. C.; McAtee, R. C.; Devery III, J. J.; Stephenson, C. R. J. *J. Org. Chem.* **2016**, *81*, 6988-6994
- (2) *APEX suite of crystallographic software, APEX 2, version 2008.4.*, Bruker AXS Inc., Madison, Wisconsin, USA (2008).
- (3) *SAINT, version 7.56a, SADABS, version 2008.1*, Bruker AXS Inc., Madison, Wisconsin, USA (2008).
- (4) Hübschle, C. B.; Sheldrick, G. M.; Dittrich, B., *SHELXL*, *J. Appl. Crystallogr.* **2011**, *44*, 1281-1284.
- (5) Sheldrick, G. M., *SHELXL-2014*, University of Göttingen, Göttingen, Germany (2014).
- (6) Sheldrick, G. M., *SHELXL-97*, University of Göttingen, Göttingen, Germany (1998).
- (7) Wilson, A. J. C., *International Tables for Crystallography*, Dordrecht, The Netherlands, Kluwer Academic Publishers (1992).
- (8) Spek, A. L., *J. Appl. Cryst.* **2003**, *36*, 7-13.
- (9) Spek, A. L., *Acta Cryst.* **2009**, *D65*, 148-155.
- (10) Xia, W.; Shao, Y.; Gui, W.; Yang, C. *Chem. Commun.* **2011**, *47*, 11098-11100.
- (11) Dong, H.; Shen, M.; Redford, J. E.; Stokes, B. J. Pumphrey, A. L.; Driver, T. G. *Org. Lett.* **2007**, *9*, 5191-5194.
- (12) Nakamura, Y.; O-kawa, K.; Minami, S.; Ogawa, T.; Tobita, S.; Nishimura, J. *J. Org. Chem.* **2002**, *67*, 1247-1252
- (13) Juteau, H.; Gareau, Y.; Labelle, M.; Sturino, C. F.; Sawyer, N.; Tremblay, N.; Lamontagne, S.; Carrière, M.-C.; Denis, D.; Metters, K. M. *Bioorg. Med. Chem.* **2001**, *9*, 1977-1984.
- (14) Xue, Q., Mao, Z.; Shi, Y.; Mao, H.; Cheng, Y.; Zhu, C. *Tetrahedron Lett.* **2012**, *53*, 1851-1854
- (15) Jeong, H. C.; Lim, S. H.; Cho, D. W.; Kim, S. H.; Mariano, P. S. *Org. Biomol. Chem.* **2016**, *14*, 10502.
- (16) Comins, D. L.; Brown, J. D.; Mantlo, N. B. *Tetrahedron Lett.* **1982**, *23*, 3979-3982.
- (17) Capkova, K.; Yoneda, Y.; Dickerson, T. J.; Janda, K. D. *Bioorg. Med. Chem. Lett.* **2007**, *17*, 6463-6466.
- (18) Biogen Ma Inc.; Capacci, A. G.; Dechantsreiter, M.; Enyedy, I.; Jones, J. H.; Lin, E. Y.-S.; Lucas, B. S. WO2018/140876, **2018**, A1.
- (19) Murry, P. M.; Bower, J. F.; Cox, D. K.; Galbraith, E. K.; Parker, J. S.; Sweeney, J. B. *Org. Process Res. Dev.* **2013**, *17*, 397-405.
- (20) Liu, J.-M.; Young, J.-J.; Li, Y.-J.; Sha, C.-K. *J. Org. Chem.* **1986**, *51*, 1120-1123.
- (21) Shiotani, S.; Hori, T.; Mitsuhashi, K. *Chem. Pharm. Bull.* **1967**, *15*, 88-93.
- (22) Grübel, M.; Bosque, I. Altmann, P. J.; Bach, T.; Hess, C. R. *Chem. Sci.* **2018**, *9*, 3313-3317.
- (23) Pavlishchuk, V. V.; Adison, A. W. *Inorg. Chim. Acta* **2000**, *298*, 97-102.

Bimetallic Nickel Mabiq complex

Synthesis of [NiNi(Mabiq)(Xanthphos)]OTf



149 mg (199 μ mol, 1.00 eq.) [Ni(Mabiq)]OTf, 72.1 mg (262 μ mol, 1.32 eq.) Ni(cod)₂ and 138 mg (238 μ mol, 1.20 eq.) xanthphos (4,5-bis(diphenylphosphino)-9,9-dimethylxanthene) were suspended in 10 ml anhydrous MeCN and stirred at room temperature. The reaction colour turned from yellow to green. After twelve hours the solvent was removed and the resulting green solid was recrystallized from a THF/Pentane/Et₂O mixture. 203 mg (146 μ mol, 73%) of crude green solid were isolated.

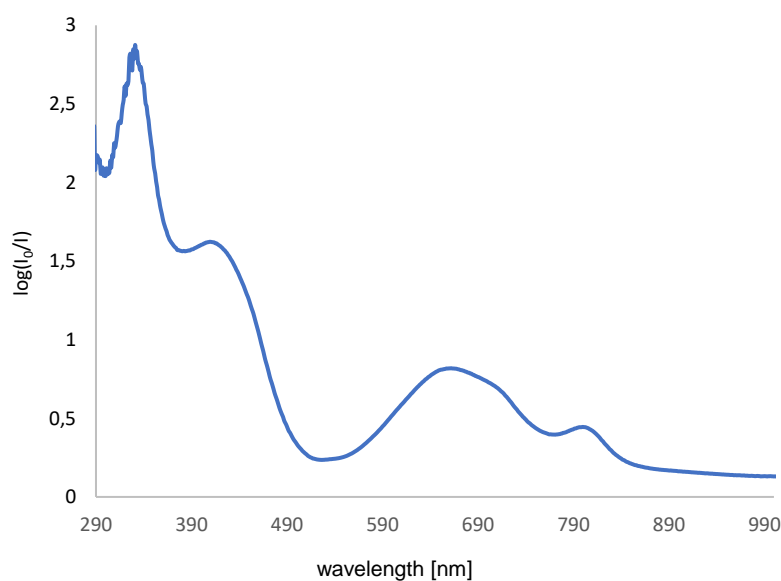


Figure 15: UV/Vis spectrum of bimetallic [NiNi(Mabiq)(Xanthphos)]OTf in THF ($c = 0.08$ mM).

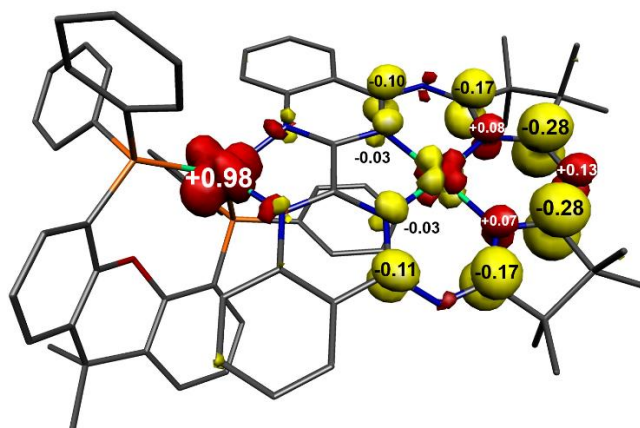


Figure 16: DFT-derived (B3LYP) spin-density plot for [NiNi(Mabiq)(Xanthphos)]OTf based on Löwdin population analysis (isosurfacevalue = ± 0.005).

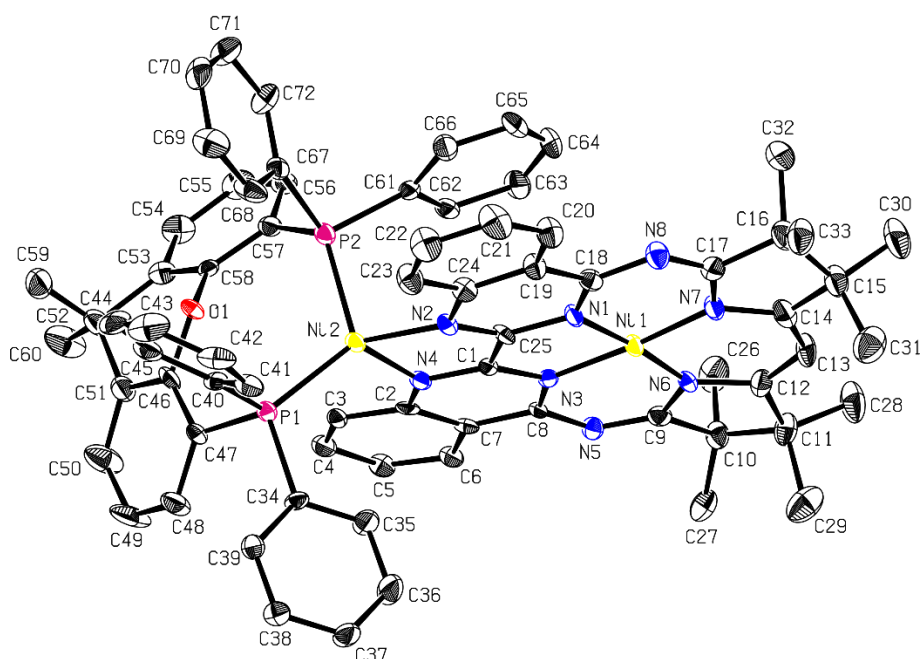


Figure 17: Molecular structure for [NiNi(Mabiq)(Xanthphos)]OTf (50% probability ellipsoids; hydrogen atoms omitted for clarity).

Table 2: Selected bond length in molecular structure of [NiNi(Mabiq)(Xanthphos)]OTf.

Bond	Length in Ångström
Ni1-N7	1.865 (4)
Ni1-N6	1.869 (4)
Ni1-N1	1.896 (4)
Ni1-N3	1.898 (4)
Ni2-N2	1.981 (4)
Ni2-N4	2.016 (4)
Ni2-P2	2.1874 (15)
Ni2-P1	2.1921 (14)
N2-C25	1.352 (6)
N4-C1	1.321 (6)
N7-C14	1.372 (6)
N6-C12	1.369 (6)

Table 3: Selected bond angles in the molecular structure of [NiNi(Mabiq)(Xanthphos)]OTf.

Bond	Angles in degrees (°)
N7-Ni1-N6	94.15 (17)
N6-Ni1-N1	174.84 (18)
N7-Ni1-N1	90.36 (17)
N7-Ni1-N3	175.32 (16)
N6-Ni1-N3	90.13 (17)
N1-Ni1-N3	85.45 (16)
N2-Ni2-P2	102.02 (12)
N4-Ni2-P2	105.59 (12)
N2-Ni2-P1	127.04 (13)
N4-Ni2-P1	117.68 (12)

Reprint permissions

Redox and photocatalytic properties of a Ni(II) complex with a macrocyclic biquinazoline (Mabiq) ligand.

You do not need to request permission to reuse your own figures, diagrams, etc, that were originally published in a Royal Society of Chemistry publication. However, permission should be requested for use of the whole article or chapter except if reusing it in a thesis. If you are including an article or book chapter published by us in your thesis please ensure that your co-authors are aware of this.

Reuse of material that was published originally by the Royal Society of Chemistry must be accompanied by the appropriate acknowledgement of the publication. The form of the acknowledgement is dependent on the journal in which it was published originally, as detailed in 'Acknowledgements'.

This article is licensed under a Creative Commons Attribution-NonCommercial 3.0 Unported Licence. Material from this article can be used in other publications provided that the correct acknowledgement is given with the reproduced material and it is not used for commercial purposes.

Reproduced material should be attributed as follows:

- For reproduction of material from NJC:[Original citation] -Published by The Royal Society of Chemistry (RSC) on behalf of the Centre National de la Recherche Scientifique (CNRS) and the RSC.
- For reproduction of material from PCCP:[Original citation] -Published by the PCCP Owner Societies.
- For reproduction of material from PPS:[Original citation] -Published by The Royal Society of Chemistry (RSC) on behalf of the European Society for Photobiology, the European Photochemistry Association, and RSC.
- For reproduction of material from all other RSC journals:[Original citation] –

Published by The Royal Society of Chemistry. Information about reproducing material from RSC articles with different licences is available on our [Permission Requests](#) page.

Synthesis of Tetrahydroisoquinolines by Visible Light-mediated 6-exo-trig Cyclization of α -Aminoalkyl Radicals.

GEORG THIEME VERLAG KG LICENSE
TERMS AND CONDITIONS

Jul 22, 2019

This Agreement between TU München -- Michael Grübel ("You") and Georg Thieme Verlag KG ("Georg Thieme Verlag KG") consists of your license details and the terms and conditions provided by Georg Thieme Verlag KG and Copyright Clearance Center.

The publisher has provided special terms related to this request that can be found at the end of the Publisher's Terms and Conditions.

License Number	4634190254540
License date	Jul 22, 2019
Licensed Content Publisher	Georg Thieme Verlag KG
Licensed Content Publication	Synlett
Licensed Content Title	Synthesis of Tetrahydroisoquinolines by Visible-Light-Mediated 6-exo-trig Cyclization of α -Aminoalkyl Radicals
Licensed Content Author	Michael Grübel, Christian Jandl, Thorsten Bach
Licensed Content Date	Jul 17, 2019
Licensed Content Issue	EFirst
Type of Use	Dissertation/Thesis
Requestor type	author of the original Thieme publication
Format	print and electronic
Portion	full article/document
Will you be translating?	no
Distribution quantity	25

Specified additional information	show the paper in the thesis
Order reference number	
Title of your dissertation / thesis	Photoredox Chemistry with Nickel-based Catalysts
Expected completion date	Sep 2019
Estimated size (number of pages)	250
	TU München Lichtenbergstraße 4
Requestor Location	Garching, 85747 Germany Attn: TU München
Publisher Tax ID	DE 147638607
Billing Type	Invoice
	TU München Lichtenbergstraße 4
Billing Address	Garching, Germany 85747 Attn: TU München
Total	0.00 EUR
Terms and Conditions	

Terms and Conditions

Introduction

The publisher for this copyrighted material is **Georg Thieme Verlag KG**, in the following referred to as **Publisher**. By clicking "accept" in connection with completing this licensing transaction, you agree that the following terms and conditions apply to this transaction (along with the Billing and Payment terms and conditions established by Copyright Clearance Center, Inc. ("CCC"), at the time that you opened your CCC account and that are available at any time at <<http://myaccount.copyright.com>>).

Limited License

Publisher hereby grants to you a non-exclusive license to use this material. Licenses are for one-time use only with a maximum distribution equal to the number specified in the license. The first instance of republication or reuse granted by this license must be completed within 12 months of the date this license was granted (although copies prepared before the end date may be distributed thereafter).

Licences for reuse in a **dissertation/thesis** are limited to the depositary copies (non-profit and password-protected) that have to be delivered within the university system. Any further use and follow-up publications require separate permission.

If you are **the author requesting full use of your article** in an Institutional Repository, special rules apply. For more detailed information, please check

<https://www.thieme.de/de/autorenounge/Autorenounge-Zeitschriftenautoren-Autorenrechte-95029.htm>

If you have identified yourself as a signatory to the **STM Permissions Guidelines**, permission is given according to the current version of these Guidelines (<https://www.stm-assoc.org/copyright-legal-affairs/permissions/permissions-guidelines/>).

Geographic Rights: Scope

Licenses may be exercised anywhere in the world.

Altering/Modifying Material: Not Permitted

You may not alter or modify the material in any manner (except that you may use, within the scope of the license granted, one or more excerpts from the copyrighted material, provided that the process of excerpting does not alter the meaning of the material or in any way reflect negatively on the publisher or any writer of the material), nor may you translate the material into another language.

Reservation of Rights

Publisher reserves all rights not specifically granted in the combination of (i) the license details provided by you and accepted in the course of this licensing transaction, (ii) these terms and conditions and (iii) CCC's Billing and Payment terms and conditions.

License Contingent on Payment

While you may exercise the rights licensed immediately upon issuance of the license at the end of the licensing process for the transaction, provided that you have disclosed complete and accurate details of your proposed use, no license is finally effective unless and until full payment is received from you (either by publisher or by CCC) as provided in CCC's Billing and Payment terms and conditions. If full payment is not received on a timely basis, then any license preliminarily granted shall be deemed automatically revoked and shall be void as if never granted. Further, in the event that you breach any of these terms and conditions or any of CCC's Billing and Payment terms and conditions, the license is automatically revoked and shall be void as if never granted. Use of materials as described in a revoked license, as well as any use of the materials beyond the scope of an unrevoked license, may constitute copyright infringement and publisher reserves the right to take any and all action to protect its copyright in the materials.

Copyright Notice: Disclaimer

Must include the following copyright and permission notice in connection with any reproduction of the licensed material: "© Georg Thieme Verlag KG."

Warranties: None

Publisher makes no representations or warranties with respect to the licensed material and adopts on its own behalf the limitations and disclaimers established by CCC on its behalf in its Billing and Payment terms and conditions for this licensing transaction.

Indemnity

You hereby indemnify and agree to hold harmless publisher and CCC, and their respective officers, directors, employees and agents, from and against any and all claims arising out of your use of the licensed material other than as specifically authorized pursuant to this license.

No Transfer of License

This license is personal to you, but may be assigned or transferred by you to a business associate (or to your employer) if you give prompt written notice of the assignment or transfer to the publisher. No such assignment or transfer shall relieve you of the obligation to pay the designated license fee on a timely basis (although payment by the identified assignee can fulfill your obligation).

No Amendment Except in Writing

This license may not be amended except in a writing signed by both parties (or, in the case of publisher, by CCC on publisher's behalf).

Objection to Contrary Terms

Publisher hereby objects to any terms contained in any purchase order, acknowledgment, check endorsement or other writing prepared by you, which terms are inconsistent with these terms and conditions or CCC's Billing and Payment terms and conditions. These terms and conditions, together with CCC's Billing and Payment terms and conditions (which are incorporated herein), comprise the entire agreement between you and publisher (and CCC) concerning this licensing transaction. In the event of any conflict between your obligations established by these terms and conditions and those established by CCC's Billing and Payment terms and conditions, these terms and conditions shall control.

Jurisdiction:

This license transaction shall be governed by and construed in accordance with the laws of the Federal Republic of Germany. You hereby agree to submit to the jurisdiction of the federal and state courts located in Berlin, Germany for purposes of resolving any disputes that may arise in connection with this licensing transaction.

Special Terms: Diese Einwilligung gilt für die Nutzung in Print und in elektronischer Form in den Pflichtexemplaren der o.g. wissenschaftlichen Arbeit. Der Artikel darf nur in der akzeptierten und für den Druck verwendeten WORD-Version ohne Thieme-Layout veröffentlicht werden. Nutzung/Bereitstellung der von uns veröffentlichten PDF-Version ist ausdrücklich ausgeschlossen. Weitere Verwertungsrechte und die Erlaubnis zur

Bereitstellung auf anderen, kommerziellen Servern werden nicht erteilt. Soll die Dissertation in den ersten 12 Monaten nach Erscheinen des Artikels bei Thieme über die Hochschule im Internet frei zugänglich gemacht werden, darf der Artikel nicht im Volltext enthalten sein. 12 Monate nach der Erstveröffentlichung der Verlagsversion dürfen die Autoren die akzeptierte Manuskriptversion auf einem nicht kommerziellen institutionellen Dokumentenserver zugänglich machen.

References

- [1] R. Willstätter, A. Stoll, *Untersuchungen über Chlorophyll. Methoden und Ergebnisse*, Springer Berlin Heidelberg, Berlin, Heidelberg, s.l., **1913**.
- [2] R. Willstätter, *J. Am. Chem. Soc.* **1915**, *37*, 323–345.
- [3] H. Fischer, H. Wenderoth, *Liebigs Ann. Chem.* **1940**, *545*, 140–147.
- [4] I. Fleming, *Nature* **1967**, *216*, 151–152.
- [5] P. H. Raven, R. F. Evert, S. E. Eichhorn, *Biology of plants*, Freeman, New York, NY, **2005**.
- [6] N. S. Lewis, D. G. Nocera, *Proc. Natl. Acad. Sci.* **2006**, *103*, 15729–15735.
- [7] G. Ciamician, *Science* **1912**, *36*, 385–394.
- [8] T. P. Yoon, M. A. Ischay, J. Du, *Nature Chem.* **2010**, *2*, 527 EP -.
- [9] I. McConnell, G. Li, G. W. Brudvig, *Chem. Biol.* **2010**, *17*, 434–447.
- [10] T. J. Meyer, *Acc. Chem. Res.* **1989**, *22*, 163–170.
- [11] V. Balzani, A. Credi, M. Venturi, *Chem. Sus. Chem.* **2008**, *1*, 26–58.
- [12] G. J. Meyer, *Inorg. Chem.* **2005**, *44*, 6852–6864.
- [13] V. Balzani, G. Bergamini, F. Marchioni, P. Ceroni, *Coord. Chem. Rev.* **2006**, *250*, 1254–1266.
- [14] A. Juris, V. Balzani, F. Barigelletti, S. Campagna, P. Belser, A. von Zelewsky, *Coord. Chem. Rev.* **1988**, *84*, 85–277.
- [15] K. Kalyanasundaram, *Coord. Chem. Rev.* **1982**, *46*, 159–244.
- [16] Q.-Q. Zhou, Y.-Q. Zou, L.-Q. Lu, W.-J. Xiao, *Angew. Chem. Int. Ed.* **2019**, *58*, 1586–1604.
- [17] K. Kalyanasundaram, *Photochemistry of polypyridine and pophyrin complexes*, Acad. Pr, London, **1992**.
- [18] M. S. Lowry, S. Bernhard, *Chem. Eur. J.* **2006**, *12*, 7970–7977.
- [19] K. Kalyanasundaram, M. Grätzel, *Coord. Chem. Rev.* **1998**, *177*, 347–414.
- [20] D. M. Hedstrand, W. H. Kruizinga, R. M. Kellogg, *Tetrahedron Lett.* **1978**, *19*, 1255–1258.
- [21] H. Cano-Yelo, A. Deronzier, *J. Chem. Soc., Perkin Trans. 2* **1984**, 1093–1098.
- [22] M. A. Ischay, M. E. Anzovino, J. Du, T. P. Yoon, *J. Am. Chem. Soc.* **2008**, *130*, 12886–12887.
- [23] D. A. Nicewicz, D. W. C. MacMillan, *Science* **2008**, *322*, 77–80.
- [24] J. M. R. Narayanam, J. W. Tucker, C. R. J. Stephenson, *J. Am. Chem. Soc.* **2009**, *131*, 8756–8757.
- [25] C. K. Prier, D. A. Rankic, D. W. C. MacMillan, *Chem. Rev.* **2013**, *113*, 5322–5363.
- [26] M. H. Shaw, J. Twilton, D. W. C. MacMillan, *J. Org. Chem.* **2016**, *81*, 6898–6926.

- [27] D. M. Arias-Rotondo, J. K. McCusker, *Chem. Soc. Rev.* **2016**, *45*, 5803–5820.
- [28] N. A. Romero, D. A. Nicewicz, *Chem. Rev.* **2016**, *116*, 10075–10166.
- [29] Y. Xi, H. Yi, A. Lei, *Org. Biomol. Chem.* **2013**, *11*, 2387–2403.
- [30] J. M. R. Narayanam, C. R. J. Stephenson, *Chem. Soc. Rev.* **2011**, *40*, 102–113.
- [31] C. Beemelmans, H.-U. Reissig, *Chem. Soc. Rev.* **2011**, *40*, 2199–2210.
- [32] C. R. J. Stephenson, D. W. C. MacMillan, T. P. Yoon (Eds.) *Visible light photocatalysis in organic chemistry*, Wiley-VCH Verlag GmbH & Co, Weinheim, Germany, **2018**.
- [33] B. Happ, A. Winter, M. D. Hager, U. S. Schubert, *Chem. Soc. Rev.* **2012**, *41*, 2222–2255.
- [34] B. M. Hockin, C. Li, N. Robertson, E. Zysman-Colman, *Catal. Sci. Technol.* **2019**, *9*, 889–915.
- [35] D. Wöhrle, M. W. Tausch, W.-D. Stohrer, *Photochemie. Konzepte, Methoden, Experimente*, Wiley-VCH, Weinheim, **2010**.
- [36] F. E. Lytle, D. M. Hercules, *J. Am. Chem. Soc.* **1969**, *91*, 253–257.
- [37] J. W. Tucker, C. R. J. Stephenson, *J. Org. Chem.* **2012**, *77*, 1617–1622.
- [38] Z. Ding, R. G. Wellington, P. F. Brevet, H. H. Girault, *J. Phys. Chem.* **1996**, *100*, 10658–10663.
- [39] J. I. Day, K. Teegardin, J. Weaver, J. Chan, *Org. Process. Res. Dev.* **2016**, *20*, 1156–1163.
- [40] T. Koike, M. Akita, *Inorg. Chem. Front.* **2014**, *1*, 562–576.
- [41] Y. Ohsawa, S. Sprouse, K. A. King, M. K. DeArmond, K. W. Hanck, R. J. Watts, *J. Phys. Chem.* **1987**, *91*, 1047–1054.
- [42] C. Pac, M. Ihama, M. Yasuda, Y. Miyauchi, H. Sakurai, *J. Am. Chem. Soc.* **1981**, *103*, 6495–6497.
- [43] A. Nitelet, D. Thevenet, B. Schiavi, C. Hardouin, J. Fournier, R. Tamion, X. Pannecoucke, P. Jubault, T. Poisson, *Chem. Eur. J.* **2019**, *25*, 3262–3266.
- [44] J. D. Nguyen, E. M. D'Amato, J. M. R. Narayanam, C. R. J. Stephenson, *Nature Chem.* **2012**, *4*, 854 EP -.
- [45] R. Maidan, Z. Goren, J. Y. Becker, I. Willner, *J. Am. Chem. Soc.* **1984**, *106*, 6217–6222.
- [46] R. Maidan, I. Willner, *J. Am. Chem. Soc.* **1986**, *108*, 1080–1082.
- [47] T. J. van Bergen, D. M. Hedstrand, W. H. Kruizinga, R. M. Kellogg, *J. Org. Chem.* **1979**, *44*, 4953–4962.
- [48] T. Hirao, J. Shiori, N. Okahata, *Bull. Chem. Soc. Jpn.* **2004**, *77*, 1763–1764.
- [49] Y. Chen, A. S. Kamlet, J. B. Steinman, D. R. Liu, *Nature Chem.* **2011**, *3*, 146 EP -.
- [50] J. W. Tucker, J. M. R. Narayanam, P. S. Shah, C. R. J. Stephenson, *Chem. Commun.* **2011**, *47*, 5040–5042.

- [51] J. W. Tucker, J. D. Nguyen, J. M. R. Narayanam, S. W. Krabbe, C. R. J. Stephenson, *Chem. Commun.* **2010**, 46, 4985–4987.
- [52] J. W. Tucker, J. M. R. Narayanam, S. W. Krabbe, C. R. J. Stephenson, *Org. Lett.* **2010**, 12, 368–371.
- [53] P. Kohls, D. Jadhav, G. Pandey, O. Reiser, *Org. Lett.* **2012**, 14, 672–675.
- [54] Y. Miyake, K. Nakajima, Y. Nishibayashi, *J. Am. Chem. Soc.* **2012**, 134, 3338–3341.
- [55] L. Ruiz Espelt, E. M. Wiensch, T. P. Yoon, *J. Org. Chem.* **2013**, 78, 4107–4114.
- [56] H. Cano-Yelo, A. Deronzier, *Tetrahedron Lett.* **1984**, 25, 5517–5520.
- [57] A. G. Condie, J. C. González-Gómez, C. R. J. Stephenson, *J. Am. Chem. Soc.* **2010**, 132, 1464–1465.
- [58] C. Dai, F. Meschini, J. M. R. Narayanam, C. R. J. Stephenson, *J. Org. Chem.* **2012**, 77, 4425–4431.
- [59] M. Rueping, C. Vila, R. M. Koenigs, K. Poscharny, D. C. Fabry, *Chem. Commun.* **2011**, 47, 2360–2362.
- [60] M. Rueping, S. Zhu, R. M. Koenigs, *Chem. Commun.* **2011**, 47, 8679–8681.
- [61] Y.-Q. Zou, L.-Q. Lu, L. Fu, N.-J. Chang, J. Rong, J.-R. Chen, W.-J. Xiao, *Angew. Chem. Int. Ed.* **2011**, 50, 7171–7175.
- [62] M. Rueping, S. Zhu, R. M. Koenigs, *Chem. Commun.* **2011**, 47, 12709–12711.
- [63] D. B. Freeman, L. Furst, A. G. Condie, C. R. J. Stephenson, *Org. Lett.* **2012**, 14, 94–97.
- [64] Z.-Q. Wang, M. Hu, X.-C. Huang, L.-B. Gong, Y.-X. Xie, J.-H. Li, *J. Org. Chem.* **2012**, 77, 8705–8711.
- [65] Y. Pan, S. Wang, C. W. Kee, E. Dubuisson, Y. Yang, K. P. Loh, C.-H. Tan, *Green Chem.* **2011**, 13, 3341.
- [66] P. Renaud, L. Giraud, *Synthesis* **1996**, 1996, 913–926.
- [67] U. C. Yoon, P. S. Mariano, *Acc. Chem. Res.* **1992**, 25, 233–240.
- [68] G. Pandey, *Synlett* **1992**, 1992, 546–552.
- [69] H. Cano-Yelo, A. Deronzier, *J. Photochem.* **1987**, 37, 315–321.
- [70] M. A. Ischay, Z. Lu, T. P. Yoon, *J. Am. Chem. Soc.* **2010**, 132, 8572–8574.
- [71] J. Du, T. P. Yoon, *J. Am. Chem. Soc.* **2009**, 131, 14604–14605.
- [72] A. E. Hurtley, M. A. Cismesia, M. A. Ischay, T. P. Yoon, *Tetrahedron* **2011**, 67, 4442–4448.
- [73] S. Lin, M. A. Ischay, C. G. Fry, T. P. Yoon, *J. Am. Chem. Soc.* **2011**, 133, 19350–19353.
- [74] Y. Miyake, Y. Ashida, K. Nakajima, Y. Nishibayashi, *Chem. Commun.* **2012**, 48, 6966–6968.
- [75] L. Ruiz Espelt, I. S. McPherson, E. M. Wiensch, T. P. Yoon, *J. Am. Chem. Soc.* **2015**, 137, 2452–2455.
- [76] D. Lenhart, A. Bauer, A. Pöthig, T. Bach, *Chem. Eur. J.* **2016**, 22, 6519–6523.

- [77] D. W. Cho, U. C. Yoon, P. S. Mariano, *Acc. Chem. Res.* **2011**, *44*, 204–215.
- [78] M. Jonas, S. Blechert, E. Steckhan, *J. Org. Chem.* **2001**, *66*, 6896–6904.
- [79] L. Chu, C. Ohta, Z. Zuo, D. W. C. MacMillan, *J. Am. Chem. Soc.* **2014**, *136*, 10886–10889.
- [80] A. Millet, Q. Lefebvre, M. Rueping, *Chem. Eur. J.* **2016**, *22*, 13464–13468.
- [81] Z. Zuo, D. W. C. MacMillan, *J. Am. Chem. Soc.* **2014**, *136*, 5257–5260.
- [82] D. W. C. MacMillan, *Nature* **2008**, *455*, 304 EP -.
- [83] S. Mukherjee, J. W. Yang, S. Hoffmann, B. List, *Chem. Rev.* **2007**, *107*, 5471–5569.
- [84] D. A. Nagib, M. E. Scott, D. W. C. MacMillan, *J. Am. Chem. Soc.* **2009**, *131*, 10875–10877.
- [85] H.-W. Shih, M. N. Vander Wal, R. L. Grange, D. W. C. MacMillan, *J. Am. Chem. Soc.* **2010**, *132*, 13600–13603.
- [86] E. R. Welin, A. A. Warkentin, J. C. Conrad, D. W. C. MacMillan, *Angew. Chem. Int. Ed.* **2015**, *54*, 9668–9672.
- [87] G. Cecere, C. M. König, J. L. Alleva, D. W. C. MacMillan, *J. Am. Chem. Soc.* **2013**, *135*, 11521–11524.
- [88] D. Uraguchi, N. Kinoshita, T. Kizu, T. Ooi, *J. Am. Chem. Soc.* **2015**, *137*, 13768–13771.
- [89] D. C. Miller, K. T. Tarantino, R. R. Knowles, *Topics Curr. Chem.* **2016**, *374*, 30.
- [90] D. S. Hamilton, D. A. Nicewicz, *J. Am. Chem. Soc.* **2012**, *134*, 18577–18580.
- [91] A. J. Perkowski, D. A. Nicewicz, *J. Am. Chem. Soc.* **2013**, *135*, 10334–10337.
- [92] T. M. Nguyen, D. A. Nicewicz, *J. Am. Chem. Soc.* **2013**, *135*, 9588–9591.
- [93] J.-M. M. Grandjean, D. A. Nicewicz, *Angew. Chem. Int. Ed.* **2013**, *52*, 3967–3971.
- [94] D. J. Wilger, J.-M. M. Grandjean, T. R. Lammert, D. A. Nicewicz, *Nature Chem.* **2014**, *6*, 720 EP -.
- [95] can be found under <https://www.nobelprize.org/prizes/chemistry/2010/press-release/>, **2010**.
- [96] D. Kalyani, K. B. McMurtrey, S. R. Neufeldt, M. S. Sanford, *J. Am. Chem. Soc.* **2011**, *133*, 18566–18569.
- [97] S. R. Neufeldt, M. S. Sanford, *Adv. Synth. Catal.* **2012**, *354*, 3517–3522.
- [98] J. Zoller, D. C. Fabry, M. A. Ronge, M. Rueping, *Angew. Chem. Int. Ed.* **2014**, *53*, 13264–13268.
- [99] Z. Zuo, D. T. Ahneman, L. Chu, J. A. Terrett, A. G. Doyle, D. W. C. MacMillan, *Science* **2014**, *345*, 437–440.
- [100] J. C. Tellis, D. N. Primer, G. A. Molander, *Science* **2014**, *345*, 433–436.
- [101] M. Jouffroy, D. N. Primer, G. A. Molander, *J. Am. Chem. Soc.* **2016**, *138*, 475–478.
- [102] V. Corcé, L.-M. Chamoreau, E. Derat, J.-P. Goddard, C. Ollivier, L. Fensterbank, *Angew. Chem. Int. Ed.* **2015**, *54*, 11414–11418.

- [103] K. Nakajima, S. Nojima, Y. Nishibayashi, *Angew. Chem. Int. Ed.* **2016**, *55*, 14106–14110.
- [104] J. A. Milligan, J. P. Phelan, S. O. Badir, G. A. Molander, *Angew. Chem. Int. Ed.* **2019**, *58*, 6152–6163.
- [105] D. T. Ahneman, A. G. Doyle, *Chem. Sci.* **2016**, *7*, 7002–7006.
- [106] C. L. Joe, A. G. Doyle, *Angew. Chem. Int. Ed.* **2016**, *55*, 4040–4043.
- [107] B. J. Shields, B. Kudisch, G. D. Scholes, A. G. Doyle, *J. Am. Chem. Soc.* **2018**, *140*, 3035–3039.
- [108] Y. Yamashita, J. C. Tellis, G. A. Molander, *Proc. Natl. Acad. Sci.* **2015**, *112*, 12026–12029.
- [109] D. N. Primer, I. Karakaya, J. C. Tellis, G. A. Molander, *J. Am. Chem. Soc.* **2015**, *137*, 2195–2198.
- [110] I. Karakaya, D. N. Primer, G. A. Molander, *Org. Lett.* **2015**, *17*, 3294–3297.
- [111] M. El Khatib, R. A. M. Serafim, G. A. Molander, *Angew. Chem. Int. Ed.* **2016**, *55*, 254–258.
- [112] C. P. Johnston, R. T. Smith, S. Allmendinger, D. W. C. MacMillan, *Nature* **2016**, *536*, 322 EP -.
- [113] N. A. Till, R. T. Smith, D. W. C. MacMillan, *J. Am. Chem. Soc.* **2018**, *140*, 5701–5705.
- [114] J. Twilton, C. Le, P. Zhang, M. H. Shaw, R. W. Evans, D. W. C. MacMillan, *Nature Chem. Rev.* **2017**, *1*, 0052 EP -.
- [115] Y. Ye, M. S. Sanford, *J. Am. Chem. Soc.* **2012**, *134*, 9034–9037.
- [116] Y. Liang, X. Zhang, D. W. C. MacMillan, *Nature* **2018**, *559*, 83–88.
- [117] A. Tlahuext-Aca, M. N. Hopkinson, B. Sahoo, F. Glorius, *Chem. Sci.* **2016**, *7*, 89–93.
- [118] Y. He, H. Wu, F. D. Toste, *Chem. Sci.* **2015**, *6*, 1194–1198.
- [119] X.-z. Shu, M. Zhang, Y. He, H. Frei, F. D. Toste, *J. Am. Chem. Soc.* **2014**, *136*, 5844–5847.
- [120] J. Um, H. Yun, S. Shin, *Org. Lett.* **2016**, *18*, 484–487.
- [121] G. Zhang, C. Liu, H. Yi, Q. Meng, C. Bian, H. Chen, J.-X. Jian, L.-Z. Wu, A. Lei, *J. Am. Chem. Soc.* **2015**, *137*, 9273–9280.
- [122] X. Sun, J. Chen, T. Ritter, *Nature Chem.* **2018**, *10*, 1229–1233.
- [123] A. F. Holleman, E. Wiberg, N. Wiberg, *Lehrbuch der anorganischen Chemie*, de Gruyter, Berlin, **2007**.
- [124] V. Balzani, G. Bergamini, S. Campagna, F. Puntoriero in *Topics in Current Chemistry*, Vol. 281 (Eds.: V. Balzani, S. Campagna, G. Accorsi), Springer, Berlin, New York, **2007**, pp. 1–36.
- [125] J. v. Caspar, T. J. Meyer, *J. Am. Chem. Soc.* **1983**, *105*, 5583–5590.
- [126] L. A. Büldt, C. B. Larsen, O. S. Wenger, *Chem. Eur. J.* **2017**, *23*, 8577–8580.

- [127] A. Cannizzo, C. J. Milne, C. Consani, W. Gawelda, C. Bressler, F. van Mourik, M. Chergui, *Coord. Chem. Rev.* **2010**, *254*, 2677–2686.
- [128] O. S. Wenger, *J. Am. Chem. Soc.* **2018**, *140*, 13522–13533.
- [129] A. Barbieri, G. Accorsi, N. Armaroli, *Chem. Commun.* **2008**, 2185–2193.
- [130] D. V. Scaltrito, D. W. Thompson, J. A. O'Callaghan, G. J. Meyer, *Coord. Chem. Rev.* **2000**, *208*, 243–266.
- [131] B.-T. Ahn, D. R. McMillin, *Inorg. Chem.* **1978**, *17*, 2253–2258.
- [132] D. R. McMillin, J. R. Kirchhoff, K. V. Goodwin, *Coord. Chem. Rev.* **1985**, *64*, 83–92.
- [133] M. T. Buckner, D. R. McMillin, *J. Chem. Soc., Chem. Commun.* **1978**, 759.
- [134] D. R. McMillin, K. M. McNett, *Chem. Rev.* **1998**, *98*, 1201–1220.
- [135] F. Dumur, *Org. Electron.* **2015**, *21*, 27–39.
- [136] D. G. Cuttell, S.-M. Kuang, P. E. Fanwick, D. R. McMillin, R. A. Walton, *J. Am. Chem. Soc.* **2002**, *124*, 6–7.
- [137] R. Czerwieniec, M. J. Leitzl, H. H.H. Homeier, H. Yersin, *Coord. Chem. Rev.* **2016**, *325*, 2–28.
- [138] M. Iwamura, S. Takeuchi, T. Tahara, *Acc. Chem. Res.* **2015**, *48*, 782–791.
- [139] N. Armaroli, *Chem. Soc. Rev.* **2001**, *30*, 113–124.
- [140] C. E. Housecroft, E. C. Constable, *Chem. Soc. Rev.* **2015**, *44*, 8386–8398.
- [141] A. J. J. Lennox, S. Fischer, M. Jurrat, S.-P. Luo, N. Rockstroh, H. Junge, R. Ludwig, M. Beller, *Chem. Eur. J.* **2016**, *22*, 1233–1238.
- [142] J.-M. Kern, J.-P. Sauvage, *J. Chem. Soc., Chem. Commun.* **1987**, 546–548.
- [143] M. Pirtsch, S. Paria, T. Matsuno, H. Isobe, O. Reiser, *Chem. Eur. J.* **2012**, *18*, 7336–7340.
- [144] S. Paria, M. Pirtsch, V. Kais, O. Reiser, *Synthesis* **2013**, *45*, 2689–2698.
- [145] X.-J. Tang, W. R. Dolbier, *Angew. Chem. Int. Ed.* **2015**, *54*, 4246–4249.
- [146] G. Fumagalli, P. T. G. Rabet, S. Boyd, M. F. Greaney, *Angew. Chem. Int. Ed.* **2015**, *54*, 11481–11484.
- [147] H. Baguia, C. Deldaele, E. Romero, B. Michelet, G. Evano, *Synthesis* **2018**, *50*, 3022–3030.
- [148] L. Traub, O. Reiser, *Phys. Sci. Rev.* **2019**, *0*, 4320.
- [149] J. M. Ahn, J. C. Peters, G. C. Fu, *J. Am. Chem. Soc.* **2017**, *139*, 18101–18106.
- [150] S. E. Creutz, K. J. Lotito, G. C. Fu, J. C. Peters, *Science* **2012**, *338*, 647–651.
- [151] C. D. Matier, J. Schwaben, J. C. Peters, G. C. Fu, *J. Am. Chem. Soc.* **2017**, *139*, 17707–17710.
- [152] S. Otto, M. Grabolle, C. Förster, C. Kreitner, U. Resch-Genger, K. Heinze, *Angew. Chem. Int. Ed.* **2015**, *54*, 11572–11576.

- [153] S. Otto, A. M. Nauth, E. Ermilov, N. Scholz, A. Friedrich, U. Resch-Genger, S. Lochbrunner, T. Opatz, K. Heinze, *Chem. Photo. Chem.* **2017**, *1*, 344–349.
- [154] S. M. Stevenson, M. P. Shores, E. M. Ferreira, *Angew. Chem. Int. Ed.* **2015**, *54*, 6506–6510.
- [155] X. Shen, Y. Li, Z. Wen, S. Cao, X. Hou, L. Gong, *Chem. Sci.* **2018**, *9*, 4562–4568.
- [156] M. Grübel, I. Bosque, P. J. Altmann, T. Bach, C. R. Hess, *Chem. Sci.* **2018**, *9*, 3313–3317.
- [157] T. Mandal, S. Das, S. de Sarkar, *Adv. Synth. Catal.* **2019**, *0*.
- [158] M. Kaspar, P. J. Altmann, A. Pöthig, S. Sproules, C. R. Hess, *Chem. Commun.* **2017**, *53*, 7282–7285.
- [159] P. Banerjee, A. Company, T. Weyhermüller, E. Bill, C. R. Hess, *Inorg. Chem.* **2009**, *48*, 2944–2955.
- [160] E. V. Puttock, P. Banerjee, M. Kaspar, L. Drennen, D. S. Yufit, E. Bill, S. Sproules, C. R. Hess, *Inorg. Chem.* **2015**, *54*, 5864–5873.
- [161] H. S. Stark, P. J. Altmann, S. Sproules, C. R. Hess, *Inorg. Chem.* **2018**, *57*, 6401–6409.
- [162] L. Gan, T. L. Groy, P. Tarakeshwar, S. K. S. Mazinani, J. Shearer, V. Mujica, A. K. Jones, *J. Am. Chem. Soc.* **2015**, *137*, 1109–1115.
- [163] E. E. Benson, C. P. Kubiak, A. J. Sathrum, J. M. Smieja, *Chem. Soc. Rev.* **2009**, *38*, 89–99.
- [164] F. Burg, M. Gicquel, S. Breitenlechner, A. Pöthig, T. Bach, *Angew. Chem. Int. Ed.* **2018**, *57*, 2953–2957.
- [165] J. R. Frost, S. M. Huber, S. Breitenlechner, C. Bannwarth, T. Bach, *Angew. Chem. Int. Ed.* **2015**, *54*, 691–695.
- [166] M. A. Elban, W. Sun, B. M. Eisenhauer, R. Gao, S. M. Hecht, *Org. Lett.* **2006**, *8*, 3513–3516.
- [167] P. F. H. Schwab, F. Fleischer, J. Michl, *J. Org. Chem.* **2002**, *67*, 443–449.